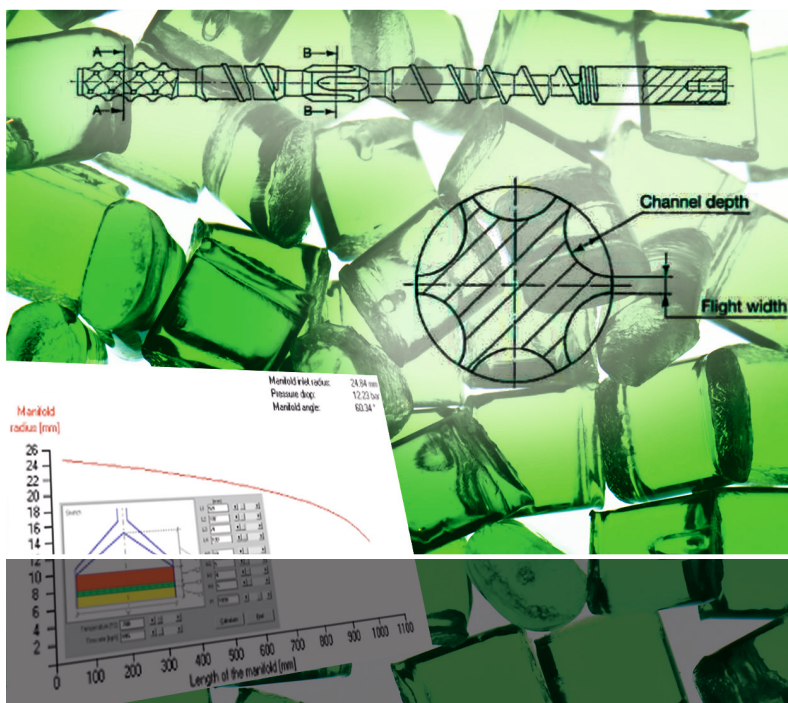


Natti S. Rao

Basic Polymer Engineering Data



HANSER

Natti S. Rao

Basic Polymer Engineering Data

Hanser Publishers, Munich

HANSER
Hanser Publications, Cincinnati

The Author:

Dr. Natti S. Rao, Schieferkopf 6, 67434 Neustadt, Germany

Distributed in the Americas by:

Hanser Publications

6915 Valley Avenue, Cincinnati, Ohio 45244-3029, USA

Fax: (513) 527-8801

Phone: (513) 527-8977

www.hanserpublications.com

Distributed in all other countries by:

Carl Hanser Verlag

Postfach 86 04 20, 81631 München, Germany

Fax: +49 (89) 98 48 09

www.hanser-fachbuch.de

The use of general descriptive names, trademarks, etc., in this publication, even if the former are not especially identified, is not to be taken as a sign that such names, as understood by the Trade Marks and Merchandise Marks Act, may accordingly be used freely by anyone. While the advice and information in this book are believed to be true and accurate at the date of going to press, neither the authors nor the editors nor the publisher can accept any legal responsibility for any errors or omissions that may be made. The publisher makes no warranty, express or implied, with respect to the material contained herein.

The final determination of the suitability of any information for the use contemplated for a given application remains the sole responsibility of the user.

Cataloging-in-Publication Data is on file with the Library of Congress

All rights reserved. No part of this book may be reproduced or transmitted in any form or by any means, electronic or mechanical, including photocopying or by any information storage and retrieval system, without permission in writing from the publisher.

© Carl Hanser Verlag, Munich 2017

Editor: Dr. Mark Smith

Production Management: Jörg Strohbach

Coverconcept: Marc Müller-Bremer, www.rebranding.de, München

Coverdesign: Stephan Rönigk

Typesetting: Kösel Media GmbH, Krugzell

Printed and bound by Hubert & Co GmbH, Göttingen

Printed in Germany

ISBN: 978-1-56990-649-1

E-Book ISBN: 978-1-56990-650-7

Preface

Mechanical, thermal, and rheological properties of polymers form the basic group of property values required for designing polymer machinery. In addition, knowledge of the properties of the resin, such as stock temperature of the melt, is necessary for optimizing the process. Furthermore, while designing a plastic part, performance properties of the resin, depending on the application, are to be considered. Examples of which are flammability, weather resistance, and optical properties, to name a few. Hence, a variety of property values is needed to accomplish machine design, part design, and process optimization.

The bulk of polymer machinery is comprised of extruders and injection molding machines. Their designs can be accomplished empirically by trial and error procedures based on experiments. However, these methods are costly and time-consuming and not always feasible if one has to work with large units like a high speed blown film line or a sheet making unit of a thermoforming plant.

As a result, the use of software based on numerical analysis of the processes occurring in these machine elements has found more applications and become a state-of-the-art design tool. The property data required to perform design calculations using software exists in databanks, which are available on the market. However, for a number of practical applications, these databanks are too extensive to justify their use; for example, to obtain a quick estimate of the dimensions of an extrusion die or the cooling of a part in an injection molding die.

The intent of this book, first of all, is to create an easy to use quick reference that covers basic design data on resin, machine, part, and process, and second, to show how this data can be applied to solve practical problems. With this aim in mind, numerous examples are given to illustrate the use of this data. The calculations involved in these examples can be easily handled with the help of handheld calculators.

Chapters 1 to 5 deal with the description of physical properties—mechanical, thermal, rheological, electrical, and optical—of polymers and principles of their measurement. In Chapter 6 the effect of external influences on the performance of polymers is treated. General property data for different materials such as liquid crystal

polymers, structural foams, thermosetting resins, and reinforced plastics are given at the end of this chapter.

In Chapter 7 the processing properties and machine related data are presented for continuous extrusion processes; namely, blown film, pipe, and flat film extrusion. Resin and machine parameters for thermoforming and compounding have also been included in this chapter.

Chapter 8 deals with blow molding and the influence of resin and machine variables on different kinds of blow molding processes. Finally, Chapter 9 covers resin-dependent and machine-related parameters concerning the injection molding process.

Machine element design, covered in Chapters 7 to 9, includes screw design for extruders and injection molding machines, die design for extruders, mold design for molding and forming operations, and downstream equipment for extrusion. Wherever appropriate, the properties and machine related parameters are described by mathematical formulas that are, as already mentioned, illustrated by worked-out examples. The solution procedure used in these examples describes the application of polymer data to solve practical problems. On the basis of this approach, the importance of polymer data in dealing with design and process optimization is explained.

Thanks are due to Dr. Benjamin Dietrich of The Karlsruhe Institute of Technology for his cooperation in preparing the manuscript, and to Prof. Stephen Orroth of the University of Massachusetts at Lowell, for his fruitful suggestions.

I am extremely grateful to Dr. Mark Smith of Hanser for his careful review of the manuscript and corrections needed to attain compatibility with the printing requirements. Thanks are also due to Cheryl Hamilton for her great help in editing the text. The careful proofreading and various suggestions for improving the manuscript by Julia Diaz, associate editor of Hanser, are also thankfully acknowledged.

Natti S. Rao, Ph. D.

About the Author

Natti S. Rao obtained his B. Tech (Hons) in Mechanical Engineering and M. Tech in Chemical Engineering from the Indian Institute of Technology Kharagpur, India. After receiving his Ph.D. in Chemical Engineering from the University of Karlsruhe, Germany, he worked for many years as a senior research assistant with the BASF AG. Later, he served as a technical advisor to the leading machine and resin manufacturers in various countries.

Dr. Rao has published over 70 papers and authored six books on designing polymer machinery with the help of computer programs. Prior to starting his consulting company in 1987, he worked as a visiting professor at the Indian Institute of Technology, Madras. Besides consulting, he conducts seminars on the computer-aided design of polymer machinery. Dr. Rao has given lectures on polymer engineering at the University of Texas, Austin, and he is presently involved in the Continuing Education Department of UMASS Lowell, MA.

Dr. Rao is a Fellow of the Society of Plastics Engineers USA.

Contents

Preface	V
About the Author	VII
1 Mechanical Properties of Solid Polymers	1
1.1 Ideal Solids	1
1.2 Tensile Properties	2
1.2.1 Stress-Strain Behavior	3
1.2.2 Tensile Modulus	5
1.2.3 Effect of Temperature on Tensile Strength	7
1.3 Shear Properties	7
1.3.1 Shear Modulus	8
1.3.2 Effect of Temperature on Shear Modulus	8
1.4 Compressive Properties	10
1.4.1 Bulk Modulus	11
1.5 Time Related Properties	12
1.5.1 Creep Modulus	12
1.5.2 Creep Rupture	14
1.5.3 Relaxation Modulus	14
1.5.4 Fatigue Limit	15
1.6 Hardness	18
1.7 Impact Strength	19
1.8 Coefficient of Friction	19
1.9 References	24
2 Thermal Properties of Solid and Molten Polymers	25
2.1 Specific Volume	25
2.2 Specific Heat	28

2.3	Thermal Expansion Coefficient	30
2.4	Enthalpy	31
2.5	Thermal Conductivity	32
2.6	Thermal Diffusivity	33
2.7	Coefficient of Heat Penetration	35
2.8	Heat Deflection Temperature	36
2.9	Vicat Softening Point	37
2.10	Flammability	38
2.11	References	41
3	Transport Properties of Molten Polymers	43
3.1	Newtonian and Non-Newtonian Fluids	43
3.2	Viscous Shear Flow	45
3.2.1	Apparent Shear Rate	45
3.2.2	Entrance Loss	46
3.2.3	True Shear Stress	47
3.2.4	Apparent Viscosity	48
3.2.5	True Shear Rate	50
3.2.6	True Viscosity	51
3.3	Rheological Models	51
3.3.1	Hyperbolic Function of Eyring and Prandtl	51
3.3.2	Power Law of Ostwald and de Waele	52
3.3.3	Polynomial of Münstedt	54
3.3.3.1	Shift Factor for Crystalline Polymers	55
3.3.3.2	Shift Factor for Amorphous Polymers	55
3.3.4	Viscosity Equation of Carreau	57
3.3.5	Viscosity Formula of Klein	60
3.4	Effect of Pressure on Viscosity	61
3.5	Dependence of Viscosity on Molecular Weight	62
3.6	Viscosity of Two-Component Mixtures	63
3.7	Melt Flow Index	63
3.8	Tensile Viscosity	65
3.9	Viscoelastic Properties	65
3.9.1	Primary Normal Stress Coefficient, Q	65
3.9.2	Shear Compliance, J_e	66
3.9.3	Die Swell	67
3.10	Rheology of Glass Fiber-Filled Polypropylene Melts	67

3.10.1	Introduction	67
3.10.2	Model	68
3.10.3	Shift Factor as a Function of Fiber Content	70
3.10.4	Example	71
3.10.5	Summary	73
3.11	Practical Computational Rheology Primer	73
3.11.1	Introduction	73
3.11.2	Shear Flow	75
3.11.2.1	Relationship between Flow Rate and Pressure Drop	75
3.11.2.2	Shear Rates for Blown Film and Extrusion Coating Dies	78
3.11.2.3	Extensional Flow	80
3.11.2.4	Melt Elasticity	80
3.12	Conclusions	84
3.13	References	84
4	Electrical Properties	87
4.1	Surface Resistivity	87
4.2	Volume Resistivity	87
4.3	Dielectric Strength	88
4.4	Relative Permittivity	88
4.5	Dielectric Dissipation Factor or Loss Tangent	89
4.6	Comparative Tracking Index (CTI)	90
4.7	References	92
5	Optical Properties of Solid Polymers	93
5.1	Light Transmission	93
5.2	Haze	93
5.3	Refractive Index	94
5.4	Gloss	95
5.5	Color	95
5.6	References	96
6	External Influences	97
6.1	Physical Interactions	97
6.1.1	Solubility	97
6.1.2	Environmental Stress Cracking (ESC)	97

6.1.3	Permeability	99
6.1.4	Absorption and Desorption	100
6.1.5	Weathering Resistance	100
6.2	Chemical Resistance	101
6.2.1	Chemical and Wear Resistance to Polymers	102
6.3	General Property Data	103
6.4	References	110
7	Extrusion	111
7.1	Extrusion Screws	112
7.2	Processing Parameters	114
7.2.1	Resin-Dependent Parameters	114
7.2.1.1	Blown Film	115
7.2.1.2	Pipe Extrusion	116
7.2.1.3	Flat Film Extrusion	117
7.2.1.4	Sheet Extrusion	117
7.2.1.5	Wire Coating	118
7.2.2	Machine-Related Parameters	118
7.2.2.1	Extruder Output	118
7.2.2.1.1	Feed Zone	118
7.2.2.1.2	Metering Zone (Melt Zone)	120
7.2.2.2	Melting Parameter	127
7.2.2.3	Melting Profile	129
7.2.2.4	Screw Power	130
7.2.2.5	Melt Temperature and Melt Pressure	132
7.2.2.5.1	Melt Temperature	132
7.2.2.5.2	Temperature Fluctuation	133
7.2.2.5.3	Melt Pressure	134
7.2.2.5.4	Pressure Fluctuation	134
7.3	Extrusion Dies	145
7.3.1	Pipe Extrusion	147
7.3.1.1	General Cross Section	149
7.3.1.2	Drawdown and Haul-Off Rates	153
7.3.2	Blown Film	155
7.3.3	Sheet Extrusion	161
7.4	Thermoforming	163
7.5	Compounding	167
7.5.1	Coextrusion	168

7.6	Extrudate Cooling	170
7.6.1	Dimensionless Groups	173
7.7	References	175
8	Blow Molding	177
8.1	Processes	177
8.1.1	Resin-Dependent Parameters	179
8.1.1.1	Melt Temperature and Pressure	179
8.1.1.1.1	Processing Data for Stretch Blow Molding	180
8.1.1.1.2	Volume Shrinkage	180
8.1.1.1.3	Choice of Material	181
8.1.2	Machine-Related Parameters	181
8.1.2.1	Blow Molding Dies	181
8.2	References	183
9	Injection Molding	185
9.1	Resin-Dependent Parameters	188
9.1.1	Injection Pressure	188
9.1.2	Mold Shrinkage and Processing Temperature	188
9.1.3	Drying Temperatures and Times	191
9.1.4	Flow Characteristics of Injection-Molding Resins	191
9.2	Machine-Related Parameters	196
9.2.1	Injection Unit	196
9.2.2	Injection Molding Screw	197
9.2.2.1	Nonreturn Valves	198
9.2.2.1.1	Nozzle	199
9.2.3	Injection Mold	200
9.2.3.1	Runner Systems	200
9.2.3.2	Design of Gates	202
9.2.3.3	Injection Pressure and Clamp Force	204
9.2.4	Mechanical Design of Mold	212
9.3	Melting in Injection Molding Screws	214
9.3.1	Model	214
9.3.2	Calculation Procedure	216
9.3.3	Sample Calculation	216
9.3.4	Results of Simulation	217
9.3.5	Screw Dimensions	219

9.4	Injection Mold	220
9.4.1	Runner Systems	220
9.4.2	Calculated Example	220
9.4.3	Mold Filling	222
9.4.4	Injection Pressure	222
9.4.5	Calculated Example with Symbols and Units	223
9.5	Flow Characteristics of Injection Molding Resins	225
9.5.1	Model	226
9.5.2	Melt Viscosity and Power Law Exponent	227
9.5.3	Experimental Results and Discussion	228
9.5.4	Sample Calculation	230
9.6	Cooling of Melt in the Mold	231
9.6.1	Crystalline Polymers	231
9.6.2	Amorphous Polymers	233
9.6.3	Calculations with Varying Mold Wall Temperature	234
9.6.3.1	Sample Calculation with Symbols and Units	235
9.6.3.2	Iteration Procedure	236
9.6.3.3	Results of Calculations with the Model	236
9.7	Rheological Design of the Mold	240
9.7.1	Sample Calculation	240
9.7.2	General Channel Shape	243
9.8	References	243
9.9	Appendix	245
	Index	247

1

Mechanical Properties of Solid Polymers

The properties of polymers are required to select a material that enables the desired performance of the plastics component under conditions of its application. Furthermore, properties are essential in design work to dimension a part from a stress analysis or to predict the performance of a part under different stress situations. Knowledge of polymer properties is, as already mentioned in the preface, a prerequisite for designing and optimizing polymer processing machinery.

In addition to the physical properties, there are certain properties known as performance or engineering properties that correlate with the performance of the polymer under varied type of loading and environmental influences like impact, fatigue, high and low temperature behavior, and chemical resistance. The following sections deal with the physical as well as with the important performance properties of polymers.

■ 1.1 Ideal Solids

Ideal elastic solids deform according to Hooke's law that states that the stress is directly proportional to the strain. The behavior of a polymer that is subjected to shear or tension can be described by comparing its reaction to an external force with that of an elastic solid under load. To characterize ideal solids, it is necessary to define certain quantities as follows [3].

■ 1.2 Tensile Properties

The axial force F_n in Fig. 1.1 causes an elongation Δl of the sample of diameter d_0 and length l_0 fixed at one end. The following equations apply for this case:

Engineering strain:

$$\varepsilon' = \frac{\Delta l}{l_0} \quad (1.1)$$

Hencky strain:

$$\varepsilon = \ln\left(\frac{l}{l_0}\right) \quad (1.2)$$

Tensile stress:

$$\sigma_z = \frac{F_n}{A_0} \quad (1.3)$$

Reference area:

$$A_0 = \frac{\pi d_0^2}{4} \quad (1.4)$$

Poisson's ratio:

$$\mu = -\frac{\Delta d / d_0}{\Delta l / l_0} \quad (1.5)$$

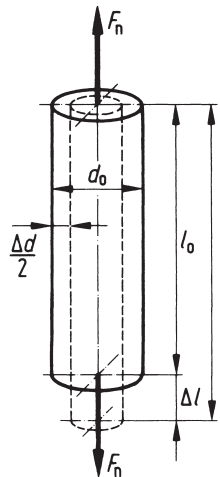


Figure 1.1 Deformation of a Hookean solid by a tensile stress [10]

1.2.1 Stress-Strain Behavior

As shown in Fig. 1.2, most metals exhibit a linear stress-strain relationship (curve 1), while polymers, being viscoelastic, show a nonlinear behavior (curve 2). When the stress is directly proportional to the strain, the material is said to obey Hooke's law. The slope of the straight line portion of curve 1 is equal to the modulus of elasticity. The maximum stress point on the curve, up to which stress and strain remain proportional, is called the proportional limit (point P in Fig. 1.2) [1].

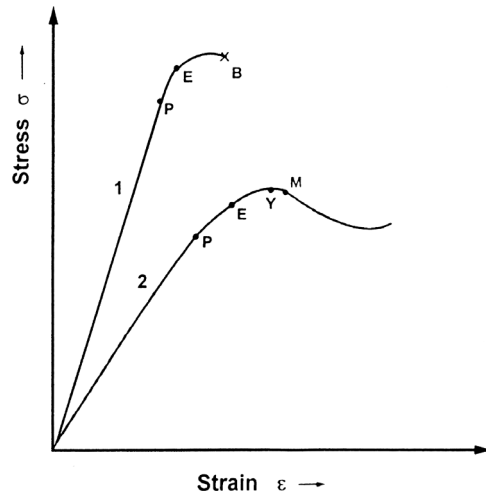


Figure 1.2 Typical stress-strain curves of metals and polymers

Most materials return to their original size and shape, even if the external load exceeds the proportional limit. The elastic limit, represented by the point E in Fig. 1.2, is the maximum load that may be applied without leaving any permanent deformation of the material. If the material is loaded beyond its elastic limit, it does not return to its original size and shape, and it is said to have been permanently deformed. On continued loading, a point is reached at which the material starts yielding. This point (point Y in Fig. 1.2) is known as the yield point, where an increase in strain occurs without an increase in stress. It should however be noted that some materials may not exhibit a yield point. The point B in Fig. 1.2 represents the break of the material.

Owing to their nonlinear nature, it is difficult to locate the straight line portion of the stress-strain curve for polymeric materials (Fig. 1.3). The secant modulus represents the ratio of stress to strain at any point (S in Fig. 1.3) on the stress-strain diagram and is equal to the slope of the line OS. It is an approximation to a linear response over a narrow, but prespecified and standard level of strain [2], which is usually 0.2%.

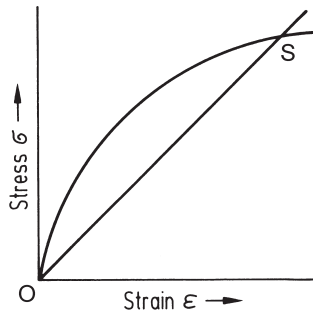


Figure 1.3 Secant modulus [3]

The initial modulus is a straight line drawn tangent to the initial region of the stress-strain curve to obtain a fictive modulus as shown in Fig. 1.4. As this is ambiguous, the resin manufacturers provide a modulus with the stress; for example, $\sigma_{0.5}$ corresponding to a strain of 0.5%, to characterize the material behavior on a practical basis (Fig. 1.4) [3]. This stress $\sigma_{0.5}$ is also known as the proof stress.

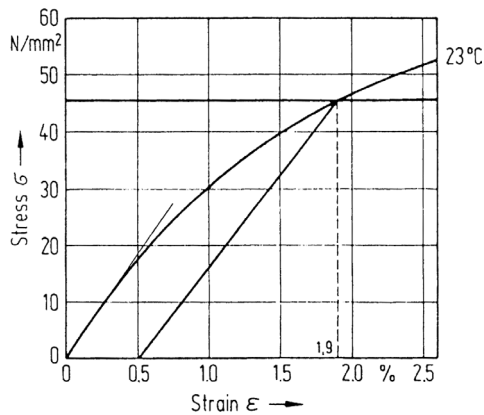


Figure 1.4 Stress at a strain of 0.5% [3]

Stress-strain diagrams are given in Fig. 1.5 for a number of materials [4]. It can be seen from Fig. 1.5 that the advantage of metals lies in their high strength, whereas that of plastics lies in their high elongation at break.

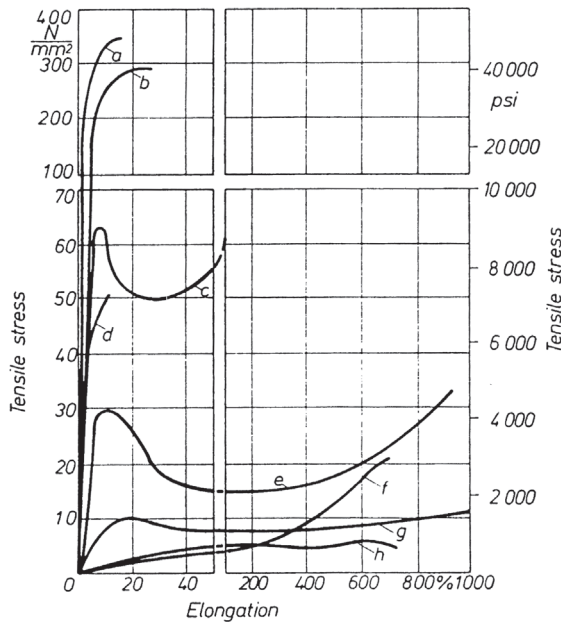


Figure 1.5 Tensile stress diagrams of materials at 23 °C [4];
a: steel, b: copper, c: polycarbonate, d: PMMA, e: PE-HD, f: rubber, g: PE-LD, h: PVC-P

1.2.2 Tensile Modulus

According to Eqs. 1.1 and 1.3, one obtains the modulus of elasticity E , which is known as Young's Modulus, by

$$E = \sigma_z / \varepsilon' \quad (1.6)$$

The modulus of elasticity in a tension test is given in Table 1.1 for different polymers [7].

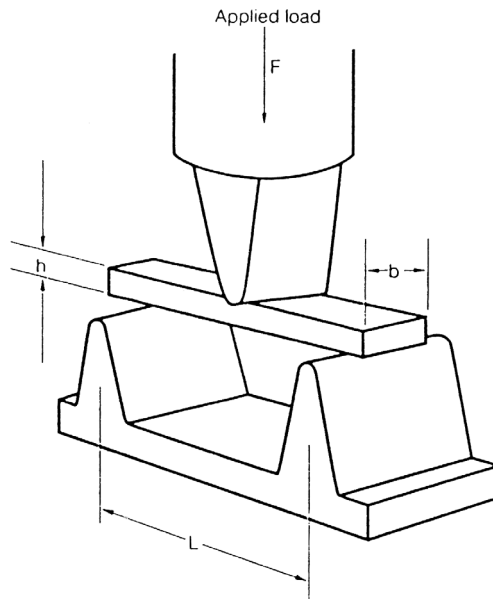
Table 1.1 Guide Values of Modulus of Elasticity of Various Plastics [4]

Material	Modulus of elasticity N mm^{-2}
PE-LD	200/ 500
PE-HD	700/1400
PP	1100/1300
PVC-U	1000/3500
PS	3200/3500
ABS	1900/2700
PC	2100/2500
POM	2800/3500

Table 1.1 Guide Values of Modulus of Elasticity of Various Plastics [4] (*Continued*)

Material	Modulus of elasticity N mm^{-2}
PA6	1200/1400
PA66	1500/2000
PMMA	2700/3200
PET	2600/3100
PBT	1600/2000
PSU	2600/2750
CA	1800/2200
CAB	1300/1600
Phenol-Formaldehyde Resins	5600/12000
Urea-Formaldehyde Resins	7000/10500
Melamin-Formaldehyde Resins	4900/9100
Unsaturated Polyester Resins	14000/20000

The 3.5% flexural stresses of thermoplastics obtained on a 3-point bending fixture (Fig. 1.6) [6] lie in the range from 100 to 150 N mm^{-2} and those of thermosets from around 60 to 150 N mm^{-2} [7].

**Figure 1.6** Three point bending fixture [6]

1.2.3 Effect of Temperature on Tensile Strength

The tensile strength is obtained by dividing the maximum load (point M in Fig. 1.2) the specimen under test will withstand by the original area of cross-section of the specimen. Figure 1.7 shows the temperature dependence of the tensile strength of some thermoplastics [4].

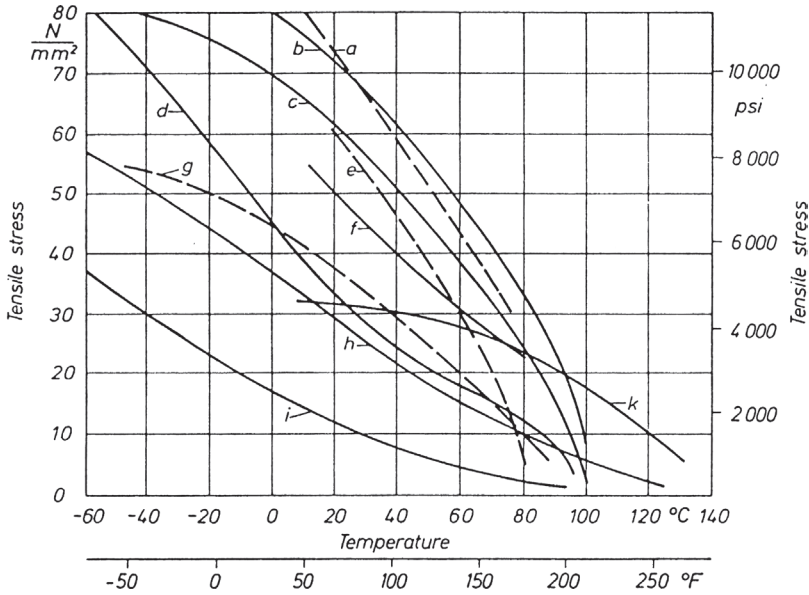


Figure 1.7 Temperature dependence of the tensile stress of some thermoplastics under uniaxial loading [4]; a: PMMA, b: SAN, c: PS, d: SB, e: PVC-U, f: ABS, g: CA, h: PE-HD, i: PE-LD, k: PE-LD-V

■ 1.3 Shear Properties

Figure 1.8 shows the influence of a shear force F_t acting on the area A of a rectangular sample and causing the displacement ΔU . The valid expressions are defined by:

Shear strain:

$$\gamma = \frac{\Delta U}{l} \quad (1.7)$$

Shear stress:

$$\tau = \frac{F_t}{A} \quad (1.8)$$

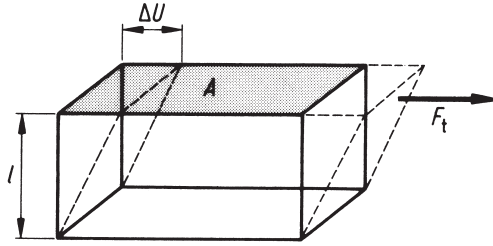


Figure 1.8 Deformation of a Hookean solid by shearing stress [10]

1.3.1 Shear Modulus

The ratio of shear stress to shear strain represents the shear modulus G . From the Eqs. 1.7 and 1.8 results:

$$G = \tau / \gamma \quad (1.9)$$

1.3.2 Effect of Temperature on Shear Modulus

The viscoelastic properties of polymers over a wide range of temperatures can be better characterized by the complex shear modulus G^* , which is measured in a torsion pendulum test by subjecting the specimen to an oscillatory deformation; see Fig. 1.9 [2]. The complex shear modulus G^* is given by the expression [2]

$$|G^*| = [(G')^2 + (G'')^2]^{0.5} \quad (1.10)$$

The storage modulus G' in Eq. 1.10 represents the elastic behavior associated with energy storage, and it is a function of shear amplitude, strain amplitude, and the phase angle δ between stress and strain. The loss modulus G'' , which is a component of the complex modulus, depicts the viscous behavior of the material and arises due to viscous dissipation.

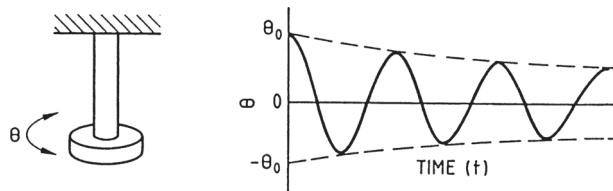


Figure 1.9 Torsion pendulum; loading mode and sinusoidal angular displacement t [2]

The tangent of the phase angle δ is often used to characterize viscoelastic behavior, and is known as loss factor. The loss factor d can be obtained from

$$d = \frac{G''}{G'} = \tan \delta \quad (1.11)$$

The modulus-temperature relationship is represented schematically in Fig. 1.10 [2], from which the influence of the transition regions described by the glass transition temperature T_g and melting point T_m is evident.

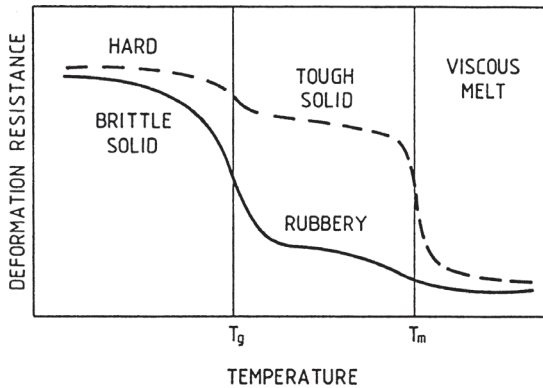


Figure 1.10 Generalized relationship between deformation resistance and temperature for amorphous (solid line) and semi-crystalline (broken line) high polymers [2]

This kind of data provides information on the molecular structure of the polymer. The storage modulus G' , which is a component of the complex shear modulus G^* , and the loss factor d are plotted as functions of temperature for high density polyethylene in Fig. 1.11 [4]. These data for various polymers are given in the reference [4].

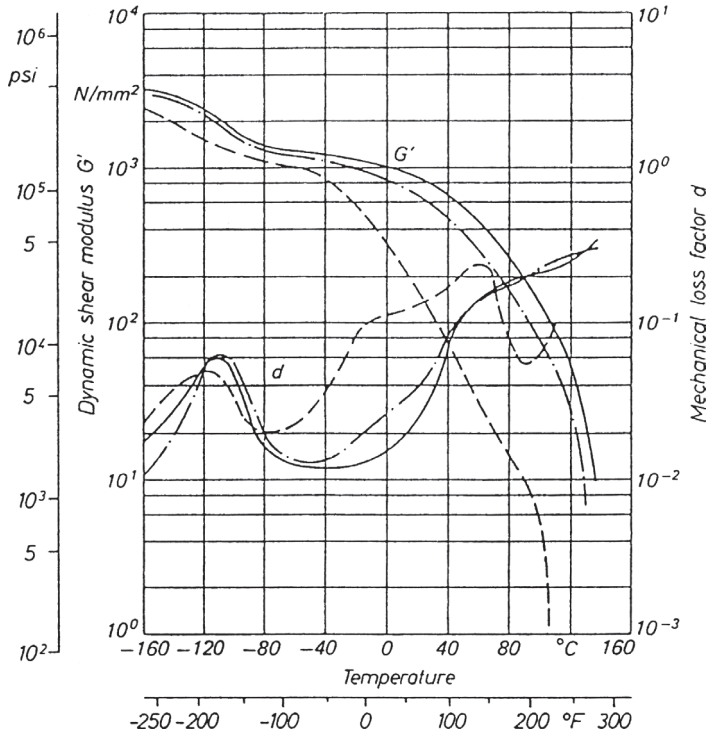


Figure 1.11 Temperature dependence of the dynamic shear modulus G' and the loss factor d obtained in the torsion pendulum test DIN 53445 [4]: PE-HD (highly crystalline; solid line), PE-HD (crystalline; broken line), PE-LD (less crystalline; dashed line)

■ 1.4 Compressive Properties

The isotropic compression due to the pressure acting on all sides of the parallelepiped, shown in Fig. 1.12, is given by the engineering compression ratio κ .

$$\kappa = \frac{\Delta V}{V_0} \quad (1.12)$$

where ΔV is the reduction of volume due to deformation of the body with the original volume V_0 .

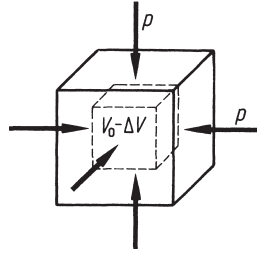


Figure 1.12 Hookean solid under compression [44]

1.4.1 Bulk Modulus

The bulk modulus K is defined by

$$K = -p/\kappa \quad (1.13)$$

Where κ is calculated from Eq. 1.12. The reduction of volume, for instance for PE-LD, when the pressure is increased by 100 bar, follows from Table 1.2

$$\Delta V / V_0 = -100 / (0.7 \cdot 10^4) = -1.43\%$$

Furthermore, the relationship between E , G , and K is expressed as [3]

$$E = 2G(1 + \mu) = 3K(1 - 2\mu) \quad (1.14)$$

This leads for an incompressible solid ($K \rightarrow \infty$, $\mu \rightarrow 0.5$) to

$$E = 3G \quad (1.15)$$

Typical values of moduli and Poisson's ratios for some materials are given in Table 1.2 [10]. Although the moduli of polymers compared with those of metals are very low, at equal weights, i.e., the ratio of modulus to density, polymers compare favorably.

Table 1.2 Poisson Ratio, μ , Density, ρ , Bulk Modulus, K , and Specific Bulk Modulus, K/ρ , for Various Materials [10]

Material	Poisson ratio μ	Density ρ at 20 °C g/cm ³	Bulk modulus K N/m ²	Specific bulk modulus K/ ρ m ² /s ²
Mild steel	0.27	7.8	$1.66 \cdot 10^{11}$	$2.1 \cdot 10^7$
Aluminum	0.33	2.7	$7 \cdot 10^{10}$	$2.6 \cdot 10^7$
Copper	0.25	8.9	$1.34 \cdot 10^{11}$	$1.5 \cdot 10^7$
Quartz	0.07	2.65	$3.9 \cdot 10^{10}$	$1.47 \cdot 10^7$
Glass	0.23	2.5	$3.7 \cdot 10^{10}$	$1.49 \cdot 10^7$
Polystyrene	0.33	1.05	$3 \cdot 10^9$	$2.85 \cdot 10^7$

Table 1.2 Poisson Ratio, μ , Density, ρ , Bulk Modulus, K , and Specific Bulk Modulus, K/ρ , for Various Materials [10] (Continued)

Material	Poisson ratio μ	Density ρ at 20 °C g/cm ³	Bulk modulus K N/m ²	Specific bulk modulus K/ρ m ² /s ²
Polymethyl-methacrylate	0.33	1.17	$4.1 \cdot 10^9$	$3.5 \cdot 10^7$
Polyamide 66	0.33	1.08	$3.3 \cdot 10^9$	$2.3 \cdot 10^7$
Rubber	0.49	0.91	$0.033 \cdot 10^9$	$0.04 \cdot 10^7$
PE-LD	0.45	0.92	$0.7 \cdot 10^9$	$3.7 \cdot 10^7$
Water	0.5	1	$2 \cdot 10^9$	$2 \cdot 10^6$
Organic liquids	0.5	0.9	$1.33 \cdot 10^9$	$1.5 \cdot 10^6$

■ 1.5 Time Related Properties

1.5.1 Creep Modulus

In addition to stress and temperature, time is an important factor for characterizing the performance of plastics. Under the action of a constant load, a polymeric material experiences a time dependent increase in strain called creep. Creep is therefore the result of increasing strain over time under constant load [6]. Creep behavior can be examined by subjecting the material to tensile, compressive, or flexural stress and measuring the strain for a range of loads at a given temperature.

The creep modulus $E_c(t)$ in tension can be calculated from

$$E_c(t) = \tau / \varepsilon(t) \quad (1.16)$$

and is independent of stress only in the linear elastic region.

As shown in Fig. 1.13, the creep data can be represented by creep plots, from which the creep modulus, according to Eq. 1.16, can be obtained. The time dependence of tensile creep modulus of some thermoplastics at 20 °C is shown in Fig. 1.14 [5]. The 2% elasticity limits of some thermoplastics under uniaxial stress are given in Fig. 1.15. Creep data measured under various conditions for different polymers are available in [4].

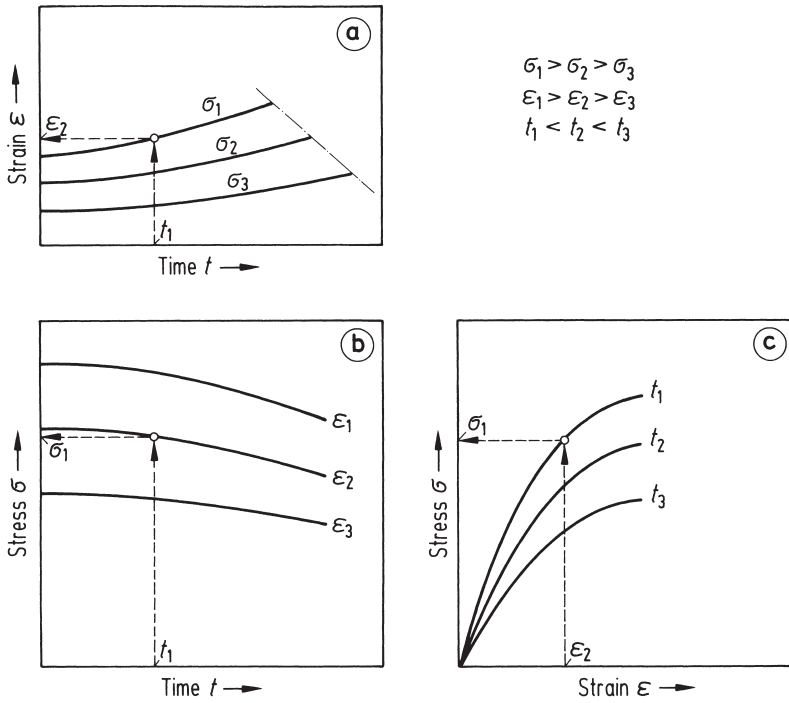


Figure 1.13 Long-term stress-strain behavior [3]

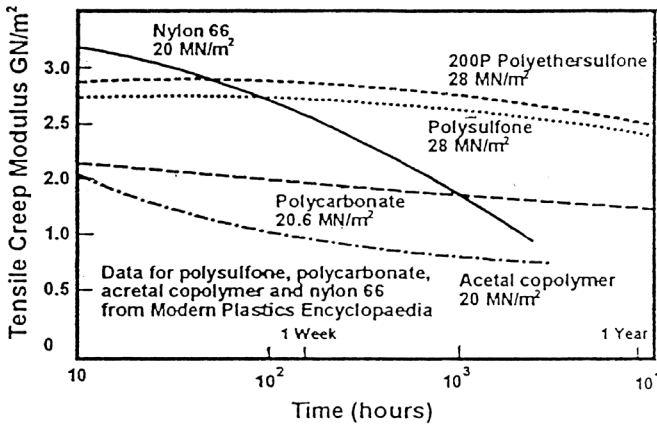


Figure 1.14 Tensile creep modulus vs. time for engineering thermoplastics [5]

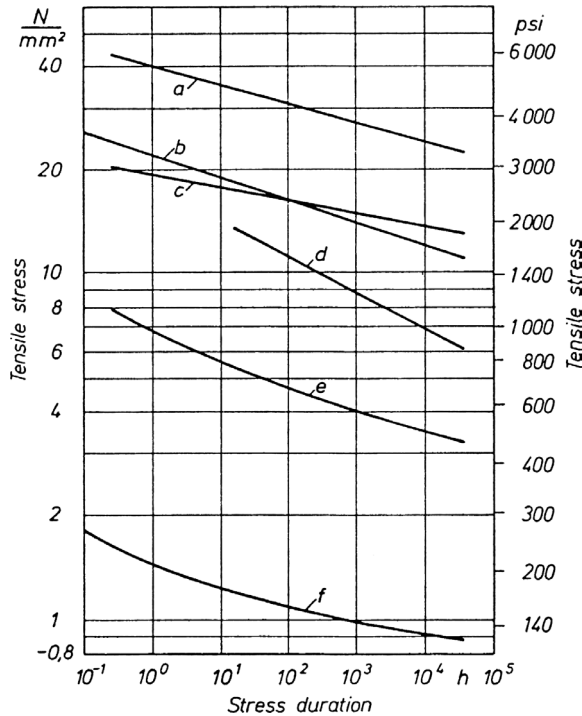


Figure 1.15 2% elasticity limits of some thermoplastics under uniaxial stress at 20 °C [4]; a: SAN, b: ABS, c: SB, d: chlorinated polyether, e: PE-HD, f: PE-LD

1.5.2 Creep Rupture

Failure with creep can occur when a component exceeds an allowable deformation or when it fractures or ruptures [6]. Creep rupture curves are obtained in the same manner as creep, except that the magnitude of the stresses used is higher and the time is measured up to failure. Data on creep rupture for a number of polymers are presented in [4]. According to [4], the extrapolation of creep data should not exceed one unit of logarithmic time and a strain elongation limit of 20% of the ultimate strength.

1.5.3 Relaxation Modulus

The relaxation behavior of a polymer is shown in Fig. 1.16 [3]. Relaxation is the stress reduction that occurs in a polymer when it is subjected to a constant strain. This data is of significance in the design of parts that are to undergo long-term deformation. The relaxation modulus of PE-HD-HMW, as a function of stress duration, is given in Fig. 1.17 [4]. Similar plots for different materials are to be found in [4].

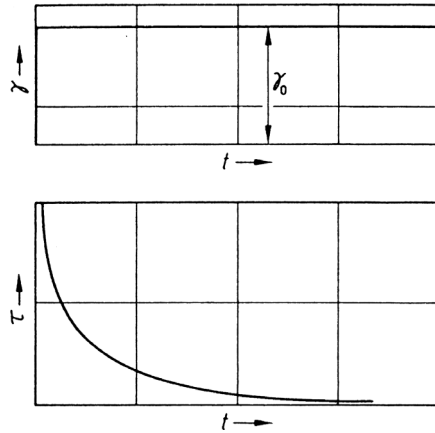


Figure 1.16 Relaxation after step shear strain γ_0 [3]

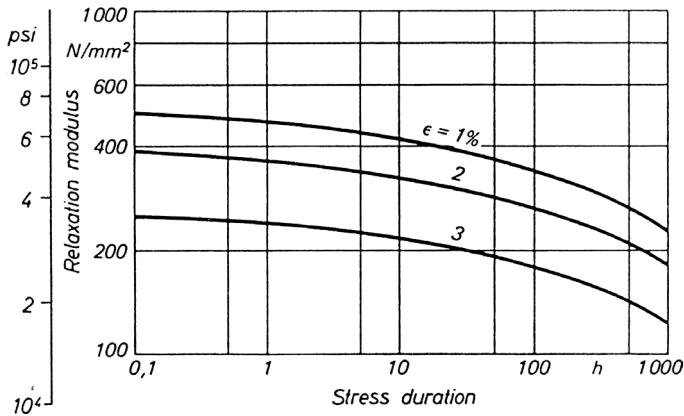


Figure 1.17 Relaxation modulus of PE-HD-HMW as a function of stress duration at 23 °C [4]

1.5.4 Fatigue Limit

Fatigue is a failure mechanism that results when the material is stressed repeatedly or when it is subjected to a cyclic load. Examples of fatigue situations are components subjected to vibration or repeated impacts. Cyclic loading can cause mechanical deterioration and fracture propagation resulting in ultimate failure of the material.

Fatigue is usually measured under conditions of bending where the specimen is subjected to constant deflection at constant frequency until failure occurs. The asymptotic value of stress shown in the schematic fatigue curve (S-N plot) in Figs. 1.18 and 1.19 [6] is known as the fatigue limit. At stresses or strains that are less than this value, failure does not occur normally.

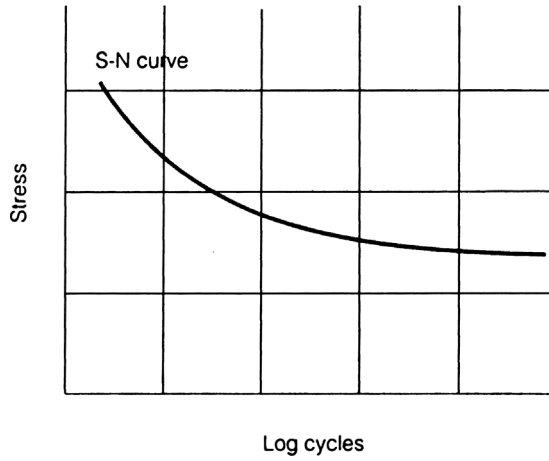


Figure 1.18 Fatigue curve [6]

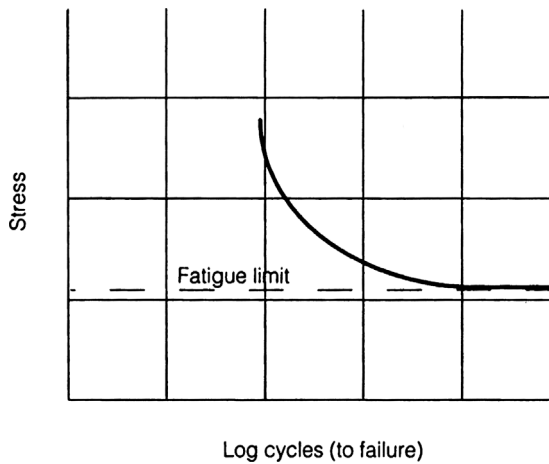


Figure 1.19 Fatigue limit [6]

Some materials do not exhibit an asymptotic fatigue limit. In these cases, the endurance limit that gives stress or strain at failure at a certain number of cycles is used (Fig. 1.20) [6].

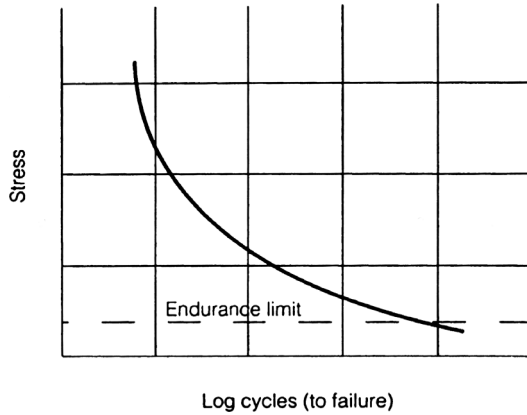


Figure 1.20 Endurance limit [6]

For most plastics, the fatigue limit is about 20 to 30% of the ultimate strength measured in short-term tensile investigations [6]. Woehler plots for the oscillating flexural stress of some thermoplastics are given in Fig. 1.21. Fatigue limits decrease with increasing temperature, increasing frequency, and stress concentrations in the part [4].

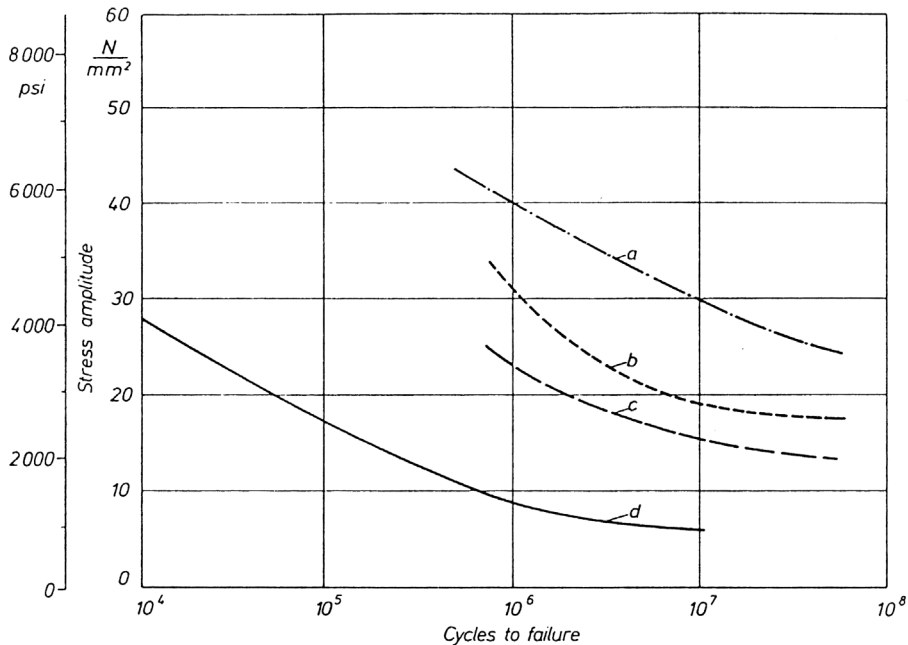


Figure 1.21 Flexural fatigue strength of some thermoplastics [4];
a: acetal polymer, b: PP, c: PE-HD, d: PVC-U

■ 1.6 Hardness

Various methods of measuring the hardness of plastics are in use. Their common feature is measuring the deformation in terms of the depth of penetration, which follows indentation by a hemisphere, cone, or pyramid depending on the test procedure under defined load conditions. According to the type of indenter (Fig. 1.22) used, the Shore hardness, for example, is given as Shore A or Shore D: Shore A data referring to soft plastics and Shore D referring to hard plastics. The results of both methods are expressed on a scale between 0 (very soft plastics) and 100 (very hard surface).

The ball-indentation hardness that represents the indentation depth of a spherical steel indenter is given in Table 1.3 for some thermoplastics [2].

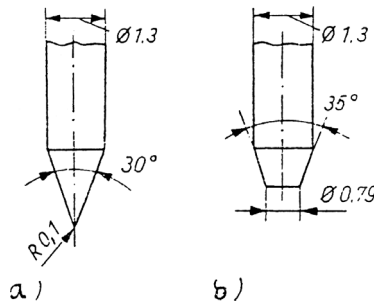


Figure 1.22 Types of indenter [7]; a: Shore, b: Shore C and A

Table 1.3 Ball-Indentation Hardness for Some Plastics [7]

Material	Hardness N/mm ²
PE-LD	13/20
PE-HD	40/65
PP	36/70
PVC-U	75/155
PS	120/130
ABS	80/120
PC	90/110
POM	150/170
PA6	70/75
PA66	90/100
PMMA	180/200
PET	180/200
PBT	150/180

Material	Hardness N/mm ²
Phenol-Formaldehyde Resins	250/320
Urea-Formaldehyde Resins	260/350
Melamin-Formaldehyde Resins	260/410
Unsaturated Polyester Resins	200/240

■ 1.7 Impact Strength

Impact strength is the ability of the material to withstand a sudden impact blow as in a pendulum test, and indicates the toughness of the material at high rates of deformation. The test procedures are varied. In the Charpy impact test (Fig. 1.23) [2], the pendulum strikes the specimen centrally leading to fracture.

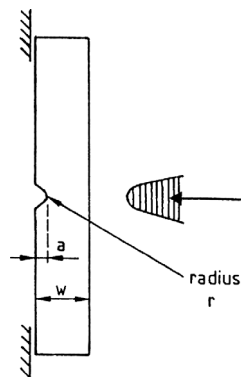


Figure 1.23 Charpy impact test [2]

■ 1.8 Coefficient of Friction

Although there is no consistent relationship between friction and wear, the factors affecting the two processes, such as roughness of the surfaces, relative velocities of the parts in contact, and area under pressure, are often the same. Table 1.4 shows the coefficients of sliding friction and sliding wear against steel for different materials [4]. In applications where low friction and high wear resistance are required, a smooth surface and a low coefficient of friction of the resin components involved are to be recommended.

Table 1.4 Coefficient of Sliding Friction of Polymer/Case Hardened Steel after 5 or 24 Hours [4]

Polymer	Coefficient of sliding friction	Sliding frictional wear
Polyamide 66	0.25/0.42	0.09
Polyamide 6	0.38/0.45	0.23
Polyamide 6 (in situ polymer)	0.36/0.43	0.10
Polyamide 6 10	0.36/0.44	0.32
Polyamide 11	0.32/0.38	0.8
Polyethyleneterephthalate	0.54	0.5
Acetal homopolymer	0.34	4.5
Acetal copolymer	0.32	8.9
Polypropylene	0.30	11.0
PE-HD (high molecular weight)	0.29	1.0
PE-HD (low molecular weight)	0.25	4.6
PE-LD	0.58	7.4
Polytetrafluoroethylene	0.22	21.0
PA 66 + 8% PE-LD	0.19	0.10
Polyacetal + PTFE	0.21	0.16
PA 66 + 3% MoS ₂	0.32/0.35	0.7
PA 66 – GF 35	0.32/0.36	0.16
PA 6 – GF 35	0.30/0.35	0.28
Standard polystyrene	0.46	11.5
Styrene/Acrylonitrile copolymer	0.52	23
Polymethylmethacrylate	0.54	4.8
Polyphenylene ether	0.35	90

A typical impact curve as a function of temperature is shown in Fig. 1.24 [6]. This type of data provides the designer with information about the temperature at which the ductile fracture changes to brittle fracture, thus enabling the ability to evaluate the performance of the material in a given application. The results of impact tests depend on the manufacturing conditions of the specimen, notch geometry, and on the test method. Impact strengths for various plastics are given by Domininghaus [4]. Charpy notched impact strengths of some plastics as functions of notch radius are given in Fig. 1.25 [5].

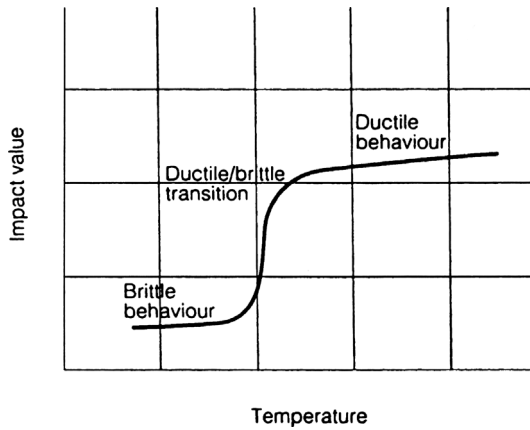


Figure 1.24 Impact curve [6]

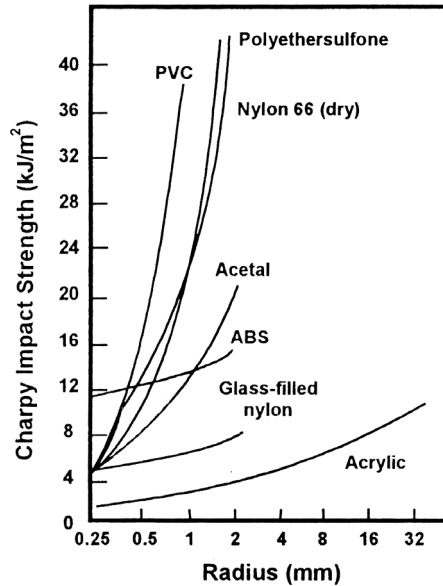


Figure 1.25 Charpy impact strength vs. notch radius for some engineering thermoplastics [5]

Example [8]:

The minimum depth of the simple beam of SAN shown in Fig. 1.26 is to be determined for the following conditions:

The beam should support a midspan load of 11.13 N for 5 years without fracture and without causing a deflection greater than 2.54 mm.

Solution:

The maximum stress is given by

$$\sigma_{\max} = \frac{1.5 F \cdot l}{b \cdot d^2} \quad (1.17)$$

where F = load (N)

l, b, d = dimensions (in mm) as shown in Fig. 1.26.

The creep modulus E_c is calculated from

$$E_c = \frac{F \cdot l^3}{4 \cdot f \cdot b \cdot d^3} \quad (1.18)$$

where f is deflection in mm.

The maximum stress from Fig. 1.27 at a period of 5 years (= 43,800 h) is

$$\sigma_{\max} = 23.44 \text{ N/mm}^2$$

Working stress σ_w with an assumed safety factor $S = 0.5$,

$$\sigma_w = 23.44 \cdot 0.5 = 11.72 \text{ N/mm}^2$$

Creep modulus E_c at $\sigma < \sigma_w$ and a period of five years from Fig. 1.27:

$$E_c = 2413 \text{ N/mm}^2$$

Creep modulus with a safety factor $S = 0.75$:

$$E_c = 2413 \cdot 0.75 = 1809.75 \text{ N/mm}^2$$

The depth of the beam results from Eq. 1.17

$$d = \left(\frac{1.5 \cdot F \cdot l}{b \cdot \sigma_w} \right)^{0.5} = \left(\frac{1.5 \cdot 11.13 \cdot 76.2}{12.7 \cdot 11.72} \right)^{0.5} = 2.92 \text{ mm}$$

The deflection is calculated from Eq. 1.18

$$f = \frac{F \cdot l^3}{4 \cdot E_c \cdot b \cdot d^3} = \frac{11.13 \cdot 76.2^3}{4 \cdot 1809.75 \cdot 12.7 \cdot 2.92^3} = 2.15 \text{ mm}$$

Under these assumptions the calculated f is less than the allowable value of 2.54 mm.

This example shows why creep data are required in design calculations and how they can be applied to solve design problems.

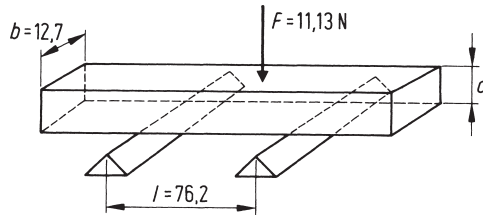


Figure 1.26 Beam under midspan load [8]

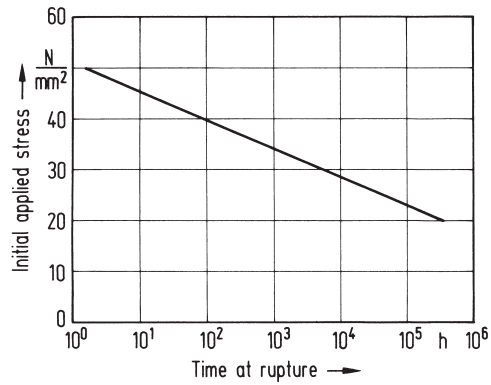


Figure 1.27 Creep curve of SAN [8]

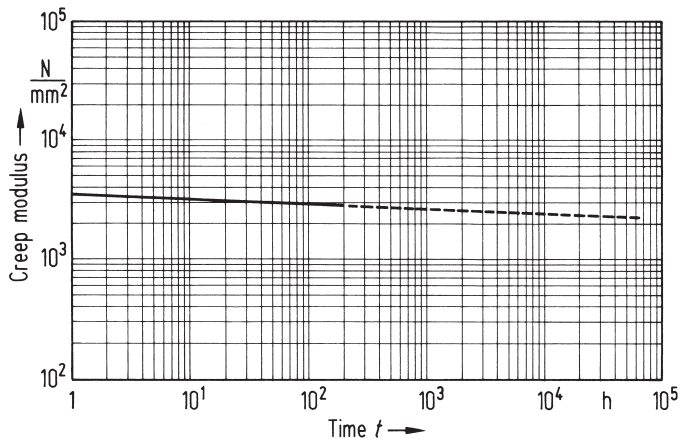


Figure 1.28 Creep modulus of SAN [8]

■ 1.9 References

- [1] *Nat, D.S.*: A Text Book of Materials and Metallurgy, Katson Publishing House, Ludhiana, India, 1980
- [2] *Birley, A. W., Haworth, B., Bachelor, T.*: Physics of Plastics, Hanser, Munich, 1991
- [3] *Rao, N.S.*: Design Formulas for Plastics Engineers, Hanser, Munich, 1991
- [4] *Domininghaus, H.*: Plastics for Engineers, Hanser, Munich, 1993
- [5] *Rigby, R.B.*: Polyethersulfone in Engineering Thermoplastics: Properties and Applications, Ed. James M. Margolis, Marcel Dekker, Basel, 1985
- [6] General Electric Plastics Brochure: Engineering Materials Design Guide
- [7] *Schmiedel, H.*: Handbuch der Kunststoffprüfung, Hanser, Munich, 1992
- [8] Design Guide, Modern Plastics Encyclopedia, 1978–79
- [9] Brochure: Advanced CAE Technology Inc., 1992
- [10] *Pahl, M., Gleißle, W., Laun, H.M.*: Praktische Rheologie der Kunststoffe und Elastomere, VDI-Kunststofftechnik, Düsseldorf, 1995

2

Thermal Properties of Solid and Molten Polymers

In addition to the mechanical and melt flow properties, thermodynamic data of polymers are necessary for optimizing various heating and cooling processes which occur in plastics processing operations.

In design work, the thermal properties are often required as functions of temperature and pressure [2]. As the measured data cannot always be predicted by physical relationships accurately enough, regression equations are used to fit the data for use in design calculations.

■ 2.1 Specific Volume

The volume-temperature relationship as a function of pressure is shown for a semicrystalline PP in Fig. 2.1 [1], and for an amorphous PS in Fig. 2.2 [1]. The p - v - T diagrams are needed in many applications; for example, to estimate the shrinkage of plastics parts in injection molding [19]. Data on p - v - T relationships for a number of polymers are presented in the VDMA-handbook [8].

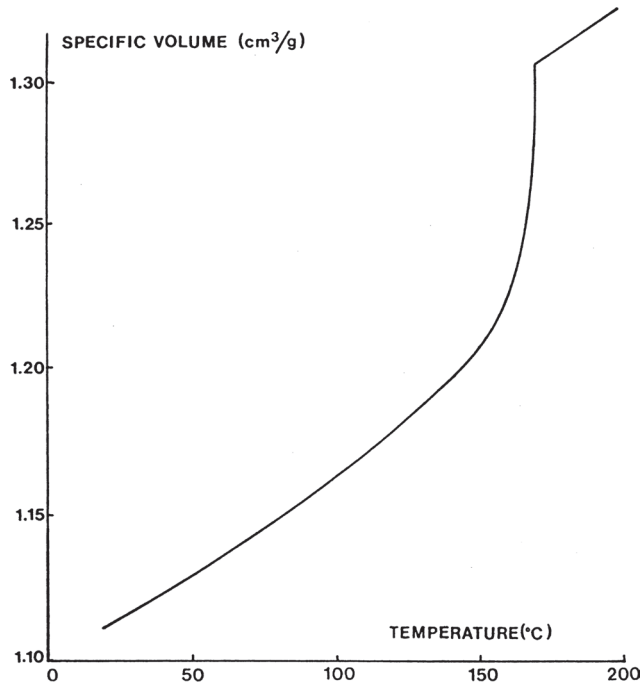


Figure 2.1 Specific volume vs. temperature for a semicrystalline polymer (PP) [1]

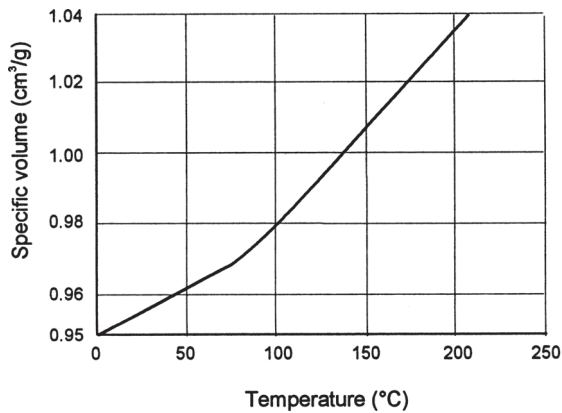


Figure 2.2 Specific volume vs. temperature for an amorphous polymer (PS) [1]

According to the Spencer-Gilmore equation, which is similar to the van der Waals equation of state for real gases, the relationship between pressure p , specific volume v , and temperature T of a polymer can be written as

$$(v - b^*)(p + p^*) = \frac{RT}{W} \quad (2.1)$$

In this equation b^* is the specific individual volume of the macromolecule, p^* the cohesion pressure, W the molecular weight of the monomer, and R the universal gas constant [9].

The values p^* and b^* can be determined from p - v - T diagrams by means of regression analysis. Spencer and Gilmore and other workers evaluated these constants from measurements for the polymers listed in Table 2.1 [9, 18].

Table 2.1 Constants for the Equation of State [9]

Material	W g/mol	p^* atm	b^* cm ³ /g
PE-LD	28.1	3240	0.875
PP	41.0	1600	0.620
PS	104	1840	0.822
PC	56.1	3135	0.669
PA 610	111	10768	0.9064
PMMA	100	1840	0.822
PET	37.0	4275	0.574
PBT	113.2	2239	0.712

Example:

Following values are given for a PE-LD:

$$W = 28.1 \text{ g/mol}$$

$$b^* = 0.875 \text{ cm}^3/\text{g}$$

$$p^* = 3240 \text{ atm}$$

Calculate the specific volume at $T = 190 \text{ }^\circ\text{C}$ and $p = 1 \text{ bar}$

Solution:

Using Eq. 2.1 and the conversion factors to obtain the volume v in cm³/g, we obtain

$$v = \frac{10 \cdot 8.314 \cdot (273 + 190)}{28.1 \cdot 3240 \cdot 99 \cdot 1.013} + 0.875 = 1.292 \text{ cm}^3/\text{g}$$

The density ρ is the reciprocal value of specific volume so that

$$\rho = \frac{1}{v}$$

The p - v - T data can also be fitted by a polynomial of the form

$$v = A(0)_v + A(1)_v \cdot p + A(2)_v \cdot T + A(3)_v \cdot T \cdot p \quad (2.2)$$

if measured data is available (Fig. 2.3) [10, 11, 17]. The empirical coefficients $A(0)_v \dots A(3)_v$ can be determined by means of the computer program given in [11]. With the modified two-domain Tait equation [16], a very accurate fit can be obtained both for the solid and melt regions.

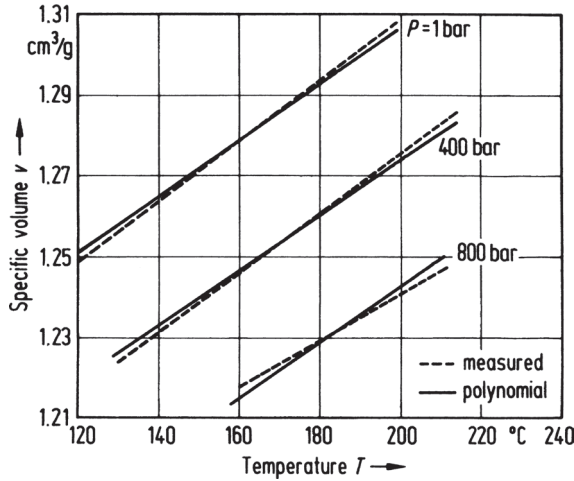


Figure 2.3 Specific volume as a function of temperature and pressure for PE-LD [2, 13]

■ 2.2 Specific Heat

The specific heat c_p is defined as

$$c_p = \left(\frac{\partial h}{\partial T} \right)_p \quad (2.3)$$

where h = enthalpy
 T = Temperature

The specific heat c_p gives the amount of heat that is supplied to a system in a reversible process at a constant pressure in order to increase the temperature of the substance by ∂T . The specific heat at constant volume c_v is given by

$$c_v = \left(\frac{\partial u}{\partial T} \right)_v \quad (2.4)$$

where u = internal energy
 T = Temperature

In the case of c_v the supply of heat to the system occurs at constant volume.

c_p and c_v are related to each other through the Spencer-Gilmore equation, Eq. 2.1:

$$c_v = c_p - \frac{R}{W} \quad (2.5)$$

The numerical values of c_p and c_v differ by roughly 10%, so that for approximate calculations c_v can be made equal to c_p .

Plots of c_p as function of temperature are shown in Fig. 2.4 for amorphous, semi-crystalline, and crystalline polymers.

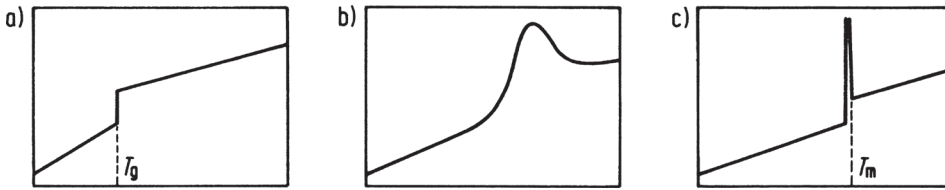


Figure 2.4 Specific heat as a function of temperature for: amorphous (a), semicrystalline (b), and crystalline polymers (c) [14]

As shown in Fig. 2.5, measured values can be fitted by a polynomial of the type [11]:

$$c_p(T) = A(0)c_p + A(1)c_p \cdot T + A(2)c_p \cdot T^2 \quad (2.6)$$

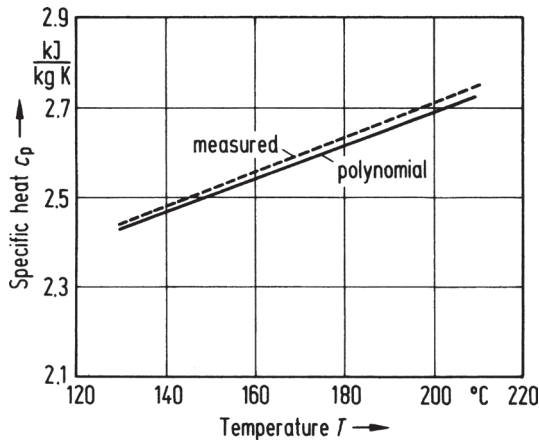


Figure 2.5 Comparison between measured values of c_p [13] and polynomial for PE-LD [2]

■ 2.3 Thermal Expansion Coefficient

The expansion coefficient α_v at constant pressure is given by [14]

$$\alpha_v = \frac{1}{v} \left(\frac{\partial v}{\partial T} \right)_p \quad (2.7)$$

The isothermal compression coefficient γ_k is defined as [14]

$$\gamma_k = -\frac{1}{v} \left(\frac{\partial v}{\partial p} \right)_T \quad (2.8)$$

Further, α_v and γ_k are related to each other by the expression [14]

$$c_p = c_v + \frac{T \cdot v \cdot \alpha_v^2}{\gamma_k} \quad (2.9)$$

The linear expansion coefficient α_{lin} is approximately

$$\alpha_{lin} = \frac{1}{3} \alpha_v \quad (2.10)$$

Table 2.2 shows the linear expansion coefficients of some polymers at 20 °C. The linear expansion coefficient of mild steel lies around $11 \times 10^{-6} \text{ K}^{-1}$, and that of aluminum is about $25 \times 10^{-6} \text{ K}^{-1}$. As can be seen from Table 2.2, plastics expand about 3 to 20 times more than metals. Factors affecting thermal expansion are crystallinity, cross-linking, and fillers [1].

Table 2.2 Coefficients of Linear Thermal Expansion [1, 5]

Polymer	Coefficient of linear expansion at 20 °C α_{lin} 10^{-6} K^{-1}
PE-LD	250
PE-HD	200
PP	150
PVC-U	75
PVC-P	180
PS	70
ABS	90
PMMA	70
POM	100
PSU	50
PC	65

Polymer	Coefficient of linear expansion at 20 °C α_{lin} $10^{-6} K^{-1}$
PET	65
PBT	70
PA 6	80
PA 66	80
PTFE	100
TPU	150

■ 2.4 Enthalpy

Equation 2.3 leads to

$$dh = c_p \cdot dT \quad (2.11)$$

As shown in Fig. 2.6, the measured data on $h = h(T)$ [13] for a polymer melt can be fitted by the polynomial

$$h(T) = A(0)_h + A(1)_h \cdot T + A(2)_h \cdot T^2 \quad (2.12)$$

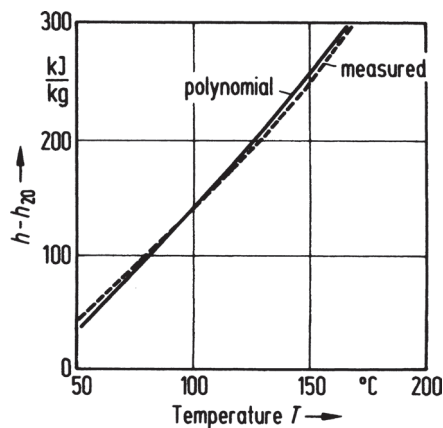


Figure 2.6 Comparison between measured values of h [13] and polynomial for PA 6 [11]

The specific enthalpy, defined as the total energy supplied to the polymer divided by the throughput of the polymer, is a useful parameter for designing extrusion and injection molding equipment, such as screws. It gives the theoretical amount of energy required to bring the solid polymer to the process temperature. Values of this parameter for different polymers are given in Fig. 2.7 [14].

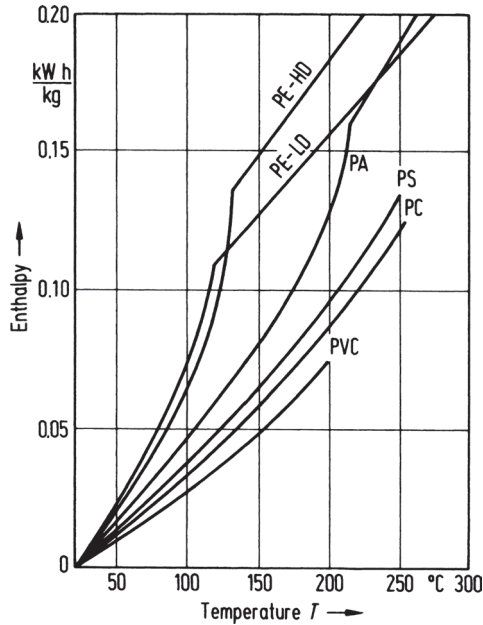


Figure 2.7 Specific enthalpy as a function of temperature [14]

If, for example, the throughput of an extruder is 100 kg/h of polyamide (PA) and the processing temperature is 260 °C, the theoretical power requirement would be 20 kW. This can be assumed to be a safe design value for the motor horse power, although theoretically it includes the power supply to the polymer by the heater bands of the extruder as well.

■ 2.5 Thermal Conductivity

The thermal conductivity λ is defined as

$$\lambda = \frac{Q \cdot l}{t \cdot A \cdot (T_1 - T_2)} \quad (2.13)$$

where Q = heat flow through the surface of area A in a period of time t
 $(T_1 - T_2)$ = temperature difference over the length l .

Analogous to the specific heat c_p and enthalpy h , the thermal conductivity λ , as shown in Fig. 2.8, can be expressed as [2]

$$\lambda(T) = A(0)_\lambda + A(1)_\lambda \cdot T + A(2)_\lambda \cdot T^2 \quad (2.14)$$

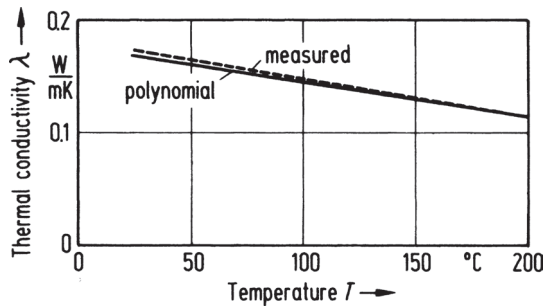


Figure 2.8 Comparison between measured values of λ [13] and polynomial for PP [2]

The thermal conductivity increases only slightly with the pressure. A pressure increase from 1 bar to 250 bar leads to an increase of less than 5% of its value at 1 bar.

As in the case of other thermal properties, the thermal conductivity is, in addition to its dependence on temperature, strongly influenced by crystallinity and orientation and by the amount and type of filler in the polymer [1]. Foamed plastics have, for example, thermal conductivities at least an order of magnitude less than those of solid polymers [1].

■ 2.6 Thermal Diffusivity

Thermal diffusivity a is defined as the ratio of thermal conductivity to the heat capacity per unit volume [1]

$$a = \frac{\lambda}{\rho \cdot c_p} \quad (2.15)$$

and is of importance in dealing with transient heat transfer phenomena, such as the cooling of melt in an injection mold [2]. Although for approximate calculations, average values of thermal diffusivity can be used, more accurate computations require functions of λ , ρ , and c_p against temperature for the solid as well as melt regions of the polymer. Thermal diffusivities of some polymers at 20 °C are listed in Table 2.3 [14, 15].

Table 2.3 Thermal Diffusivities of Polymers at 20 °C

Polymer	Thermal diffusivity at 20 °C a $10^6 \text{ m}^2/\text{s}$
PE-LD	0.12
PE-HD	0.22
PP	0.14
PVC-U	0.12
PVC-P	0.14
PS	0.12
PMMA	0.12
POM	0.16
ABS	0.15
PC	0.13
PBT	0.12
PA 6	0.14
PA 66	0.12
PET	0.11

Exhaustive measured data of the quantities c_p , h , λ , and p - v - T diagrams of polymers are given in the VDMA-Handbook [8]. Approximate values of thermal properties of use to plastics engineers are summarized in Table 2.4 [14, 15].

Experimental techniques of measuring enthalpy, specific heat, melting point, and glass transition temperature by differential thermal analysis (DTA), such as differential scanning calorimetry (DSC), are described in detail in the brochure [12]. Methods of determining thermal conductivity, p - v - T values, and other thermal properties of plastics have been treated in this brochure [12].

Table 2.4 Approximate Values for Thermal Properties of Some Polymers [14]

Polymer	Thermal conductivity (20 °C) λ W/m·K	Specific heat (20 °C) c_p kJ/kg K	Density (20 °C) ρ g/cm ³	Glass transition temperature T_g °C	Melting point range T_m °C
PS	0.12	1.20	1.06	101	-
PVC	0.16	1.10	1.40	80	-
PMMA	0.20	1.45	1.18	105	-
SAN	0.12	1.40	1.08	115	-
POM	0.25	1.46	1.42	-73	About 175
ABS	0.15	1.40	1.02	115	-
PC	0.23	1.17	1.20	150	-
PE-LD	0.32	2.30	0.92	-120/-90	About 110
PE-LLD	0.40	2.30	0.92	-120/-90	About 125

Polymer	Thermal conductivity (20 °C) λ W/m·K	Specific heat (20 °C) c_p kJ/kg K	Density (20 °C) ρ g/cm ³	Glass transition temperature T_g °C	Melting point range T_m °C
PE-HD	0.49	2.25	0.95	-120/0	About 130
PP	0.15	2.40	0.91	-10	160/170
PA6	0.36	1.70	1.13	50	215/225
PA 66	0.37	1.80	1.14	55	250/260
PET	0.29	1.55	1.35	70	250/260
PBT	0.21	1.25	1.35	45	About 220

■ 2.7 Coefficient of Heat Penetration

The coefficient of heat penetration is used in calculating the contact temperature, which results when two bodies of different temperature are brought into contact with each other [2, 16].

As shown in Table 2.5, the coefficients of heat penetration of metals are much higher than those of polymer melts. Owing to this, the contact temperature of the wall of an injection mold at the time of injection lies in the vicinity of the mold wall temperature before injection.

The contact temperature $\theta_{w_{\max}}$ of the wall of an injection mold at the time of injection is [17]

$$\theta_{w_{\max}} = \frac{b_w \theta_{w_{\min}} + b_p \theta_M}{b_w + b_p} \quad (2.16)$$

where b = coefficient of heat penetration = $\sqrt{\lambda \rho c}$
 $\theta_{w_{\min}}$ = temperature before injection
 θ_M = melt temperature

Indices w and p refer to mold and polymer respectively.

Table 2.5 Coefficients of Heat Penetration of Metals and Plastics [17]

Material	Coefficient of heat penetration b $W \cdot s^{0.5} \cdot m^{-2} \cdot K^{-1}$
Beryllium Copper (BeCu25)	17.2×10^3
Unalloyed Steel (C45W3)	13.8×10^3
Chromium Steel (X40Cr13)	11.7×10^3
Polyethylene (PE-HD)	0.99×10^3

Table 2.5 Coefficients of Heat Penetration of Metals and Plastics [17] (*Continued*)

Material	Coefficient of heat penetration b $W \cdot s^{0.5} \cdot m^{-2} \cdot K^{-1}$
Polystyrene (PS)	0.57×10^3
Stainless Steel	7.56×10^3
Aluminum	21.8×10^3

The values given in Table 2.5 refer to the following units of the properties:

Thermal conductivity λ : $W/(m \cdot K)$

Density ρ : kg/m^3

Specific heat c : $kJ/(kg \cdot K)$

The approximate values for steel are

$$\lambda = 50 \text{ W/(m} \cdot \text{K)}$$

$$\rho = 7850 \text{ kg/m}^3$$

$$c = 0.485 \text{ kJ/(kg} \cdot \text{K)}$$

The coefficient of heat penetration is

$$b = \sqrt{\lambda \cdot \rho \cdot c} = \sqrt{50 \cdot 7.85 \cdot 10^3 \cdot 0.485 \cdot 10^3} = 13.8 \cdot 10^3 \text{ W s}^{0.5} \cdot \text{m}^{-2} \cdot \text{K}^{-1}$$

■ 2.8 Heat Deflection Temperature

Heat deflection temperature (HDT) or the deflection temperature under load (DTUL) is a relative measure of the polymer's ability to retain shape at elevated temperatures while supporting a load. In amorphous materials, the HDT almost coincides with the glass transition temperature T_g . Crystalline polymers may have lower values of HDT but are dimensionally more stable at elevated temperatures [5]. Additives like fillers have more significant effect on crystalline polymers than on amorphous polymers. The heat deflection temperatures are listed for some materials in Table 2.6. Owing to the similarity of the measuring principle, Vicat softening point, HDT, and Martens temperature often lie close to each other (Fig. 2.9) [6].

Table 2.6 Heat Deflection Temperatures (HDT) According to the Method A of Measurement [3, 6]

Material	HDT (Method A) $^{\circ}\text{C}$
PE-LD	35
PE-HD	50
PP	45

Material	HDT (Method A) °C
PVC	72
PS	84
ABS	100
PC	135
POM	140
PA 6	77
PA 66	130
PMMA	103
PET	80
PBT	65

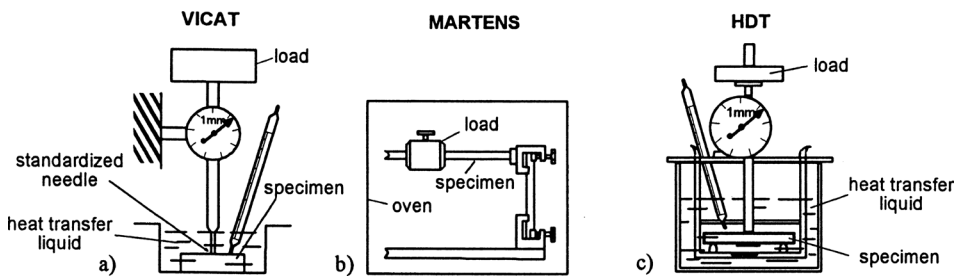


Figure 2.9 Principles of measurement of heat distortion of plastics [6]

■ 2.9 Vicat Softening Point

Vicat softening point is the temperature at which a small lightly loaded, heated test probe penetrates a given distance into a test specimen [5].

The Vicat softening point gives an indication of the material's ability to withstand contact with a heated object for a short duration. It is used as a guide value for demolding temperature in injection molding. Vicat softening points of crystalline polymers have more significance than amorphous polymers, as the latter tend to creep during the test [5]. Both Vicat and HDT values serve as a basis to judge the resistance of a thermoplastic to distortion at elevated temperatures.

Guide values of Vicat softening temperatures of some polymers according to DIN 53460 (Vicat 5 kg) are given in Table 2.7 [6].

Table 2.7 Values for Vicat Softening Points [6]

Polymer	Vicat softening point °C
PE-HD	65
PP	90
PVC	92
PS	90
ABS	102
PC	138
POM	165
PA 6	180
PA 66	200
PMMA	85
PET	190
PBT	180

■ 2.10 Flammability

Most plastics are flammable and can act as fuel in a fire situation. The aim of various flammability tests is to measure the burning characteristics of plastics materials once ignition has occurred. The critical oxygen is the most accepted laboratory test. It measures the minimum volume concentration of oxygen in a mixture of oxygen and nitrogen that is required to initiate combustion of the plastic and propagate flame-burning to a prespecified extent (a flame-spread time or a distance along the test sample) [1]. Data are presented in the form of limiting oxygen index (LOI) value. These values are summarized in Table 2.8 [1]. The non-flammability of PTFE is manifested by its exceptionally high LOI value. Other flame-resistant plastics include thermosets, PVC, and PVDC. Resistance to flammability can be enhanced by adding flame retarding additives to the polymer [1].

The Underwriters' Laboratory test (UL 94) is a rating system that classifies flammability behavior of plastics according to their ability to maintain combustion after the flame is removed (see Fig. 2.10 [1]). In general, plastics that extinguish rapidly and do not drip flaming particles obtain high ratings. Ratings are given on the basis of minimum wall thickness of the material which corresponds to a particular flame class [1]. These thicknesses are important for plastics component design.

Table 2.8 Limiting Oxygen Indices (LOI) of Polymers (23 °C) [1]

Material	LOI
POM	14.9/15.7
PMMA	17.4
PE	17.4
PP	17.4
PS	17.6/18.3
ABS	18.3/18.8
PET	20.0
PA 66	24/29
PSU	30/32
PI	36.5
PVDC	60.0
PVC (chlorinated)	60.0/70.0
PTFE	95.0

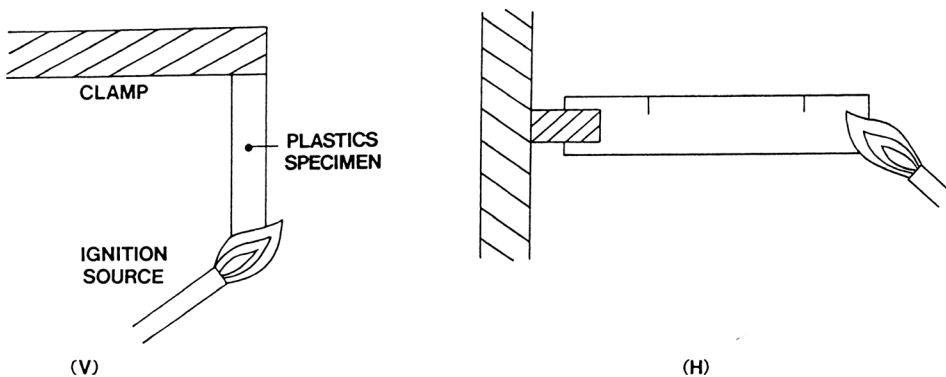


Figure 2.10 Typical arrangements for the UL flammability test: (V) UL 94 v; vertical small flame ignitability (variable sample thickness); (H) UL 94; HB horizontal small flame ignitability/flame spread [1]

The temperature index determined on the basis of the tensile half-life concept of the Underwriters' Laboratories is shown for various polymers in Fig. 2.11 [4]. The smoke emission for a number of plastics is given in Fig. 2.12 [4].

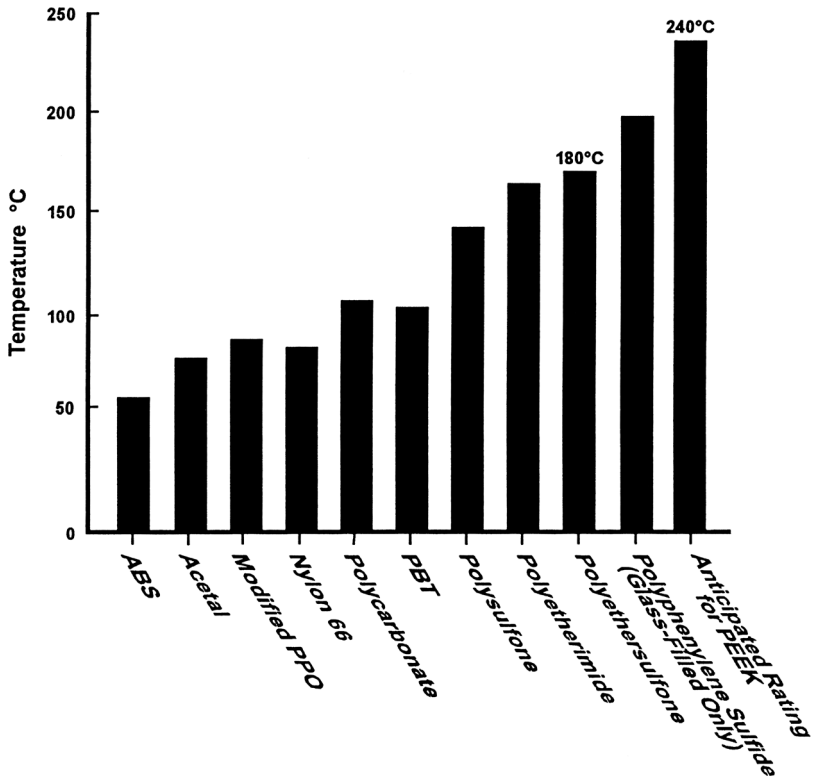


Figure 2.11 UL temperature index for some thermoplastics [4]

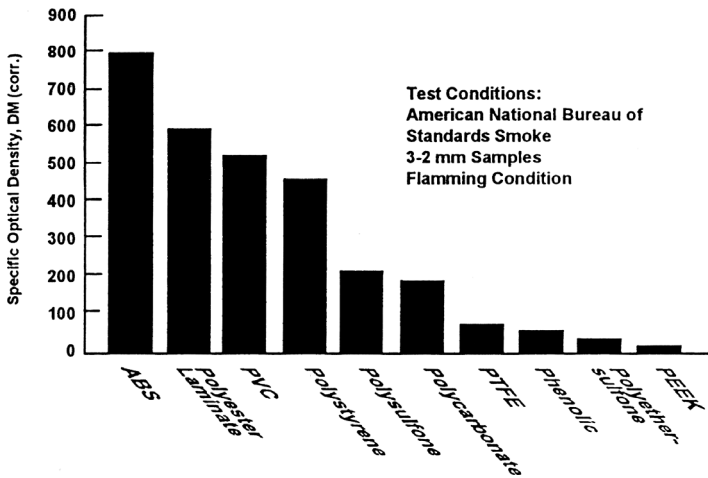


Figure 2.12 Smoke emission behavior of some thermoplastics [4]

■ 2.11 References

- [1] *Birley, A. W., Haworth, B., Bachelor, T.*: Physics of Plastics, Hanser, Munich, 1991
- [2] *Rao, N. S.*: Design Formulas for Plastics Engineers, Hanser, Munich, 1991
- [3] *Dominghaus, H.*: Plastics for Engineers, Hanser, Munich, 1993
- [4] *Rigby, R. B.*: Polyethersulfone in Engineering Thermoplastics: Properties and Applications, Ed. James M. Margolis, Marcel Dekker, Basel, 1985
- [5] General Electric Plastics Brochure: Engineering Materials Design Guide
- [6] *Schmiedel, H.*: Handbuch der Kunststoffprüfung, Hanser, Munich, 1992
- [7] Design Guide, Modern Plastics Encyclopedia, 1978 - 79
- [8] Kenndaten für die Verarbeitung thermoplastischer Kunststoffe, Teil I, Thermodynamik, Hanser, Munich, 1979
- [9] *McKelvey, J. M.*: Polymer Processing, John Wiley, New York, 1962
- [10] *Münstedt, H.*: Berechnen von Extrudierwerkzeugen, VDI-Verlag, Düsseldorf, 1978
- [11] *Rao, N. S.*: Designing Machines and Dies Polymer Processing, Hanser, Munich, 1981
- [12] Brochure: Advanced CAE Technology Inc., 1992
- [13] Proceedings, 9. Kunststofftechnisches Kolloquium, IKV, Aachen, 1978
- [14] *Rauwendaal, C.*: Polymer Extrusion, Hanser, Munich, 1986
- [15] *Ogorkiewicz, R. M.*: Thermoplastics Properties and Design, John Wiley, New York, 1973
- [16] *Martin, H.*: VDI-Wärmeatlas, VDI-Verlag, Düsseldorf, 1984
- [17] *Wübken, G.*: Berechnen von Spritzgießwerkzeugen, VDI-Verlag, Düsseldorf, 1974
- [18] *Progelhof, R. C., Throne, J. L.*: Polymer Engineering Principles - Properties, Processes, Tests for Design, Hanser, Munich, 1993
- [19] *Kurfess, W.*: Kunstst. 61, 1971, p 421

3

Transport Properties of Molten Polymers

The basic principle of making parts out of polymeric materials lies in creating a melt from the solid material and forcing the melt into a die, the shape of which corresponds to that of the part. Thus, as Fig. 3.1 indicates, melt flow and thermal properties of polymers play an important role in the operations of polymer processing.

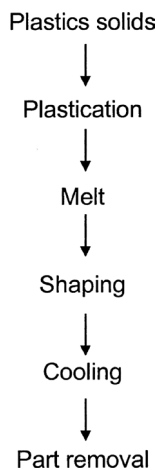


Figure 3.1 Principle of manufacturing of plastics parts

■ 3.1 Newtonian and Non-Newtonian Fluids

Analogous to the ideal elastic solids, there exists a linear relationship between stress and strain in the case of Newtonian fluids (Fig. 3.2).

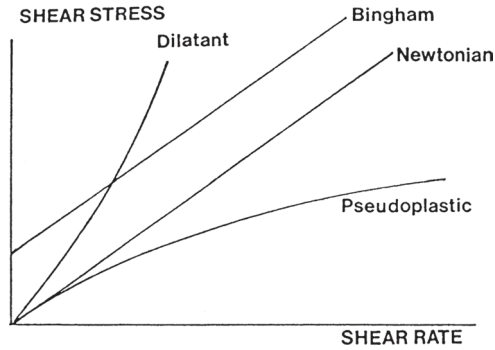


Figure 3.2 Flow curves of idealized fluids [1]

The fluid between the upper plate in Fig. 3.3, moving at a constant velocity U_x , and the lower stationary plate, experiences a shear stress τ

$$\tau = \frac{F_t}{A} \quad (3.1)$$

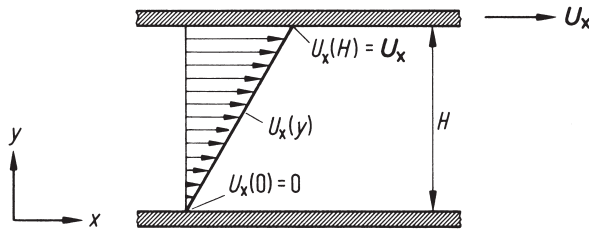


Figure 3.3 Shear flow

The shear or deformation rate of the fluid is equal to

$$\dot{\gamma} = \frac{U_x}{H} = \frac{du}{dy} \quad (3.2)$$

The shear viscosity is then defined as

$$\eta = \frac{\tau}{\dot{\gamma}} \quad (3.3)$$

For an extensional flow, which corresponds to the tension test of a Hookean solid, we get

$$\sigma_z = \lambda \cdot \dot{\epsilon} \quad (3.4)$$

where σ_z = normal stress
 λ = Trouton viscosity
 $\dot{\epsilon}$ = strain rate

The Trouton viscosity can be expressed as [2]

$$\lambda = 3\eta \quad (3.5)$$

■ 3.2 Viscous Shear Flow

Macromolecular fluids, such as thermoplastic melts, exhibit significant non-Newtonian behavior. This is noticed in the marked decrease of melt viscosity when the melt is subjected to shear or tension as shown in Figs. 3.4 and 3.5. The flow of melt in the channels of dies and polymer processing machinery is mainly shear flow. Therefore, knowledge of the laws of shear flow is necessary for designing machines and dies for polymer processing. For practical applications the following summary of the relationships was found to be useful.

3.2.1 Apparent Shear Rate

The apparent shear rate for a melt flowing through a capillary is defined as

$$\dot{\gamma}_a = \frac{4\dot{Q}}{\pi R^3} \quad (3.6)$$

where \dot{Q} is the volume flow rate per second, and R the radius of capillary.

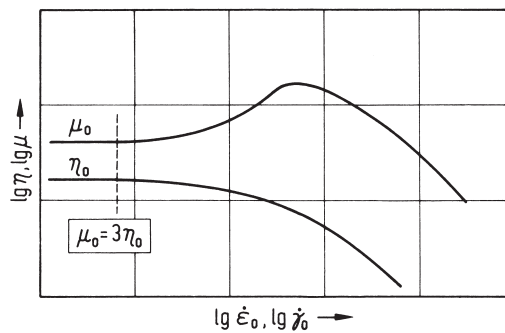


Figure 3.4 Tensile viscosity and shear viscosity of a polymer melt as a function of strain rate [14]

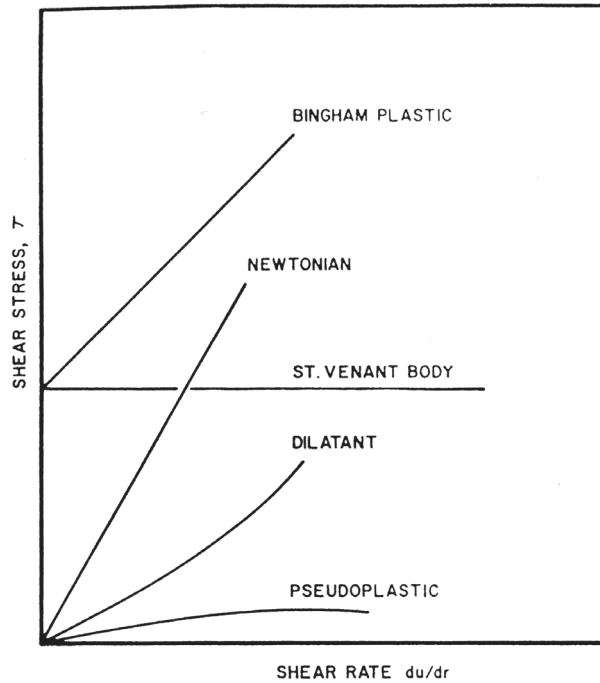


Figure 3.5 Shear stress as a function of shear rate for different types of plastics [24]

3.2.2 Entrance Loss

Another rheological parameter, which is of practical importance, is the entrance loss p_c , representing the loss of energy of flow at the entrance to a round nozzle. This is correlated empirically by the relation [4]

$$p_c = c \cdot \tau^m \quad (3.7)$$

where c and m are empirical constants and τ the shear stress. These constants can be determined from the well-known Bagley curves as shown in Fig. 3.6. The values of these constants are given in Table 3.1 for some thermoplastics. The units of shear stress and entrance loss used in the calculation of c and m are Pa.

Table 3.1 Resin-Dependent Constants c and m in Equation 3.7 [4]

Product	c	m
Polypropylene (Novolen 1120 H)	$2.551 \cdot 10^{-5}$	2.116
Polypropylene (Novolen 1120 L)	$1.463 \cdot 10^{-4}$	1.976
Polypropylene (Novolen 1320 L)	$2.871 \cdot 10^{-7}$	2.469
PE-LD (Lupolen 1800 M)	$1.176 \cdot 10^{-1}$	1.434

Product	c	m
PE-LD (Lupolen 1800 S)	$6.984 \cdot 10^0$	1.072
PE-LD (Lupolen 1810 D)	$5.688 \cdot 10^{-4}$	1.905
PE-HD (Lupolen 6011 L)	$3.940 \cdot 10^{-2}$	1.399
PE-HD (Lupolen 6041 D)	$1.788 \cdot 10^0$	1.187
Polyisobutylene (Oppanol B10)	$6.401 \cdot 10^{-3}$	1.575
Polyisobutylene (Oppanol B15)	$1.021 \cdot 10^{-7}$	2.614

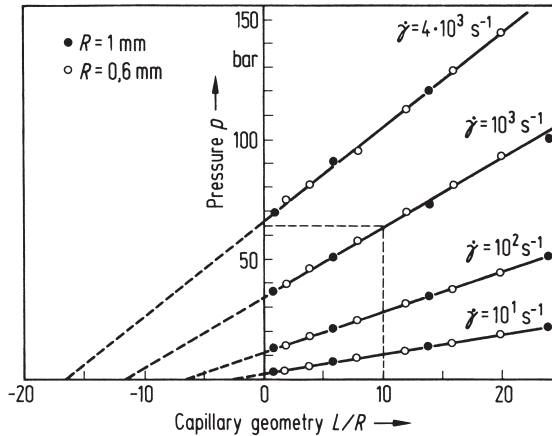


Figure 3.6 Bagley plots of polystyrene with the capillary length L and radius R [15]

3.2.3 True Shear Stress

The flow curves of a particular PE-LD measured with a capillary rheometer are given in Fig. 3.7. The plot shows the apparent shear rate $\dot{\gamma}_a$ as a function of the true shear stress τ at the capillary wall with the melt temperature as a parameter. The entrance loss p_c was obtained from the Bagley plot shown in Fig. 3.6.

Thus, the true shear stress τ is given by

$$\tau = \frac{p - p_c}{2(L/R)} \quad (3.8)$$

where L = length of the capillary
 R = radius of the capillary
 p = pressure of the melt (see Fig. 3.6)

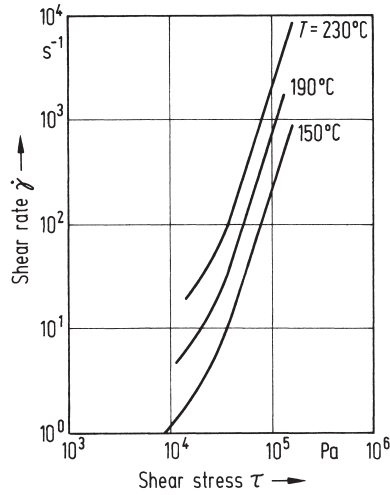


Figure 3.7 Flow curves of a PE-LD [2]

3.2.4 Apparent Viscosity

The apparent viscosity η_a is defined as

$$\eta_a = \frac{\tau}{\dot{\gamma}_a} \quad (3.9)$$

and is shown in Fig. 3.8 as a function of shear rate and temperature for a PE-LD. Viscosity functions for several polymers are given in Figs. 3.9 and 3.10.

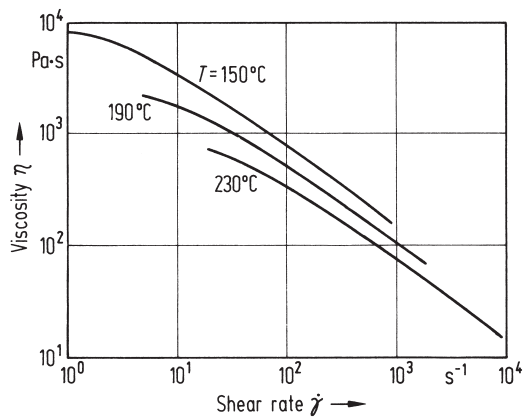


Figure 3.8 Viscosity functions of a PE-LD [2]

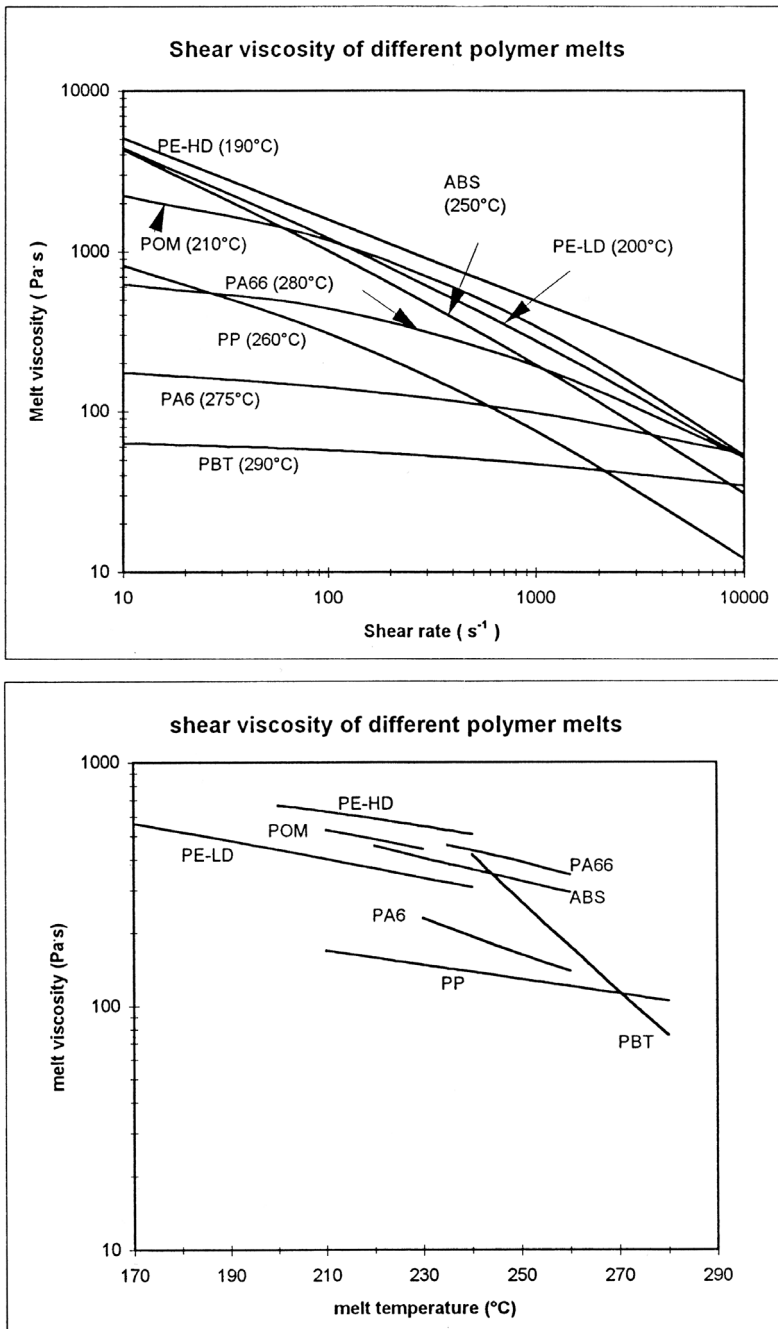


Figure 3.9 Shear viscosity of some polymer melts

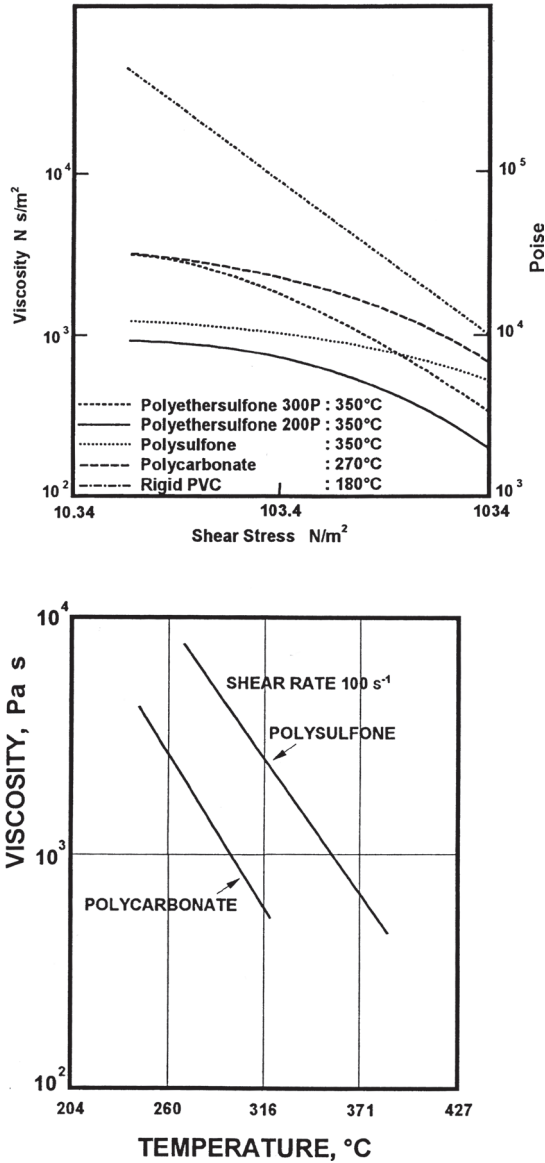


Figure 3.10 Shear viscosity of some engineering thermoplastics [3, 16]

3.2.5 True Shear Rate

The true shear rate $\dot{\gamma}_t$ is obtained from the apparent shear rate by applying the correction for the non-Newtonian behavior of the melt according to Rabinowitsch:

$$\dot{\gamma}_t = \left(\frac{n+3}{4} \right) \dot{\gamma}_a \quad (3.10)$$

3.2.6 True Viscosity

The true viscosity η_w is given by

$$\eta_w = \frac{\tau}{\dot{\gamma}_t} \quad (3.11)$$

In Fig. 3.11, the true and apparent viscosities are plotted as functions of the corresponding shear rates at different temperatures for polystyrene. As can be seen, the apparent viscosity function is a good approximation for engineering calculations.

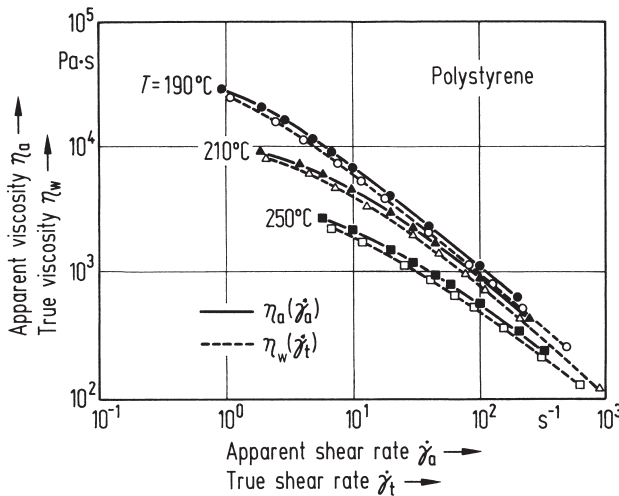


Figure 3.11 True and apparent viscosity functions of a polystyrene at different temperatures [4]

■ 3.3 Rheological Models

Various fluid models have been developed to calculate the apparent shear viscosity η_a [2]. The following sections deal with an important few of these relationships, which are frequently used in design calculations.

3.3.1 Hyperbolic Function of Eyring and Prandtl

The relation between shear rate $\dot{\gamma}_a$ and shear stress τ according to the fluid model of Eyring [19] and Prandtl [20] can be written as

$$\dot{\gamma}_a = -C \sinh(\tau/A) \quad (3.12)$$

where C and A are temperature-dependent material constants.

The evaluation of the constants C and A for the flow curve of PE-LD at 190°C in Fig. 3.12 leads to $C = 4\text{ s}^{-1}$ and $A = 3 \cdot 10^4\text{ N/m}^2$. It can be seen from Fig. 3.12 that the hyperbolic function of Prandtl and Eyring holds well at low shear rates.

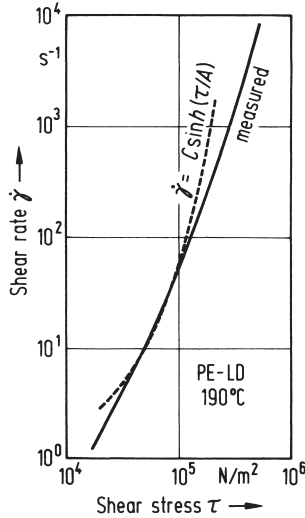


Figure 3.12 Comparison between measurements and values calculated with Eq. 3.12 [2]

3.3.2 Power Law of Ostwald and de Waele

The power law of Ostwald [21] and de Waele [22] is easy to use, hence, it is widely employed in design work [5]. This relation can be expressed as

$$\dot{\gamma}_a = K \tau^n \quad (3.13)$$

or

$$\dot{\gamma}_a = K \left| \tau^{n-1} \right| \tau \quad (3.14)$$

where K denotes a factor of proportionality and n the power law exponent.

Another form of power law often used is

$$\tau_a = K_R \dot{\gamma}_a^{n_R} \quad (3.15)$$

or

$$\tau_a = K_R \left| \dot{\gamma}_a^{n_R-1} \right| \dot{\gamma}_a \quad (3.16)$$

In this case, n_R is the reciprocal of n and $K_R = K^{-n_R}$.

From Eq. 3.13, the exponent n can be expressed as

$$n = \frac{d \lg \dot{\gamma}_a}{d \lg \tau} \quad (3.17)$$

As shown in Fig. 3.13, in a double log-plot, the exponent n represents the local gradient of the curve $\dot{\gamma}_a$ vs. τ .

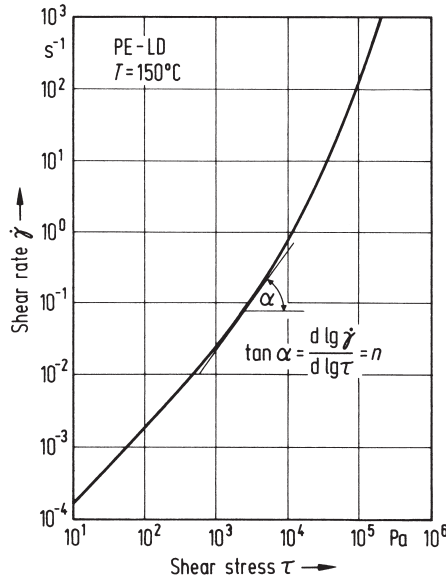


Figure 3.13 Determination of the power law exponent n in the Eq. 3.13

Furthermore

$$\frac{1}{n} = \frac{d \lg \tau}{d \lg \dot{\gamma}_a} = \frac{d \lg \eta_a + d \lg \dot{\gamma}_a}{d \lg \dot{\gamma}_a} = \frac{d \lg \eta_a}{d \lg \dot{\gamma}_a} + 1 \quad (3.18)$$

The values of K and n determined from the flow curve of PE-LD at 190 °C, shown in Fig. 3.14, were found to be $K = 1.06 \cdot 10^{-11}$ and $n = 2.57$.

As can be seen from Fig. 3.14, the power law fits the measured values much better than the hyperbolic function of Eyring [19] and Prandtl [20]. The deviation between the power law and experiment is a result of the assumption that the exponent n is constant throughout the range of shear rates considered, whereas n actually varies with the shear rate. The power law can be extended to consider the effect of temperature on viscosity as follows:

$$\eta_a = K_{OR} \cdot \exp(-\beta \cdot T) \cdot \dot{\gamma}_a^{n_R - 1} \quad (3.19)$$

where K_{OR} = consistency index
 β = temperature coefficient
 T = temperature of melt

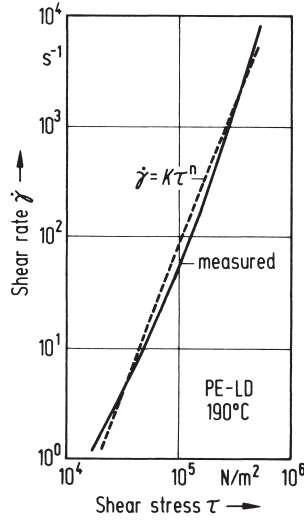


Figure 3.14 Comparison between measured values and power law

Example:

The following values are given for a PE-LD:

$$n_R = 0.3286$$

$$\beta = 0.00863 \text{ } ^\circ\text{C}^{-1}$$

$$K_{OR} = 135,990 \text{ N} \cdot \text{s}^{n_R} \cdot \text{m}^{-2}$$

The viscosity η_a at $T = 200 \text{ } ^\circ\text{C}$ and $\dot{\gamma}_a = 500 \text{ s}^{-1}$ is calculated from Eq. 3.19

$$\eta_a = 373.1 \text{ Pa}\cdot\text{s}$$

3.3.3 Polynomial of Münstedt

The fourth degree polynomial of Münstedt provides a good fit for the measured values of viscosity. For a definite temperature this is expressed as

$$\lg \eta_a = A_0 + A_1 \lg \dot{\gamma}_a + A_2 (\lg \dot{\gamma}_a)^2 + A_3 (\lg \dot{\gamma}_a)^3 + A_4 (\lg \dot{\gamma}_a)^4 \quad (3.20)$$

where A_0, A_1, A_2, A_3, A_4 represent resin-dependent constants. These constants can be determined with the help of the program of Rao [13], which is based on multiple linear regressions.

This program in its general form fits an equation of the type $y = a_0 + a_1x_1 + a_2x_2 + \dots + a_nx_n$ and prints out the coefficients a_0, a_1 , and so on for the best fit.

3.3.3.1 Shift Factor for Crystalline Polymers

The influence of temperature on viscosity can be taken into account by the shift factor a_T [4]. For crystalline polymers this can be expressed as

$$a_T = b_1(T_0) \exp(b_2/T) \quad (3.21)$$

where b_1, b_2 = resin-dependent constants
 T = melt temperature (K)
 T_0 = reference temperature (K)

3.3.3.2 Shift Factor for Amorphous Polymers

The shift factor a_T for amorphous polymers is derived from the WLF equation and can be written as

$$\lg a_T = \frac{-c_1(T - T_0)}{c_2 + (T - T_0)} \quad (3.22)$$

where c_1, c_2 = resin-dependent constants
 T = melt temperature ($^{\circ}\text{C}$)
 T_0 = reference temperature ($^{\circ}\text{C}$)

The expression for calculating both the effect of temperature and shear rate on viscosity follows from Eq. 3.20

$$\begin{aligned} \lg \eta_a = \lg a_T + A_0 + A_1 \lg(a_T \dot{\gamma}_a) + A_2 [\lg(a_T \dot{\gamma}_a)]^2 \\ + A_3 [\lg(a_T \dot{\gamma}_a)]^3 + A_4 [\lg(a_T \dot{\gamma}_a)]^4 \end{aligned} \quad (3.23)$$

With Eq. 3.18 we get

$$\frac{1}{n} = 1 + A_1 + 2A_2 \lg(a_T \dot{\gamma}_a) + 3A_3 [\lg(a_T \dot{\gamma}_a)]^2 + 4A_4 [\lg(a_T \dot{\gamma}_a)]^3 \quad (3.24)$$

The power law exponent is often required in the design work as a function of shear rate and temperature. Figure 3.15 illustrates this relationship for a PE-LD. The curves shown are computed with Eqs. 3.21 and 3.24. As can be inferred from Fig. 3.15, the assumption of a constant value for the power law exponent holds good for a wide range of shear rates.

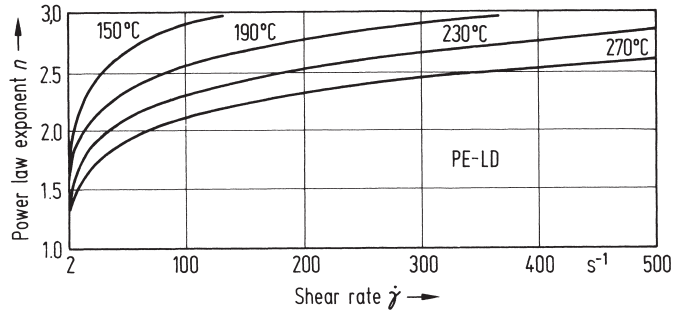


Figure 3.15 Power law exponent of a PE-LD as a function of shear rate and temperature

Example:

$$A_0 = 4.2541$$

$$A_1 = -0.4978$$

$$A_2 = -0.0731$$

$$A_3 = 0.0133$$

$$A_4 = -0.0011$$

$$b_1 = -5.13 \cdot 10^{-6}$$

$$b_2 = 5640 \text{ K}$$

$$\text{at } \dot{\gamma}_a = 500 \text{ s}^{-1} \text{ and } T = 200 \text{ }^\circ\text{C}.$$

Solution:

$$a_T \text{ from Eq. 3.21}$$

$$a_T = 5.13 \cdot 10^{-6} \cdot \exp(5640/473) = 0.774$$

$$\text{With } X = \lg(a_T \cdot \dot{\gamma}_a)$$

$$X = \lg(0.774 \cdot 500) = 2.588$$

$$\text{With } \eta_a \text{ from Eq. 3.23}$$

$$\eta_a = 10^{(\lg a_T + A_0 + A_1 X + A_2 X^2 + A_3 X^3 + A_4 X^4)}$$

Substituting the values of A_0 , A_1 , and so on, one gets

$$\eta_a = 351.78 \text{ Pa} \cdot \text{s}$$

The power law exponent is obtained from Eq. 3.24

$$n = (1 + A_1 + 2A_2 X + 3A_3 X^2 + 4A_4 X^3)^{-1}$$

Using the values of A_0 , A_1 , and so on

$$n = 3.196$$

3.3.4 Viscosity Equation of Carreau

As shown in Fig. 3.16, the Carreau equation [23] gives the best fit for the viscosity function, reproducing the asymptotic form of the plot at high and low shear rates correctly.

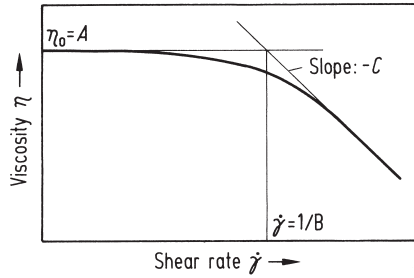


Figure 3.16 Determination of Carreau parameters from a viscosity function [9]

The equation is expressed as

$$\eta_a = \frac{A}{(1 + B \dot{\gamma}_a)^C} \quad (3.25)$$

where A , B , and C are resin-dependent constants. By introducing the shift factor a_T into Eq. 3.25, the temperature-invariant form of the Carreau equation can be given as (Fig. 3.17)

$$\eta_a = \frac{A a_T}{(1 + B a_T \dot{\gamma}_a)^C} \quad (3.26)$$

For a number of resins, the shift factor can be calculated as a function of temperature from the following equation with good approximation [5, 6]

$$\lg a_T(T_1, T_2) = \frac{8.86(T_1 - T_{ST})}{101.6 + (T_1 - T_{ST})} - \frac{8.86(T_2 - T_{ST})}{101.6 + (T_2 - T_{ST})} \quad (3.27)$$

where T_1 (°C) is the temperature at which the viscosity is given and T_2 (°C) the temperature at which the viscosity is to be found out.

The standard temperature T_{ST} is given by [6]

$$T_{ST} = T_g + 50 \text{ } ^\circ\text{C} \quad (3.28)$$

Data on typical glass transition temperatures of polymers are given in Table 2.4.

The power law exponent n can be obtained from Eq. 3.26:

$$\frac{1}{n} = -C \cdot \frac{B \cdot a_T}{1 + B \cdot a_T \cdot \dot{\gamma}_a} \cdot \dot{\gamma}_a + 1 \tag{3.29}$$

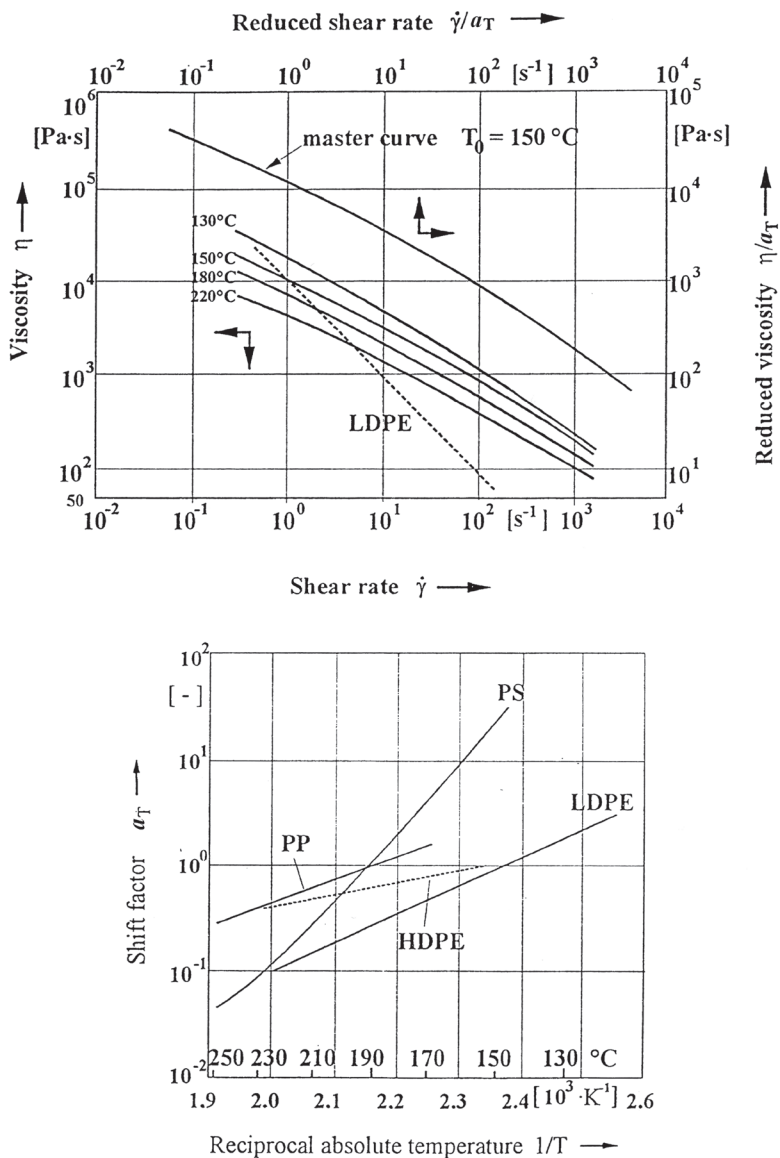


Figure 3.17 Use of shift factor a_T for calculating temperature invariant viscosity [17]

For high shear rates n becomes [4]

$$n = \frac{1}{1-C} \quad (3.30)$$

Computer disks containing the resin-dependent constants A , B , and C can be obtained for the respective resins from the resin manufacturers [12]. These constants can also be determined by using the software VISRHEO [13], and can be stored in a data bank for viscosity data.

Example:

The following constants are given for a particular PE-LD.

$$A = 32400 \text{ Pa} \cdot \text{s}$$

$$B = 3.1 \text{ s}$$

$$C = 0.62$$

$$T_{ST} = -133 \text{ }^\circ\text{C}$$

$$T_1 = 190 \text{ }^\circ\text{C}$$

The viscosity is to be calculated at

$$T_2 = 200 \text{ }^\circ\text{C} \text{ and } \dot{\gamma}_a = 500 \text{ s}^{-1}$$

Solution:

One obtains from Eq. 3.27

$$X = \frac{8.86(T_1 - T_{ST})}{101.6 + (T_1 - T_{ST})} = \frac{8.86(190 - (-133))}{101.6 + (190 - (-133))} = 6.74$$

and

$$Y = \frac{8.86(T_2 - T_{ST})}{101.6 + (T_2 - T_{ST})} = \frac{8.86(200 - (-133))}{101.6 + (200 - (-133))} = 6.79$$

The power law exponent is calculated from Eq. 3.29

$$n = \left(\frac{-C \cdot Z}{1+Z} + 1 \right)^{-1} = \left(\frac{-0.62 \cdot 1379.5}{1+1379.5} + 1 \right)^{-1} = 2.63$$

The viscosity η_a follows from Eq. 3.26

$$\eta_a = \frac{32400 \cdot 0.89}{(1+1379.5) \cdot 0.62} = 325.8 \text{ Pa s}$$

3.3.5 Viscosity Formula of Klein

The regression equation of Klein et al. [25] is given by

$$\lg \eta_a = a_0 + a_1 \ln \dot{\gamma}_a + a_{11} (\ln \dot{\gamma}_a)^2 + a_2 T + a_{22} T^2 + a_{12} T \ln \dot{\gamma}_a \quad (3.31)$$

T = Temperature of the melt ($^{\circ}\text{F}$)

η_a = Viscosity ($\text{lb}_f \cdot \text{s}/\text{in}^2$)

The resin-dependent constants a_0 to a_{22} can be determined with the help of the computer program given in [13], as has been the case in finding out the a -coefficients in Eq. 3.20.

Example:

The following constants are valid for a particular type of PE-LD. What is the viscosity η_a at $\dot{\gamma}_a = 500 \text{ s}^{-1}$ and $T = 200 \text{ }^{\circ}\text{C}$?

$$a_0 = 3.388$$

$$a_1 = -6.351 \cdot 10^{-1}$$

$$a_{11} = -1.815 \cdot 10^{-2}$$

$$a_2 = -5.975 \cdot 10^{-3}$$

$$a_{22} = -2.51 \cdot 10^{-6}$$

$$a_{12} = 5.187 \cdot 10^{-4}$$

Solution:

$$T(^{\circ}\text{F}) = 1.8 \cdot T(^{\circ}\text{C}) + 32 = 1.8 \cdot 200 + 32 = 392$$

With the constants above and Eq. 3.31 one gets

$$\eta_a = 0.066 \text{ lb}_f \cdot \text{s}/\text{in}^2$$

and in SI-units

$$\eta_a = 6857 \cdot 0.066 = 449.8 \text{ Pa} \cdot \text{s}$$

The expression for the power law exponent n can be derived from Eqs. 3.18 and 3.30. The exponent n is given by

$$\frac{1}{n} = 1 + a_1 + 2a_{11} \ln \dot{\gamma}_a + a_{12} \cdot T \quad (3.32)$$

Putting the constants a_1, \dots, a_{12} into this equation one obtains

$$n = 2.919$$

■ 3.4 Effect of Pressure on Viscosity

Compared to the influence of temperature the effect of pressure on viscosity is not of much significance.

However, the relative measure of viscosity can be obtained from [8,6,4]

$$\eta_p = \eta_0 \exp(\alpha_p \cdot p) \quad (3.33)$$

where η_p = viscosity at pressure p and constant shear stress τ_0
 η_0 = viscosity at constant shear stress τ_0
 α_p = pressure coefficient

For styrene polymers η_p is calculated from [8]

$$\eta_p = \eta_0 \exp(p / 1000) \quad (3.34)$$

Where p = pressure in bar.

Thus the change of viscosity with the pressure can be obtained from Eq. 3.34. Table 3.2 shows the values of viscosity calculated according to Eq. 3.34 for a polystyrene of average molecular weight. It can be seen that a pressure of 200 bar causes an increase of viscosity of 22% as compared to the value at 1 bar. The pressure coefficient of PE-LD is less than that of PS by factor of 3 to 4, and the value of PE-HD is again less than a factor of 2 than that of PE-LD. This means that in the case of polyethylene, an increase of pressure by 200 bar would enhance the viscosity only by 3 to 4%. Consequently, the effect of pressure on viscosity can be neglected in the case of extrusion processes, in which generally low pressures exist. However, in injection molding, where usually one has to deal with high pressures, the dependence of viscosity on pressure has to be considered.

Table 3.2 Effect of Pressure on Viscosity for Polystyrene, Equation 3.34

p bar	η_p
30	1.03
100	1.105
200	1.221
300	1.35
500	1.65
1000	2.72
3000	20

Figure 3.18 shows the melt viscosity at constant stress and temperature as a function of pressure for some polymers [7].

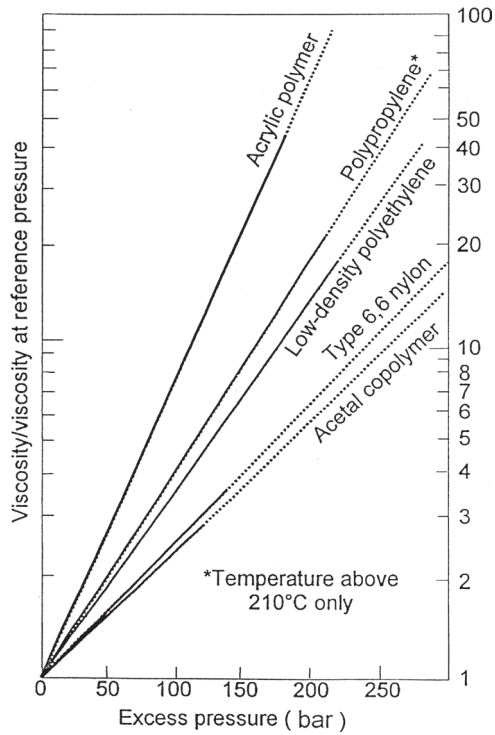


Figure 3.18 Melt viscosity at constant stress and temperature as a function of pressure [7]

■ 3.5 Dependence of Viscosity on Molecular Weight

The relationship between viscosity and molecular weight can be described by [10]

$$\eta_a = K' M_w^{3.5} \quad (3.35)$$

where M_w = molecular weight
 K' = resin dependent constant.

The approximate value of K' for PE-LD is

$$K' = 2.28 \cdot 10^{-4}$$

and for Polyamide 6

$$K' = 5.21 \cdot 10^{-14}$$

according to the measurements of Laun [10]. These values are based on zero viscosity.

■ 3.6 Viscosity of Two-Component Mixtures

The viscosity of a mixture consisting of the component A and the component B can be obtained from [11]

$$\lg \eta_M = C_A \lg \eta_A + C_B \lg \eta_B \quad (3.36)$$

where η = viscosity
 C = weight percent

Indices:

M : mixture
 A, B : components

■ 3.7 Melt Flow Index

The melt flow index (MFI), which is also known as the melt flow rate (MFR), indicates the flowability of a constant polymer melt, and is measured by forcing the melt through a capillary under a dead load at constant temperature (Fig. 3.19). The MFI value is the mass of melt flowing in a certain time. A MFR or MFI of 2 at 200 °C and 2.16 kg means, for example, that the melt at 200 °C flows at a rate of 2 g in ten minutes under a dead load of 2.16 kg.

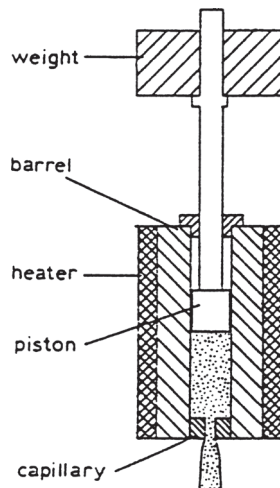


Figure 3.19 Melt flow tester [6]

In the case of the melt volume rate, which is also known as melt volume index (MVI), the volume flow rate of the melt instead of mass flow rate is set as the basis. The unit here is ml/10 min.

The effect of MFI on the properties of polyethylene, as an example, is illustrated in Fig. 3.20 [18].

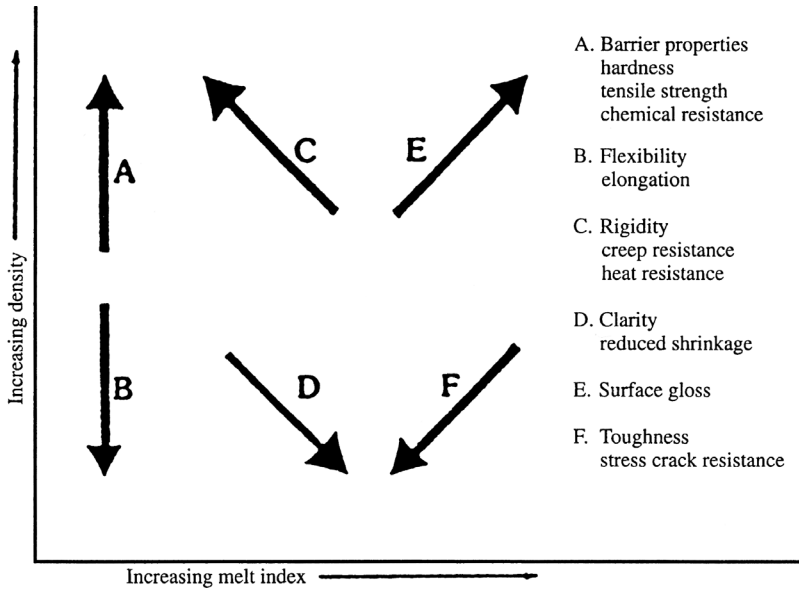


Figure 3.20 Melt index and density vs. polymer properties [18]

Ranges of melt indices for common processing operations are given in Table 3.3 [18].

Table 3.3 Ranges of MFI Values (ASTM D1238) for Common Processes [18]

Process	MFI range
Injection molding	5/100
Rotational molding	5/20
Film extrusion	0.5/6
Blow molding	0.1/1
Profile extrusion	0.1/1

■ 3.8 Tensile Viscosity

Although the flow of melt in the channels of dies and machines of polymer machinery is mainly shear flow, the elongational flow is of importance in such applications as film blowing and blow molding. The elongational or tensile viscosity can be measured with a tensile rheometer [1], and is much higher than shear viscosity. As shown in Fig. 3.4, the tensile viscosity of a Newtonian fluid is three times the shear viscosity. The tensile viscosity is defined as

$$\mu = \frac{\sigma}{\dot{\epsilon}} \quad (3.37)$$

$$\dot{\epsilon} = \frac{1}{l} \cdot \frac{dl}{dt} \quad (3.38)$$

where l = length at any instant of a volume element,
 t = time

■ 3.9 Viscoelastic Properties

Polymer machinery can be designed sufficiently accurate on the basis of the relationships for viscous shear flow alone. However, a complete analysis of melt flow should include both viscous and elastic effects, although the design of machines and dies by considering melt elasticity is rather difficult and seldom in use. Similar attempts to dimension the dies taking elastic effects into account have been made as described in the work of Wagner [26] and Fischer [27].

To give a more complete picture of melt rheology, the following expressions for the viscoelastic quantities according to Laun [10, 14] are presented.

The material functions characterizing the elastic behavior of a polymer melt are shear compliance and primary normal stress coefficient, which are defined as follows [14, 2]:

3.9.1 Primary Normal Stress Coefficient, Θ

$$\Theta = \frac{N_1}{\dot{\gamma}_0^2} \quad (3.39)$$

N_1 : normal stress difference,
 $\dot{\gamma}_0$: shear rate

3.9.2 Shear Compliance, J_e

$$J_e = \frac{\gamma_{r,s}}{\tau_0} \quad (3.40)$$

$\gamma_{r,s}$: recoverable shear strain,
 τ_0 : shear stress

Further on we have [14]

$$J_e = \frac{\Theta}{2\eta^2} \quad (3.41)$$

The equations above shown as functions of shear rate can be determined from measurements with a cone and plate rheometer (Fig. 3.21, [1]).

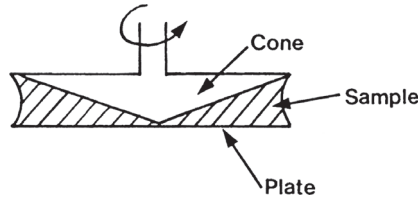


Figure 3.21 Schematic diagram of a cone and plate rheometer [1]

The limiting values of these equations are Θ_0 , η_0 , and J_e^0 (see Fig. 3.22).

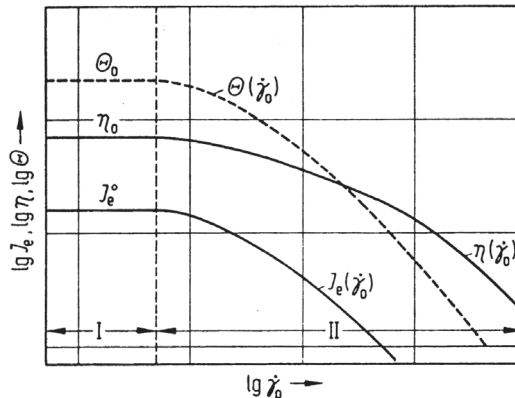


Figure 3.22 Parameters for steady shear flow [14]
 (I = linear region, II = nonlinear region)

3.9.3 Die Swell

Die swell, which can be measured with a capillary viscometer, gives a measure of the elastic deformation of the melt. Die swell is shown in Fig. 3.23 [14] as a function of length L to radius R of the capillary. The value is highest for an orifice of negligible length where the effect of converging entrance flow is largest. With increasing L/R ratios the molecular orientation decays, and the swell attains a constant value. For certain applications smaller L/R ratios of dies are preferred in order to have a high molecular orientation.

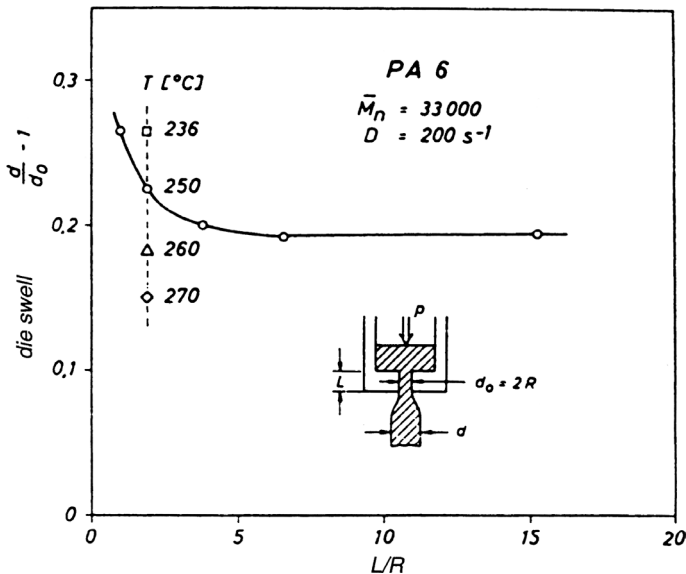


Figure 3.23 Die swell vs. length to radius L/R [14]

The viscoelastic behavior of polymer melts is discussed in [2] in more detail.

■ 3.10 Rheology of Glass Fiber-Filled Polypropylene Melts

3.10.1 Introduction

The advantages of glass-reinforced plastics in various branches of the industry, such as automotive and aircraft, and also in the manufacturing of furniture and sports goods, are well-known. In all these applications, knowledge of the melt flow

of the composite material is required, in order to design machinery for processing the filled polymer. This section is a contribution to the quantitative description of the rheology of glass fiber-filled polypropylene melts. The effects of shear rate, melt temperature, and fiber concentration on the melt viscosity have been studied by means of a high-pressure capillary rheometer. A novel equation has been presented to correlate the melt viscosity with the fiber content, using a modified shift factor taking the melt temperature and the fiber content into account. The proposed modeling can be applied to any filled thermoplastic melt.

Owing to their ease of processing and availability, glass fibers are common reinforcing agents used as fillers for imparting strength to the polymer. Knowledge of the flow behavior of the melt is important to the design of processing equipment and process optimization. In the present work, shear viscosities of polypropylene melts with glass fiber content by weight percent of 0, 20, 25, and 30 were measured at temperatures of 200, 220, 240, and 260 °C with a high pressure capillary rheometer. Based on these experimental results, a model for predicting the melt viscosity as a function of the fiber content was developed. The methodology described is applicable to any polymer.

3.10.2 Model

The shear viscosity can be expressed as a function of melt temperature, shear rate, and shift factor a_T as [28, 29]

$$\log \eta = \log(a_T) + A_0 + A_1 [\log(a_T \dot{\gamma})] + A_2 [\log(a_T \dot{\gamma})]^2 + A_3 [\log(a_T \dot{\gamma})]^3 + A_4 [\log(a_T \dot{\gamma})]^4 \quad (3.42)$$

where $A_0, A_1, A_2, A_3,$ and A_4 are the corresponding coefficients of the polynomial at the reference temperature T_r . The shift factor a_T is obtained by moving the individual plots of η vs. $\dot{\gamma}$ along a 45° line as shown in Fig. 3.24. If η / a_T is then plotted as a function of $\dot{\gamma} a_T$, we have the temperature-independent master curve; see Fig. 3.25.

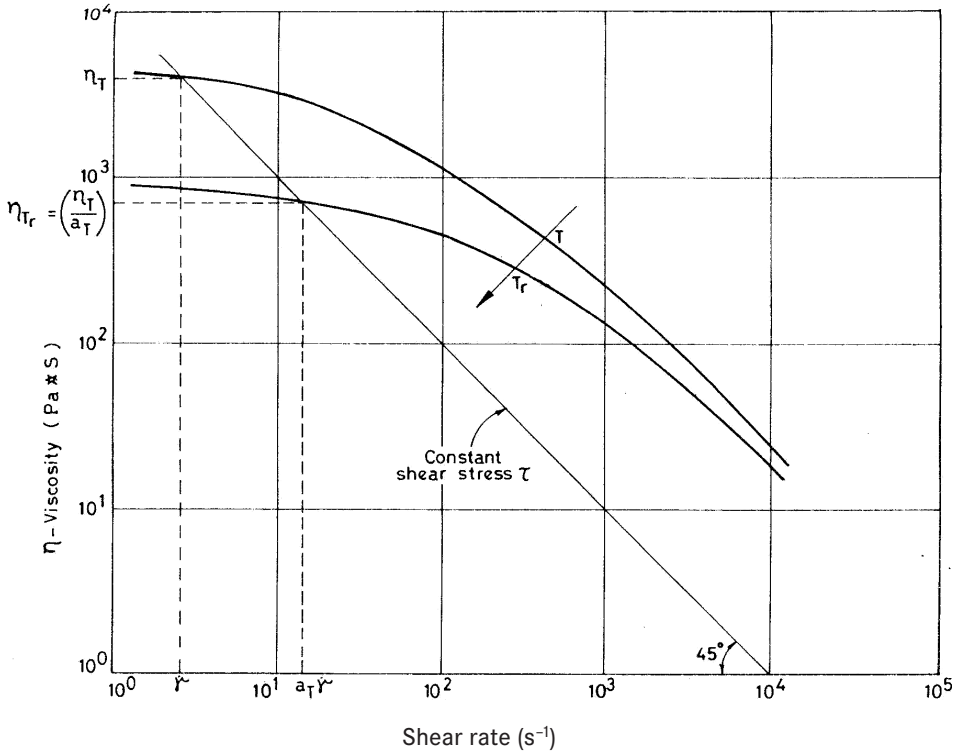


Figure 3.24 Determining the shift factor a_T

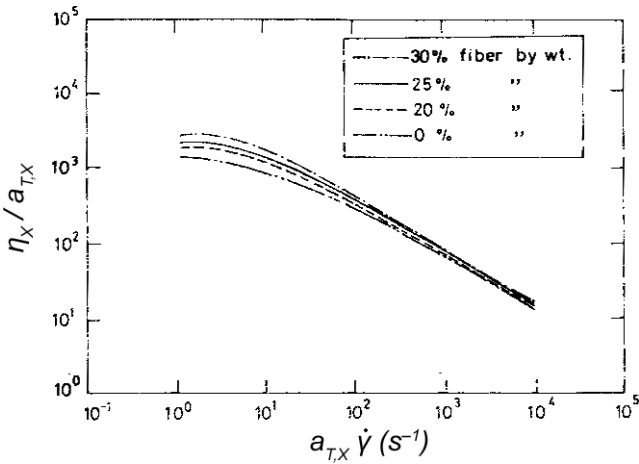


Figure 3.25 Master plot of polypropylene ($T_r = 220^\circ\text{C}$)

3.10.3 Shift Factor as a Function of Fiber Content

The experimental shear viscosity data for filled and unfilled melts are represented in Figs. 3.26 and 3.27 [30]. From these and other experiments a single relationship has been developed to express a_T as a function of temperature and fiber fraction,

$$a_{T,X} = \exp \left[-6.88(1+X)^{1.02} + \frac{3392.3(1+X)^{1.02}}{T} \right] \quad (3.43)$$

where X is the weight fraction of fibers and T in K.

By means of Eq. 3.43, the viscosity curve can be calculated for any fiber content and temperature, if $\eta(\dot{\gamma})$ is known at the reference temperature.

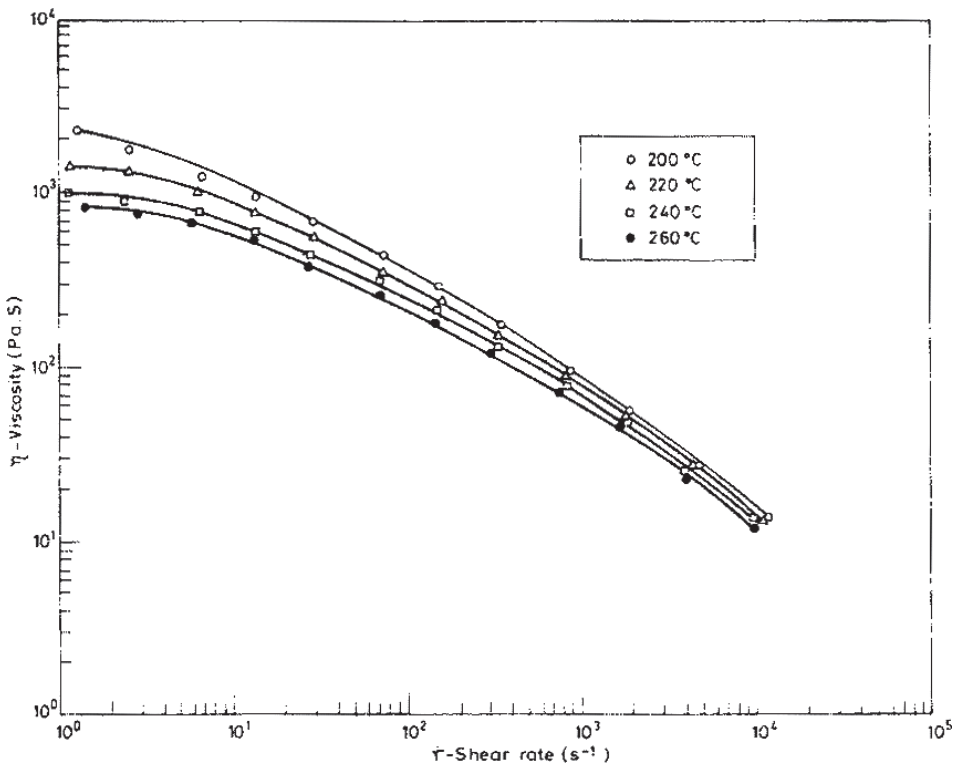


Figure 3.26 Viscosity vs. shear rate of unfilled polypropylene

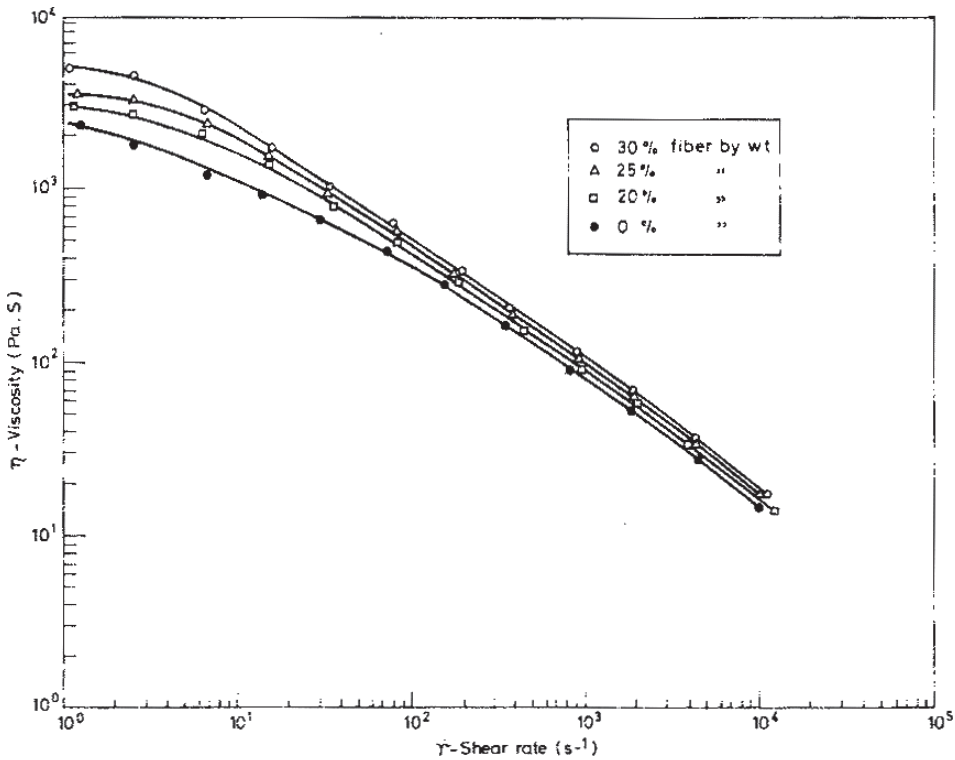


Figure 3.27 Viscosity vs. shear rate of polypropylene for different filler loadings ($T = 200\text{ }^{\circ}\text{C}$)

3.10.4 Example

The A -constants for a fiber content of 20% at a reference temperature of $220\text{ }^{\circ}\text{C}$ are found to be, from a polynomial fit of the experimental results,

$$A_0 = 3.370$$

$$A_1 = -0.0245$$

$$A_2 = -0.2862$$

$$A_3 = 0.0527$$

$$A_4 = -0.00352$$

Calculate the melt viscosity at $\dot{\gamma} = 500\text{ s}^{-1}$ and $T = 260\text{ }^{\circ}\text{C}$.

According to Eq. 3.43, $a_T = 0.553$ for $X = 0.2$ and $T = 260\text{ }^{\circ}\text{C}$.

Using this value, the viscosity η for $X = 0.2$ follows from Eq. 3.42:

$$\eta = 97.3\text{ Pa}\cdot\text{s}$$

Comparisons between experiments and calculations are shown in the Figs. 3.28 and 3.29.

Equations for the die swell can be derived on the basis of measurements on filled melts with variable fiber content, as shown in Fig. 3.30 in a similar manner as above.

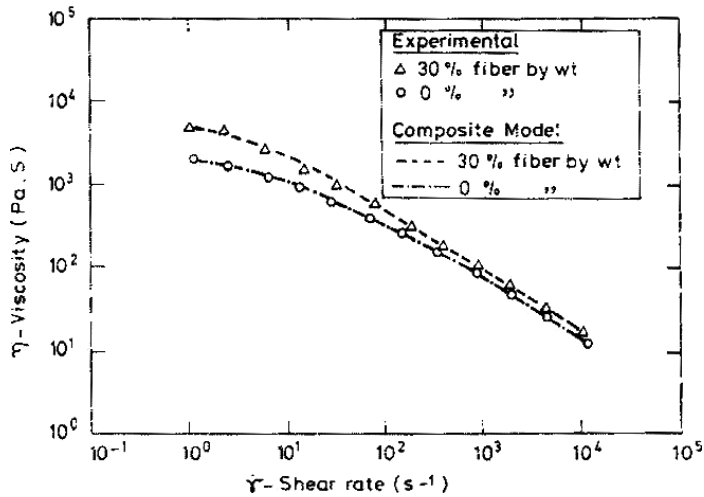


Figure 3.28 Comparison between experiment and prediction ($T = 200\text{ }^{\circ}\text{C}$)

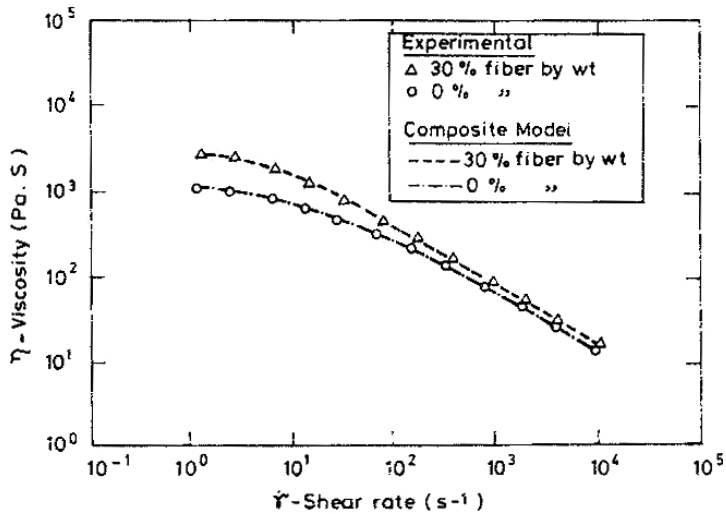


Figure 3.29 Comparison between experiment and prediction ($T = 240\text{ }^{\circ}\text{C}$)

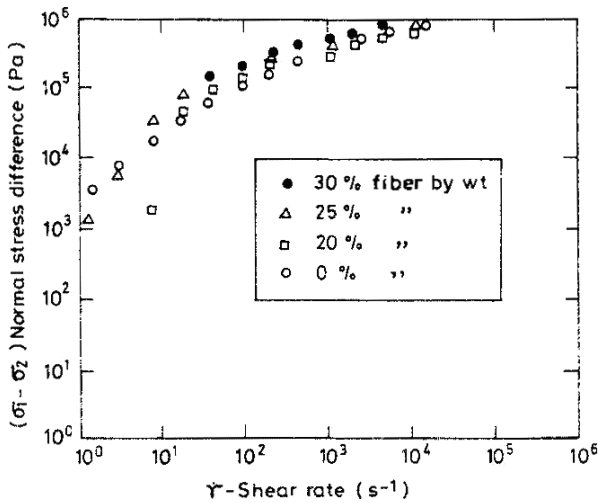


Figure 3.30 Normal stress difference vs. shear rate at $T = 200\text{ }^{\circ}\text{C}$

3.10.5 Summary

The shear viscosities of polypropylene melts with variable glass-fiber content were measured with a high pressure capillary rheometer. On the basis of these results, a single explicit relationship for the shift factor as a function of the fiber content and temperature has been developed. Using the viscosity function at a reference temperature, the viscosity of the filled melt can be predicted with this equation for the shift factor at any temperature and shear rate. The method of calculation presented can be applied to any thermoplastic material with filler.

■ 3.11 Practical Computational Rheology Primer

3.11.1 Introduction

Unlike other primers on rheology, this primer focuses on easily applicable calculation procedures for obtaining rheological resin process data required for optimizing blown film, cast film, and extrusion coating processes. Starting from laboratory measurements of rheological properties measured with a capillary rheometer and cone and plate rheometer, it is shown how, by using simple rheology equations, the process related melt flow data can be derived from these physical measurements. This data pertains to process relevant viscoelastic values, such as melt shear and

elongational viscosity, dynamic moduli, shear compliance, entrance pressure, and die swell. Correlations between these quantities and resin behavior in film making and extrusion coating are described. The use of the rheology formulas treated is illustrated by numerous practical examples.

Analogous to the ideal elastic solids, there exists a linear relationship between stress and strain in the case of Newtonian fluids (Fig. 3.31). Macromolecular fluids, such as thermoplastic melts, exhibit significant non-Newtonian behavior. This is noticed in the marked decrease of the melt viscosity when the melt is subjected to shear or tension, as shown in Fig. 3.32 [31]. The flow of melt in the channels of dies and machines used for polymer processing is normally shear flow. Therefore, knowledge of laws of shear flow is, first of all, necessary for designing and optimizing polymer machinery. In addition to shear flow, this primer presents practical formulas for extensional flow and viscoelastic properties, which are required for describing the interaction between the resin and the processing machine.

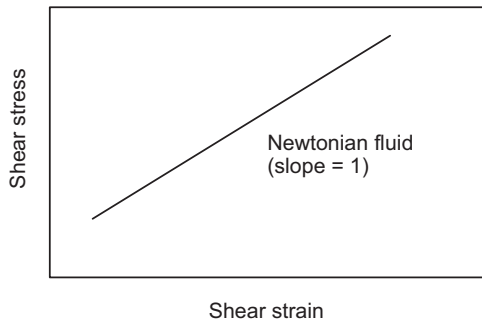


Figure 3.31 Flow curve of Newton fluid (logarithmic coordinates)

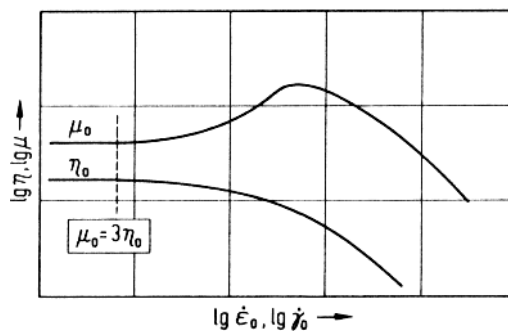


Figure 3.32 Extensional viscosity and shear viscosity of a polymer melt as a function of strain rate [31]

3.11.2 Shear Flow

3.11.2.1 Relationship between Flow Rate and Pressure Drop

To illustrate the behavior of polymer melt flow, the flow curves, in which the flow rate is plotted against die pressure, are given for water and LDPE in Fig. 3.33. The diameter and length of the nozzle used are 1 mm and 30 mm, respectively. Figure 3.33 shows that the flow rate of water increases linearly with the pressure, whereas in the case of LDPE, the increase is exponential. To put it in numbers, increasing pressure of water tenfold would bring forth a tenfold flow rate. A tenfold pressure of LDPE, however, leads to about five hundredfold flow rate. The flow of the melt is indeed viscous, but pressure changes are accompanied by much larger changes in output. The relation between volume flow rate and pressure drop of the melt in a die can be expressed in the general form [33]

$$\dot{Q} = K \cdot G^n \cdot \Delta p^n \quad (3.44)$$

where \dot{Q} = volume flow rate
 G = die constant
 Δp = pressure difference
 K = factor of proportionality
 n = power law exponent

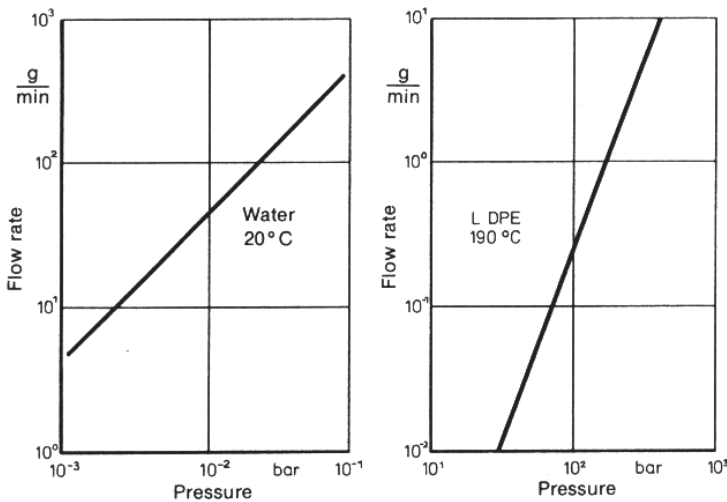


Figure 3.33 Flow curves of water and LDPE [32]

The power law exponent n is illustrated in Fig. 3.34 [34], in which the shear rate $\dot{\gamma}$ in a capillary is plotted as a function of shear stress τ . This curve can be represented by the equation

$$\dot{\gamma} = K\tau^n \quad (3.45)$$

The approximate ranges of shear rates for different methods of polymer processing are shown in Fig. 3.35 [35].

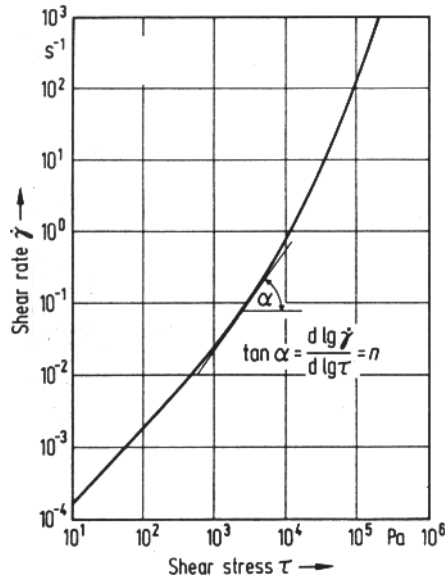


Figure 3.34 Determination of the power law exponent n in the Eq. 3.45 [34]

The power law exponent n in Eq. 3.44 can be calculated from

$$\frac{1}{n} = 1 + a_1 + 2a_{11} \ln \dot{\gamma} + a_{12}T \quad (3.46)$$

where a_1 , a_{11} , and a_{12} are viscosity coefficients in the Klein viscosity model and T the melt temperature in $^{\circ}\text{F}$ [36].

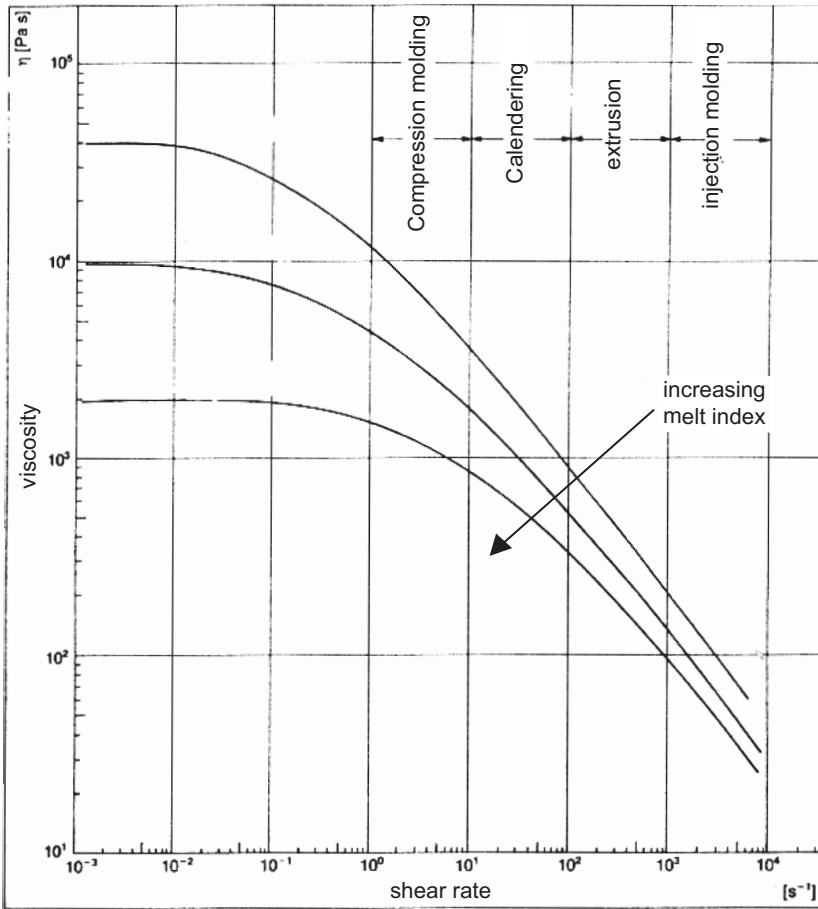


Figure 3.35 Ranges of shear rates for different methods of processing for LDPE [35]

The exponent n is given as a function of shear rate in Fig. 3.36 for LDPE [34]. This value for other materials can be obtained from the Eq. 3.46 by using the respective viscosity coefficients.

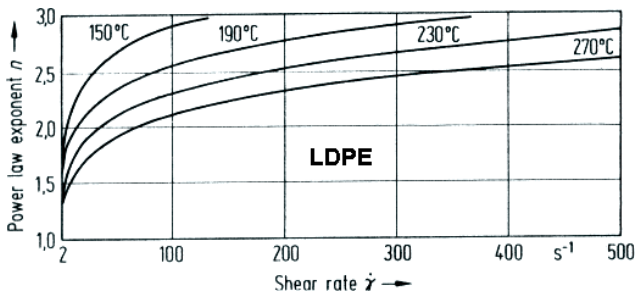


Figure 3.36 Power law exponent n as a function of shear rate $\dot{\gamma}$ and melt temperature T [34]

Choosing a value of $n = 2.7$ for LDPE, Eq. 3.44 can be written for a given die and processing conditions

$$\dot{Q} \sim \Delta p^{2.7} \quad (3.47)$$

Increasing the pressure by tenfold would increase the volume flow rate by about five hundredfold because $10^{2.7}$ equals 501.2.

3.11.2.2 Shear Rates for Blown Film and Extrusion Coating Dies

The formulas for calculating the shear rates in these dies are presented in the Table 3.4, and the channel shapes in Fig. 3.37 [37]. Other channel shapes can be taken into account by the formula developed by Schenkel [38].

Table 3.4 Shear Rates and Die Constants for Some Die Channel Shapes [37]

Channel shape	Shear rate $\dot{\gamma}$ [s ⁻¹]	Die constant G
Circle	$4\dot{Q} / \pi R^3$	$\left(\frac{\pi}{4}\right)^{\frac{1}{n}} \cdot \frac{R^{\frac{1}{n}+1}}{2L}$
Slit	$\frac{6\dot{Q}}{W \cdot H^2}$	$\left(\frac{W}{6}\right)^{\frac{1}{n}} \cdot \frac{H^{\frac{2}{n}+1}}{2L}$
Annulus	$\frac{6\dot{Q}}{\pi(R_o + R_i)(R_o - R_i)^2}$	$\left(\frac{\pi}{6}\right)^{\frac{1}{n}} \cdot \frac{(R_o + R_i)^{\frac{1}{n}} \cdot (R_o - R_i)^{\frac{2}{n}+1}}{2L}$
Triangle	$\frac{10}{3} \cdot \frac{\dot{Q}}{d^3}$	$\frac{1}{\sqrt{3}} \cdot \left(\frac{3}{10}\right)^{\frac{1}{n}} \cdot \frac{d^{\frac{3}{n}+1}}{2L}$
Square	$\frac{3}{0.42} \cdot \frac{\dot{Q}}{a^3}$	$\frac{1}{2} \left(\frac{0.42}{3}\right)^{\frac{1}{n}} \cdot \frac{a^{\frac{3}{n}+1}}{2L}$

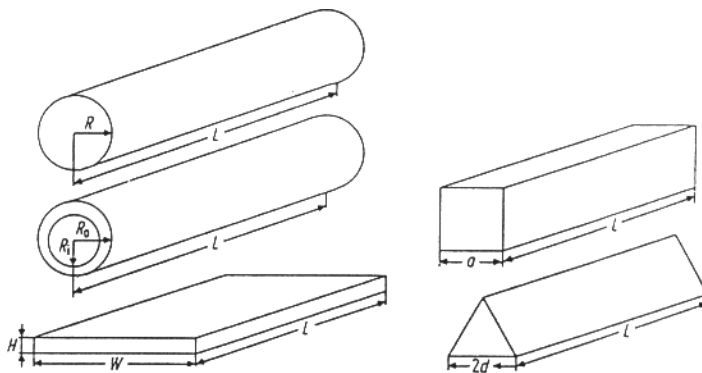


Figure 3.37 Common shapes of flow channels in extrusion dies [34]

The following examples illustrate the use of the formulas just given:

Example 1. What is the shear rate of a LDPE melt at 200 °C flowing through a round channel of 25 mm diameter at a mass flow rate of $\dot{m} = 36$ kg/h with a melt density of $\rho_n = 0.7$ g/cm³?

Solution: Volume shear rate $\dot{Q} = \dot{m} / \rho_n = 1.429 \cdot 10^{-5} \text{ m}^3/\text{s}$
 Shear rate $\dot{\gamma} = 4\dot{Q} / (\pi R^3) = 9.361 \text{ s}^{-1}$

Example 2. Melt flow through an annulus of a blown film die with an outside radius $R_o = 40$ mm and an inside radius $R_i = 39$ mm. The resin is LDPE with the same viscosity as above. Mass flow rate and the melt temperature remain the same.

Solution: Volume shear rate $\dot{Q} = \dot{m} / \rho_n = 1.429 \cdot 10^{-5} \text{ m}^3/\text{s}$
 Shear rate $\dot{\gamma} = 6\dot{Q} / (\pi(R_o + R_i)(R_o - R_i)^2) = 345.47 \text{ s}^{-1}$

Example 3. For the same conditions above it is required to calculate the shear rate when the melt flows through a slit of width $W = 75$ mm and height $H = 1$ mm of an extrusion coating die.

Solution: Shear rate $\dot{\gamma} = 6\dot{Q} / (WH^2) = 1143.2 \text{ s}^{-1}$

The calculated shear rates in different dies enable the ability to obtain the shear viscosity from the plot η vs. $\dot{\gamma}$, which then can be used in a comparative study of the resin behavior.

Example 4. Calculation of the pressure drop Δp for the conditions given in Example 2. Using the Klein model [36]

$$\ln \eta = a_0 + a_1 \ln \dot{\gamma} + a_{11} \ln \dot{\gamma}^2 + a_2 T + a_{22} T^2 + a_{12} T \ln \dot{\gamma}$$

with viscosity coefficients [36]

$$a_0 = 3.388, a_1 = -0.635, a_{11} = -0.01815$$

$$a_2 = -0.005975, a_{22} = -0.0000025, a_{12} = 0.0005187$$

η at $\dot{\gamma} = 9.316 \text{ s}^{-1}$ is found to be $\eta = 4624.5 \text{ Pa}\cdot\text{s}$ with $T = 392$ °F. The power law exponent n follows from Eq. 3.46

$$n = 2.052.$$

Shear stress

$$\tau = \eta \cdot \dot{\gamma} = 43077 \text{ N/m}^2.$$

Factor of proportionality K in Eq. 3.44 from Eq. 3.45

$$K = 28824 \cdot 10^{-9}.$$

Die constant

$$G_{\text{circle}} = \left(\frac{\pi}{4} \right)^{\frac{1}{2.052}} \frac{0.0125^{\frac{3}{2.052} + 1}}{2 \cdot 0.1} = 9.17 \cdot 10^{-5}$$

Finally,

$$\Delta p = \frac{(1.429 \cdot 10^{-5})^{\frac{1}{2.052}}}{(2.8824 \cdot 10^{-9})^{\frac{1}{2.052}} \cdot 9.17 \cdot 10^{-5}} = 6.845 \text{ bar}$$

3.11.2.3 Extensional Flow

Extensional flow plays a great role in the bubble formation in blown film. As seen from Fig. 3.32, it is three times larger than the shear viscosity at zero shear rate. It is defined as

$$\mu = \sigma / \dot{\epsilon} \quad (3.48)$$

$$\dot{\epsilon} = \frac{1}{l} \times \frac{dl}{dt} \quad (3.49)$$

where l = length,
 t = time.

3.11.2.4 Melt Elasticity

Whereas the melt flow can be described by the shear viscosity, the melt elasticity is characterized by a number of quantities depending on the type of measuring equipment used. These can be summarized as

- normal stress coefficient,
- shear compliance,
- complex dynamic moduli,
- die swell, and
- entrance pressure loss.

Normal stress coefficient. The components of stress acting on a volume element of the melt in simple shear are shown in Fig. 3.38(A). The cone and plate rheometer for calculating the normal stress difference $\sigma_{11} - \sigma_{22}$ is shown in Fig. 3.38(B) [39]. The normal stress coefficient is defined as

$$\Theta = (\sigma_{11} - \sigma_{22}) / \dot{\gamma}^2 \quad (3.50)$$

and its limiting value, the zero normal stress coefficient Θ_0 , is given by

$$\Theta_0 = \lim_{\dot{\gamma} \rightarrow 0} \Theta(\dot{\gamma}) \quad (3.51)$$

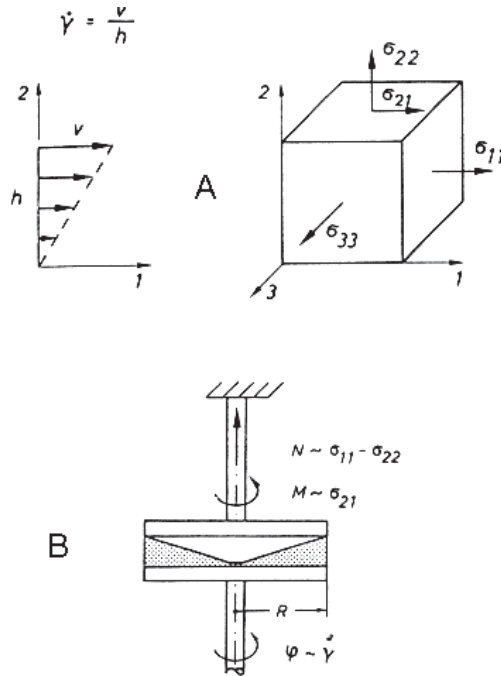


Figure 3.38 A: Stress acting on a volume element in simple shear flow; B: cone and plate rheometer [39] (N : normal force, M : torque, R : Radius, φ : angular speed, $\dot{\gamma}$: shear rate)

Shear compliance. The shear compliance is defined as

$$J_e = \gamma_r / \sigma_{21} \quad (3.52)$$

where γ_r = reversible shear.

The value of the shear compliance at small shear rates is denoted as the steady state shear compliance

$$J_e^0 = \lim_{\dot{\gamma} \rightarrow 0} J_e(\dot{\gamma}) \quad (3.53)$$

The relationship combining the elastic properties treated above and the zero shear viscosity η_0 is represented as

$$J_e^0 = \frac{\Theta_0}{2\eta_0^2}$$

Figure 3.39 shows these properties as a function of the molar mass for the polyamide melts. Neck-in of the web in extrusion coating can be correlated with the normal stress coefficient [9] and draw-down with the extensional viscosity [40].

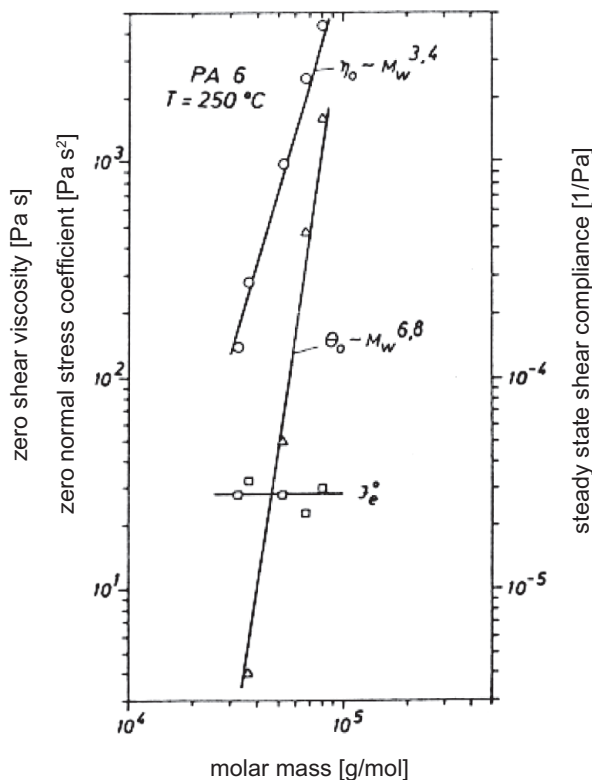


Figure 3.39 Zero viscosity η_0 , zero normal stress Θ_0 , and steady state shear compliance J_e^0 for 6-polyamides of similar molecular weight distributions [39]

Dynamic moduli. The storage modulus $G'(\omega)$ characterizes the elastic behavior, whereas the loss modulus $G''(\omega)$ depicts the viscous behavior of the melt subjected to periodic shear deformation (Fig. 3.40). Formulas giving the relationship between storage modulus and shear compliance, and zero shear viscosity and loss modulus, are given in the book [34].

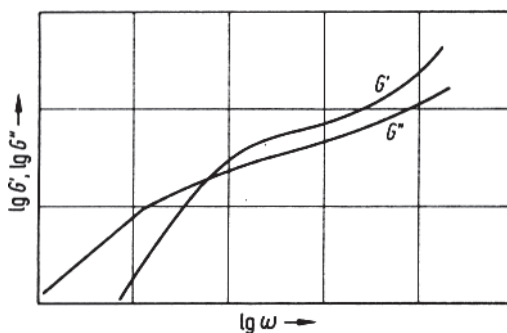


Figure 3.40 Storage modulus G' and loss modulus G'' as functions of frequency [34]

Die swell. Elastic effects are responsible for the die swell, which occurs when the melt flows through a die, as shown in Fig. 3.41 [39]. Figure 3.41 gives the die swell for two polypropylenes having different distributions of the molar mass [39].

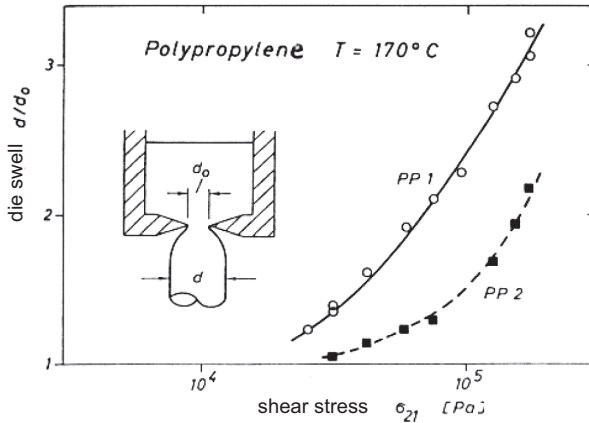


Figure 3.41 Die swell for two polypropylene melts of different molecular weight distributions [39]

Entrance pressure loss. Another important quantity resulting from elongational flow as shown in Figure 3.42 is the entrance pressure loss p_c , which can be calculated empirically by means of the formula [34]

$$p_c = c\tau^m \quad (3.54)$$

where c and m are resin-dependent constants.

The pressure p_c can be read from the Bagley plot.

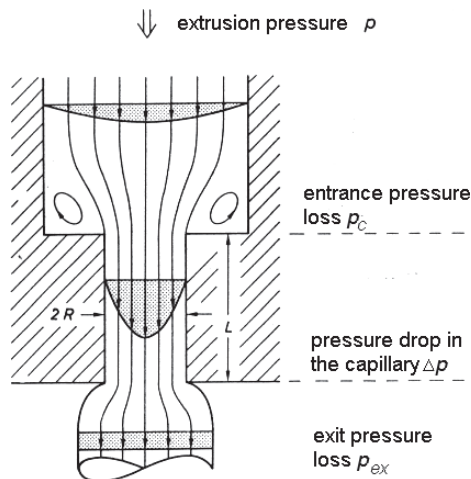


Figure 3.42 Flow through a capillary [39]

■ 3.12 Conclusions

Polymer machinery can be designed sufficiently accurate on the basis of the relationships for viscous shear flow alone. However, elastic effects play a significant role in processes, such as blown film and extrusion coating. This overview summarizes some important practical formulas for shear flow and melt elasticity, which are useful for characterizing the behavior of the resin with respect to the process. Worked-out examples illustrate the application of the equations treated.

■ 3.13 References

- [1] *Birley, A. W., Haworth, B., Bachelor, T.*: Physics of Plastics, Hanser, Munich, 1991
- [2] *Rao, N. S.*: Design Formulas for Plastics Engineers, Hanser, Munich, 1991
- [3] *Rigby, R. B.*: Polyethersulfone in Engineering Thermoplastics: Properties and Applications, Ed. James M. Margolis, Marcel Dekker, Basel, 1985
- [4] *Münstedt, H.*: Berechnen von Extrudierwerkzeugen, VDI-Verlag, Düsseldorf, 1978
- [5] *Rao, N. S.*: Designing Machines and Dies Polymer Processing, Hanser, Munich, 1981
- [6] *Rauwendaal, C.*: Polymer Extrusion, Hanser, Munich, 1986
- [7] *Ogorkiewicz, R. M.*: Thermoplastics Properties and Design, John Wiley, New York, 1973
- [8] *Avenas, P., Agassant, J.F., Sergent, J.P.*: La Mise en Forme des Matières Plastiques, Technique & Documentation (Lavoisier), Paris, 1982
- [9] *Hertlein, T., Fritz, H. G.*: Kunstst. 78, p. 606, 1988
- [10] *Laun, H. M.*: Progr. Colloid & Polymer Sci., v. 75, p. 111, 1987
- [11] *Carley, J. F.*: ANTEC 84, p. 439, 1984
- [12] CAMPUS Databank
- [13] *Rao, N. S., O'Brien, K. T., Harry, D. H.*: Computer Modeling for Extrusion and other Continuous Polymer Processes, Ed. Keith T. O'Brien, Hanser, Munich, 1992
- [14] *Laun, H. M.*: Rheol. Acta 18, p. 478, 1979
- [15] BASF Brochure: Kunststoff-Physik im Gespräch, 1977
- [16] *Harris, J. E.*: Polysulfone in Engineering Thermoplastics: Properties and Applications, Ed. James M. Margolis, Marcel Dekker, Basel, 1985
- [17] *Geiger, K.*: Private Communication
- [18] *Rosato, D. V., Rosato, D. V.*: Plastics Processing Data Handbook, Van Nostrand Reinhold, New York, 1990
- [19] *Eyring, H.*: I. Chem. Phys. 4, p. 283, 1963
- [20] *Prandtl, L.*: Phys. Blätter 5, p. 161, 1949
- [21] *Ostwald, W.*: Kolloid-Z. 36, p. 99, 1925
- [22] *de Waele, A.*: Oil and Color Chem. Assoc. J. 6, p. 33, 1923
- [23] *Carreau, P.J.*: Dissertation, Univ. Wisconsin, Madison, 1968

- [24] *Bernhardt, E. C.*: Processing of Thermoplastic Materials, Reinhold, New York, 1963
- [25] *Klein, I., Marshall, D. I., Friehe, C. A.*: SPE J. 21, p. 1299, 1965
- [26] *Wagner, M. H.*: Dissertation, Univ. Stuttgart, 1976
- [27] *Fischer, E.*: Dissertation, Univ. Stuttgart, 1983
- [28] *Muenstedt, H.*: Kunstst. 68, p. 92, 1978
- [29] *Rao, N. S.*: Design Formulas for Plastics Engineers, Hanser, Munich, 1991
- [30] *Nanguneri, S. R. et al.*: Rheological Characteristics of glass-fiber-filled polypropylene melts, Rheologica Acta 26, p. 301, 1987, and the literature referred to within
- [31] *Laun, H. M.*: Progr. Colloid & Polymer Sci. 75, p. 111, 1987
- [32] *Rao, N. S.*: Berechnen von Extrudierwerkzeugen, VDI-Verlag, Düsseldorf, 1978
- [33] *Procter, B.*: SPE J. 28, p. 34, 1972
- [34] *Rao, N. S.*: Design Formulas for Plastics Engineers, Hanser, Munich, 1991
- [35] BASF Brochure: Kunststoff-Physik im Gespräch, 1977
- [36] *Klein, I., Marschall, D. I., Friehe, C. A.*: SPE J. 21, p. 1299, 1965
- [37] *Rao, N. S., O'Brien, K.*: Design Data for Plastics Engineers, Hanser, Munich, 1998
- [38] *Schenkel, G.*: Private Communication
- [39] *Laun, H. M.*: Kautschuk, Gummi + Kunststoffe 6, p. 554, 1987
- [40] *Oveby, C., Clevenhag, P.*: Nordic Rheology Conference 1997, Reykjavik, 1997

4

Electrical Properties

The use of plastics in the electrical industry as insulators for wire and cable insulation is well known. The application of engineering resins to make miniature electric components, printed circuit boards, conductive housings of computer equipment, and the like, although not so well known, is increasing. Some of the electrical properties that are of importance in selecting a resin for these applications are treated in this chapter.

■ 4.1 Surface Resistivity

Surface resistivity is defined as the ratio of electrical field strength to the current density in a surface layer of an insulating material. It is the measure of a material's ability to resist the flow of current along its surface when a direct voltage is applied between surface mounted electrodes of unit width and unit spacing. The unit of surface resistivity is ohm [1, 3].

■ 4.2 Volume Resistivity

Volume resistivity is the volume resistance reduced to a cubical unit volume of the material. Volume resistance is the ratio of the direct voltage applied to the electrodes in contact with the test material, to the steady-state current flowing between them [1, 3]. The unit of volume resistivity is ohm · m ($\Omega \cdot m$) or ohm · cm ($\Omega \cdot cm$).

■ 4.3 Dielectric Strength

Dielectric strength is the measure of the electrical breakdown resistance of a material under an applied voltage [1]. It is the ratio of the voltage reached just before breakdown to the material's thickness and is expressed as kV/mm or MV/m. Dielectric strength data for some materials are given in Table 4.1.

Table 4.1 Dielectric Strength Data for Plastics (Method ASTM D149) [6]

Material	Dielectric strength kV/25 μm
PE-LD	> 700
PE-HD	> 700
PP	800
PVC	300
PS	500
ABS	400
PC	350
POM	700
PA 6	350
PA 66	400
PMMA	300
PET	500
PBT	500

■ 4.4 Relative Permittivity

Relative permittivity (ϵ_R), formerly known as dielectric constant, is the ratio of capacitance (C) of a given configuration of electrodes with the plastics material as the dielectric medium, to the capacitance (C_v) of the same configuration of electrodes with vacuum as the dielectric [1, 3].

$$\epsilon_R = \frac{C}{C_v} \quad (4.1)$$

The performance of plastics as insulators increases with decreasing relative permittivity.

■ 4.5 Dielectric Dissipation Factor or Loss Tangent

Dielectric dissipation factor is the ratio of the electrical power dissipated in a material to the total power circulating in the circuit. It is the tangent of the loss angle (δ) and is analogous to $\tan \delta$, which is the ratio between the loss and storage moduli described in Section 3.11.2.4. A low dissipation factor is important for plastics insulators in high frequency applications such as radar and microwave equipment. Relative permittivity and the dissipation factor are dependent on temperature, moisture, frequency, and voltage [3]. Typical values of volume resistivity, relative permittivity, and loss tangent are given in Table 4.2 for some polymers [1, 5] (see also Fig. 4.1 [2]).

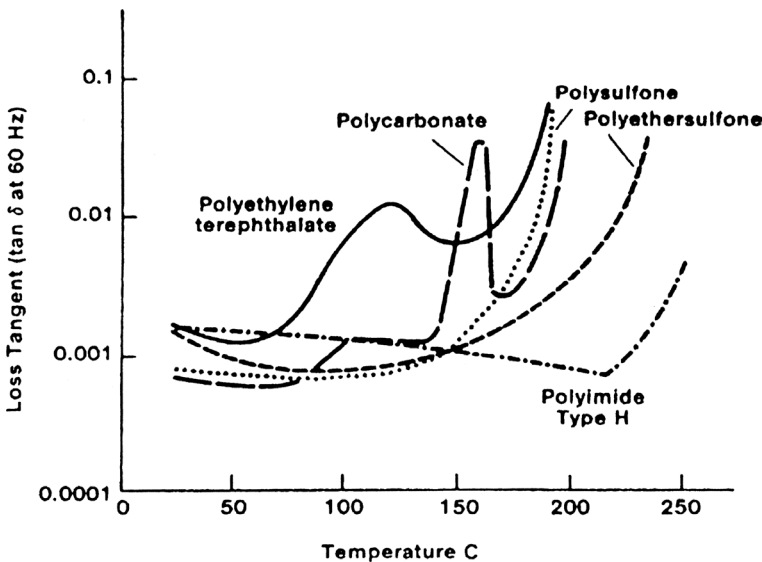


Figure 4.1 Loss tangent as a function of temperature for some engineering thermoplastics [2]

Table 4.2 Typical Values of Volume Resistivity, Relative Permittivity, and Loss Tangent [1, 5]

Material	Volume resistivity ohm \times cm	Relative permittivity at 50 Hz	Dielectric dissipation factor or loss tangent $\tan \delta \times 10^4$ at 20 °C and 1 MHz
PE-LD	10^{17}	2.3	1.2
PE-HD	10^{17}	2.35	2
PP	10^{17}	3.5	400
PVC	10^{15}	2.27	230
PS	10^{17}	2.5	1

Table 4.2 Typical Values of Volume Resistivity, Relative Permittivity, and Loss Tangent [1, 5]
(Continued)

Material	Volume resistivity ohm \times cm	Relative permittivity at 50 Hz	Dielectric dissipation factor or loss tangent $\tan \delta \times 10^4$ at 20 °C and 1 MHz
ABS	10^{15}	2.9	200
PC	10^{17}	3	7
POM	10^{15}	3.7	50
PA 6	10^{12}	3.8	300
PA 66	10^{12}	8.0	800
PMMA	10^{15}	3.3	40
PET	10^{16}	4.0	200
PBT	10^{16}	3.0	200

■ 4.6 Comparative Tracking Index (CTI)

Comparative tracking index indicates a plastics material's ability to resist development of an electrical conducting path when subjected to current in the presence of a contaminating solution [1, 3]. Contaminants, such as salt and moisture, allow increased conduction over the surface, which may lead to tracking, which is the appearance of conducting paths over the surface. The deterioration of the surface quality is hence the cause of failure of high voltage insulation systems [1]. The CTI is given in terms of maximum voltage, at which no failure occurs, according to different test procedures. Typical values of CTI are given in Table 4.3 [5].

Table 4.3 Typical Values of Comparative Tracking Index [5]

Material	Test method KB
PE-LD	> 600
PE-HD	> 600
PP	> 600
PVC	600
PS	200
ABS	300
PC	> 600
POM	> 600
PA 6	> 600
PA 66	> 600
PMMA	> 600
PBT	450

Owing to their high electrical resistance, plastics retain electrostatic charge, which leads to undesirable effects, such as marked attraction of dust or the creation of discharges when the material comes into contact with other surfaces. This situation can be alleviated by using antistatic agents in the polymer formulation. Polymers with intrinsic electrical conductivity can also be used as antistatic coatings [1].

In addition to the properties treated in the foregoing sections, the optical properties of plastics products, such as transparency and gloss of films, play an important role in selecting a resin in applications where these properties are required. The test procedures to measure the optical properties are treated in [1].

A list of properties for which data can be obtained from the resin manufacturers, for example, on CAMPUS computer disks, is presented in Table 4.4. Example of material data used as input to the software VISMELT [4] for designing extruders is given in Table 4.5.

Table 4.4 List of Properties Obtainable from Resin Manufacturers

Mechanical properties	Thermal properties	Electrical properties	Optical properties	Rheological properties
Tensile strength	Material density	Dielectric strength	Comparative Tracking Index (CTI)	Melt Flow Rate (MFR)
Tensile elongation	Bulk density	Surface resistivity	Light transmission	Melt Volume Rate (MVR)
Tensile modulus	ρ - v - T diagrams	Volume resistivity	Refractive Index	Shear viscosity as a function of shear rate and temperature of melt
Flexural strength	Specific heat	Relative permittivity		
Flexural modulus	Enthalpy	Dielectric dissipation factor or loss tangent		
Compressive strength	Thermal conductivity			
Hardness	Vicat temperature			
Abrasion	HDT (Heat distortion temperature)			
Izod impact strength	Flammability UL 94 rating LOI (Limiting Oxygen Index)			

Table 4.5 Example of Input Data to the Software Design Package VISMELT [4]

Type of Polymer:	PE-HD				
Trade name of polymer:	HOECHST GM 9255 F				
thermal properties:					
melting point	TM	=	130.0 Grad Celsius		
specific heat of melt	CPM	=	2.51 kJ / (kg K)		
specific heat of solid	CPS	=	2.30 kJ / (kg K)		
thermal conductivity of melt	KM	=	.2700 W / (m K)		
thermal conductivity of solid	KS	=	.2800 W / (m K)		
heat of fusion	LAM	=	200.000 kJ / kg		
density of melt	RHOM	=	.78 g / cm**3		
density of solid	RHOS	=	.9430 g / cm**3		
bulk density	RHOSO	=	.40 g / cm**3		
Viscosity coefficients:					
Carreau-coefficients:					
A	=	28625. Pa s	B	=	.7126 s
C	=	.6535			
T0	=	200.0 Grad Celsius			
b	=	2447. K			
Münstedt-coefficients:					
A0	=	4.2410	A1	=	-.01304
A2	=	-.55251	A3	=	.222252
A4	=	-.033758			
T0	=	200.0 Grad Celsius			
b	=	2425. K			
Klein-coefficients:					
A0	=	.653721E+01	A1	=	-.722213E+00
A11	=	-.989580E-02	A2	=	-.213261E-01
A22	=	.204288E-04	A12	=	.473881E-03
Power law coefficients:					
NR	=	.4022			
BETA	=	.003919 1/Grad Celsius	KOR	=	60889. N s**n / m**2

■ 4.7 References

- [1] *Birley, A. W., Haworth, B., Bachelor, T.*: Physics of Plastics, Hanser, Munich, 1991
- [2] *Rigby, R. B.*: Polyethersulfone in Engineering Thermoplastics: Properties and Applications, Ed. James M. Margolis, Marcel Dekker, Basel, 1985
- [3] General Electric Plastics Brochure: Engineering Materials Design Guide
- [4] *Rao, N. S., O'Brien, K. T., Harry, D. H.*: Computer Modeling for Extrusion and other Continuous Polymer Processes, Ed. Keith T. O'Brien, Hanser, Munich, 1992
- [5] BASF Brochure: Kunststoff-Physik im Gespräch, 1977
- [6] *Dominghaus, H.*: Plastics for Engineers, Hanser, Munich, 1993

5

Optical Properties of Solid Polymers

■ 5.1 Light Transmission

The intensity of light incident on the surface of a plastic is reduced as the light enters the plastic because some light is always reflected away from the surface. The intensity of light entering the plastic is further reduced as the light passes through the plastic since some light is absorbed, or scattered, by the plastic. The luminous transmittance is defined as the percentage of incident light that is transmitted through the plastic. For comparison purposes the exact test parameters are documented in ASTM D 1003. Some typical light transmission values for the most common optical plastics are presented in Table 5.1. Light transmission is a measurement of the transparency of a plastic.

Table 5.1 Light Transmission or Luminous Transmittance of Some Common Optical Plastics

Material	Luminous transmittance D 1003
ABS	85
PC	89
PMMA	92
PMMA/PS	90
PS	88
SAN	88

■ 5.2 Haze

Haze is defined as the percentage of transmitted light which deviates from the incident light beam by more than 2.5 degrees. Its measurement is also defined by ASTM D 1003. Some typical haze values are presented in Table 5.2 for the most common optical plastics. Haze is a measure of the clarity of a plastic.

Table 5.2 Haze of Some Common Optical Plastics

Material	Haze
ABS	10
PC	1 – 3
PMMA	1 – 8
PMMA/PS	2
PS	3
SAN	3

■ 5.3 Refractive Index

The refractive index n of an isotropic material is defined as the ratio of the speed of light in the material v to the speed of light in vacuum c , that is,

$$n = v/c$$

The speed of light in vacuum is 300,000 km/s. The refractive index decreases as the wavelength of the light increases. Therefore, the refractive index is measured and reported at a number of standard wavelengths, or atomic emission spectra (AES) lines, as indicated in Table 5.3.

Table 5.3 Refractive Indices as Functions of Wavelength

AES line	Wavelength	PMMA	PS	PC
F	486 nm	1.497	1.607	1.593
D	589 nm	1.491	1.590	1.586
C	651 nm	1.489	1.584	1.576

The refractive index is usually measured using an Abbe refractometer according to ASTM D542. The Abbe refractometer also measures the dispersions, which is required for lens design. An extensive list of refractive indices is provided in Table 5.4. Since the speed of light in the polymer v is a function of the density, polymers which exhibit a range of densities also exhibit a range of refractive indices. Since density is a function of crystallinity, the refractive index is dependent on whether the polymer is amorphous or crystalline, and on its degree of crystallinity. Since density is also a function of temperature, decreasing as temperature increases, the refractive index also decreases with increasing temperature.

Table 5.4 Refractive Indices of Some Plastics as Functions of Density [1]

Polymer	Refractive index n_D^{20}	Density kg/m ³	Transparency
PE-LD	1.51	914/928	transparent
PE-HD	1.53	940/960	opaque
PP	1.50/1.51	890/910	transparent/opaque
PVC	1.52/1.55	1380/1550	transparent/opaque
PS	1.59	1050	transparent
PC	1.58	1200	transparent
POM	1.48	1410/1420	opaque
PA 6	1.52	1130	transparent/opaque
PA 66	1.53	1140	transparent/opaque
PMMA	1.49	1170/1200	transparent
PET	1.64	1380	transparent/opaque

■ 5.4 Gloss

Surface gloss is the percentage of light intensity reflected relative to that reflected by an ideal surface. Also called specular reflectance or specular gloss, the gloss is measured within a specific angular range of the ideal reflected angle. It is then compared to a standard, polished black glass with a refractive index of 1.567, which possesses a specular gloss of 100%. The gloss reduces rapidly as the surface roughness increases. The specular gloss is measured according to ASTM D 523-80.

■ 5.5 Color

Color may be measured using tristimulus colorimeters (i.e., colorimeters), or spectrophotometers (i.e., spectrocolorimeters). These instruments measure color by illuminating a sample and collecting the reflected light. Colorimeters use filters to simulate the color response of the eye. They are used for quick and simple measurements of color differences. Spectrocolorimeters measure color as a certain wavelength of light. The color is reported as three numbers. The *L*-value measures the grayness, with pure white scoring 100 and pure black scoring 0. The *a*-value measures the redness when positive and the greenness when negative. The *b*-value

measures the yellowness when positive and the blueness when negative. So from the L , a , and b values a color can be defined.

■ 5.6 References

- [1] *Dominghaus, H.*: Plastics for Engineers, Hanser, Munich, 1993

6

External Influences

Plastics parts are often used in an environment in which an interaction between the polymer and a fluid like water, gas, or organic liquids can take place. This may lead to deterioration or even failure of the part. Furthermore, plastics used in certain applications, as in packaging foodstuffs, should be resistant to the entry of oxygen or moisture, so that the contents do not deteriorate during the prescribed time span.

The behavior of polymers under external influences is dependent on the combination of polymer and fluid, exposure time, temperature, stress level, and processing history [1]. The properties of polymers which manifest themselves under external effects are the topic of this chapter.

■ 6.1 Physical Interactions

6.1.1 Solubility

Most thermoplastics have a solubility parameter [1, 3]. Common solvents are paraffins, ethers, ketones, alcohols, and chlorinated organic liquids. The solvation leads to swelling, weight, and dimensional changes, together with property loss.

6.1.2 Environmental Stress Cracking (ESC)

ESC is a failure mechanism that occurs under conditions when an external or residual stress is imposed on the part that is in contact with an external environment such as liquid or vapor. It is the combination of stress and the liquid medium what gives rise to premature failure. The failure is initiated by microcrazing, into which the aggressive liquid or vapor penetrates [1]. The term ESC is applied to amorphous polymers, whereas in the case of crystalline polymers the failure is denoted as stress corrosion failure.

One of the standard ESC tests is the Bell Telephone technique in which bent strips of material containing a defect are totally immersed in a chemical medium before being examined for visible signs of damage (Fig. 6.1) [1]. The environmental behavior of some plastics is presented in Figs. 6.2 [7] and 6.3 [4].

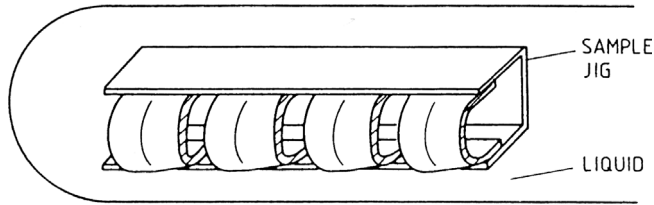


Figure 6.1 Bell test for determining ESC [1]

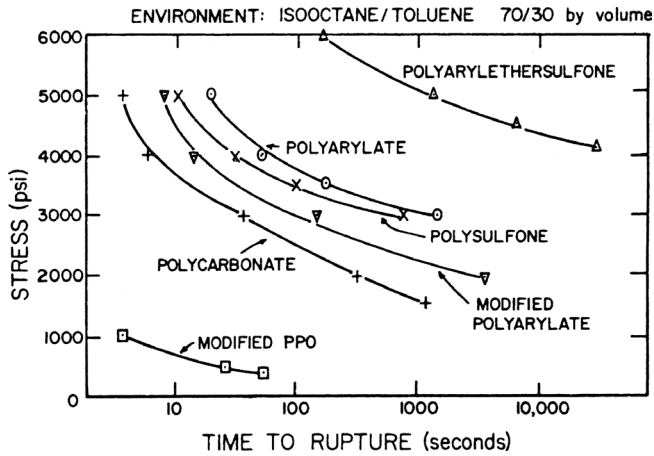


Figure 6.2 ESC resistance of polyarylate vs. other thermoplastics [7]

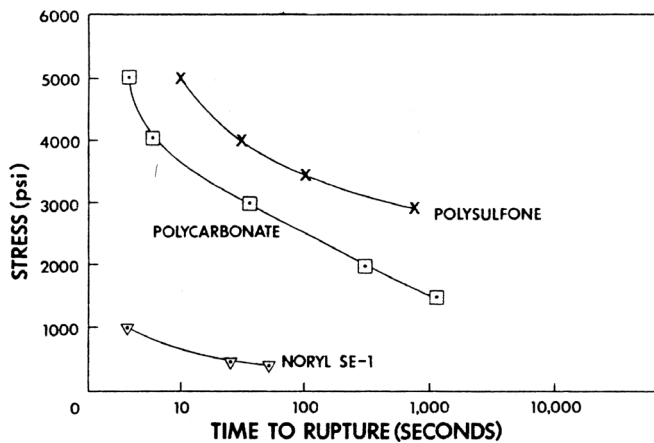


Figure 6.3 ESC rupture comparison of several engineering thermoplastics in a 70/30 isooctane/toluene mixture at 25 °C [4]

6.1.3 Permeability

Plastics are to some extent permeable to gases, vapors, and liquids. The diffusional characteristics of polymers can be described in terms of a quantity known as permeability.

The mass of the fluid permeating through the polymer at equilibrium conditions is given by [3]

$$m = \frac{P \cdot t \cdot A \cdot (p_1 - p_2)}{s} \quad (6.1)$$

where m = mass of fluid permeating [g]

P = permeability $\left[\frac{\text{g}}{\text{m} \cdot \text{s} \cdot \text{Pa}} \right]$

t = time of diffusion [s]

A = Area of the film or membrane [m^2]

p_1, p_2 = partial pressures on the side 1 and 2 of the film [Pa]

s = thickness of the film [m]

Besides its dependence on temperature, the permeability is influenced by the difference in partial pressures of the fluid and thickness of the film. Other factors that affect permeability are the structure of the polymer film such as crystallinity and type of the fluid.

Permeability is a barrier property of plastics and is important in applications like packaging. Permeation data for some resins is summarized in Table 6.1 [3].

Table 6.1 Relative Permeability of Various Polymers Compared to PVDC [3]

Polymer	Gas permeability			
	N_2	O_2	CO_2	H_2O (25 °C, 90% R. H.)
PVDC	1	1	1	1
PCTFE	3.19	10.64	2.48	0.21
PET	5.32	4.15	5.28	93
PA6	8.51	7.17	5.52	500
PVC-U	42.55	22.64	34.5	111
CA	298	147	235	5357
PE-HD	287	200	121	9.3
PE-LD	2021	1038	1214	57
PP	479	434	317	49
PS	309	208	303	857
Butyl Rubber	332	245	179	–
Polybutadiene	862	3604	4800	–
Natural Rubber	8600	4400	4517	–

One of the reasons for using PET for making bottles for carbonated drinks is that PET is relatively impermeable to carbon dioxide, as can be seen from Table 6.2 [3].

Table 6.2 Relative Permeability to CO₂ of Different Polymers Compared to PET [3]

Polymer	Relative permeability
PET	1
PVC-U	6.53
PP	60
PE-HD	23
PE-LD	230

6.1.4 Absorption and Desorption

The process by which a fluid is absorbed or desorbed by a plastics material is time-dependent, governed by its solubility and by the diffusion coefficient [3]. The period until the equilibrium value is reached can be very long. Its magnitude can be estimated by the half-life of the process given by

$$t_{0.5} = \frac{0.04919 s^2}{D} \quad (6.2)$$

where $t_{0.5}$ = half-life of the process
 s = thickness of the polymer assumed to be penetrated by one side
 D = diffusion coefficient

The value of $t_{0.5}$ for moisture in PMMA for $D = 0.3 \times 10^{-12}$ m²/s and $s = 3$ mm is

$$t_{0.5} = \frac{0.04919 \cdot 3 \cdot 3 \cdot 10^{-6}}{0.3 \cdot 10^{-12} \cdot 3600 \cdot 24} = 17.1 \text{ days}$$

when the sheet is wetted from one side only [3]. However, the equilibrium absorption takes much longer, as the absorption rate decreases with saturation.

6.1.5 Weathering Resistance

Weathering is the deterioration of the polymer under atmospheric conditions which by the action of oxygen, temperature, humidity, and above all, ultraviolet radiation on the resin lead to loss of properties and finally failure of the part. Performance data of the resin under weathering is supplied by resin makers (see also Table 6.3) [8].

Table 6.3 Ultraviolet, Thermal, and Biological Resistance of Some Plastics [8]

Polymer	Service temperature range °C	Ultraviolet resistance	Fungus resistance
Acetals	90/104	fair	excellent
Polyamides	-50/150	poor	excellent
PC	120	excellent	excellent
Polyethylene	75/100	poor	poor
Polypropylene	110	poor	excellent
PS	75	fair	excellent
Polysulfone	170	fair	excellent
PVC	55	poor	poor
Epoxy, aromatic	100/150	fair to good	poor
Epoxy, cycloaliphatic	100/150	excellent	poor
Polyurethanes	100/130	fair	poor
Silicones	260	excellent	excellent
Butyl rubber	-45/150	excellent	excellent

■ 6.2 Chemical Resistance

Good chemical resistance of polymers is of importance in many applications. Table 6.4 shows the performance of some polymers according to a rating when they are in direct contact with the chemical agents listed in the Table 6.3 [6].

Table 6.4 Chemical Resistance of Resin to Different Liquid Agents [6]

Polymer	Salt solution	Concentrated acids	Organic acids	Concentrated bases	Aliphatic hydrocarbons	Halogenated hydrocarbons	Aromatic hydrocarbon	Monovalent alcohols	Oils and greases	Ketones	Esters	Ethers
PE-LD	1	2	1	1	1	5	3	3	2	3	3	3
PE-HD	1	2	1	1	1	4	3	1	3	1	1	1
PVC-U	1	1	2	1	1	5	5	1	1	5	5	1
PMMA	1	3	5	3	1	5	5	5	1	5	5	5

Table 6.4 Chemical Resistance of Resin to Different Liquid Agents [6] (*Continued*)

Polymer	Salt solution	Concentrated acids	Organic acids	Concentrated bases	Aliphatic hydrocarbons	Halogenated hydrocarbons	Aromatic hydrocarbon	Monovalent alcohols	Oils and greases	Ketones	Esters	Ethers
PS	1	3	5	3	1	5	5	5	1	5	5	5
PA	1	5	4	5	1	4	1	1	1	1	1	1
PC	1	2	4	5	1	5	5	2	1	5	5	5
POM	1	5	1	1	1	1	2	1	1	3	5	1
PTFE	1	1	1	1	1	1	1	1	1	1	1	1

Rating: 1: resistant; 2: sufficiently resistant; 3: conditionally resistant; 4: mostly not resistant; 5: completely nonresistant

Data on chemical resistance of resins can be obtained from resin manufacturers.

6.2.1 Chemical and Wear Resistance to Polymers

As polymers are converted into products they contact the walls of the various machines in which they are converted. Such walls include barrel walls, the plasticating screw surfaces, the interior die surfaces, and the mold cavity surfaces. It is important that the correct materials be chosen for these surfaces or reduced performance and premature failure may arise. In the case of screws and barrels, the contacting surfaces must also exhibit wear resistance to each other.

One of the approaches is to select the barrel that provides the greatest resistance to corrosion and wear by particular plastic, including any additives, fillers, or reinforcements. Then to select a material for the screw flights which performs well against that particular barrel material, and finally to select a coating for the remaining surfaces of the screw which exhibits the greatest corrosion and wear resistance to the plastic.

■ 6.3 General Property Data

General property data for some plastics is presented in Tables 6.5 to 6.11. Some properties of the reinforced plastics are illustrated in Fig. 6.4 [5]. The comparability of different test methods is discussed in Table 6.12.

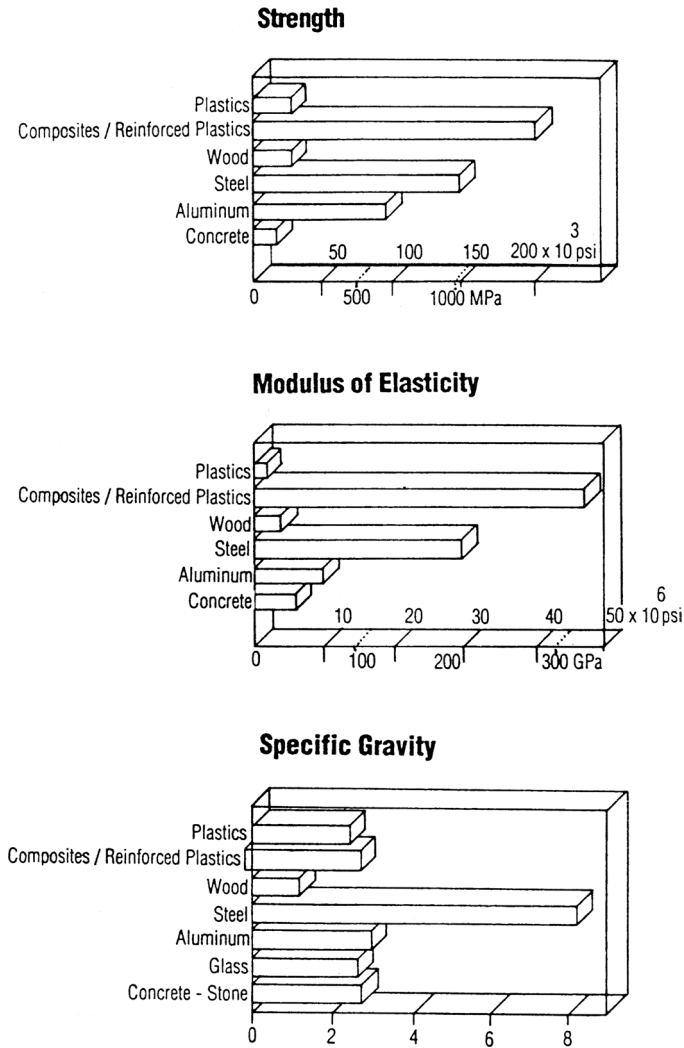


Figure 6.4 Reinforced plastics and composites vs. other materials [5]

Table 6.5 Polymer Parameters and Their Influence Properties [8]

	Density		Molecular weight		Molecular weight distribution	
	Increases	Decreases	Increases	Decreases	Broadens	Narrows
Environmental stress	-			-		-
Impact strength	-			-	-	
Stiffness	↑	↓	-	-	-	-
Hardness	↑	↓	-	-	-	-
Tensile strength		-	-	-	-	-
Permeation	-		-	-	-	-
Warpage		-	-	-		-
Abrasion resistance	-	-		-		
Flow processibility	-	-	↓	↑	↑	↓
Melt strength	-	-		-		-
Melt viscosity	-	-	↑	↓	↓	↑
Copolymer content	↓	↑	-	-	-	-

Table 6.6 Properties of Some Thermoplastic Structural Foams (Physical Properties Guidelines at 0.25 Wall with 20% Density Reduction) [9]

Property	PE-HD	ABS	modified PPO	PC
Specific gravity	0.6	0.86	0.85	0.9
Deflection temperature [°C]				
under load at 0.462 N/mm ²	54.2	86	96	138
at 1.85 N/mm ²	34.2	78	82	127
Coefficient of thermal expansion [K ⁻¹ ·10 ⁻⁵]	22	8.9	6.9	3.64
Tensile strength [N/mm ²]	9.2	27.3	23.8	42.7
Flexural modulus [N/mm ²]	840	1960	1827	2500
Compressive strength 10% deformation [N/mm ²]	12.9	31	36.4	36.4

Table 6.7 General Properties of Liquid-Crystal Polymers [8]

Property	Value
Flexural strength, N/mm ²	147/308
Unnotched izod, J/m	150/300
Notched izod, J/m	400/500
Rockwell hardness	M62/99
Dielectric constant at 10 ³ Hz	2.9/4.5
Dissipation factor at 10 ³ Hz	4–6 × 10 ⁻³
Volume resistivity, Ω · cm	10 ¹² /10 ⁻¹³

Table 6.7 General Properties of Liquid-Crystal Polymers [8] (Continued)

Property	Value
Dielectric strength, V/mil	780/1000
Arc resistance, s	63/185
Water absorption, equilibrium at 23 °C, %	0.02/0.04
Specific gravity	1.4/1.9
Glass transition temperature, °C	-
Melt temperature, °C	275/330
Heat distortion temperature, °C	
at 0.455 N/m ²	250/280
at 1.848 N/m ²	180/240
Continuous-use temperature, °C	200/240
Coefficient of thermal expansion, ppm/°C	0–25 × 10 ⁻⁶ flow direction
	25–50 × 10 ⁻⁶ transverse
Flammability, UL-94	V/O
Oxygen index	35/50
Tensile modulus, N/mm ²	9.8/40.6
Tensile strength, yield N/mm ²	140/245
Tensile elongation, %	1.2/6.9
Flexural modulus, N/mm ²	9.8/35

Table 6.8 Some Physical Properties of Polyurethane Structural Foams [9]

Property vs. specific gravity			
Specific gravity	0.4	0.5	0.6
Flexural strength [N/mm ²]	24.5	32.2	36.4
Flexural modulus [N/mm ²]	602	742	847
Tensile strength [N/mm ²]	9.8	12.6	16.8
Heat deflection temperature [°C] at 0.462 N/mm ²	81	91	96
Charpy impact, unnotched [kJ/m ²]	13.25	18.1	21
Skin hardness, D scale	70	75	80
Property vs. thickness			
Thickness	1/4 in	3/8 in	1/2 in
Specific gravity	0.6	0.6	0.6
Flexural strength (N/mm ²)	37.8	37.8	36.4
Flexural modulus (N/mm ²)	1092	1001	847
Tensile strength (N/mm ²)	18.2	17.5	16.8
Charpy impact, unnotched [ft · lb/in ²]	12.0	11.0	10.0

Table 6.9 Properties of Some Thermosetting Resins [8]

	Epoxy		General	Phenolics	
	glass filled	mineral filled	purpose	glass filled	mineral filled
Specific gravity	1.8	2.1	1.45	1.95	1.83
Water absorption [% 24 h]	0.2	0.04	0.7	0.5	0.5
Heat deflection temperature at 1.85 N/m ² [°C]	204	121	172	204	260
Tensile strength [N/mm ²]	210	105	70	49	77
Impact strength [J/m] [Izod]	530.4	21.4	16	187	801
Coefficient of thermal expansion [10 ⁻⁵ · K ⁻¹]	3.1	4	4.55	-	1.76
Thermal conductivity [W/m · K]	0.864	-	0.043	0.05	0.03

Table 6.10 Properties of Some Elastomers [8]

Property	EPM/EPDM	Chloroprene	Fluoro-elastomers	Natural rubber
Tensile strength (N/mm ²)	3.5/24.5	3.5/24.5	10.5	16.8/32.2
Tensile modulus (N/mm ²)	700/21000	700/21000	1400/14000	3360/5950
Elongation	100/700	100/800	150/450	300/750
Resilience	good	excellent	fair	outstanding
Brittleness temperature (°C)	-55	-45	-15/-50	-60
Thermal expansion coefficient (10 ⁻⁵ · K ⁻¹)	58	62	55	67
Durometer hardness	30A/90A	30A/95A	55A/95A	30A/100A
Compression set	20/60	20/60	15/30	10/30

Table 6.11 Comparative Physical Properties of Metals and Reinforced Plastics at Room Temperature [10]

Property	Carbon steel 1020	Stainless steel 316	Hastelloy C	Aluminum	Glassmat laminate	Composite structure glassmat woven roving	Glass reinforced epoxy filament wound
Density [kg/m ³]	7860	7916	8968	2712	1384	1522	1800
Coefficient of thermal expansion [K ⁻¹ · 10 ⁻⁶]	11.83	16.7	11.5	24	31	24	16.4/22
Modulus of elasticity [N/mm ²]	210000	196000	196000	70000	4900/7000	7000/10500	21000

Table 6.11 Comparative Physical Properties of Metals and Reinforced Plastics at Room Temperature [10] (Continued)

Property	Carbon steel 1020	Stainless steel 316	Hastelloy C	Aluminum	Glassmat laminate	Composite structure glassmat woven roving	Glass reinforced epoxy filament wound
Tensile strength [N/mm ²]	462	595	560	84	63/84	84/140	420/700
Yield strength [N/mm ²]	231	245	354	28	63/84	84/140	420/700
Thermal conductivity [W/m · K]	48.5	16.3	11.3	234	2.6	2.6	2.6/3.5
Ratio of tensile strength to density	0.0588	0.0752	0.0624	0.031	0.0607	0.092	0.39

Table 6.12 Comparability of DIN/ISO and ASTM Test Methods for Plastics [2]

Test	Standard	Symbol	Units	Comparability
Density	DIN 1306	d	g/cm ³ at 20 °C	comparable at same temperature
	DIN 53479	d_R		
	ASTM D 792 ASTM D 1505	d^{23C}		
Melt index	DIN 53735 (~ISO/R 292)	MFI	g/10 min	comparable under same conditions
	ASTM D 1338	-	g/10 min	
Mechanical properties				
Elastic modulus	DIN 53457	E	kN/mm ²	comparable only under same conditions: shape and state of specimen, measured length, test rate
	ASTM D 638 (Tensile)	E	psi (= lb/in ²)	
	ASTM D 695 (Compression)	-		
	ASTM D 790 (Flexural)	E_B	psi	
	ASTM D 882 (Film)	-	kgf/cm ² *)	
Shear modulus	DIN 53445 (ISO/DR 533)	G	kN/mm ²	comparable
Torsion modulus	ASTM D 2236	G	dyn/cm ² psi	
Torsional stiffness	DIN 53447 (ISO/DR 458)	T	kN/mm ²	comparable
Stiffness properties	ASTM D 1043	G (!)	dN/cm ²	

*) kgf = kiloforce = dN

Table 6.12 Comparability of DIN/ISO and ASTM Test Methods for Plastics [2] (Continued)

Test	Standard	Symbol	Units	Comparability
Tensile properties				
Tensile strength (at maximum load)	DIN 53455 (ISO/DR 468)	σ_B	N/mm ²	
	DIN 53371	σ_B	N/mm ²	comparable only under same conditions
	ASTM D 638	-	psi	
	ASTM D 882	-	dN/cm ²	
Elongation at maximum force	DIN 53455 DIN 53371	ϵ_B δP_{max}	% %	shape and state of specimen, measured length, test rate
Percentage elongation	ASTM D 638 ASTM D 882	% El -	% %	
Ultimate tensile strength	DIN 53455 DIN 53371	σ_R σ_R	N/mm ² N/mm ²	
Tensile strength (at break)	ASTM D 638 ASTM D 882	σ_U -	psi dN/cm ²	
Percentage elonga- tion (at break)	DIN 53455 DIN 53371	δ_R δ_R	% %	
	ASTM D 638	-	%	
	ASTM D 882	-	%	
Yield stress (Yield point)	DIN 53455 DIN 53371	σ_S σ_S	N/mm ² N/mm ²	comparable only under same conditions
Yield point	ASTM D 638	-	psi	shape and state of specimen, measured length, test rate
Yield strength	ASTM D 882	-	dN/cm ²	
Percentage	DIN 53455	E_S	%	
Elongation (at yield)	ASTM D 882	-	%	
Flexural properties	DIN 53452	σ_{bB}	N/mm ²	
Flexural strength	ASTM D 790	-	psi	
Limiting flexural stress	DIN 53452 ASTM D 790	σ_{bG} -	N/mm ² psi	limited compara- bility
Flexural stress (at 5% strain or at conventional deflection)				
Flexural impact	DIN 53453	a_n	kJ/m ²	not comparable
Impact resistance	(ISO/R 179)			
Impact strength	ASTM D 256 (ISO/R 180)	-	J/m	
Impact strength (notched)	DIN 53453 (ISO/R 179)	a_K	kJ/m ²	not comparable
	ASTM D 256 (ISO/R 180)	-	J/m	
Shore hardness	DIN 53505	-	Shore scale A, C, D	comparable
Durometer (Shore hardness)	ASTM D 1706 ASTM D 2240	- H	Scale A, D gram force	

Table 6.12 Comparability of DIN/ISO and ASTM Test Methods for Plastics [2] (Continued)

Test	Standard	Symbol	Units	Comparability
Ball indentation hardness	DIN 53456	H	N/mm^2	not comparable
α -Rockwell hardness	ASTM D 785	-	Rockwell scale	
Thermal properties				
Vicat softening point	DIN 53460	VSP	$^{\circ}\text{C}$	comparable if measured under same load in liquid
	(ISO/R 306) ASTM D 1525	-	$^{\circ}\text{C}$	
Martens heat distortion temperature	DIN 53458	-	$^{\circ}\text{C}$	comparable if load, specimen shape, and slate are the same
Heat distortion temperature	DIN 53461 (ISO/R 75)	F_{ISO}	$^{\circ}\text{C}$	
Deflection temperature (HDT)	ASTM D 648	-	$^{\circ}\text{C}$, $^{\circ}\text{F}$	
Water absorbption	DIN 53472	-	22°C ,	comparable (converted), if pre- and post-treatment, specimen, and times are the same
	DIN 53475 (ISO/R 62)	-	4 d, mg 23°C ,	
	ASTM D 570	-	24 h, mg 23°C ,	
		-	24 h, % 2 h	
Electrical properties				
Volume resistivity	DIN 53482 (VDE 0303 Part 3)	ρ_D	$\Omega \cdot \text{cm}$	comparable
	ASTM D 257	ρ	$\Omega \cdot \text{cm}$	
Surface resistivity	DIN 53482 (VDE 0303 Part 3)	R_0	Ω	comparable
	ASTM D 257	σ	Ω	
Dielectrical constant	DIN 53483 (VDE 0303 Part 4)	ϵ_r	-	comparable
	ASTM D 150	ϵ	-	
Dissipation factor (tan δ)	DIN 53483 (VDE 0303 Part 4)	-	-	comparable
	ASTM D 150	$D-$	-	
Dielectrical loss factor ($\epsilon = \tan \delta$)	-	-	-	
	ASTM D 150	-	-	
Dielectrical strength	DIN 53481 (VDE 0303 Part 2)	E_d	kV/mm	not comparable
	ASTM D 149	-	V/mil (1 mil = $25 \mu\text{m}$)	
Arc resistance	DIN 53484 (VDE 0303 Part 5)	-	s	not comparable
	ASTM D 495	-	s	
Tracking resistance	DIN 53480 (VDE 0303 Part 1)	-	-	not comparable
	ASTM D 2132	-	-	

■ 6.4 References

- [1] *Birley, A. W., Haworth, B., Bachelor, T.*: Physics of Plastics, Hanser, Munich, 1991
- [2] *Domininghaus, H.*: Plastics for Engineers, Hanser, Munich, 1993
- [3] *Ogorkiewicz, R. M.*: Thermoplastics Properties and Design, John Wiley, New York, 1973
- [4] *Harris, J.E.*: Polysulfone in Engineering Thermoplastics: Properties and Applications, Ed. James M. Margolis, Marcel Dekker, Basel, 1985
- [5] *Rosato, D. V., Rosato, D. V.*: Plastics Processing Data Handbook, Van Nostrand Reinhold, New York, 1990
- [6] *Schmiedel, H.*: Handbuch der Kunststoffprüfung, Hanser, Munich, 1992
- [7] *Maresca, L. M., Robeson, L. M.*: Polyarylates in Engineering Thermoplastics, Properties and Applications, Ed. James M. Margolis, Marcel Dekker, Basel, 1985
- [8] *Alvino, W.M.*: Plastics for Electronics – Materials, Properties, and Design Applications, McGraw Hill, New York, 1994
- [9] *Wendle, B.A.*: Structural Foam, A Purchasing and Design Guide, Marcel Dekker, New York, 1985
- [10] *Mallinson, J.H.*: Corrosion-resistant Plastic Composites in Chemical Plant Design, Marcel Dekker, New York, 1969

7

Extrusion

Extrusion is one of the most widely used unit operations of polymer processing. Basically it consists of transporting the solid polymer in an extruder by means of a rotating screw, melting the solid, homogenizing the melt, and forcing the melt through a die (Fig. 7.1).

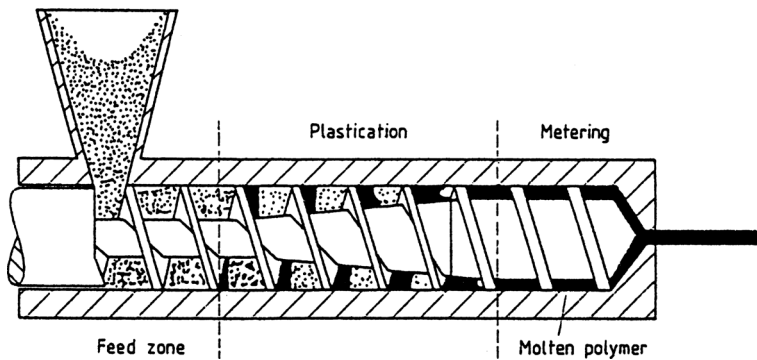


Figure 7.1 Plasticating extrusion [2]

The extruder screw of a conventional plasticating extruder has three geometrically different zones (Fig. 7.2), whose functions can be described as follows:

- feed zone:
transport and preheating of the solid material,
- transition zone:
compression and plastication of the polymer,
- metering zone:
melt conveying, melt mixing, and pumping of the melt to the die.

However, the functions of a zone are not limited to that particular zone alone. The processes mentioned can continue to occur in the adjoining zone as well.

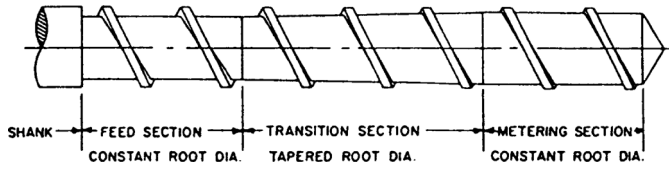


Figure 7.2 Three zone screw

■ 7.1 Extrusion Screws

To perform these processing operations, optimally screws of varied geometry as shown in Fig. 7.3 are used. Higher melting capacities compared to the three zone screws (Fig. 7.1) are achieved with screws having shearing and mixing devices (Fig. 7.3(a)). Barrier type screws enable the separation of solid polymers from the melt, and thus lead to lower and constant melt temperatures over a wide range of screw speeds (Fig. 7.3(c)(d)). Devolatilizing screws are applied to extract volatile components from the melt (Fig. 7.3(b)) [27].

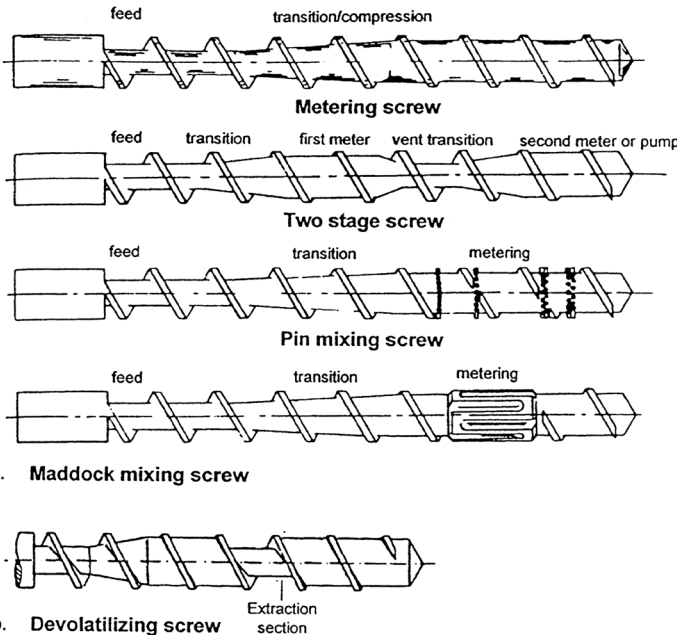


Figure 7.3 Geometries of some extrusion screws [20, 27]

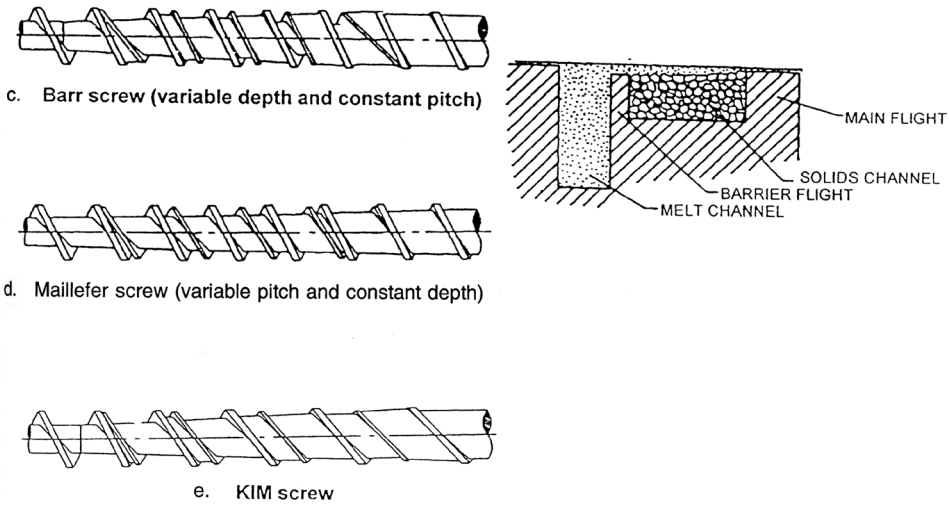


Figure 7.3 Geometries of some extrusion screws [20, 27] (*Continued*)

Twin screw extruders are mainly used in the compounding of polymers; for example, in the pelletizing and compounding of PVC or in the profile extrusion of PVC. The positive conveying characteristics of the twin screw extruders are achieved by forcing the material to move in compartments formed by the two screws and the barrel. The degree of intermeshing between the flight of one screw and the channel of the other screw, sense of rotation, and speed distinguish the different kinds of screws (Fig. 7.4 [9]) from one another.

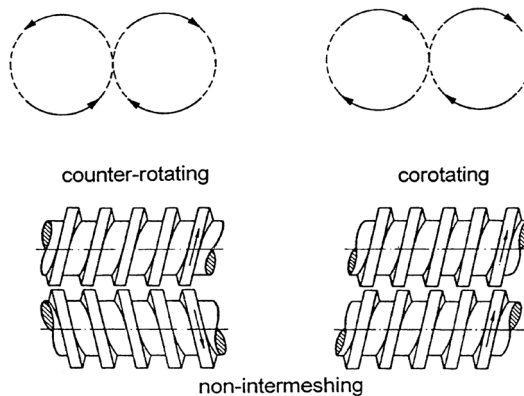


Figure 7.4 Geometries of some twin screws [9]

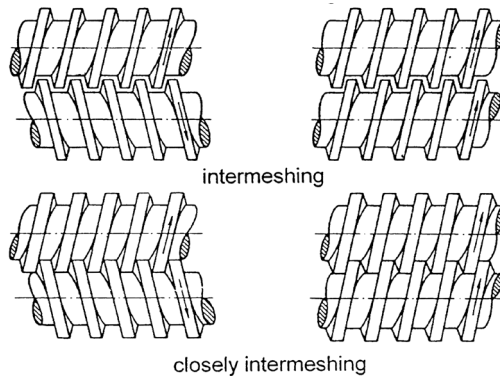


Figure 7.4 Geometries of some twin screws [9] (*Continued*)

■ 7.2 Processing Parameters

The factors affecting extrusion can be classified into resin-dependent and machine-related parameters.

7.2.1 Resin-Dependent Parameters

Resin-dependent parameters are not the physical constants that one obtains by measuring the physical properties of the polymeric material. They are, however, similar to these constants with the difference that they relate more to the process and processing conditions. If, for example, the processing temperature of a polymer is too high, degradation of the material leading to adverse material properties of the product might occur. Too low a processing temperature, on the other hand, may create a melt containing unmelted solids. The appropriate processing temperatures and pressures suited to a particular resin and process are usually quoted by the resin manufacturers. These values can be maintained during the process by optimizing the processing conditions and, if necessary, the machinery such as extrusion screw or die [1].

Melt temperature and pressure are important resin-dependent parameters that affect the quality of the product. Approximate values of these parameters are given in Tables 7.1 – 7.4 for a few resins and extrusion processes. They refer to the temperature and pressure of the melt at the die entrance as shown in Fig. 7.5. These values are also known in practice as stock temperature and stock pressure, and depend not only on the type of the resin, but also on the grade of the resin used, which is characterized, for example, by the MFR value.

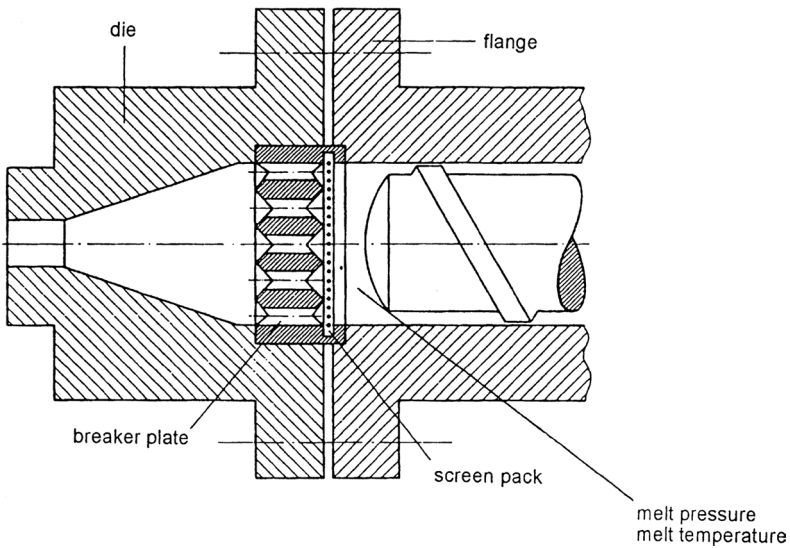


Figure 7.5 Position of measurement of melt pressure and melt temperature [9]

7.2.1.1 Blown Film

Characteristic values of melt temperature and pressure are given in Table 7.1, with the blown film process shown in Fig. 7.6.

Table 7.1 Typical Values of Melt Temperature and Pressure for Blown Film

Material	Melt temperature °C	Melt pressure bar
PE-LD	140/210	100/300
PE-HD	180/230	150/300
PE-LLD	190/230	250/350
PP	220/240	200/300
PA 6	270/280	160/200
PC	260/290	150/250
PET	260/280	150/250
EVA	150/200	100/200
EVOH	200/220	100/200

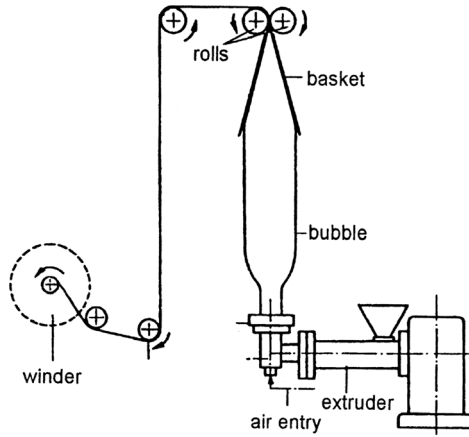


Figure 7.6 Blown film [9]

7.2.1.2 Pipe Extrusion

Table 7.2 shows some guide values of melt temperature and pressure for pipe extrusion, seen in Fig. 7.7.

Table 7.2 Typical Values of Melt Temperature and Melt Pressure for Pipe Extrusion

Material	Melt temperature °C	Melt pressure bar
PVC-U	180/185	100/200
PVC-P	160/165	100/200
PEHD	180/200	150/250
PP	230/240	150/200

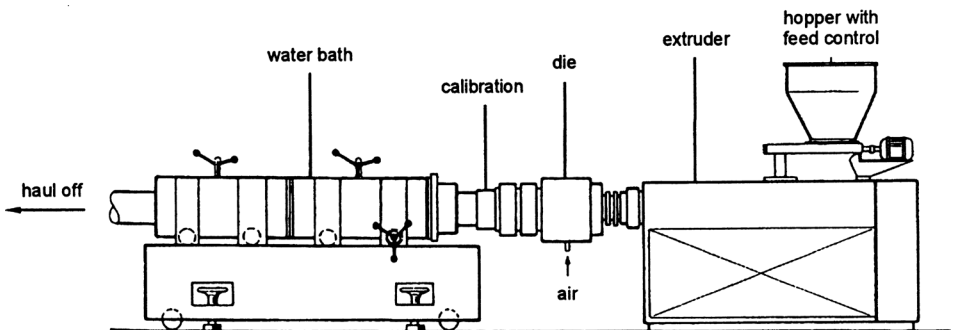


Figure 7.7 Pipe extrusion [9]

7.2.1.3 Flat Film Extrusion

Typical values of melt temperature and pressure for flat film extrusion are given in Table 7.3 and shown in Fig. 7.8.

Table 7.3 Typical Values of Melt Temperature and Pressure for Flat Film Extrusion

Material	Melt temperature °C	Melt pressure bar
PP	230/260	150/200
PA 6	260/280	100/200
PELD	220/250	100/250
PEHD	220/230	150/250

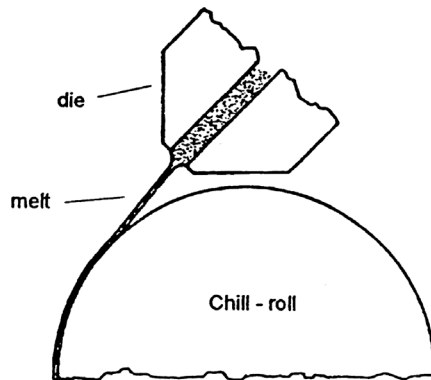


Figure 7.8 Flat film extrusion [9]

7.2.1.4 Sheet Extrusion

A flat die is used in both flat film and sheet extrusion processes. Depending on the thickness of the product the term film or sheet is applied. Typical values for sheet extrusion are presented in Table 7.4.

Table 7.4 Typical Values of Melt Temperature and Pressure for Sheet Extrusion

Material	Melt temperature °C	Melt pressure bar
PS	190/220	150/250
PMMA	200/230	200/250
SB	210/230	150/250
ABS	220/240	150/250
PET	280/285	150/200
PVC-U	180/185	100/200
PVC-P	160/165	75/150

7.2.1.5 Wire Coating

Melt temperatures for wire coating are approximately the same as those used for pipe extrusion. However, depending on the type of extrusion the pressure can range from 100 bar to 400 bar.

Melt temperatures and pressures for other resins and processes can be obtained from resin makers. Data on processing conditions suited to attain resin compatible melt temperatures are also supplied by resin manufacturers. These data include values on extruder barrel temperature, die temperature, screw speed, and depending on the process, haul-off rates, and draw-ratios.

7.2.2 Machine-Related Parameters

Although machine-related parameters include effects due to resin properties, they are more influenced by the geometry of the machine elements involved, such as extrusion screw and die, than by resin properties. The following examples taken from single screw extrusion illustrate the influence of the geometry of machinery on the target quantities of the process.

7.2.2.1 Extruder Output

Depending on the type of extruder, the output is determined either by the geometry of the solids feeding zone alone, as in the case of a grooved extruder [11], or by the solids and melt zones found in a smooth barrel extruder.

7.2.2.1.1 Feed Zone

The solids transport is largely influenced by the frictional forces between the solid polymer and barrel and screw surfaces. A detailed analysis of the solids conveying mechanism was performed by Darnell and Mol [16]. In the following example, an empirical equation, which gave good results in the practice, is presented [1, 2].

Example:

The geometry of the feed zone of a screw (Fig. 7.9) is given by the following data:

barrel diameter	D_b	=	30 mm
screw lead	s	=	30 mm
number of flights	v	=	1
flight width	w_{FLT}	=	3 mm
channel width	W	=	28.6 mm
depth of the feed zone	H	=	5 mm
conveying efficiency	η_F	=	0.436

screw speed $N = 250$ rpm
 bulk density of the polymer $\rho_o = 800$ kg/m³

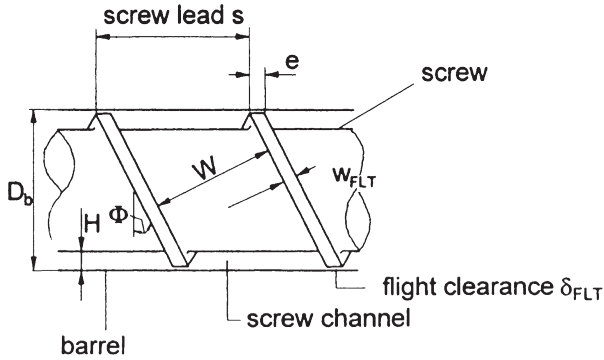


Figure 7.9 Screw zone of a single screw extruder

The solids conveying rate in the feed zone of the extruder can be calculated according to [2]

$$G = 60 \cdot \rho_o \cdot N \cdot \eta_F \cdot \pi^2 \cdot H \cdot D_b (D_b - H) \frac{W}{W + W_{FLT}} \cdot \sin \Phi \cdot \cos \Phi \quad (7.1)$$

with the helix angle Φ

$$\Phi = \tan^{-1} \left[s / (\pi \cdot D_b) \right] \quad (7.2)$$

The conveying efficiency η_F in Eq. 7.1 as defined here is the ratio between the actual extrusion rate and the theoretical maximum extrusion rate attainable under the assumption of no friction between the solid polymer and the screw. It depends on the type of polymer, bulk density, barrel temperature, friction between the polymer, barrel, and the screw. Experimental values of η_F for some polymers are given in Table 7.5.

Solution:

Inserting the values above with the dimensions in meters into Eqs. 7.1 and 7.2 we get

$$G = 60 \cdot 800 \cdot 250 \cdot 0.44 \cdot \pi^2 \cdot 0.005 \cdot 0.03 \cdot 0.025 \cdot \frac{0.0256}{0.0286} \cdot 0.3034 \cdot 0.953$$

Hence, $G \approx 50$ kg/h

Table 7.5 Conveying Efficiency η_F for Some Polymers

Polymer	Smooth barrel	Grooved barrel
PE-LD	0.44	0.8
PE-HD	0.35	0.75
PP	0.25	0.6
PVC-P	0.45	0.8
PA	0.2	0.5
PET	0.17	0.52
PC	0.18	0.51
PS	0.22	0.65

7.2.2.1.2 Metering Zone (Melt Zone)

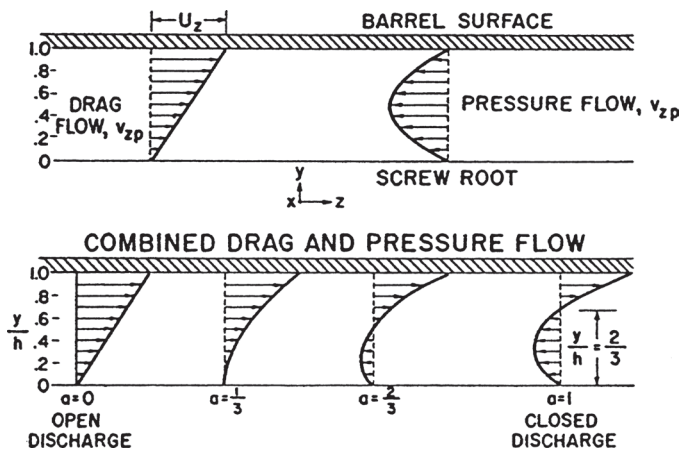
Starting from the parallel plate model and correcting it by means of appropriate correction factors [3] the melt conveying capacity of the metering zone can be calculated as follows [3]:

Although the following equations are valid for an isothermal quasi-Newtonian fluid, there were found to be useful for many practical applications [1].

These equations can be summarized as follows:

Volume flow rate of pressure flow \dot{Q}_p (Fig. 7.10):

$$\dot{Q}_p = \frac{-\pi D_b \cdot H^3 \left(1 - \frac{\nu \cdot e}{s}\right) \cdot \sin^2 \Phi \cdot \Delta p \cdot 10^{-4}}{12 \eta_a \cdot L} \quad (7.3)$$

**Figure 7.10** Drag and pressure flow in screw channel

Mass Flow Rate, \dot{m}_p

$$\dot{m}_p = 3600 \cdot 1000 \cdot \dot{Q}_p \cdot \rho_m \quad (7.4)$$

Drag Flow, \dot{Q}_d

$$\dot{Q}_d = \frac{\pi^2 \cdot D_b^2 \cdot N \cdot H \cdot \left(1 - \frac{\nu \cdot e}{s}\right) \cdot \sin \Phi \cdot \cos \Phi \cdot 10^{-9}}{120} \quad (7.5)$$

Mass Flow Rate, \dot{m}_d

$$\dot{m}_d = 3600 \cdot 1000 \cdot \dot{Q}_d \cdot \rho_m \quad (7.6)$$

Leakage Flow, \dot{Q}_L

To avoid metal to metal friction, extrusion screws have a small clearance between the top of the flight and the barrel surface. This clearance reduces the pumping rate of the melt because it enables the polymer to leak across the flights. The net flow rate \dot{Q} is therefore:

$$\dot{Q} = \dot{Q}_d + \dot{Q}_p - \dot{Q}_L \quad (7.7)$$

The melt conveying rate of the metering zone can be finally calculated from [1]

$$\dot{m} = 3 \cdot 10^{-5} \cdot \pi^2 \cdot D_b^2 \cdot N \cdot H \cdot \left(1 - \frac{\nu \cdot e}{s}\right) \cdot \rho_m \cdot \sin \Phi \cdot \cos \Phi \cdot (1 - a_d - J) \quad (7.8)$$

where $a_d = -\dot{m}_p / \dot{m}_d$ and $J = \delta_{FLT} / H$

Average shear rate in the metering channel

$$\dot{\gamma}_a = \pi \cdot D_b \cdot N / 60 \cdot H \quad (7.9)$$

Here are symbols and units used in the previous equations:

D_b = Barrel diameter [mm]

H = Channel depth [mm]

e = Flight width [mm]

s = Screw lead [mm]

δ_{FLT} = Flight clearance [mm]

L = Length of metering zone [mm]

\dot{Q}_p, \dot{Q}_d = Volume flow rate of pressure and drag flow, respectively [m^3/s]

\dot{m}_p, \dot{m}_d = Mass flow rate of pressure and drag flow, respectively [kg/h]

\dot{m} = Extruder output [kg/h]

Δp	= Pressure difference across the metering zone [bar]
v	= Number of flights
η_a	= Melt viscosity [Pa · s]
$\dot{\gamma}_a$	= average shear rate [s^{-1}]
ρ_m	= density of the melt [g/cm^3]
α_d	= Ratio of pressure flow to drag flow
N	= Screw speed [rpm]

Example:

For the following conditions the extruder output is to be determined:

$$\text{melt viscosity } \eta_a = 1406.34 \text{ Pa} \cdot \text{s}; \quad N = 80 \text{ rpm}; \quad \Delta p = 300 \text{ bar}; \quad \rho_m = 0.7 \text{ g/cm}^3$$

Solution:

Geometry of the metering zone (Fig. 7.9)

$$Db = 60 \text{ mm}; \quad H = 3 \text{ mm}; \quad e = 6 \text{ mm}; \quad s = 60 \text{ mm}; \quad \delta_{FLT} = 0.1 \text{ mm}; \quad L = 600 \text{ mm}; \\ v = 1$$

Substituting these values into the equations above one obtains

$$\dot{m}_p = -3.148 \text{ kg/h} \quad \text{from Eq. 7.4}$$

$$\dot{m}_d = 46.59 \text{ kg/h} \quad \text{from Eq. 7.6}$$

$$\dot{m} = 41.88 \text{ kg/h} \quad \text{from Eq. 7.8}$$

$$\text{Leakage flow: } \dot{m}_l = \dot{m}_d + \dot{m}_p - \dot{m} = 1.562 \text{ kg/h}$$

With the help of Eq. 7.8, the effect of different parameters on the extruder output is presented in Figs. 7.11 - 7.18 by changing one variable at a time, while keeping all other variables constant. The dimensions of the screw used in these calculations are taken from the previous example.

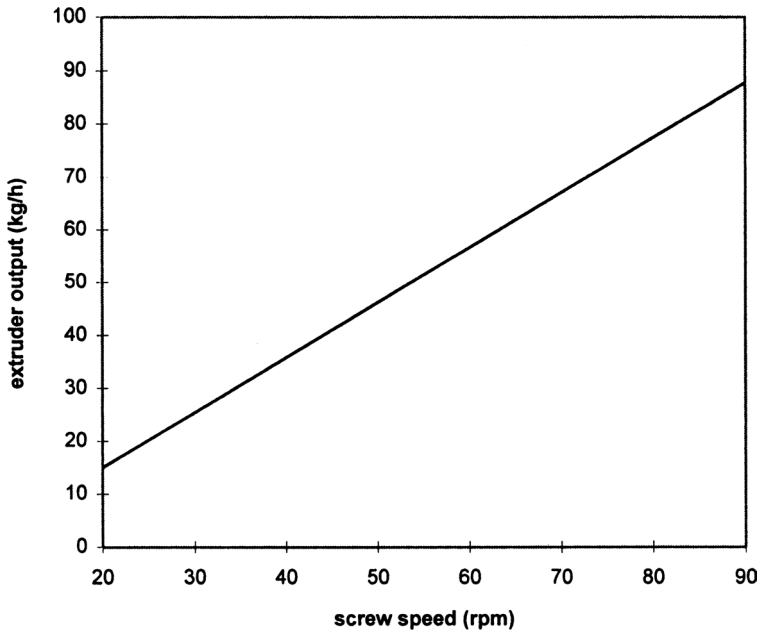


Figure 7.11 Effect of screw speed on extruder output

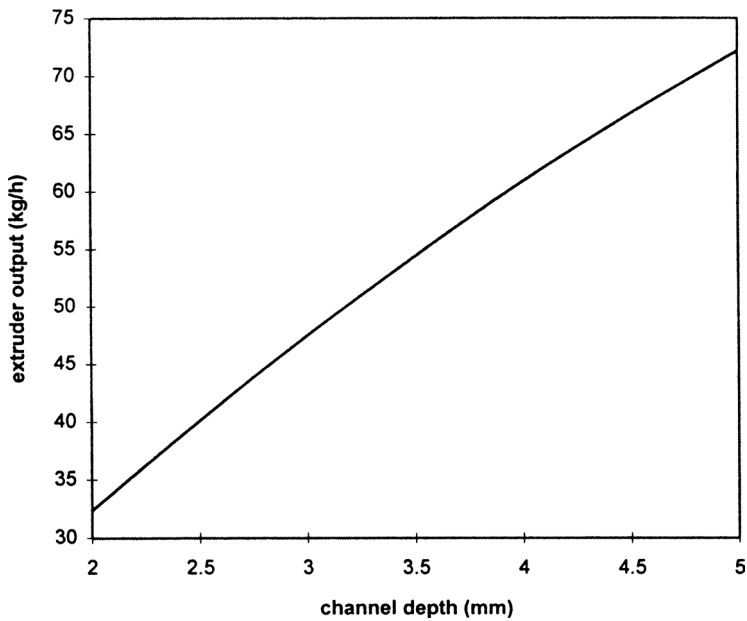


Figure 7.12 Effect of channel depth on extruder output

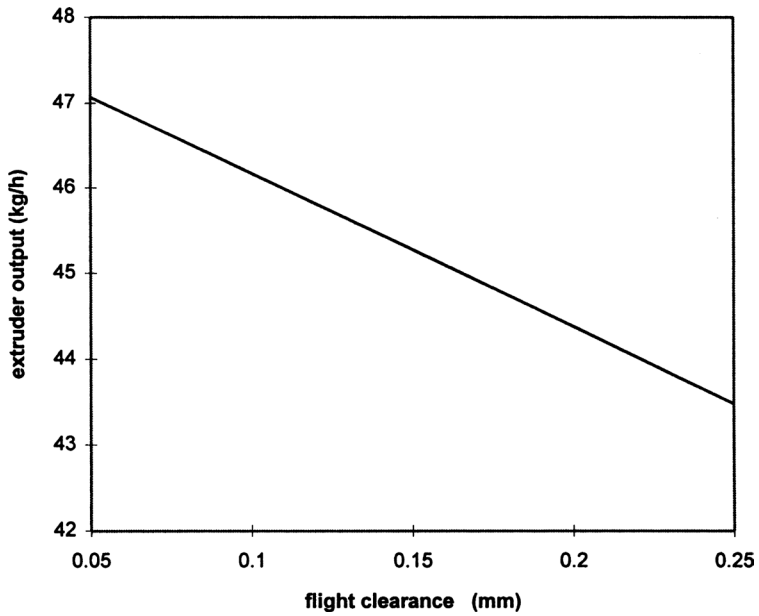


Figure 7.13 Effect of flight clearance on extruder output

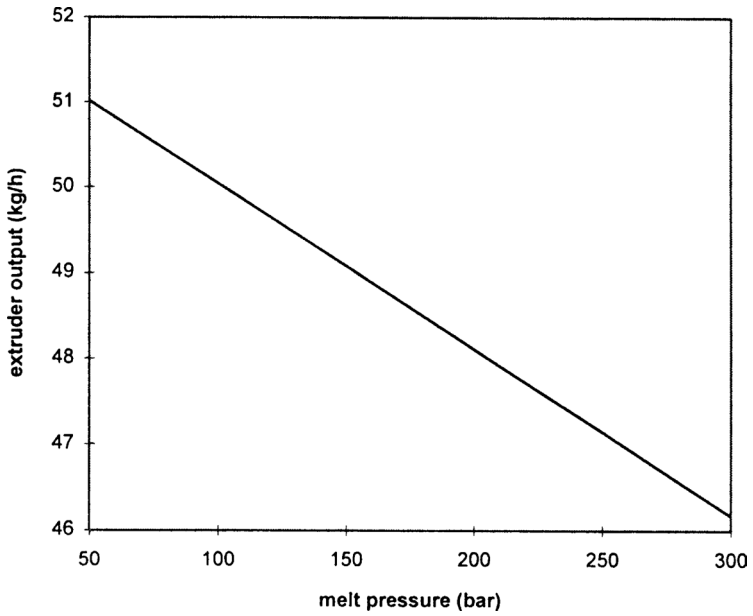


Figure 7.14 Effect of melt pressure on extruder output

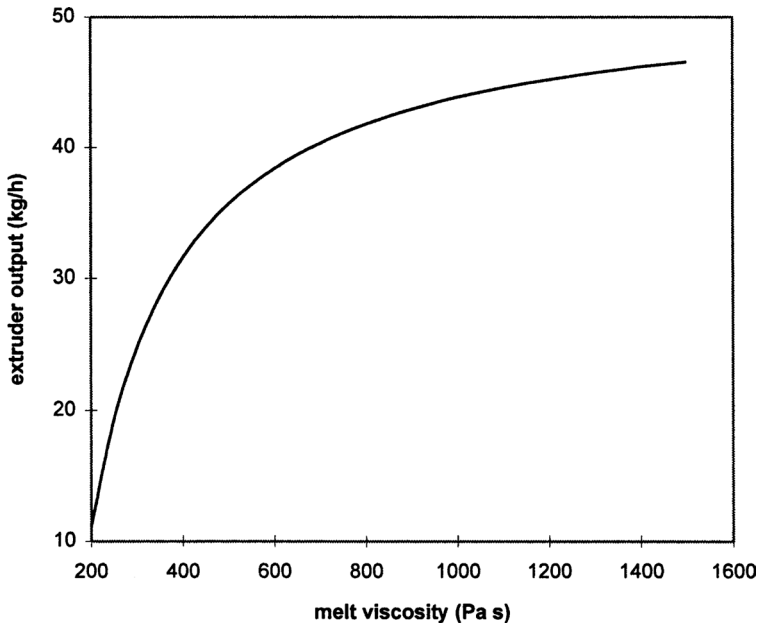


Figure 7.15 Effect of melt viscosity on extruder output

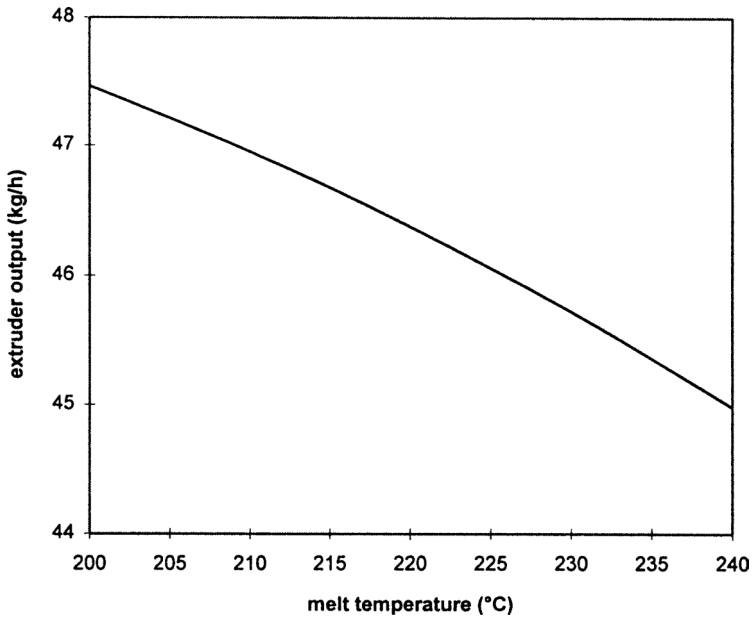


Figure 7.16 Effect of melt temperature on extruder output

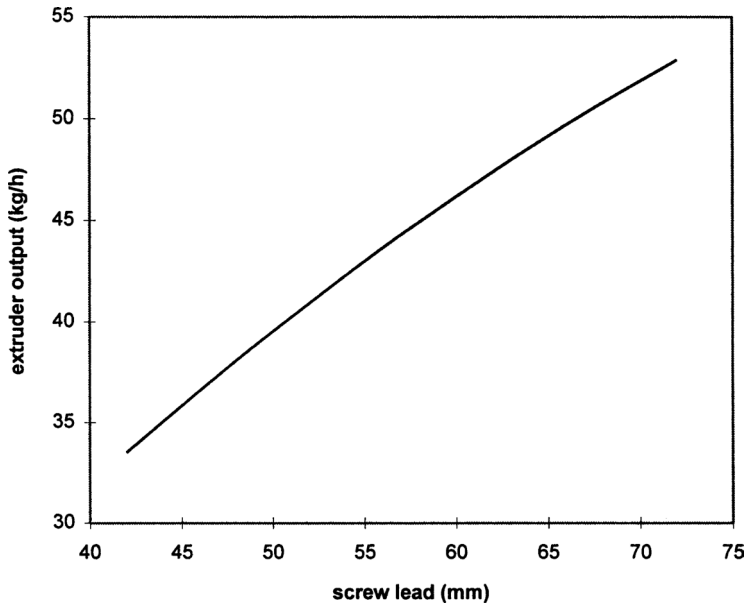


Figure 7.17 Effect of screw lead on extruder output

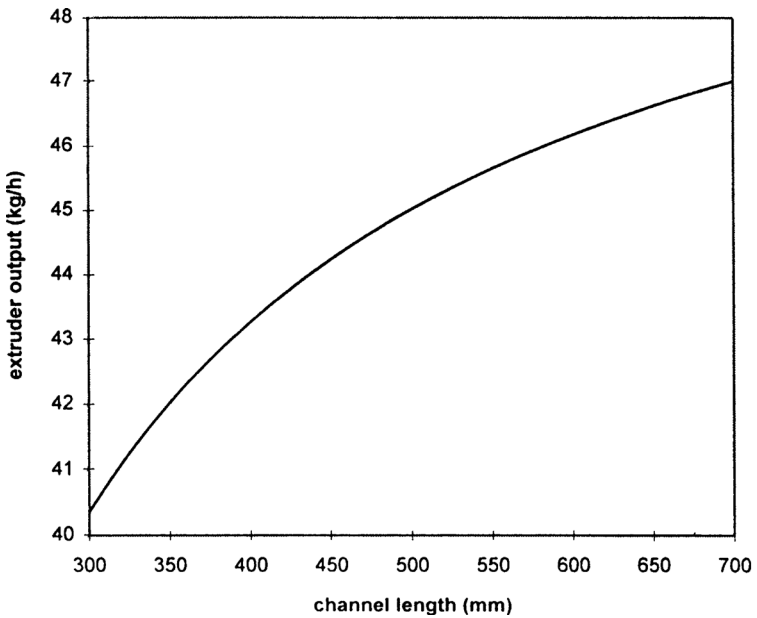


Figure 7.18 Effect of channel length on extruder output

Correction Factors

To correct the infinite parallel plate model for the flight-edge effects, the following factors can be used along with the previous equations:

With sufficient accuracy the shape factor F_d for the drag flow can be obtained from [27]

$$F_d = 1 - 0.571 \frac{H}{W} \quad (7.10)$$

and the factor F_p for the pressure flow

$$F_p = 1 - 0.625 \frac{H}{W} \quad (7.11)$$

The expressions for the corrected drag flow and pressure flow would then be

$$\dot{Q}_{dk} = F_d \cdot \dot{Q}_d \quad (7.12)$$

and

$$\dot{Q}_{pk} = F_p \cdot \dot{Q}_p \quad (7.13)$$

The correction factor for the screw power, which is treated in the next section, can be determined from [1]

$$F_x = e^x x^3 + 2.2 x^2 - 1.05x \quad (7.14)$$

with $x = H/W$.

Equation 7.14 is valid in the range of $0 < H/W < 2$. For the range of commonly occurring H/W -ratios in extruder screws, the flight-edge effect accounts for less than 5% and can therefore be neglected [27]. The influence of screw curvature is also so small that F_x can be taken as 1. Although the above mentioned factors are valid only for Newtonian fluids, their use for polymer melt flow is accurate enough for practical purposes.

7.2.2.2 Melting Parameter

The melting rate is described by Tadmor [2] through the parameter Φ_p , which is expressed as Eq. 7.15 [1, 2] (see also Fig. 7.19).

$$\Phi_p = \left\{ \frac{V_{bx} \cdot \delta_m \cdot [\lambda_m(T_b - T_m) + 0.5 \eta_f \cdot V_j^2 \cdot 10^{-4}]}{200 [c_{ps}(T_m - T_s) + i_m]} \right\}^{0.5} \quad (7.15)$$

The numerator represents the heat supplied to the polymer by conduction through the barrel and dissipation, whereas the denominator shows the enthalpy required to melt the solid polymer. The melting rate increases with increasing Φ_p . The dimensionless melting parameter Ψ is defined as [2]

$$\Psi = \frac{\varphi_p \cdot H_1 \cdot W^{0.5}}{10^{1.5} \cdot G} \quad (7.16)$$

This parameter is the ratio between the amount of melted polymer per unit down channel distance to the extruder output per unit channel feed depth.

The symbols and units used in the Eqs. 7.15 and 7.16 are as follows:

Barrel temperature	T_b	°C
Melting point of the polymer	T_m	°C
Viscosity in the melt film	η_f	Pa · s
Velocity of the barrel surface	V_b	cm/s
Velocity component	V_{bx}	cm/s (Fig. 7.19)
Relative velocity	V_j	cm/s
Output of the extruder	G	g/s
Depth of the feed zone	H_1	mm
Width of the screw channel	W	mm
Melt density	ρ_m	g/cm ³
Specific heat of the solid polymer	c_{p_s}	kJ/(kg · K)
Temperature of the solid polymer	T_s	°C
Thermal conductivity of the melt	λ_m	W/(m · K)
Heat of fusion of the polymer	i_m	kJ/kg

Numerical examples illustrating the calculation of melting rate and melting parameter according to Eqs. 7.15 and 7.16 have been given by Rao in his book [1].

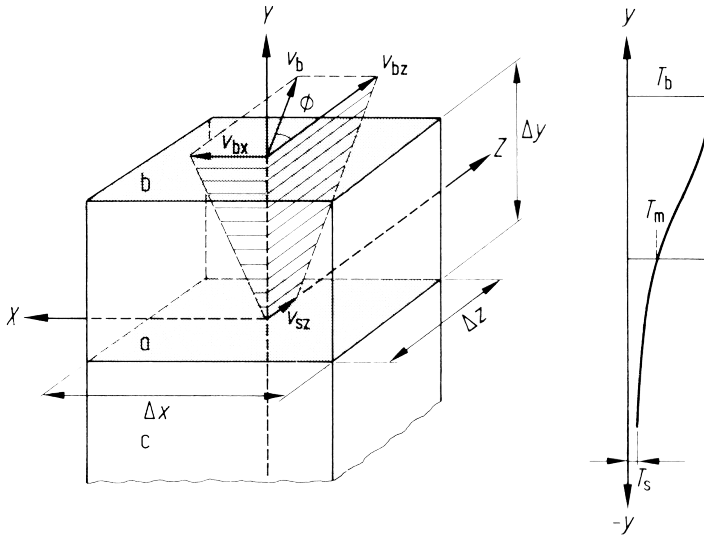


Figure 7.19 Velocity and temperature profiles in the melt and solid bed after TADMOR [2]

7.2.2.3 Melting Profile

The melting profile gives the amount of unmelted polymer as a function of screw length (Fig. 7.20), and is the basis for calculating the melt temperature and pressure along the screw. It shows whether the polymer at the end of the screw is fully melted. The plasticating and mixing capacity of a screw can be improved by incorporating mixing and shearing devices into the screw. The melting profile enables one to judge the suitable positioning of these devices in the screw [4]. Methods of calculating melting profile, melt temperature, and melt pressure are given in the book by Rao [4].

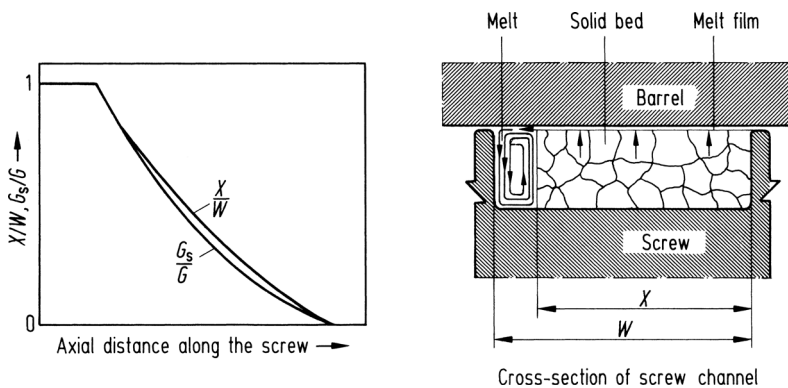


Figure 7.20 Solid bed and melting profiles X/W and G_s/G [2];
 G : total mass flow rate; G_s : mass flow rate of solids

7.2.2.4 Screw Power

The screw power consists of the power dissipated as viscous heat in the channel and flight clearance and the power required to raise the pressure of the melt. The total power Z_N is therefore for a melt filled zone [5]

$$Z_N = Z_c + Z_{FLT} + Z_{\Delta p} \quad (7.17)$$

where Z_c = power dissipated in the screw channel
 Z_{FLT} = power dissipated in the flight clearance
 $Z_{\Delta p}$ = power required to raise the pressure of the melt

The power $Z_{\Delta p}$ is small in comparison with the sum $Z_c + Z_{FLT}$, and can be neglected. In general, the power due to dissipation \dot{E}_d can be expressed for a Newtonian fluid as [1]

$$\dot{E}_d = \eta \dot{\gamma}^2 \quad (7.18)$$

Using the respective shear rates for the screw channel (Eq. 7.9) and flight clearance, the equation for the screw power can be derived [1].

The power dissipated in the screw channel Z_c is given by [1]

$$Z_c = \frac{v \cdot \pi^2 \cdot D_{FLT}^2 \cdot N^2 \cdot W \cdot \eta_c \cdot \Delta L (F_x \cos^2 \Phi + 4 \sin^2 \Phi)}{36 \cdot 10^{14} \cdot \sin \Phi \cdot H} \quad (7.19)$$

The power dissipated in the flight clearance can be calculated from [1]

$$Z_{FLT} = \frac{v \cdot \pi^2 \cdot D_{FLT}^2 \cdot N^2 \cdot W_{FLT} \cdot \Delta L \cdot \eta_{FLT}}{36 \cdot 10^{14} \cdot \delta_{FLT} \cdot \sin \Phi} \quad (7.20)$$

The power required to raise the pressure of the melt $Z_{\Delta p}$ can be written as

$$Z_{\Delta p} = 100 \cdot \dot{Q}_p \cdot \Delta p \quad (7.21)$$

The flight diameter D_{FLT} is obtained from

$$D_{FLT} = D_b - 2\delta_{FLT} \quad (7.22)$$

and the channel width W

$$W = \frac{s}{ny} \cos \Phi - W_{FLT} \quad (7.23)$$

The symbols and units used in the equations above are given in the following example:

Example:

For the following conditions the screw power is to be determined:

Resin: PE-LD

Operating conditions:

Screw speed $N = 80$ rpm

melt temperature $T = 200$ °C

die pressure $\Delta p = 300$ bar

Geometry of the metering zone:

$D_b = 60$ mm; $H = 3$ mm; $e = 6$ mm; $s = 60$ mm; $\delta_{FLT} = 0.1$ mm;

$\Delta L = 600$ mm; $v = 1$

Solution:

Power Z_c in the screw channel: $D_{FLT} = 59.8$ mm from Eq. 7.22

Viscosity of the melt in the screw channel η_c at the average shear rate 83.8 s⁻¹, according to Eq. 7.9, and $T = 200$ °C from the viscosity function of resin

$$\eta_c = 1406.34 \text{ Pa}\cdot\text{s}$$

Channel width $W = 51.46$ from Eq. 7.23

Number of flights $v = 1$

Length of the metering zone $\Delta L = 600$ mm

Factor F_x :

$$F_x = 1 \text{ for } H/W = 3/51.46 = 0.058 \text{ from Eq. 7.14}$$

Power in the screw channel Z_c from Eq. 7.19

$$Z_c = \frac{1 \cdot \pi^2 \cdot 59.82 \cdot 802 \cdot 51.46 \cdot 1406.34 \cdot 600 \cdot (1 \cdot \cos^2 17.66^\circ + 4 \cdot \sin^2 17.66^\circ)}{36 \cdot 10^{14} \cdot 3 \cdot \sin 17.66^\circ} = 3.85 \text{ kW}$$

Power in the flight clearance Z_{FLT} :

Flight width W_{FLT} (Fig. 7.9)

$$W_{FLT} = e \cos \Phi = 6 \cdot \cos 17.66^\circ = 5.7 \text{ mm}$$

Viscosity at the average shear rate in the flight clearance

$$\dot{\gamma}_{FLT} = \frac{\pi D_b \cdot N}{60 \cdot \delta_{FLT}} = 2513.3 \text{ s}^{-1}$$

and $T = 200$ °C from the viscosity function of the resin

$$\eta_{FLT} = 219.7 \text{ Pa} \cdot \text{s}$$

Power in the flight clearance Z_{FLT} from Eq. 7.20:

$$Z_{FLT} = \frac{1 \cdot \pi^2 \cdot 59.8^2 \cdot 80^2 \cdot 600 \cdot 5.7 \cdot 219.7}{36 \cdot 10^{14} \cdot 0.1 \cdot 0.303} = 1.56 \text{ kW}$$

Power to raise the melt pressure $Z_{\Delta p}$:

Pressure flow \dot{Q}_p :

\dot{Q}_p from the example in Section 7.2.2.1

$$\dot{Q}_p = 1.249 \cdot 10^{-6} \text{ m}^3/\text{s}$$

Die pressure Δp :

$$\Delta p = 300 \text{ bar}$$

$Z_{\Delta p}$ from Eq. 7.21:

$$Z_{\Delta p} = 100 \cdot 1.249 \cdot 10^{-6} \cdot 300 = 0.0375 \text{ kW}$$

Hence the power $Z_{\Delta p}$ is negligible in comparison with the sum $Z_c + Z_{FLT}$.

With increasing flight clearance, as might occur due to wear in extruders, the melt conveying capacity is reduced since the leakage flow over the flight increases. To compensate for this reduction, the screw speed has to be increased if the output is to remain the same. This leads to an increase in the power Z_N as shown in Table 7.6.

The power in the flight clearance Z_{FLT} does not vary much as the opposing effects of viscosity and flight clearance nearly balance each other.

Table 7.6 Effect of Flight Clearance on Screw Power for a PE-LD

δ_{FLT} mm	Z_{FLT} kW	Z_c kW	Z_N kW	N rpm
0.1	0.711	2.73	3.44	80
0.15	0.71	2.83	3.54	81.5
0.2	0.65	2.93	3.58	83
0.25	0.626	3.0	3.63	84
0.3	0.6	3.15	3.75	86

7.2.2.5 Melt Temperature and Melt Pressure

7.2.2.5.1 Melt Temperature

The exact calculation of melt temperature can be done only on an iterative basis as shown in the computer program given in [4]. The temperature rise ΔT in an increment of the screw can be found from [5] Eq. 7.24

$$\Delta T = (T_{out} - T_m) = \frac{3600 \cdot (Z_c + Z_{FLT} + N_H)}{\dot{m} \cdot c_{pm}} \quad (7.24)$$

where Z_c, Z_{FLT} = see Section 7.2.2.4 (kW)
 N_H = heat through the barrel (kW)
 \dot{m} = extruder output (kg/h)
 T_{out} = temperature of the melt leaving the increment ($^{\circ}\text{C}$)
 T_m = melting point of the polymer ($^{\circ}\text{C}$)

The average temperature $0.5 (T_{in} + T_{out})$ can be taken as the stock temperature in the increment, where T_{in} denotes the temperature of the melt entering the increment.

7.2.2.5.2 Temperature Fluctuation

Fluctuations of melt temperature in an extruder serve as a measure of the stability of extrusion and extrudate quality.

The temperature variation ΔT can be estimated for a 3-zone screw from the following empirical relationship developed by Squires [19]:

$$\Delta T = \frac{5}{9} \left[\frac{1}{4.31 N_Q^2 - 0.024} \right] \quad (7.25)$$

for $0.11 < N_Q < 0.5$. The parameter N_Q is given by

$$N_Q = 14.7 \cdot 10^{-4} \frac{D_b^2}{G} \Sigma \frac{L}{H} \quad (7.26)$$

where ΔT = temperature variation $^{\circ}\text{C}$
 D_b = barrel diameter cm
 G = output g/s
 L = length of screw zone in diameters
 H = depth of the screw zone cm

Example:

$D_b = 6 \text{ cm};$	$G = 15 \text{ g/s};$	L	H	L/H
		9	0.9	10
		3	0.6 (mean value)	3.33
		9	0.3	30

Hence $L/H = 43.33$

N_Q from Eq. 7.26

$$N_Q = 14.7 \cdot 10^{-4} \cdot \frac{36}{15} \cdot 43.33 = 0.153$$

ΔT from Eq. 7.25

$$\Delta T = \frac{5}{9} \left[\frac{1}{4.31 \cdot 0.153^2 - 0.024} \right] = 7.22^\circ\text{C} \quad \text{or} \quad \pm 3.61^\circ\text{C}$$

The constants occurring in Eqs. 7.25 and 7.26 depend on the type of polymer used. For screws other than 3-zone screws, the geometry term in Eq. 7.26 has to be defined in such a way that N_Q correlates well with the measured temperature fluctuations.

7.2.2.5.3 Melt Pressure

The melt or stock pressure can be obtained from the pressure flow by means of Eq. 7.4 [1, 5]. The more exact calculation of the melt pressure profile in an extruder should consider the effect of the ratio of pressure flow to drag flow, the so-called Drossel quotient, as shown in [5].

7.2.2.5.4 Pressure Fluctuation

The effect of pressure fluctuations of the melt on the flow rate can be estimated by the relation [2]

$$\dot{Q}_1 / \dot{Q}_2 = (\Delta p_1 / \Delta p_2)^n \quad (7.27)$$

Example:

Calculate the flow rate variation where:

pressure drop $\Delta p_1 = 200$ bar; $\Delta p_2 = 210$ bar

flow rate $\dot{Q}_1 = 39.7$ cm³/s

power law exponent n for PE-LD = 2.5

Solution:

$$\dot{Q}_1 / \dot{Q}_2 = 39.7 / \dot{Q}_2 = (200 / 210)^{2.5} = 0.885$$

$$\dot{Q}_2 = 44.9 \text{ cm}^3 / \text{s}$$

$$\text{flow rate variation} = (\dot{Q}_2 - \dot{Q}_1) / \dot{Q}_1 = \frac{44.9 - 39.7}{39.7} = 13\%$$

$$\text{pressure variation} = \frac{\Delta p_2 - \Delta p_1}{\Delta p_1} = \frac{210 - 200}{200} = 5\%$$

This means that a pressure variation of 5% can cause a flow rate fluctuation of 13%. The influence of machine-related parameters and operating variables on the melting of solid polymer is shown in Figs. 7.21 – 7.32 [2].

For a given resin, the fluctuation of the melt temperature depends mainly on the screw geometry and output rate as shown in Fig. 7.33 [2].

Empirical design data for different screw geometries, resins, and processes are given in Figs. 7.34 – 7.38 [11].

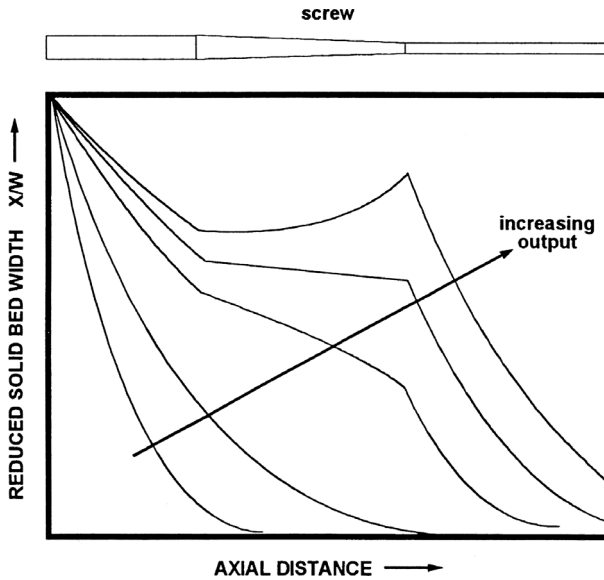


Figure 7.21 Influence of increasing output on solids melting in an extruder [2]

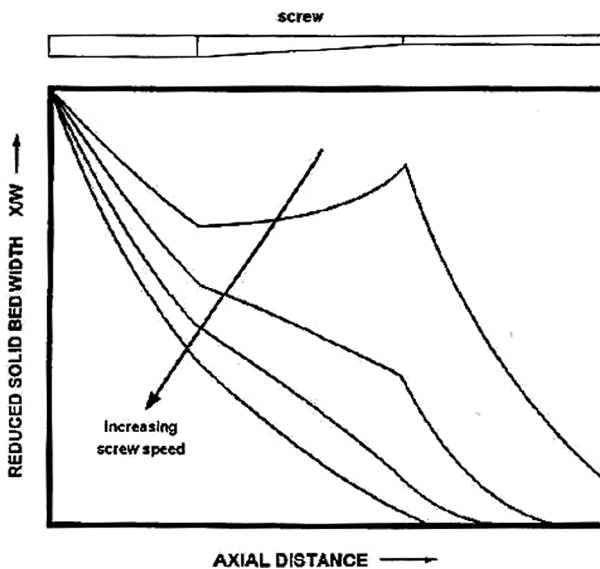


Figure 7.22 Influence of increasing screw speed on solids melting in an extruder [2]

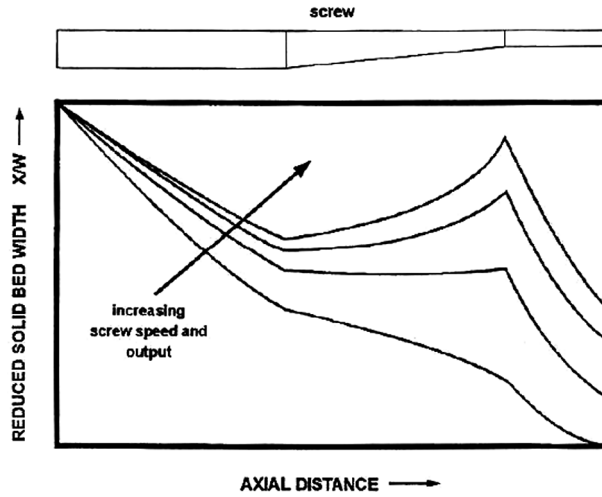


Figure 7.23 Influence of increasing screw speed and output on solids melting in an extruder [2]

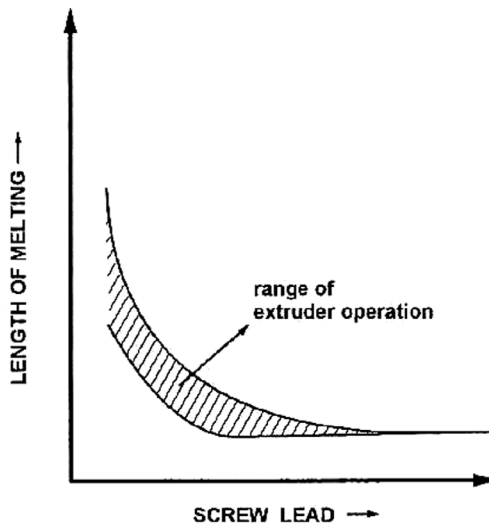


Figure 7.24 Relationship between length of melting and screw lead in an extruder [2]

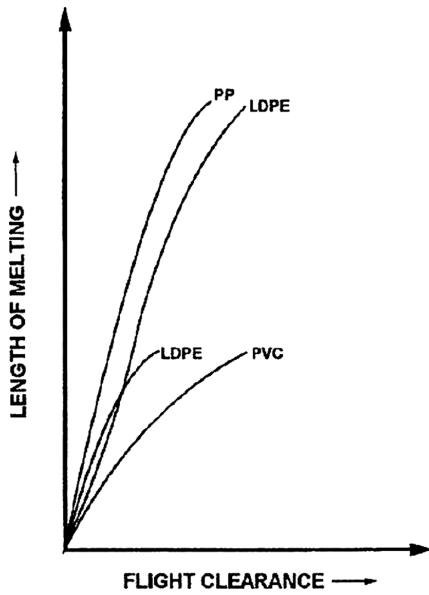


Figure 7.25 Relationship between flight clearance and length of melting for different resins in an extruder [2]

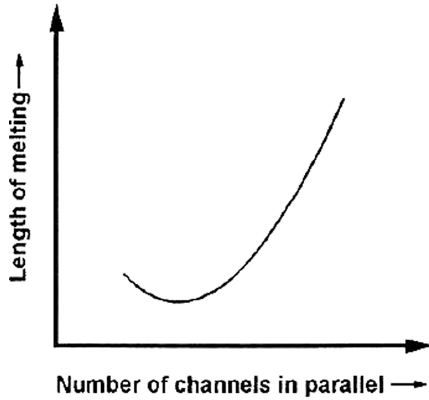


Figure 7.26 Relationship between length of melting and number of channels in an extruder [2]

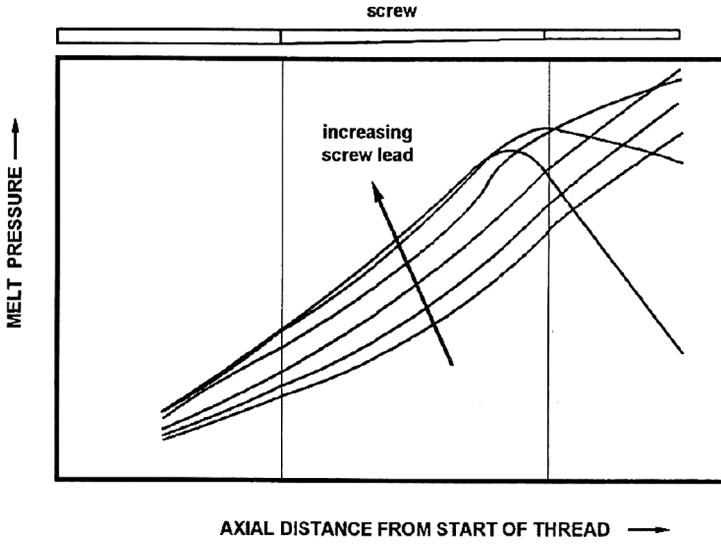


Figure 7.27 Relationship between melt pressure and screw length at increasing screw speed [2]

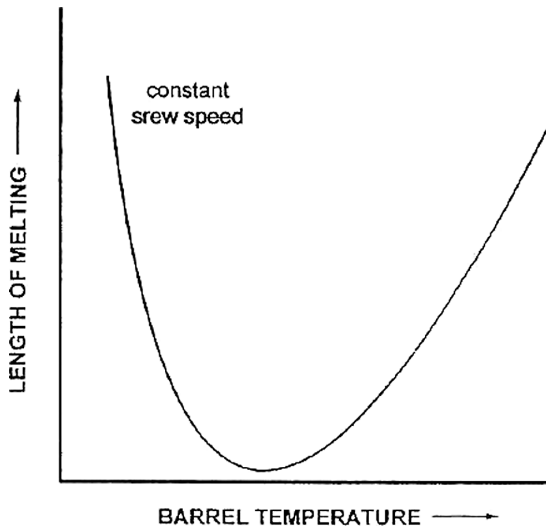


Figure 7.28 Relationship between length of melting and barrel temperature at constant screw speed [2]

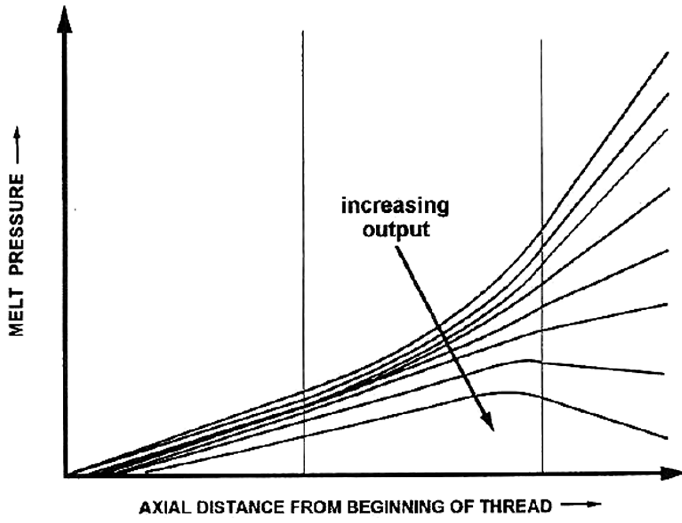


Figure 7.29 Relationship between melt pressure and screw length at constant screw speed and increasing output [2]

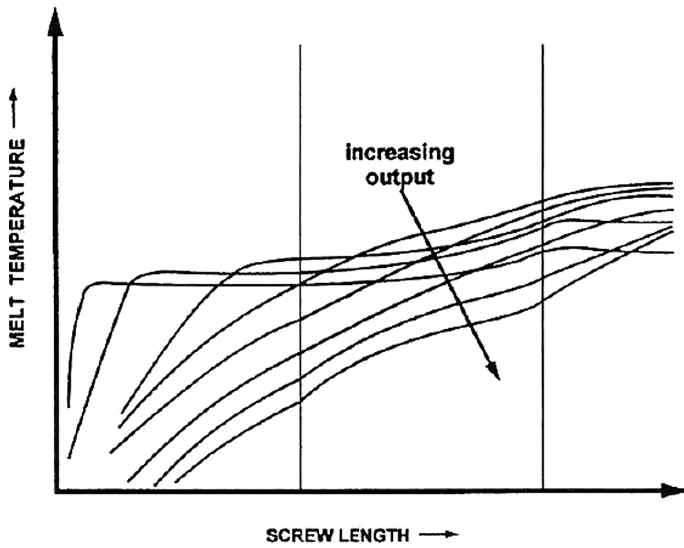


Figure 7.30 Relationship between melt temperature and screw length at increasing output [2]

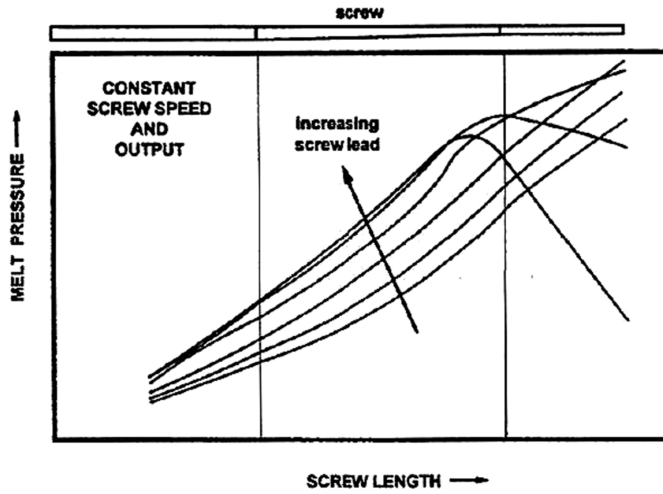


Figure 7.31 Relationship between melt pressure and screw length at constant output and screw speed and increasing screw lead [2]

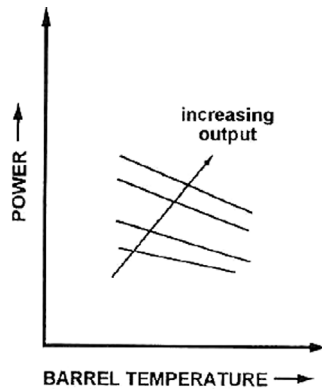


Figure 7.32 Relationship between power and barrel temperature at increasing output [2]

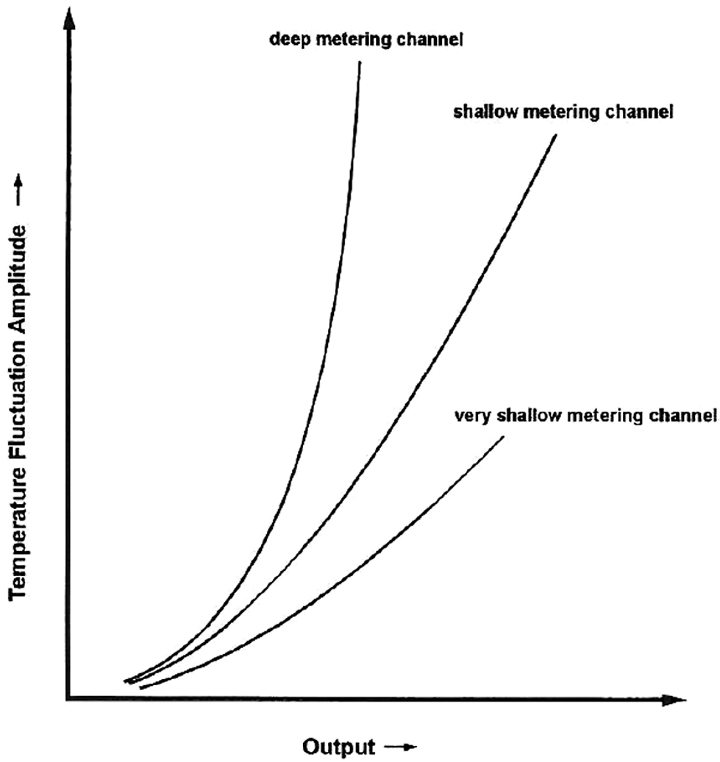


Figure 7.33 Relationship between melt temperature fluctuation, screw geometry and output [2]

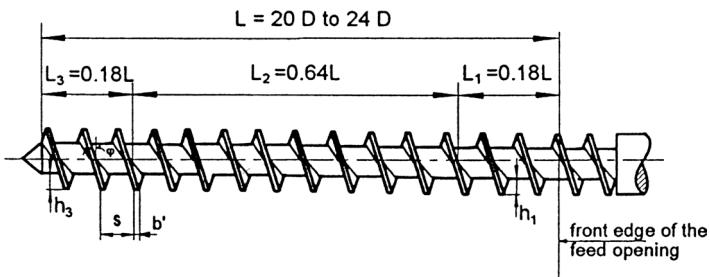


Figure 7.34 Empirical screw design data [11]

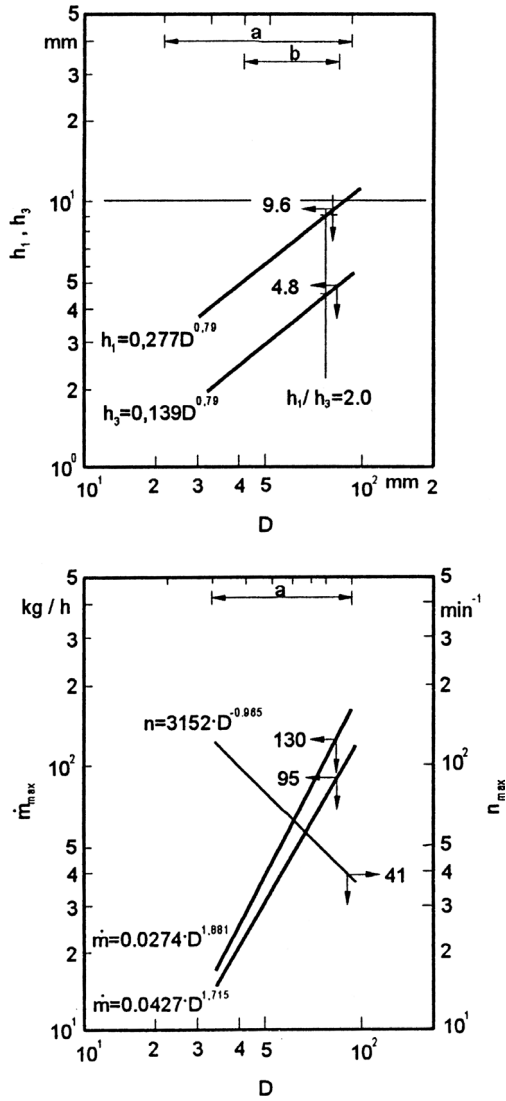


Figure 7.35 Empirical screw design data [11]

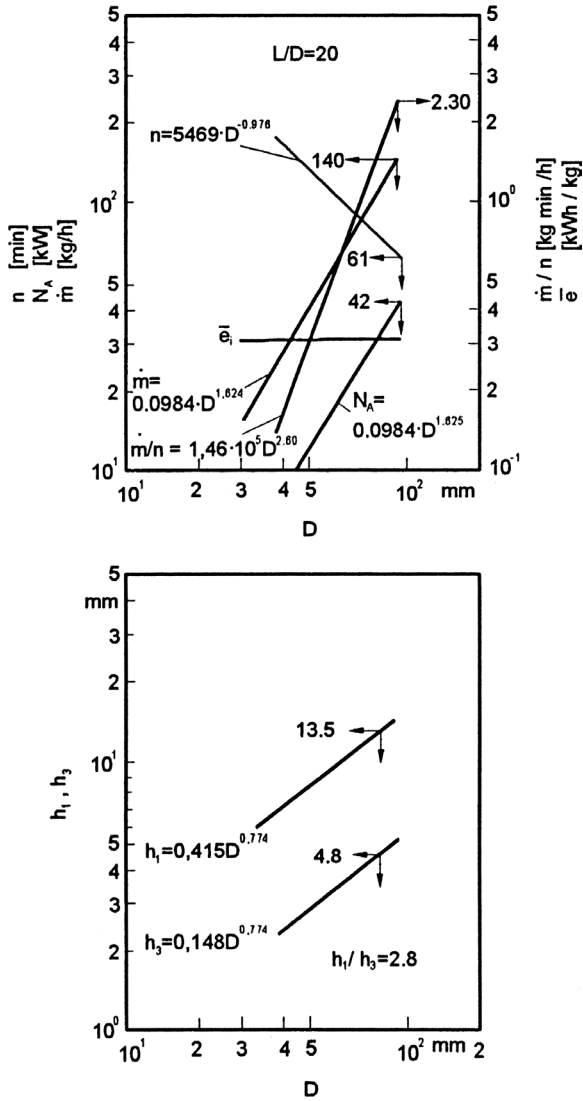
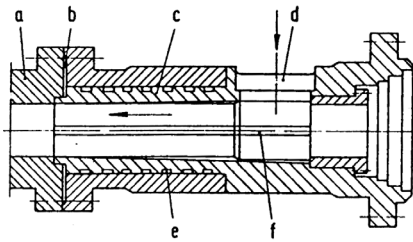
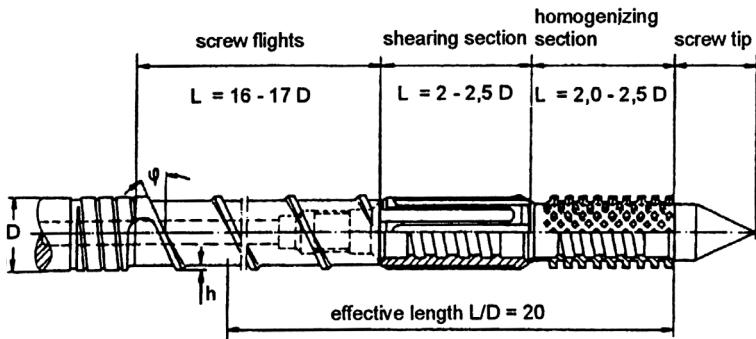


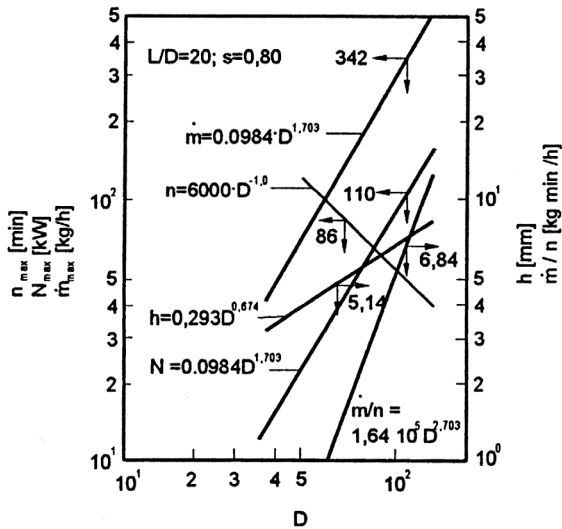
Figure 7.36 Empirical screw design data [11]



High efficiency feed zone
a extruder barrel, *b* thermal break,
c grooved sleeve, *d* feed opening,
e cooling spiral, *f* grooves



Screw built from standard modules for grooved blow molding extruders



Design data for a series of grooved extruders

Figure 7.37 Empirical screw design data [11]

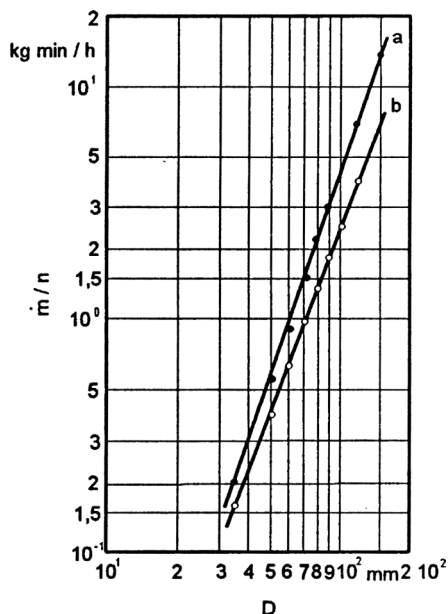


Figure 7.38 Empirical screw design data [11]

■ 7.3 Extrusion Dies

Extrusion dies can be designed by calculating shear rate, die pressure, and the residence time of the melt as functions of the flow path of melt in the die [6]. Of these quantities, the die pressure is the most important as the desired throughput cannot be attained if the die pressure does not match with the melt pressure. The interaction between screw and die is shown in Figs. 7.39 and 7.40.

Common shapes of flow channels occurring in extrusion dies are shown in Fig. 7.41. Detailed treatment of die design is presented in [1] and [17]. The following areas of application of extrusion dies serve as examples to illustrate the relationship between die geometry and processing parameters:

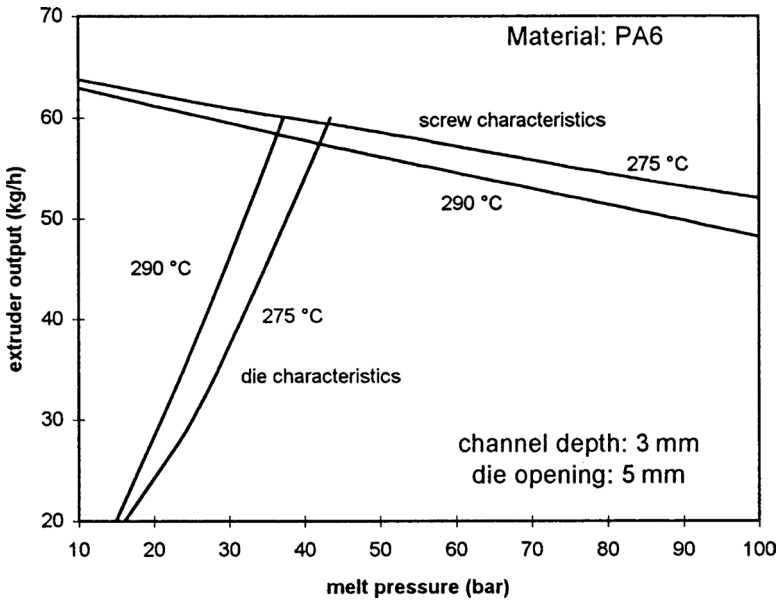


Figure 7.39 Effect of screw and die temperature

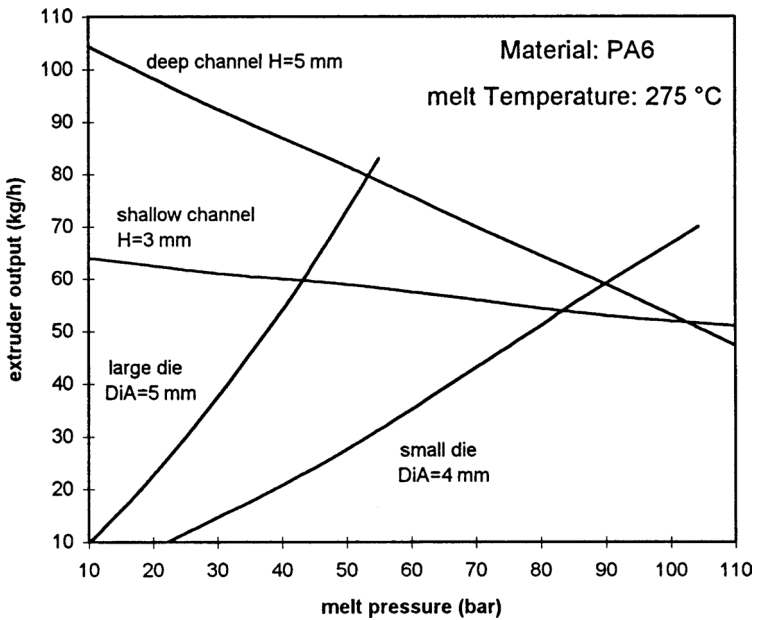


Figure 7.40 Effect of channel depth and die opening

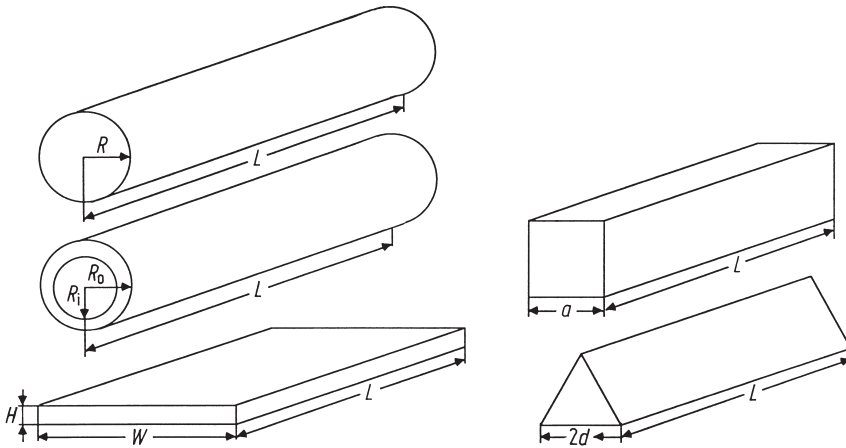


Figure 7.41 Common shapes of flow channels in extrusion dies [1]

7.3.1 Pipe Extrusion

The spider die shown in Fig. 7.42 is employed for making tubes and pipes and also for extruding a parison required to make a blow-molded article. It is also used in blown film processes.

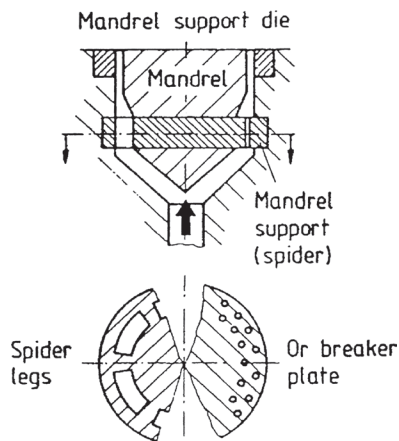


Figure 7.42 Mandrel support die with spider or breaker plate [17]

For a circular channel, the shear rate is given in Table 7.7. For an annulus, which represents the pipe cross-section, it is given by

$$\dot{\gamma}_{\text{annulus}} = \frac{6\dot{Q}}{\pi(R_o + R_i)(R_o - R_i)^2} \quad (7.28)$$

The pressure drop is obtained from [7]

$$\Delta p = \frac{\dot{Q}^{\frac{1}{n}}}{K^{\frac{1}{n}} \cdot G} \quad (7.29)$$

where G , the die constant, follows from

$$G_{\text{circle}} = \left(\frac{\pi}{4} \right)^{\frac{1}{n}} \cdot \frac{R_n^{\frac{1}{n}+1}}{2L} \quad (7.30)$$

$$G_{\text{slit}} = \left(\frac{W}{6} \right)^{\frac{1}{n}} \cdot \frac{H_n^{\frac{2}{n}+1}}{2L} \quad (7.31)$$

for $W/H \geq 20$. For $W/H < 20$, G_{slit} has to be multiplied by the correction factor F_p given in Fig. 7.43 as a function of H/W . The die constant G_{annulus} is calculated from

$$H = R_o - R_i \quad (7.32)$$

$$W = \pi (R_o + R_i) \quad (7.33)$$

G_{annulus} follows then from

$$G_{\text{annulus}} = \left(\frac{\pi}{6} \right)^{\frac{1}{n}} \cdot \frac{(R_o + R_i)^{\frac{1}{n}} \cdot (R_o - R_i)^{\frac{2}{n}+1}}{2L} \quad (7.34)$$

for $(R_o + R_i)/(R_o - R_i) \geq 37$.

For smaller values of this ratio, G_{annulus} has to be multiplied by F_p , given in Fig. 7.43. The height H and the width W are obtained in this case from Eqs. 7.32 and 7.33.

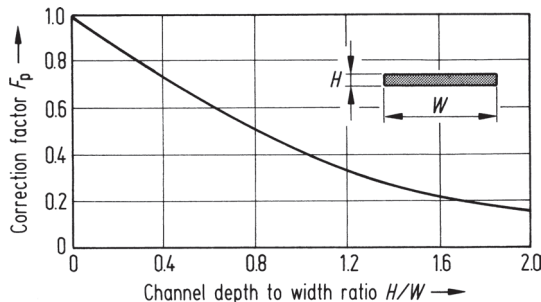


Figure 7.43 Correction factor F_p as a function of H/W [19]

In Table 7.7, the shear rates and die constants for different channel shapes are summarized.

Table 7.7 Shear Rates and Die Constants for Some Die Channel Shapes (see Fig. 7.41) [1]

Channel shape	Shear rate $\dot{\gamma}$ [s^{-1}]	Die constant G
Circle	$4\dot{Q} / \pi R^3$	$\left(\frac{\pi}{4}\right)^{\frac{1}{n}} \cdot \frac{R_n^{1+1}}{2L}$
Slit	$\frac{6\dot{Q}}{W \cdot H^2}$	$\left(\frac{W}{6}\right)^{\frac{1}{n}} \cdot \frac{H_n^{2+1}}{2L}$
Annulus	$\frac{6\dot{Q}}{\pi(R_o + R_i)(R_o - R_i)^2}$	$\left(\frac{\pi}{6}\right)^{\frac{1}{n}} \cdot \frac{(R_o + R_i)^{\frac{1}{n}} \cdot (R_o - R_i)^{\frac{2}{n}+1}}{2L}$
Triangle	$\frac{10}{3} \cdot \frac{\dot{Q}}{a^3}$	$\frac{1}{\sqrt{3}} \cdot \left(\frac{3}{10}\right)^{\frac{1}{n}} \cdot \frac{a_n^{\frac{3}{n}+1}}{2L}$
Square	$\frac{3}{0.42} \cdot \frac{\dot{Q}}{a^3}$	$\frac{1}{2} \left(\frac{0.42}{3}\right)^{\frac{1}{n}} \cdot \frac{a_n^{\frac{3}{n}+1}}{2L}$

7.3.1.1 General Cross Section

By means of the substitute radius, defined by Schenkel [18], the pressure drop in cross sections other than the ones treated previously can be calculated. The substitute radius is expressed by [18] Eq. 7.35

$$R_{rh} = \left[\frac{\left(\frac{2n+1}{\pi} \right) \cdot A^{n+2}}{B^{n+1}} \right]^{\frac{1}{n+3}} \quad (7.35)$$

where R_{rh} = substitute radius
 A = cross-sectional area
 B = circumference

On the basis of the substitute radius the pressure drop in the channel is calculated as in the case of the circular channel [1].

Another method of calculating the pressure drop in channels of varied cross section is presented in Fig. 7.44 [17, 19]. The correction factor F_p and the flow coefficient f_p have the same values in comparable ranges of height to width of the channel.

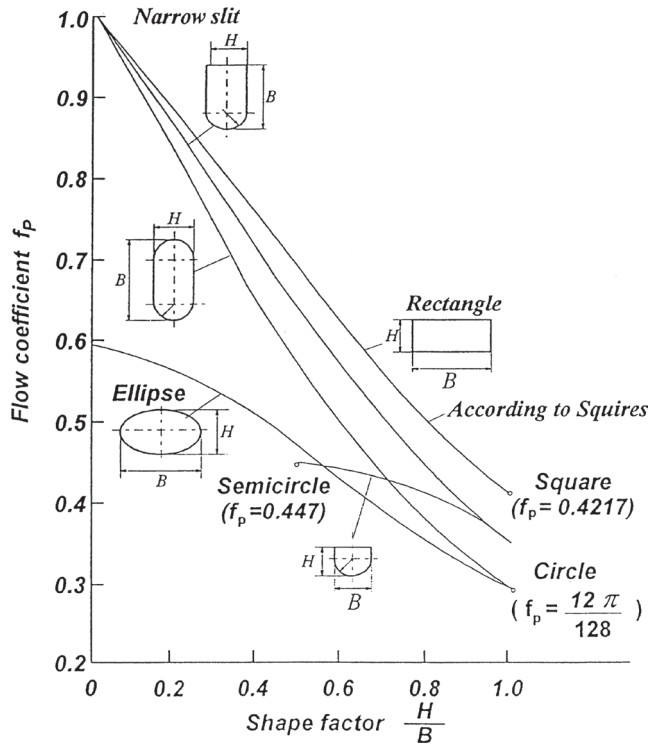


Figure 7.44 Flow coefficient f_p as a function of shape factor H/B [17]

The symbols and units used in the equations above are explained in the following example:

Example:

It is required to calculate the pressure drop Δp of a PE-LD melt at 200 °C flowing through an annular channel with an outside radius $R_o = 40$ mm, an inside radius $R_i = 39$ mm, and length $L = 100$ mm at a mass flow rate $\dot{m} = 10$ g/s.

Solution:

$$\text{Volume flow rate } \dot{Q} = \frac{\dot{m}}{\rho_m} = \frac{10}{0.7} = 14.29 \frac{\text{cm}^3}{\text{s}}$$

$$\text{or } \dot{Q} = 1.429 \cdot 10^{-5} \text{ m}^3/\text{s}$$

where $\rho_m = \text{melt density} = 0.7 \text{ g/cm}^3$

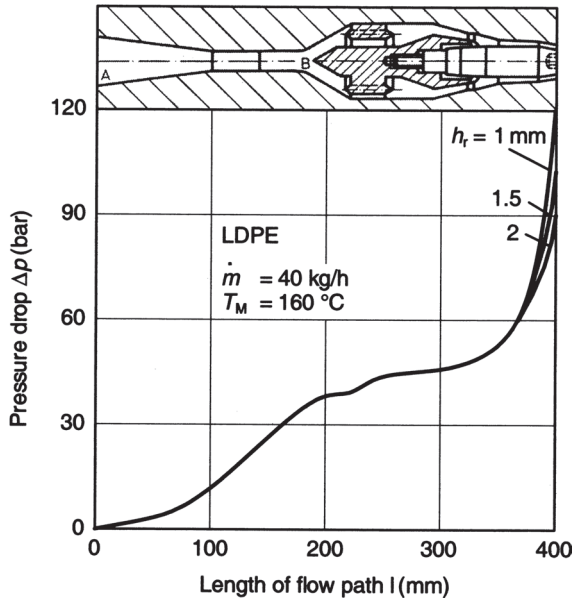


Figure 7.45 Melt pressure in a spider die [6]

Shear rate from Eq. 7.28

$$\dot{\gamma} = \frac{6\dot{Q}}{\pi(R_o + R_i)(R_o - R_i)^2} = \frac{6 \cdot 1.429 \cdot 10^{-5}}{\pi(0.04 + 0.039)(0.001)^2} = 354.47 \text{ s}^{-1}$$

The given resin-dependent values, which can also be calculated from flow curves, are

$$n = 2.907$$

$$\eta = 579.43 \text{ Pa} \cdot \text{s}$$

$$K = 1.34 \cdot 10^{-13}$$

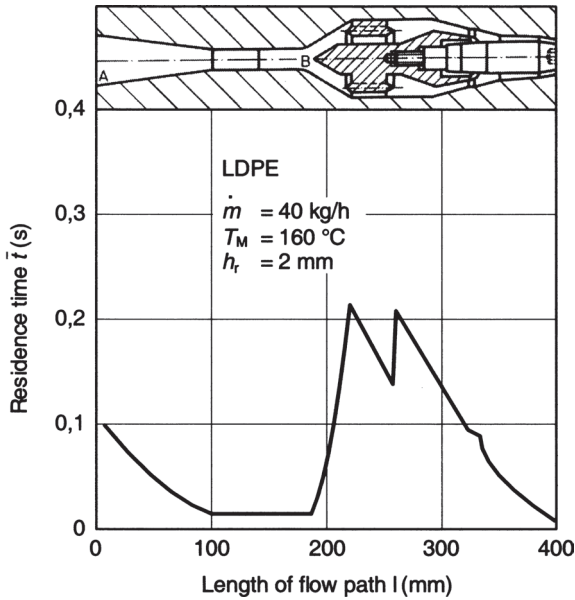


Figure 7.46 Residence time in a spider die [6]

The die constant G_{annulus} follows from Eq. 7.34

$$G_{\text{annulus}} = \frac{\left(\frac{\pi}{6}\right)^{\frac{1}{2.907}} \cdot (0.04 + 0.39)^{\frac{1}{2.907}} \cdot (0.001)^{\frac{2}{2.907} + 1}}{2 \cdot 0.1}$$

As the ratio $\pi(R_o + R_i)/(R_o - R_i) = 248.19$ is greater than 37, no correction is necessary. Therefore, $G_{\text{annulus}} = 1.443 \cdot 10^{-5}$.

The pressure drop Δp is obtained finally from Eq. 7.29

$$\Delta p = 400.26 \text{ bar}$$

The residence time \bar{t} in a channel of length ΔL can be written as

$$\bar{t} = \Delta L / \bar{u}$$

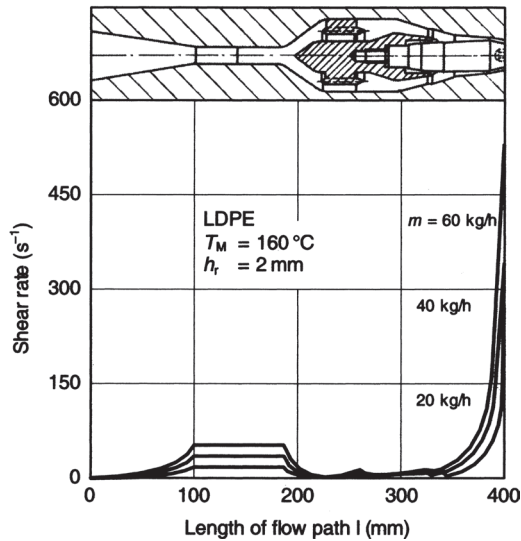


Figure 7.47 Shear rate in a spider die [6]

The average velocity \bar{u} can be expressed in terms of shear rate, channel cross section, and volume flow rate. The adiabatic temperature increase of the melt in the die can be obtained from

$$\Delta T = \frac{\Delta p}{10 \cdot \rho_m \cdot c_{p_m}} \text{ (K)} \quad (7.36)$$

where ΔT = temperature rise (K)
 Δp = pressure difference (bar)
 ρ_m = melt density (g/cm^3)
 c_{p_m} = specific heat of the melt ($\text{kJ}/\text{kg K}$)

Using the previous equations, the shear rate, residence time, and pressure of the melt along a spider die are calculated and shown in Figs. 7.45, 7.46, and 7.47. As seen from these figures the die gap has a marked influence on the pressure [6].

7.3.1.2 Drawdown and Haul-Off Rates

Drawdown occurs when the velocity of the haul-off is greater than the velocity of the extrudate at the die exit. This leads to a reduction of the extrudate cross section. The draw ratio D_R can be expressed as (Fig. 7.48).

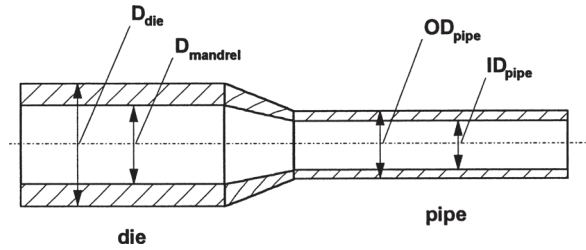


Figure 7.48 Drawdown in pipe extrusion

$$D_R = \frac{D_{die}^2 - D_{mandrel}^2}{OD_{pipe}^2 - ID_{pipe}^2} \tag{7.37}$$

The draw ratio is dependent on the resin and on the haul-off rate. In Fig. 7.49 [8], the ratio of die diameter to pipe diameter, which is referred in practice as the draw ratio, is shown as a function of the haul-off rate for a PA resin. For other resins this ratio has to be determined experimentally.

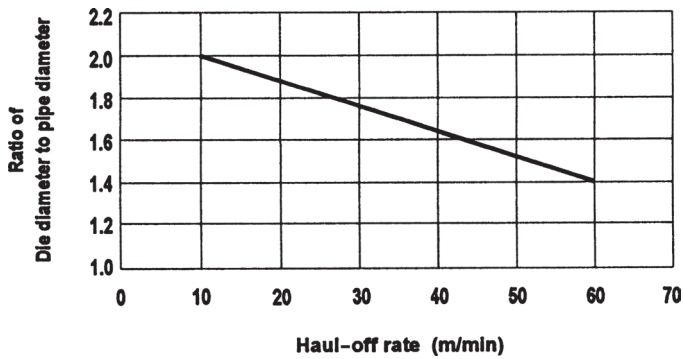


Figure 7.49 Relationship between draw ratio and Haul-off rate [8]

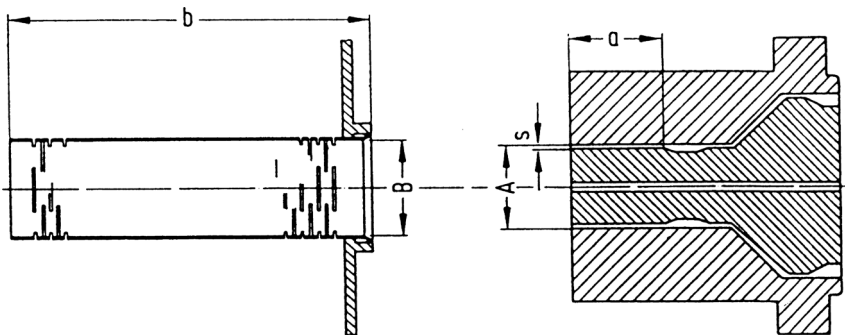
Table 7.8 shows typical data obtained on twin screw extruders for pipes. Design data for pipe dies and sizing units (Fig. 7.50) are given in Table 7.9 [12].

Table 7.8 Typical Data for Twin-Screw Extruders for Pipes out of Rigid PVC [12]

Screw diameter <i>D</i> mm	Screw length <i>L/D</i>	Screw speed min ⁻¹	Screw power kW	Specific energy kWh/kg
60/70	18/22	35/50	15/25	0.1/0.14
80/90	18/22	30/40	28/40	0.1/0.14
100/110	18/22	25/38	58/70	0.1/0.14
120/140	18/22	20/34	65/100	0.1/0.14

Table 7.9 Die and Calibration Unit Dimensions Based on Empirical Results [12]

Pipe raw material	Outer diameter of pipe mm	A mm	B mm	S in % of nominal wall thickness	a at pressure 6 to 10 bar mm	b mm	Haul-off speed m/min
PVC	20	20	20.16	4	30	100/150	20/35
	160	160	161.3	79	150	500/600	2.0/3.5
PE	20	21	21	100	20	150	25/30
	160	168	167.2	100	40/175 ¹	40	1.2/2.2
PP	20	21	21	100	20	150	25/30
	160	168	167.2	100	40/175 ¹	640	1.0/2.0
S [mm]							
PA 12 ¹	8	14.2	8.6	2.0	25	130	55/60
PA 12 ²	20	28.2	20.85	3.3	25/30 ³	130	12/15
PA 12 ²	22	30.0	23.0	3.3	35/50 ³	130	10/12

¹ wall thickness 1 mm² wall thickness 2 mm³ dependent on wall thickness**Figure 7.50** Design data for pipe dies and sizing units (see Table 7.9) [12]

7.3.2 Blown Film

The blow ratio is the ratio between the diameter of blown film to the die lip diameter (Fig. 7.51). The effect of operating variables, such as coolant temperature, in the case of water-cooled films, on some film properties like gloss and haze is shown in Figs. 7.52 – 7.58 [9]. Depending on the material and the type of film, blow ratios range from 1.3:1 to 6:1 [26].

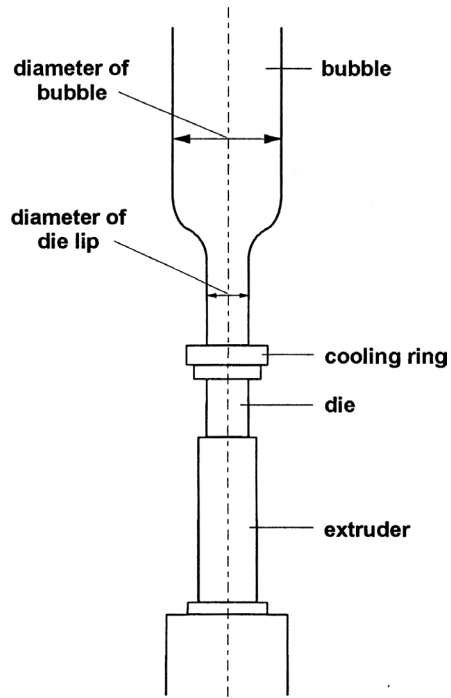


Figure 7.51 Blow-up in blown film

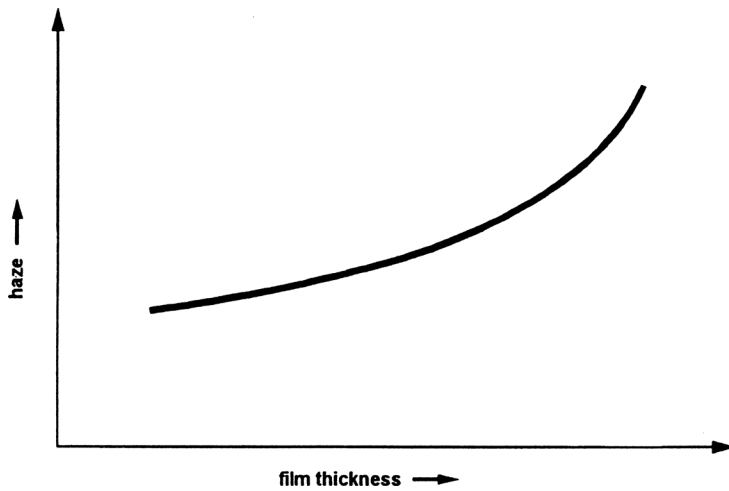


Figure 7.52 Effect of film thickness on haze [9]

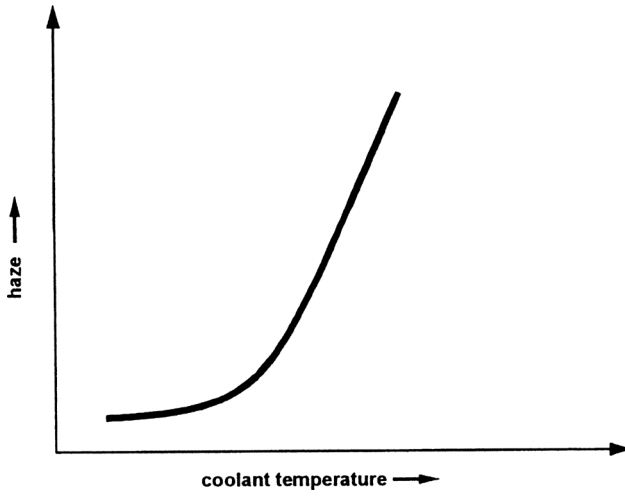


Figure 7.53 Effect of coolant temperature on haze [9]

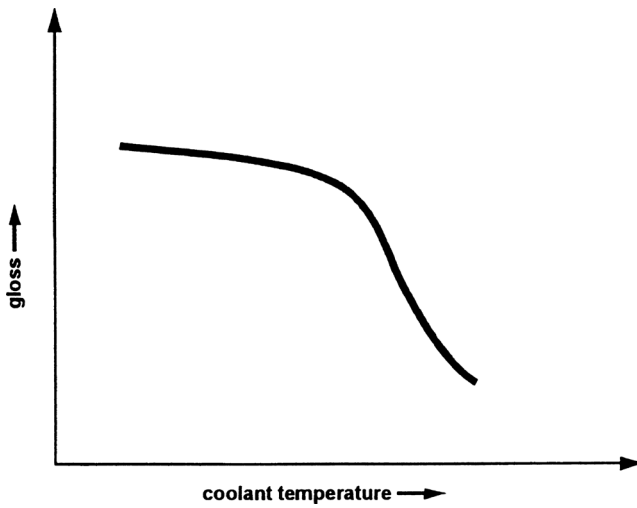


Figure 7.54 Effect of coolant temperature on gloss [9]

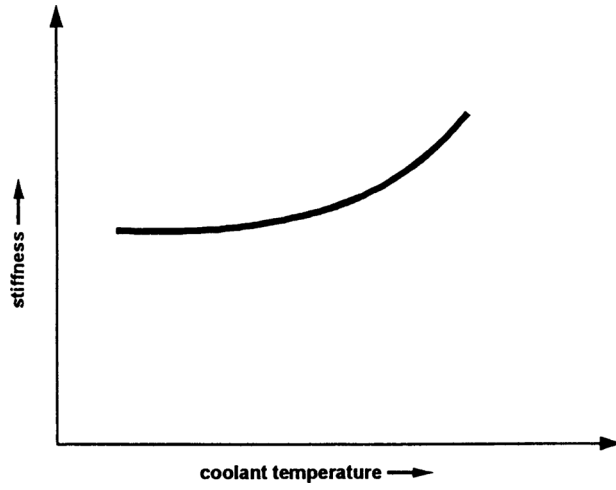


Figure 7.55 Effect of coolant temperature on stiffness [9]

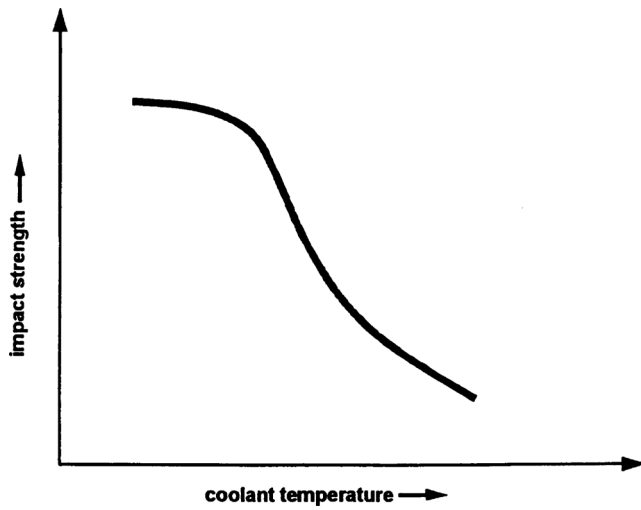


Figure 7.56 Effect of coolant temperature on impact strength [9]

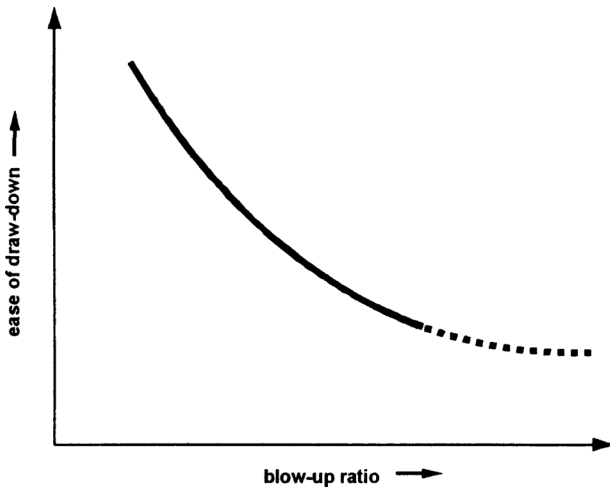


Figure 7.57 Effect of blow-up ratio on ease of draw-down [9]

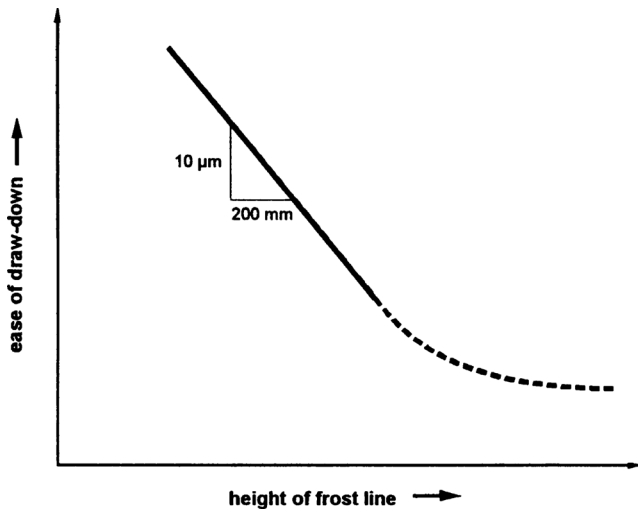


Figure 7.58 Effect of frost line on ease of draw-down [9]

Extruder throughputs for polyethylene blown film lines are given in Table 7.10 [13].

Table 7.10 Data for High Performance PE-LD Blown Film Lines [13]

Screw diameter D mm	Maximum throughput kg/h	Extruder power kW
60	200	55
90	400	110
120	550	170
150	900	300

Side fed and spiral mandrel dies are employed in processes in which the extruder is at an angle, usually 90° , to the direction of the extrudate (Fig. 7.59) [17]. These processes include making annular parisons for blow molding, cable coating, and pipe jacketing, to mention a few examples.

In the extrusion of blown film spiral mandrel dies (Fig. 7.59) are widely used today. The mixing of spiral flow and annular flow of the melt in these dies leads to uniform flow distribution at the die exit, and owing to the lack of spider legs which disturb the melt flow in a spider die there will be no weld lines on the film.

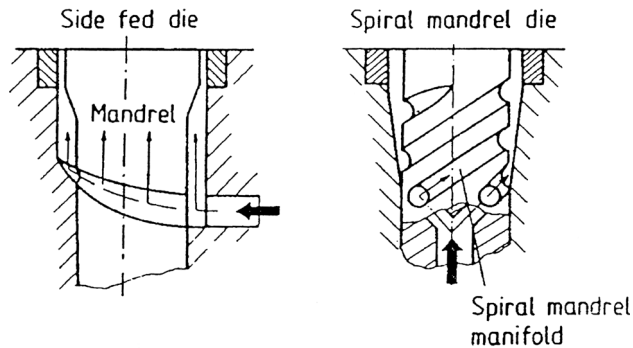


Figure 7.59 Side-fed spiral mandrel dies [17]

Side fed and spiral dies can also be designed using the equations given in the Section 7.3.1. The principle here is to divide the die into a number of segments and by applying the pressure balance to each segment calculate the height of the channel required for uniform flow.

$$\Delta p_{\text{spiral flow in the channel}} = \Delta p_{\text{annular flow in the gap}}$$

This can be done conveniently by means of a computer program such as VISPIRAL [20].

7.3.3 Sheet Extrusion

Dies for sheet and flat film extrusion have a rectangular exit cross section (Fig. 7.41), where the die width W is usually much larger than the height of the slit H . The shear rate in a rectangular channel is calculated from

$$\dot{\gamma} = \frac{6\dot{Q}}{WH^2} \quad (7.38)$$

The pressure drop in a sheet die can be obtained from the relation given by Chung and Lohkamp [10]. For a uniform flow distribution, the radius $R(x)$ along the manifold (Fig. 7.60) is deduced to be [10]

$$R(x) = R_o \left(1 - \frac{x}{L_M} \right)^{\frac{n_r}{(3n_r + 1)}} \quad (7.39)$$

where n_r is the reciprocal of the power law exponent n .

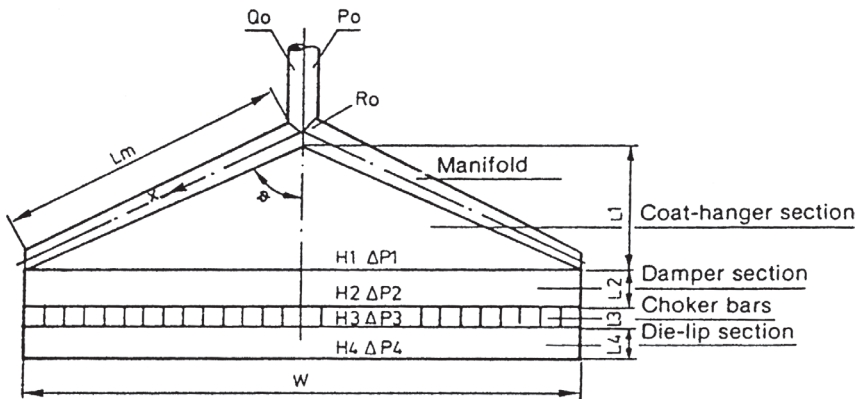


Figure 7.60 Scheme of a typical coat-hanger die [6]

In Fig. 7.61, the calculated manifold radius $R(x)$ is shown as a function of the distance x along the manifold [6]. The pressure drop in the die lip section is given in Fig. 7.62 as a function of the die gap.

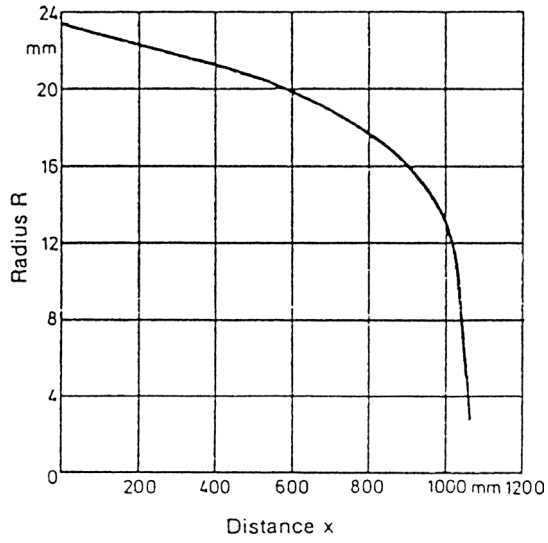


Figure 7.61 Manifold radius $R(x)$ as a function of the distance x along the manifold [6]

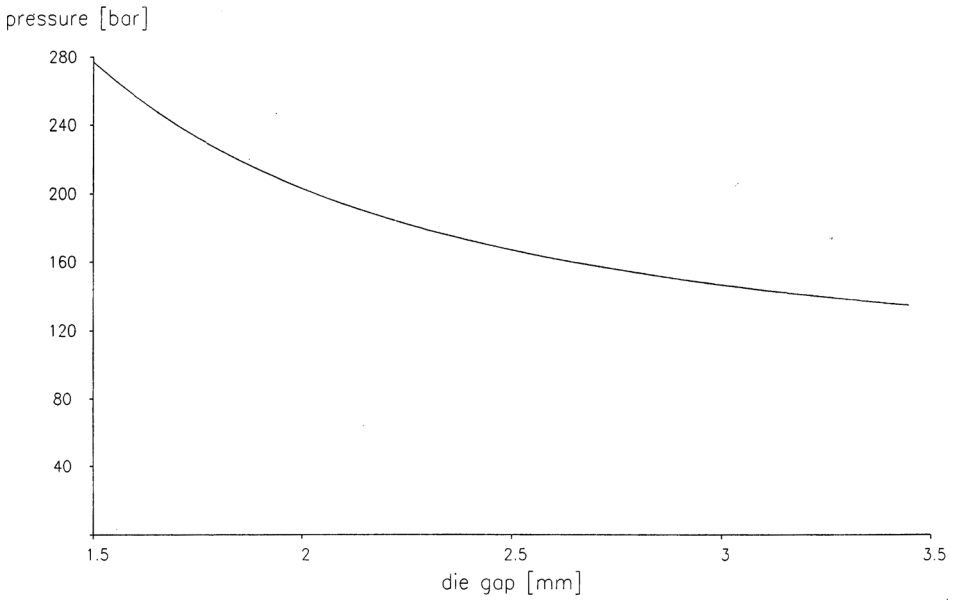


Figure 7.62 Pressure drop in a flat die as a function of die gap

■ 7.4 Thermoforming

In thermoforming, the material initially in the form of a sheet or film is shaped under vacuum or pressure after it has reached a particular temperature. At this temperature, the polymer must have a sufficiently strong viscous component to allow for flow under stress and a significant elastic component to resist flow in order to enable solid shaping. Thus, the optimal conditions for thermoforming occur at a temperature corresponding to the material's transition from a solid rubber state to a viscous liquid state [21].

The effect of different factors related to thermoforming is presented in Figs. 7.63 – 7.67 [22, 23]. Some data including machine dependent parameters are given in Tables 7.11 – 7.14.

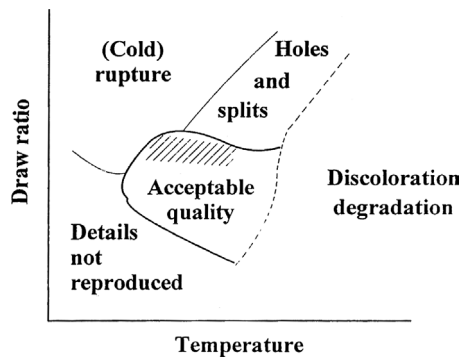


Figure 7.63 Parametrical relationship for thermoforming: draw ratio vs temperature

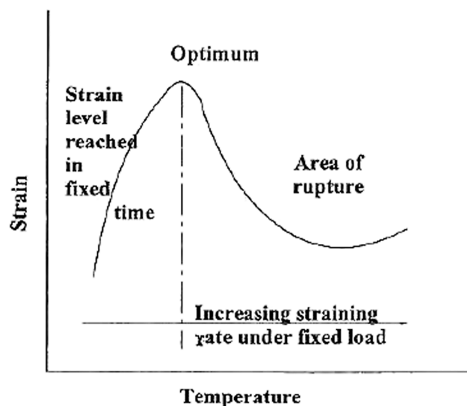


Figure 7.64 Parametrical relationship for thermoforming: strain vs temperature

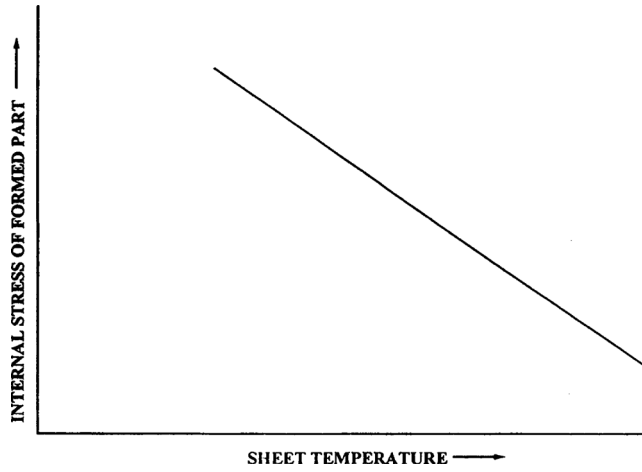


Figure 7.65 Parametrical relationship for thermoforming: internal stress vs. sheet temperature

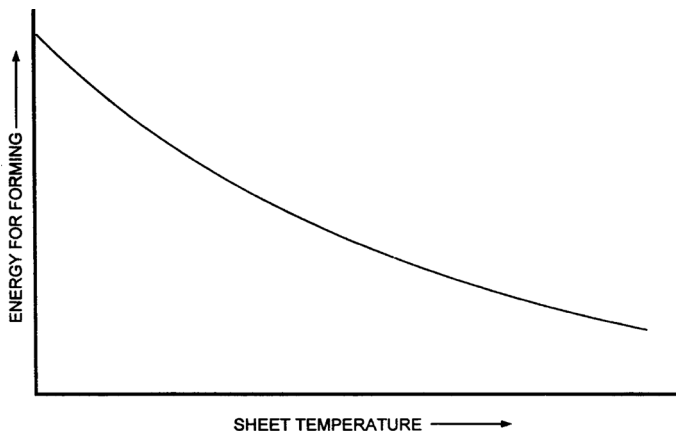


Figure 7.66 Parametrical relationship for thermoforming: energy vs. temperature

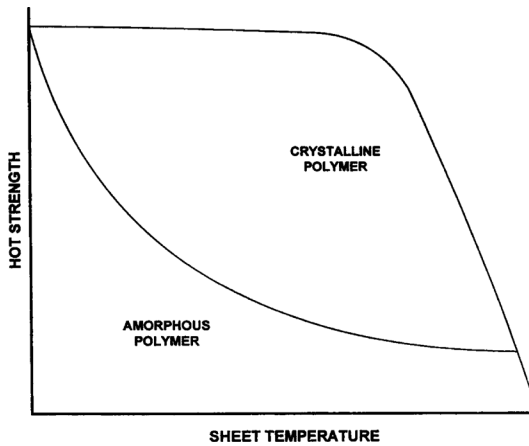


Figure 7.67 Parametrical relationship for thermoforming: hot strength vs. sheet temperature

The production rates for flat and thermoformable films are given in Figs. 7.68 and 7.69 [14] and in Table 7.12 [14]. Table 7.13 shows the thermoforming temperature ranges for various thermoplastics [14].

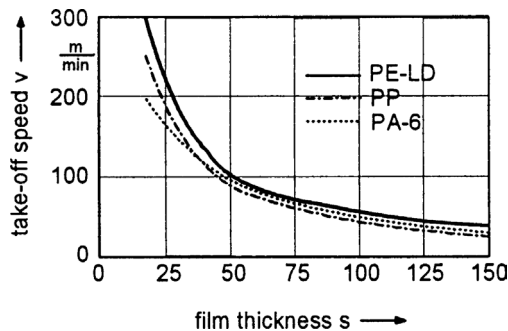


Figure 7.68 Production rates for flat films [14]

Table 7.11 Guide to Thermoforming Processing Temperatures [$^{\circ}\text{C}$] [24]

Polymer	Mold temperature	Lower processing limit	Normal forming heat	Upper limit	Set temperature
PE-HD	71	127	146	166	82
ABS	82	127	163	193	93
PMMA	88	149	177	193	93
PS	85	127	146	182	93
PC	129	168	191	204	138
PVC	60	100	135	149	71
PSU	160	200	246	302	182

Table 7.12 Extruder Outputs for Thermoformable Film Extrusion (Film Thickness Range: 0.4 to 2.0 mm) [14]

Screw diameter <i>D</i> mm	Screw length	Output kg/h			
		PP	SB	ABS	PET
75	30/36 D	180/200	300/320	220/250	120/140
90	30/36 D	260/290	450/500	360/400	180/220
105	30/36 D	320/350	600/650	450/480	240/280
120	30/36 D	480/550	750/850	600/650	320/360
150	30/36 D	650/750	1100/1200	850/900	480/540

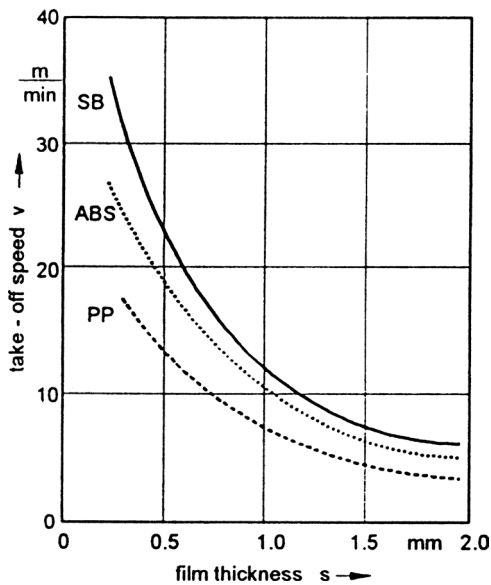


Figure 7.69 Production rates for thermoformable films [14]

Table 7.13 Ranges of Melt and Roll Temperatures Used in Thermoformable Film [14]

Material	Melt temperature °C	Chill roll temperature °C
PP	230/260	15/60
SB	210/230	50/90
ABS	220/240	60/100
PET	280/285	15/60

Table 7.14 Shrinkage Guide for Thermoformed Plastics [24]

Polymer	Shrinkage %
PE-LD	1.6/3.0
PE-HD	3.0/3.5
ABS	0.3/0.8
PMMA	0.2/0.8
SAN	0.5/0.6
PC	0.5/0.8
PS	0.3/0.5
PP	1.5/2.2
PVC-U	0.4/0.5
PVC-P	0.8/2.5

■ 7.5 Compounding

In the compounding of polymers such as polyolefins and PVC twin screw extruders find a wide application. Some machine data are given in the tables below.

Table 7.15 Machine Data of Nonintermeshing Counter-Rotating Twin-Screw Machines for Degassing [25]

Screw diameter D mm	Screw speed n min^{-1}	Drive power N kW	Throughput G kg/h
150	100/180	120/250	670/1250
200	87/150	220/460	1200/2300
250	78/135	370/750	2000/3750
305	70/120	600/1200	3300/6000
380	63/110	970/2000	5400/10000
400	58/100	1500/3000	8300/15000

Table 7.16 Machine Data of Intermeshing Corotating Twin-Screw Extruders (ZSK) for the Concentration of Melts [25]

Screw diameter D mm	Screw speed n min^{-1}	Drive power N kW	Throughput G kg/h
130	180/300	150/240	850/1500
170	150/250	300/490	1750/3000
240	140/230	680/1100	4000/7000
300	110/180	1200/2000	7000/12000

Table 7.17 Data for the Reifenhauer-Extruder with Intermeshing Counter-Rotating Screws for Compounding and Pelletizing of PVC-U and PVC-P [23]

Extruder	Screw diameter mm	Screw length L/D	Drive power N kW	Heating capacity kW	Output kg/h
BT 80 - 12 G	77	12	25	17	120/230
BT 80 - 16 G	77	16	25	17	200/400
BT 100 - 14 G	98	14	33	31	300/550
BT 100 - 18 G	98	18	37	36	450/750
BT 150 - 17 G	150	17	133	88	650/1200

7.5.1 Coextrusion

In many cases, a plastics product made from a single polymer cannot meet the requirements imposed on it. To create layered structures and benefit from the properties of several resins in combination, coextrusion is evenly employed. Examples include multiple layer flat and tubular films, cables with multiple layer insulation, multiple layer blow molded articles, and many more.

To achieve these objectives, dies of different designs are used as shown in Figs. 7.70 and 7.71 [17]. A multilayer extrudate can be produced by conventional dies when an adapter is used to feed the individual melt streams into the die inlet. They flow together through the die and leave it as a coextrudate (Fig. 7.70) [17].

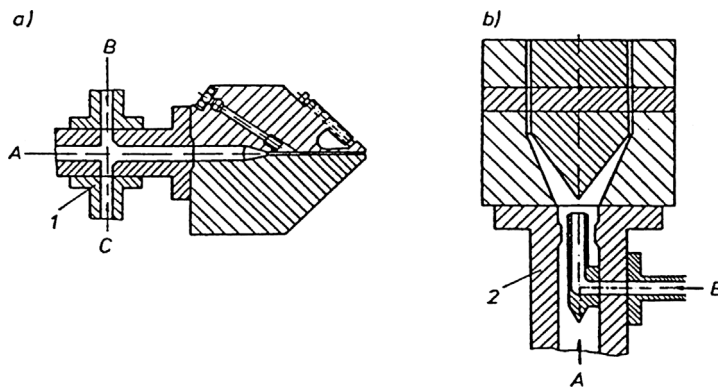


Figure 7.70 Adapter dies: a) flat slit die, b) blown film die

In the multimanifold dies (Fig. 7.71) [17], each melt is first fed separately and distributed into the desired form. These partial streams are then combined just prior to the land area.

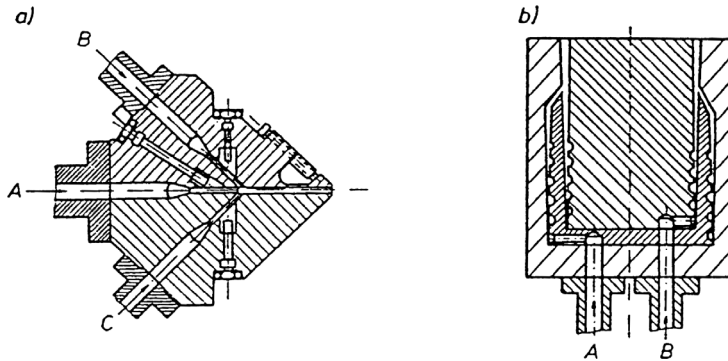


Figure 7.71 Multimanifold dies: a) flat slit die, b) blown film die [17]

Some advantages and disadvantages of adapter and multimanifold dies are summarized in Table 7.18.

Table 7.18 Comparison Between Adapter (Feedblock) Dies and Multimanifold Dies [17]

Type of die	Advantages	Disadvantages
Adapter (Feedblock) dies	Any number of individual layers can be combined.	Polymers used must have almost identical flow behavior and processing temperatures.
Multimanifold dies	<ol style="list-style-type: none"> 1. Each melt can be adjusted individually, if appropriate adjustment is available. 2. The method of combining the melts inside the die under pressure improves the mutual adhesion of the layers. 3. Materials with different flow behavior (Table 7.19) and melt temperature can be processed 	<ol style="list-style-type: none"> 1. Die design is complicated. 2. It is difficult to solve the problem of thermal insulation of the individual channels from each other. 3. For a combination of more than four layers this type of die becomes very complex and costly.

Table 7.19 Examples of Compatibility Between Plastics for Coextrusion [24]

	PE-LD	PE-HD	PP	IONOMER	PA	EVA
PE-LD	3	3	2	3	1	3
PE-HD	3	3	2	3	1	3
PP	2	2	3	2	1	3
IONOMER	3	3	2	3	3	3
PA	1	1	1	3	3	1
EVA	3	3	3	3	1	3

- 1: Layers easy to separate,
 2: Layers can be separated with moderate effort, and
 3: Layers difficult to separate.

■ 7.6 Extrudate Cooling

The cooling of extrudate is an important operation in downstream extrusion processing, as it sets a limit to the production rate. It is an unsteady heat transfer process where mostly conduction and convection determine the rate of cooling. Transient conduction can be described by means of Fourier number and simultaneous conduction and convection by a Biot number. The magnitude of heat transfer coefficients that are necessary to estimate the rate of cooling is given in Table 7.20 for different cooling media.

Table 7.20 Heat Transfer Coefficients for Different Types of Cooling

Mode of cooling	Heat transfer coefficient α_a [W/(m ² · K)]
Air cooling by natural convection	5/10
Air cooling by forced convection	20/80
Water bath	1000/1800
Water sprays	2000/2500

Example [28]:

A wire of polyacetal of diameter 3.2 mm is extruded at 190 °C into a water bath at 20 °C. Calculate the length of the water bath to cool the wire from 190 °C to a centerline temperature of 140 °C for the following conditions:

$$\text{Heat transfer coefficient } \alpha_a = 1700 \text{ W/(m}^2 \cdot \text{K)}$$

$$\text{Thermal diffusivity } a_{\text{plastic}} = 10^{-7} \text{ m}^2/\text{s}$$

$$\text{Thermal conductivity } \lambda_{\text{plastic}} = 0.23 \text{ W/(m} \cdot \text{K)}$$

$$\text{Haul-off rate of the wire } V_H = 0.5 \text{ m/s}$$

Solution:

$$\text{The Biot number } \text{Bi} = \frac{\alpha_a \cdot R}{\lambda}$$

where R = radius of the wire

$$\text{Bi} = \frac{1700 \cdot 1.6}{1000 \cdot 0.23} = 11.13; \quad \frac{1}{\text{Bi}} = 0.0846$$

The temperature ratio Θ_{T_b} :

$$\Theta_{T_b} = \frac{(T_b - T_w)}{(T_a - T_w)} = \frac{140 - 20}{190 - 20} = \frac{120}{170} = 0.706$$

The temperature ratio Θ_{T_0} , based on the centerline temperature, is given in Fig. 7.72 as a function of the Fourier number with the reciprocal of Biot number as parameter [29].

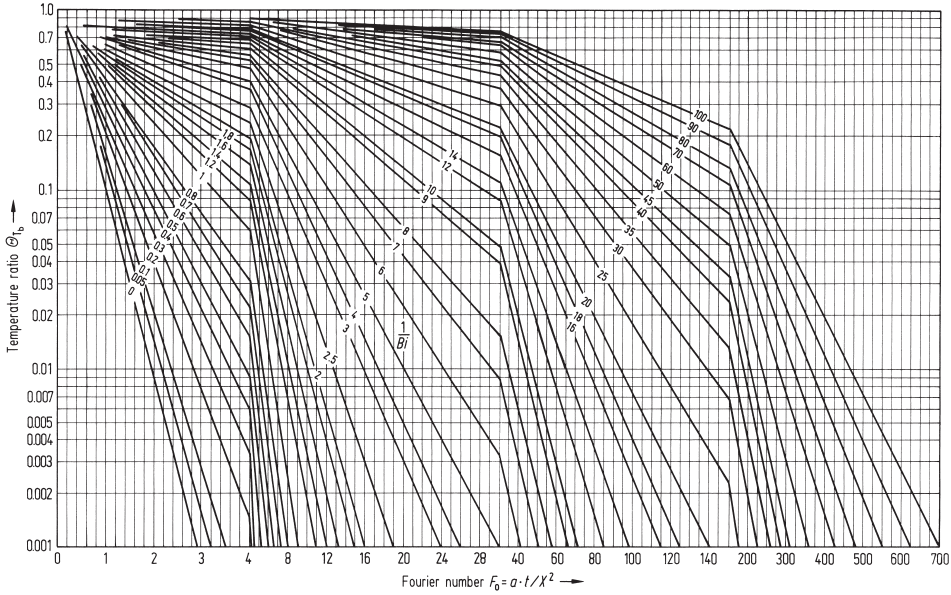


Figure 7.72 Midplane temperature for an infinite plate [29]

The Fourier number F_0 for $\Theta_{T_0} = 0.706$ and $1/\text{Bi} = 0.0846$, and from Fig. 7.72, $F_0 = 0.16$, approximately.

The cooling time t_k follows from the definition of the Fourier number

$$\frac{a \cdot t_k}{R^2} = \frac{10^{-7} \cdot t_k}{(1.6 \cdot 10^{-3})^2} = \frac{t_k}{2.56 \cdot 10} = 0.16$$

$$t_k = 4.1 \text{ s}$$

The length of the water bath is therefore

$$V_H \cdot t_k = 0.5 \cdot 4.1 = 2.05 \text{ m}$$

If the wire is cooled by spraying water onto it as it emerges from the extruder, a heat transfer coefficient of $\alpha_a = 3500 \text{ W}/(\text{m}^2 \cdot \text{K})$ can be assumed.

The Biot number is then

$$\text{Bi} = 3500 \cdot 1.6 / (1000 \cdot 0.23) = 24.35$$

$$1/\text{Bi} = 0.041$$

The Fourier number from Fig. 7.72 is approximately

$$F_0 \approx 0.15$$

The cooling time t_k follows from

$$a \cdot t_k / R^2 = 10^{-7} \cdot t_k / (1.6 \cdot 10^{-3})^2 = 0.15$$

$$t_k = 3.84 \text{ s}$$

This value is not significantly less than the one in the case of cooling in the water bath, since the resistance to heat flow is mainly due to conduction.

Example:

Cooling of a blown film for the following conditions:

thickness of the film: 70 μm

melt temperature: 220 $^\circ\text{C}$

frost line temperature: 110 $^\circ\text{C}$

air temperature: 20 $^\circ\text{C}$

α_a = 120 W / ($\text{m}^2 \cdot \text{K}$)

λ_{plastic} = 0.242 W / ($\text{m} \cdot \text{K}$)

thermal diffusivity a : $1.29 \cdot 10^{-3} \text{ cm}^2/\text{s}$

haul-off speed: 60 m/min

The cooling time t_k is to be calculated.

Solution:

Temperature ratio Θ_{Tb}

$$\Theta_{Tb} = (110 - 20)/(220 - 20) = 0.45$$

Biot number Bi

$$\text{Bi} = 120 \cdot 35 \cdot 10^{-6} / 0.242 = 0.01736$$

$$1/\text{Bi} = 57.6$$

Fourier number F_0 from Fig. 7.72 for $\Theta_{Tb} = 0.45$ and $1/\text{Bi} = 57.6$

$$F_0 = 42.5$$

$$\text{Cooling time } t_k = \frac{x^2 \cdot F_0}{a} = \frac{35 \cdot 35 \cdot 42.5 \cdot 10^3}{10^8 \cdot 1.29} = 0.4 \text{ s}$$

At a haul-off speed of 1 m/s the height of the film to the frost line will be approximately 0.4 m.

Example:

Cooling of a sheet for the following conditions:

thickness of the sheet	$s = 0.25 \text{ mm}$
melt temperature	$T_o = 240 \text{ }^\circ\text{C}$
roll temperature	$T_w = 20 \text{ }^\circ\text{C}$
thermal diffusivity	$a = 1.13 \cdot 10^{-3} \text{ m}^2/\text{s}$
	$\lambda_{\text{plastic}} = 0.12 \text{ W} / (\text{m} \cdot \text{K})$
	$\alpha_a = 1000 \text{ W} / (\text{m}^2 \cdot \text{K})$
haul-off speed	$= 130 \text{ m/min}$

The length of contact between the sheet and the roll required to attain a sheet temperature of $70 \text{ }^\circ\text{C}$ is to be calculated.

Solution:

The Biot number $\text{Bi} = \frac{\alpha_a X}{\lambda}$

$$\text{Bi} = 1000 \cdot 0.125 / 0.12 = 1.04$$

$$1 / \text{Bi} = 0.96$$

$$\Theta_{Tb} = (70 - 120) / 240 - 20 = 50 / 220 = 0.227$$

The Fourier number F_o for $1 / \text{Bi} = 0.96$ and Θ_{Tb} from Fig. 7.72

$$F_o \approx 2$$

$$\text{Cooling time } t_k = \frac{0.125 \cdot 0.125 \cdot 2 \cdot 10^3}{10^2 \cdot 1.13} = 0.276 \text{ s}$$

At a haul-off speed of 2.17 m/s , the length of contact is $L = 2.17 \cdot 0.276 = 0.6 \text{ m}$. For a roll diameter of $D = 250 \text{ mm}$, this amounts to 1.31 times the roll circumference.

These examples give only a rough estimate of the actual values. More realistic results can be obtained by using the software POLYFLOW [20].

7.6.1 Dimensionless Groups

Dimensionless groups can be used to describe complicated processes which are influenced by a large number of variables with the advantage that the whole process can be analyzed on a sound basis by means of a few dimensionless parameters.

The foregoing example shows their application in heat transfer applications. Their use in correlating experimental data and in scaling-up equipment is well known.

Table 7.21 shows some of the dimensionless groups that are often used in plastics engineering.

Table 7.21 Dimensionless Groups

Symbol	Name	Definition
Bi	Biot number	$\alpha_a \cdot l / \lambda^i$
Br	Brinkman number	$\eta w^2 / (\lambda \cdot \Delta T)$
Deb	Deborah number	t_D / t_p
F _o	Fourier number	$a \cdot t / l^2$
Gr	Grashof number	$g \cdot \beta \cdot \Delta T \cdot l^2 / \nu^2$
Gz	Graetz number	$l^2 / (a \cdot t_p)$
Le	Lewis number	a / δ_d
Na	Nahme number	$\beta_T \cdot w^2 \cdot \eta / \lambda$
Nu	Nusselt number	$\alpha l / \lambda$
Pe	Peclet number	$w l / a$
Pr	Prandtl number	ν / a
Re	Reynolds number	$\rho w l / \eta$
Sh	Sherwood number	$\beta_s \cdot l / \delta_d$
Sc	Schmidt number	ν / δ_d
Sk	Stokes number	$p \cdot l / (\eta \cdot w)$

Nomenclature:

- a = thermal diffusivity [m²/s]
- g = acceleration due to gravity [m/s²]
- l = characteristic length [m]
- p = pressure [N/m²]
- t_D = memory time [s]
- t_p = process time [s]
- ΔT = temperature difference [K]
- w = velocity of flow [m/s]
- α_a = outside heat-transfer coefficient [W/(m² · K)]
- β = coefficient of volumetric expansion [K⁻¹]
- β_T = temperature coefficient in the power law of viscosity [1] [K⁻¹]
- β_s = mass transfer coefficient [m/s]
- δ_d = diffusion coefficient [m²/s]
- η = viscosity [Pa · s]
- λ = thermal conductivity (index i refers to the inside value) [W/(m · K)]

ν = kinematic viscosity [m^2/s]

t_v = residence time [s]

t = time [s]

ρ = density [kg/m^3]

■ 7.7 References

- [1] *Rao, N. S.*: Design Formulas for Plastics Engineers, Hanser, Munich, 1991
- [2] *Tadmor, Z., Klein, I.*: Engineering Principles of Plasticating Extrusion, Van Nostrand Reinhold, New York, 1970
- [3] *Bernhardt, E. C.*: Processing of Thermoplastic Materials, Reinhold, New York, 1963
- [4] *Rao, N. S.*: Computer Aided Design of Plasticating Screws, Hanser, Munich, 1986
- [5] *Klein, I., Marshall, D. I.*: Computer Programs for Plastic Engineers, Reinhold, New York, 1968
- [6] *Rao, N. S.*: Designing Machines and Dies for Polymer Processing with Computer Programs, Hanser, Munich, 1981
- [7] *Procter, B.*: SPE J. 28, 1972, p 324
- [8] Brochure: EMS Chemie, 1992
- [9] Brochure: BASF A. G., 1992
- [10] *Chung, C. I., Lohkamp, D. T.*: SPE 33, ANTEC 21, 1975, p 363
- [11] *Fritz, H. G.*: Extrusion Blow Molding in Plastics Extrusion Technology, Ed. F. Hensen, Hanser, Munich, 1988
- [12] *Predöhl, W., Reitemyer, P.*: Extrusion of Pipes, Profiles and Cables in Plastics Extrusion Technology, Ed. F. Hensen, Hanser, Munich, 1988
- [13] *Winkler, G.*: Extrusion of Blown Films in Plastics Extrusion Technology, Ed. F. Hensen, Hanser, Munich, 1988
- [14] *Bongaerts, H.*: Flat Film Extrusion Using Chill-Roll Casting in Plastics Extrusion Technology, Ed. F. Hensen, Hanser, Munich, 1988
- [15] *Rauwendaal, C.*: Polymer Engineering and Science, 21, 1981, p 1092
- [16] *Darnell, W. H., Mol, E. A. J.*: Soc. Plastics Eng. J. 12, 1956, 20
- [17] *Michaeli, W.*: Extrusion Dies, Hanser, Munich, 1992
- [18] *Schenkel, G.*: Private Communication
- [19] *Squires, P. H.*: SPE-J, 16, 1960, p 267
- [20] *Rao, N. S., O'Brien, K. T., Harry, D. H.*: Computer Modelling for Extrusion and Other Continuous Polymer Processes, Ed. Keith T. O'Brien, Hanser, Munich, 1992
- [21] *Eckstein, Y., Jackson, R. L.*: Plastics Engineering 5, 1995
- [22] *Ogorkiewicz, R. M.*: Thermoplastics - Effects of Processing, Iliffe Books Ltd, London, 1969
- [23] *Titow, W. V.*: PVC Technology, Elsevier Applied Science Publishers, London, 1984
- [24] *Rosato, D. V., Rosato, D. V.*: Plastics Processing Data Handbook, Van Nostrand-Reinhold, New York, 1990
- [25] *Hermann, H.*: Compound Lines in Plastics Extrusion Technology, Ed. F. Hensen, Munich, 1988

- [26] *Hensen, F.*: *Plastics Extrusion Technology*, Hanser, Munich, 1988
- [27] *Rauwendaal, C.*: *Polymer Extrusion*, Hanser, Munich, 1986
- [28] *Ogorkiewicz, R. M.*: *Thermoplastics and Design*, John Wiley, New York, 1973
- [29] *Kreith, F., Black, W. Z.*: *Basic Heat Transfer*, Harper & Row, New York, 1980

8

Blow Molding

■ 8.1 Processes

The different processes of blow molding, namely extrusion blow molding, injection blow molding, and stretch blow molding, are illustrated in Figs. 8.1 to 8.4 [1, 2].

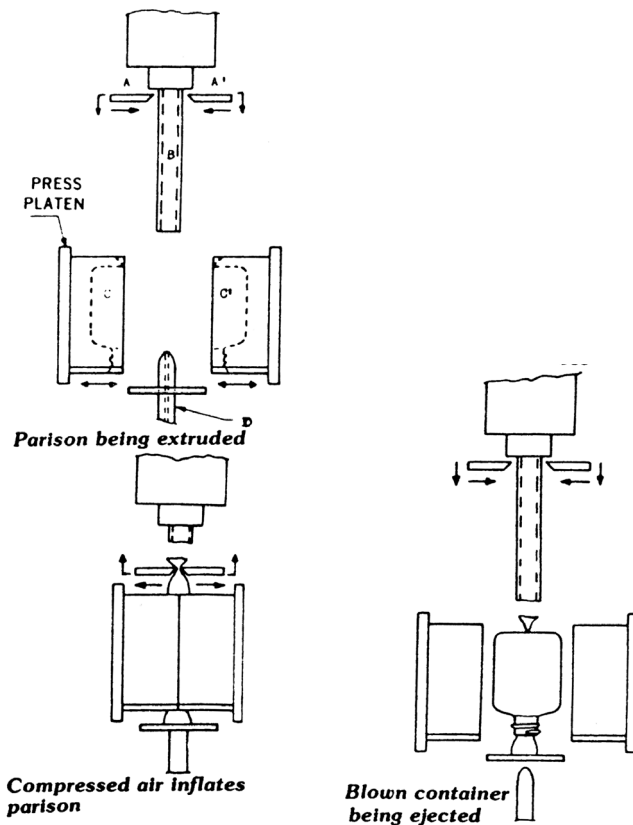


Figure 8.1 Extrusion blow molding [1]

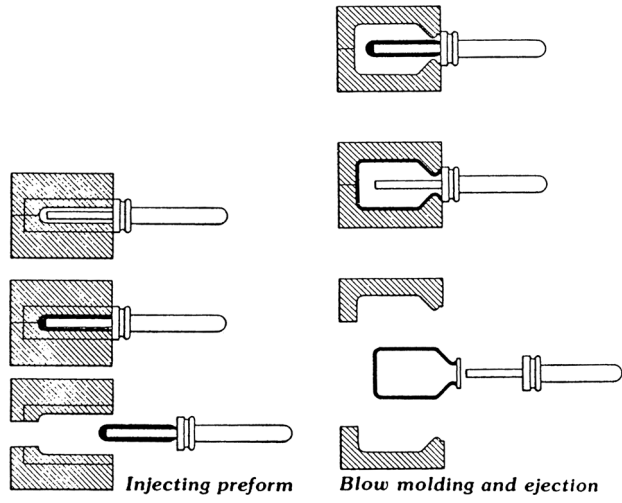


Figure 8.2 Injection blow molding [1]

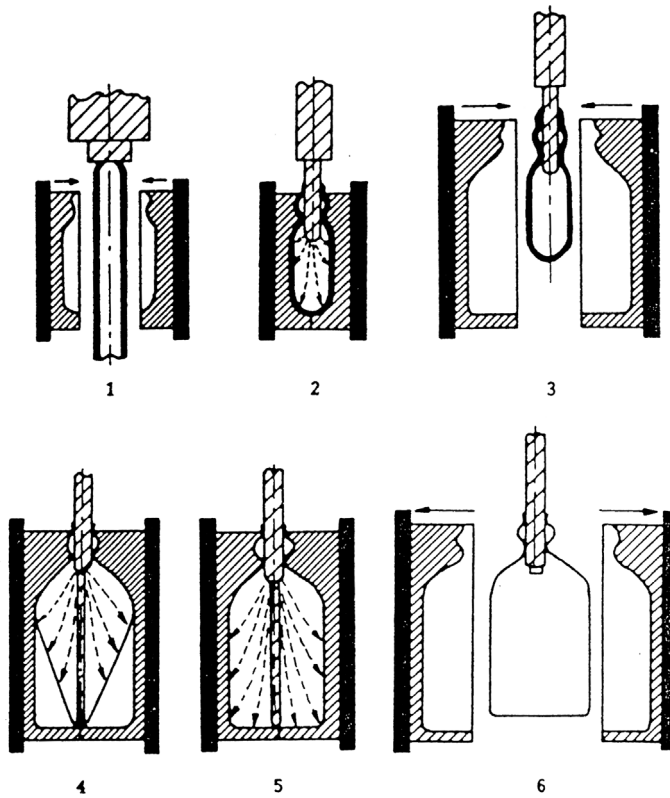


Figure 8.3 Extrusion stretch blow molding [2]

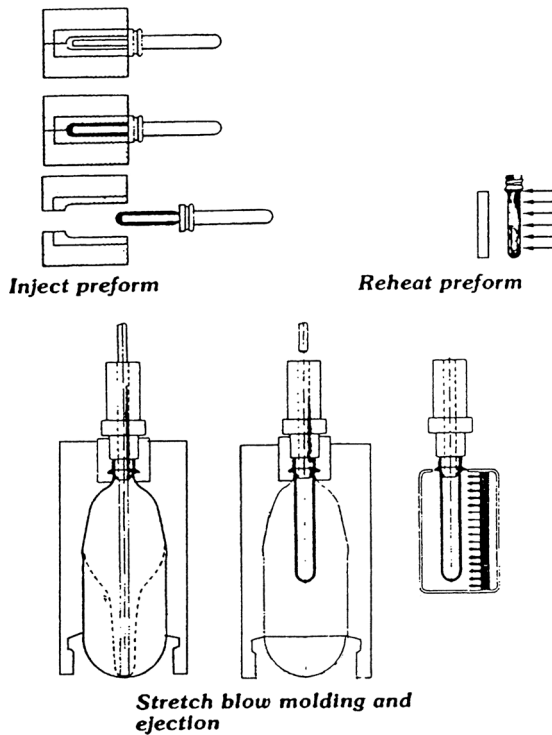


Figure 8.4 Injection stretch blow molding [2]

8.1.1 Resin-Dependent Parameters

8.1.1.1 Melt Temperature and Pressure

Typical values of melt temperature and melt pressure for extrusion blow molding are given in Table 8.1, and the average parison swell for some polymers is given in Table 8.2 [1].

Table 8.1 Melt Temperature and Pressure for Extrusion Blow Molding of Some Polymers

Material	Melt temperature °C	Melt pressure bar
PE-LD	140/150	100/150
PE-HD	160/190	100/200
PP	230/235	150/200
PVC-U	180/210	100/200
PVC-P	160/165	75/150

Table 8.2 Average Parison Swell for Some Polymers [1]

Polymer	Swell %
PE-HD (Phillips)	15/40
PE-HD (Ziegler)	25/65
PE-LD	30/65
PVC-U	30/35
PS	10/20
PC	5/10

8.1.1.1.1 Processing Data for Stretch Blow Molding

Data on some polymers used in stretch blow molding are given in Table 8.3.

Table 8.3 Data on Stretch Blow Molding for Some Polymers [1]

Polymer	Melt temperature °C	Stretch orientation temperature °C	Maximum stretch ratio
PET	250	88/116	16:1
PVC	200	99/116	7:1
PP	170	121/136	6:1
PAN	210	104/127	9:1

8.1.1.1.2 Volume Shrinkage

The volume shrinkage of various stretched blow-molded bottles at seven days is given in Table 8.4.

Table 8.4 Volume Shrinkage of Stretched Blow Molded Bottles (Seven Days at 27°C) [1]

Type of bottle	Percent
Extrusion blow molded PVC	-
Impact-modified PVC (high orientation)	4.2
Impact-modified PVC (medium orientation)	2.4
Impact-modified PVC (low orientation)	1.6
Nonimpact modified PVC (high orientation)	1.9
Nonimpact modified PVC (medium orientation)	1.2
Nonimpact modified PVC (low orientation)	0.9
PET	1.2

8.1.1.1.3 Choice of Material

Data for choosing a polymer for blow molding are given in Table 8.5, along with information about appearance and cost.

Table 8.5 Data for Choosing Blow Molding Materials [8]

Polymer	Appearance in blow molded form	Cost for equivalent stiffness (PE-LD = 100)
High-impact PVC-U	clear high gloss	104
PE-LD	translucent, high gloss	100
Low-impact PVC-U	very clear, high gloss	87
High-impact PP	rather opaque, low gloss	79
PE-HD	rather opaque, low gloss	76
Low-impact PP	translucent, moderate gloss	71

8.1.2 Machine-Related Parameters

8.1.2.1 Blow Molding Dies

As the parison is always ejected downward and the position of the extruder is usually horizontal, the term cross-head dies may be applied to blow molding dies. These can be of the spider type or side fed dies as shown schematically in [6]; see Fig. 8.5. As mentioned earlier, these dies can be designed by using the equations given in Chapter 7.

Data on air blowing pressures and temperatures for cavities in blow molds are given in Tables 8.6 and 8.7, respectively.

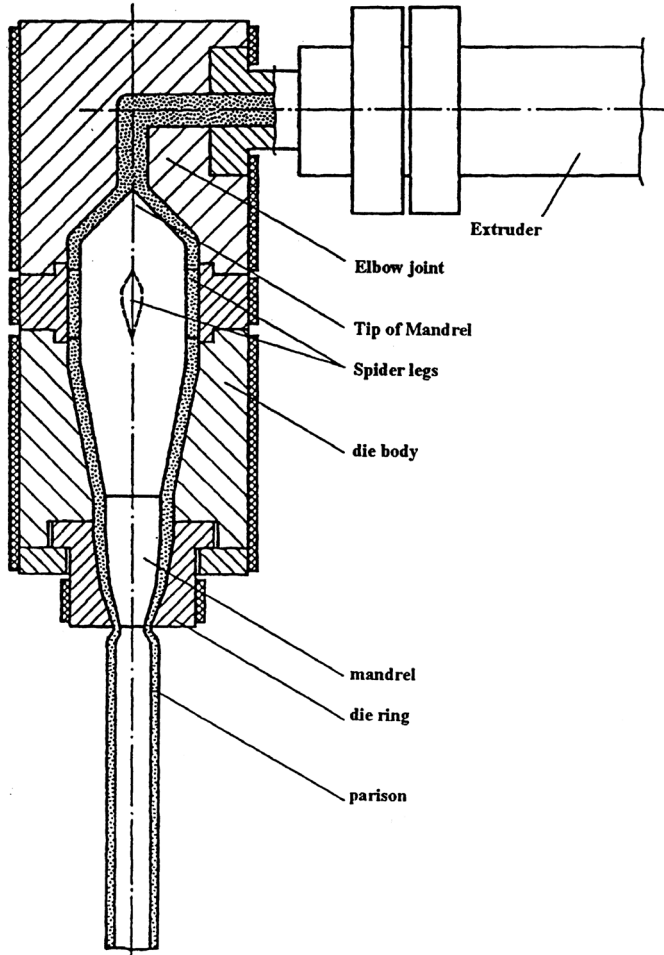


Figure 8.5 Application of spider die in blow molding [5]

Table 8.6 Data on Air Blowing Pressures [1]

Polymer	Pressure bar
Acetal	6.9/10.34
PMMA	3.4/5.2
PC	4.8/10.34
PE-LD	1.38/4.14
PE-HD	4.13/6.9
PP	5.2/6.9
PS	2.76/6.9
PVC-U	5.2/6.9
ABS	3.4/10.34

Table 8.7 Recommended Temperature for Cavities in Blow Molds [1]

Polymer	Temperature °C
PE and PVC	15/30
PC	50/70
PP	30/60
PS	40/65
PMMA	40/60

■ 8.2 References

- [1] *Rosato, D. V., Rosato, D. V.*: Plastics Processing Data Handbook, Van Nostrand-Reinhold, New York, 1990
- [2] *Titow, W. V.*: PVC Technology, Elsevier Applied Science Publishers, London, 1984
- [3] *Morton-Jones, D. H.*: Polymer Processing, Chapman and Hall, New York, 1981
- [4] *Cogswell, F. N.*: Polymer Melt Rheology, John Wiley, New York, 1981
- [5] BASF Brochure on Blow Molding, 1970
- [6] *Michaeli, W.*: Extrusion Dies, Hanser, Munich, 1992
- [7] *Rosato, D. V., Rosato, D. V.*: Injection Molding Handbook, Van Nostrand-Reinhold, New York, 1986
- [8] *Glyde, B. S.*: Blow Moulding in Thermoplastics, Effects of Processing, Ed. R. M. Ogorkiewicz, Iliffe Books Ltd, London, 1969

9

Injection Molding

Among the polymer processing operations, injection molding (Fig. 9.1) has found the widest application for making articles that can be put to direct use.

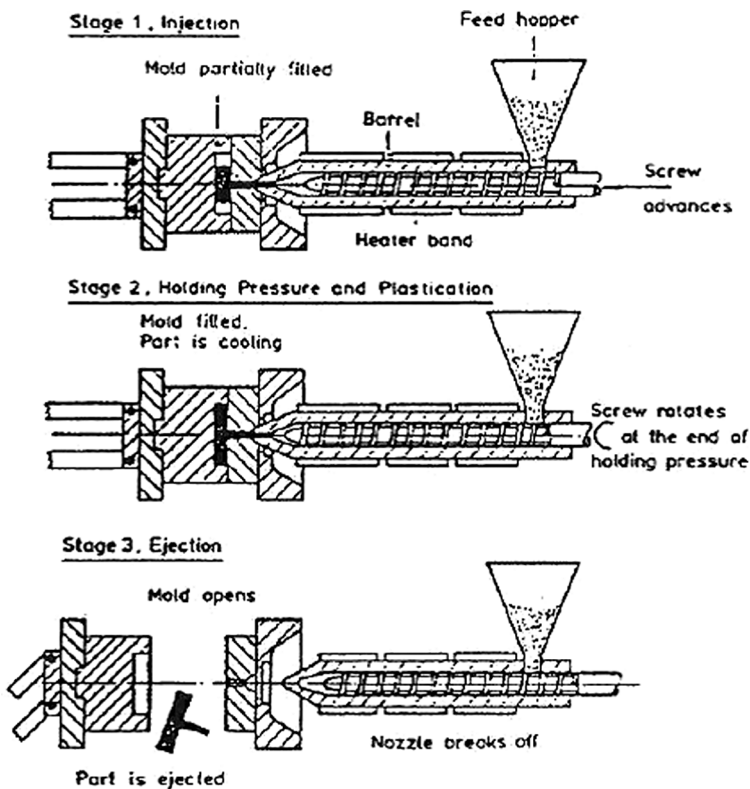
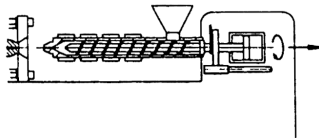


Figure 9.1 The three stages of injection molding: injection, plastication, and ejection [1]

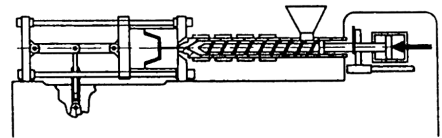
The molding equipment consists of an injection unit, an injection mold, and a mold temperature control unit. The quality of the part depends on how well the interaction between these components functions.

At an appropriate point in the typical molding cycle (Fig. 9.1), the screw remains stationary in the forward position (Fig. 9.2), as indicated by phase 5 in Fig. 9.3 [1]. At the end of dwell or holding pressure, the screw begins to rotate conveying plastic material and developing a pressure ahead of the screw. This pressure pushes the screw to move back a predetermined distance, which is dependent on the desired volume of the molded part. The screw is then idle in the back position while the previously molded plastic continues cooling in the mold, and the mold is open and part ejected. After the mold closes, the screw is forced forward by the hydraulic pressure, causing the newly recharged shot in front of the screw to flow into the empty mold. A valve, such as a cheek ring (Fig. 9.11), prevents back flow during injection. The screw then maintains pressure on the molded plastic for a specific time, which is called the dwell or hold time, thus completing the cycle [6].

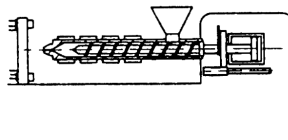
step 1: start of plastication



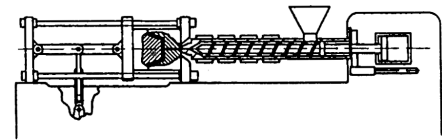
step 4: start of injection



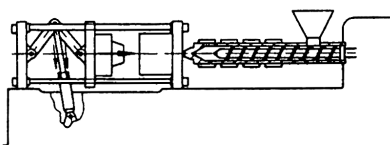
step 2: end of plastication



step 5: end of injection and cooling of the molding



step 3: closing the mold



step 6: ejection of molding

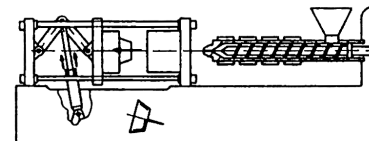


Figure 9.2 Injection molding process [2]

The important processing variables in the injection molding process, and their effect on the plastic material and final part, are shown in Fig. 9.4. Here, the cavity pressure is illustrated as a function of time during the molding of a part [1].

As in extrusion, the processing parameters can be classified into resin-dependent and machine-related parameters.

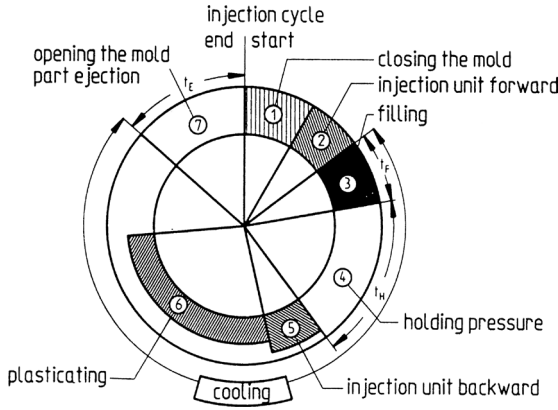


Figure 9.3 Molding cycle [3]

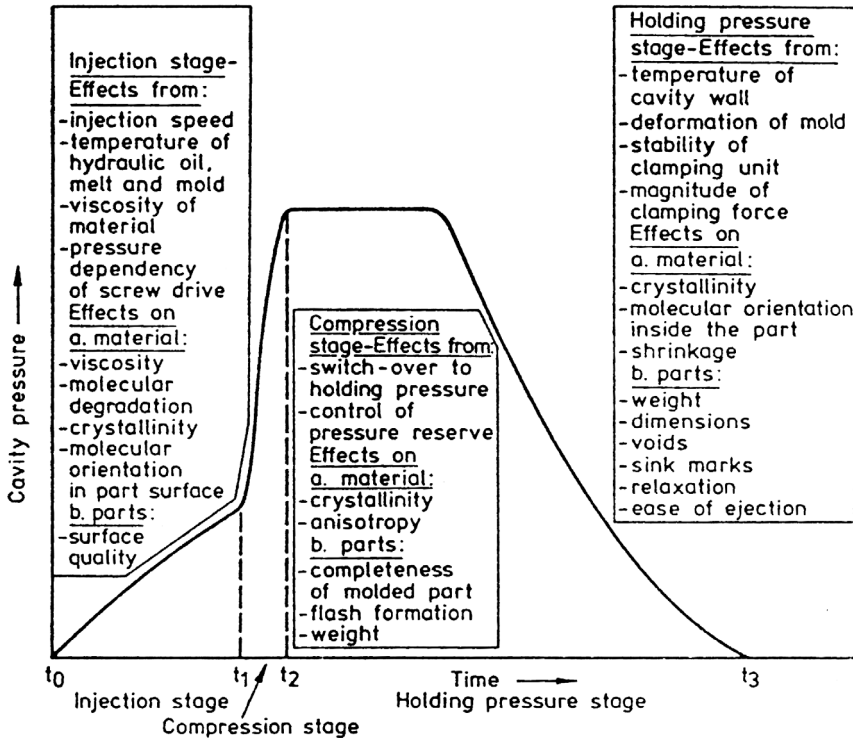


Figure 9.4 Cavity pressure profile over time [1]

■ 9.1 Resin-Dependent Parameters

9.1.1 Injection Pressure

Injection pressure is the pressure exerted on the melt in front of the screw tip during the injection stage, with the screw acting like a plunger [1]. It affects both the speed of the advancing screw and the process of filling the mold cavity with the polymer melt, and also corresponds to the flow resistance of the melt in the nozzle, sprue, runner, and cavity. The injection pressures required for some resins are given in Table 9.1 [1]. The maximum injection pressure is approximately 1.2 times the pressure listed in Table 9.1.

Table 9.1 Injection Pressure Required for Various Plastics [1]

Material	Necessary Injection Pressure [MPa]		
	Low viscosity, heavy sections	Medium viscosity, standard sections	High viscosity, thin sections, small gates
ABS	80/110	100/130	130/150
POM	85/100	100/120	120/150
PE	70/100	100/120	120/150
PA	90/110	110/140	> 140
PC	100/120	120/150	< 150
PMMA	100/120	120/150	< 150
PS	80/100	100/120	120/150
Rigid PVC	100/120	120/150	> 150
Thermosets	100/140	140/175	175/230
Elastomers	80/100	100/120	120/150

9.1.2 Mold Shrinkage and Processing Temperature

Due to their high coefficients of thermal expansion, components molded from plastics experience significant shrinkage effects during the cooling phase. Semi-crystalline polymers tend to shrink more, owing to the greater specific volume difference between melt and solid. Shrinkage S can be defined by [2]

$$S = \frac{L^* - L}{L^*} \quad (9.1)$$

where L^* is any linear dimension of the mold, and L , the corresponding dimension of the part when it is at some standard temperature and pressure. As a consequence of mold shrinkage, it is necessary to make core and cavity slightly larger in dimension than the size of the finished part.

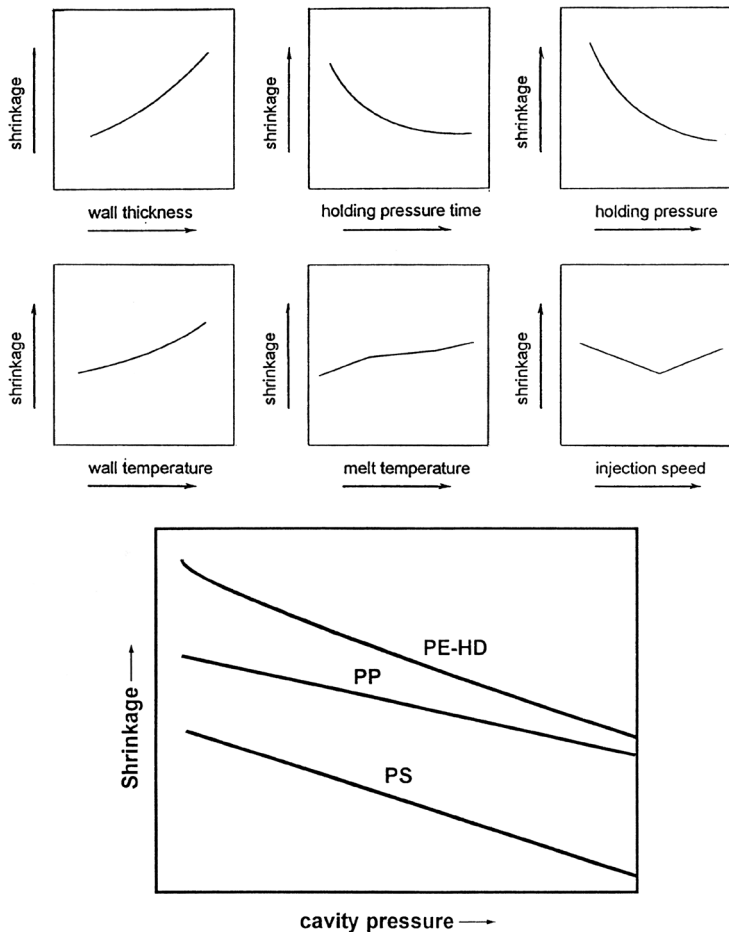
Processing temperature, mold temperature, and shrinkage are given in Table 9.2 for a number of materials [1]. The parameters influencing shrinkage behavior are shown in Fig. 9.5 [1].

Table 9.2 Processing Temperatures, Mold Temperatures, and Shrinkage for the Most Common Plastics Processed by Injection Molding [1]

Material	Glass fiber content %	Processing temperature °C	Mold temperature °C	Shrinkage %
PS		180/280	10/10	0.3/0.6
HI-PS		170/260	5/75	0.5/0.6
SAN		180/270	50/80	0.5/0.7
ABS		210/275	50/90	0.4/0.7
ASA		230/260	40/90	0.4/0.6
PE-LD		160/260	50/70	1.5/5.0
PE-HD		260/300	30/70	1.5/3.0
PP		250/270	50/75	1.0/2.5
PP-GR	30	260/280	50/80	0.5/1.2
IB		150/200		
PMP		280/310	70	1.5/3.0
PVC-soft		170/200	15/50	> 0.5
PVC-rigid		180/210	30/50	- 0.5
PVDF		250/270	90/100	3/6
PTFE		320/360	200/230	3.5/6.0
PMMA		210/240	50/70	0.1/0.8
POM		200/210	> 90	1.9/2.3
PPO		250/300	80/100	0.5/0.7
PPO-GR	30	280/300	80/100	< 0.7
CA		180/230	50/80	0.5
CAB		180/230	50/80	0.5
CP		180/230	50/80	0.5
PC		280/320	80/100	0.8
PC-GR	10/30	300/330	100/120	0.15/0.55
PET		260/290	140	1.2/2.0
PET-GR	20/30	260/290	140	1.2/2.0
PBT		240/260	60/80	1.5/2.5
PBT-GR	30/50	250/270	60/80	0.3/1.2
PA 6		240/260	70/120	0.5/2.2
PA 6-GR	30/50	270/290	70/120	0.3/1
PA 66		260/290	70/120	0.5/2.5
PA 66-GR	30/35	280/310	70/120	0.5/1.5
PA 11		210/250	40/80	0.5/1.5

Table 9.2 Processing Temperatures, Mold Temperatures, and Shrinkage for the Most Common Plastics Processed by Injection Molding [1] (Continued)

Material	Glass fiber content %	Processing temperature °C	Mold temperature °C	Shrinkage %
PA 12		210/250	40/80	0.5/1.5
PSO		310/390	100/160	0.7
PPS	40	370	> 150	0.2
PUR		195/230	20/40	0.9
PF		60/80	170/190	1.2
MF		70/80	150/165	1.2/2
MPF		60/80	160/180	0.8/1.8
UP		40/60	150/170	0.5/0.8
EP	30/80	ca. 70	150/170	0.2

**Figure 9.5** Qualitative relations between individual process parameters and shrinkage behavior [17]

9.1.3 Drying Temperatures and Times

As mentioned in Section 6.1.4, plastics absorb water at a rate that depends on the relative humidity of the air where they are stored, see Table 9.3 [3].

Table 9.3 Equilibrium Moisture Content of Various Plastics Stored in Air at 23 °C and Relative Humidity 50% [3]

	CA	CAB	ABS	PA6	PA66	PBT	PC	PMMA	PPO	PET
Equilibrium moisture (%)	2.2	1.3	1.5	3	2.8	0.2	0.19	0.8	0.1	0.15
Water content acceptable for injection molding [%]	0.2	0.2	0.2	0.15	0.03	0.02	0.08	0.05	0.02	0.02

Moisture and monomers have an adverse effect on processing and on the final part. To remove moisture, materials are dried in their solid or melt state. Table 9.4 shows the drying temperatures and times for different resins and dryers [17].

Table 9.4 Drying Temperatures and Times of Various Dryers [17]

Material	Drying temperature, °C		Drying time, h	
	fresh air/mixed air dryers	dehumidifying dryers	fresh air/mixed air dryers	dehumidifying dryers
ABS	80	80	2/3	1/2
CA	70/80	75	1/1.5	1
CAB	70/80	75	1/1.5	1
PA 6	not recommended	75/80	-	2
PA 66, 6.10	not recommended	75/80	-	2
PBT, PET	120	120	3/4	2/3
PC	120	120	2/4	2
PMMA	80	80	1/2	1/1.5
PPO	120	120	1/2	1/1.5
SAN	80	80	1/2	1/1.5

9.1.4 Flow Characteristics of Injection-Molding Resins

The flow behavior of injection-molding materials can be determined on the basis of melt flow in a spiral channel. In practice, a spiral-shaped mold of rectangular cross section with the height and width in the order of a few millimeters is often used to classify the resins according to their flowability (Fig. 9.6). The length L of the solid-

ified plastic in the spiral is taken as a measure of the viscosity of the polymer concerned (Fig. 9.7).

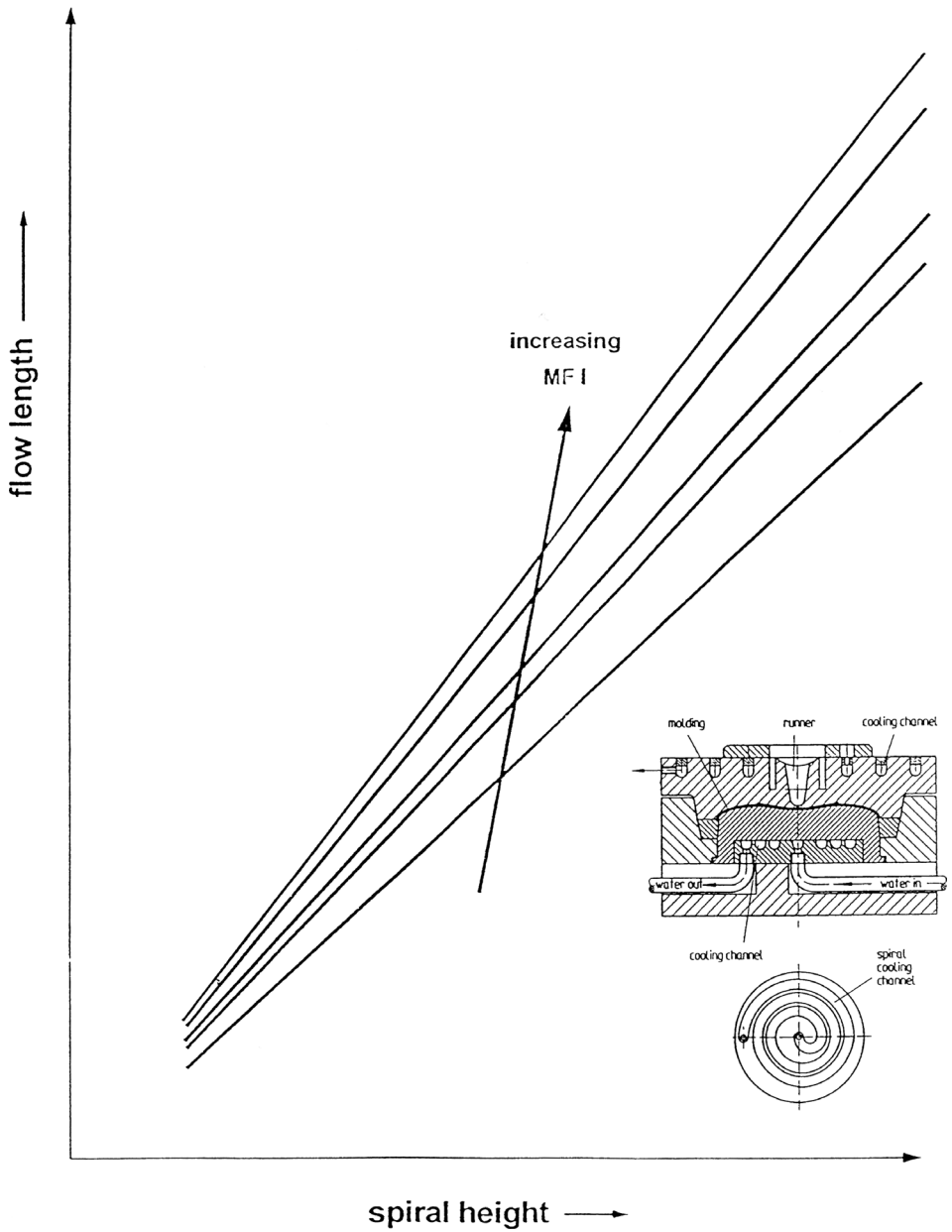


Figure 9.6 Flow length in a spiral test as a function of the resin MFI

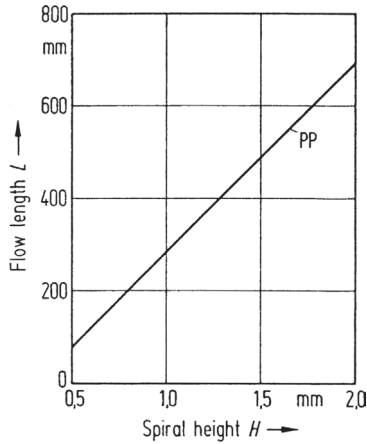


Figure 9.7 Flow Length L as function of the spiral height H [28]

Figure 9.7 shows the experimentally determined flow length L as a function of the height H of the spiral for polypropylene. A quantitative relation between L and the parameters influencing L , such as type of resin, melt temperature, mold temperature, and injection pressure, can be developed [4] by using the dimensionless numbers as defined by Throne [19]. As shown in [17], the Graetz number correlates well with the product $\text{Re} \cdot \text{Pr} \cdot \text{Br}$.

$$\text{Gz} = f(\text{Re} \cdot \text{Pr} \cdot \text{Br}) \quad (9.2)$$

from which an explicit relationship for the flow length L can be computed.

Example [1]:

This example illustrates the calculation of the dimensionless numbers, Gz , Re , Pr , and Br , for the given data and for resin-dependent constants given in [1]:

Width of the spiral	$W = 10 \text{ mm}$
Height of the spiral	$H = 2 \text{ mm}$
Flow length	$L = 420 \text{ mm}$
Melt density	$\rho = 1.06 \text{ g/cm}^3$
Specific heat	$c_p = 2 \text{ kJ}/(\text{kg} \cdot \text{K})$
Thermal conductivity	$\lambda = 1.5 \text{ W}/(\text{m} \cdot \text{K})$
Melt temperature	$T_M = 270 \text{ }^\circ\text{C}$
Mold temperature	$T_W = 70 \text{ }^\circ\text{C}$
Mass flow rate	$G = 211.5 \text{ kg/h}$

Solution:

The conversion factors for the units used in the following calculation of the dimensionless numbers are

$$F_1 = 0.001; F_2 = 1000; F_3 = 3600$$

The Graetz number Gz is calculated from

$$Gz = \frac{F_2 \cdot G \cdot c_p}{F_1 \cdot F_3 \cdot \lambda \cdot L} \quad (9.3)$$

with G in kg/h and L in mm.

From the above data, $Gz = 186.51$.

The Reynolds number (Re) is obtained from

$$Re = \frac{F_2 \cdot V_e^{(2-n_R)} \cdot \rho \cdot H^{*n_R}}{k^*} \quad (9.4)$$

where V_e = velocity of the melt front in m/s
 H^* = half-height of the spiral in mm
 n_R = reciprocal of the power law exponent
 $k^* = \eta \dot{\gamma}^{(1-n_R)}$

The viscosity η can be calculated from the melt temperature and shear rate [9].

For the given values $Re = 0.03791$ [9].

With H^* in meters (m) and V_e in m/s, we get for the Prandtl number, Pr :

$$Pr = \frac{F_2 \cdot k^* \cdot c_p \cdot H^{*(1-n_R)}}{\lambda \cdot V_e^{(1-n_R)}} \quad (9.5)$$

$$Pr = 103,302.87$$

The Brinkman number, Br [8]:

$$Br = \frac{k^* \cdot V_e^{(1+n_R)} \cdot H^{*(1-n_R)}}{\lambda \cdot (T_M - T_W)} \quad (9.6)$$

V_e follows from $V_e = \frac{\dot{Q}}{W \cdot H}$ with $\dot{Q} = \frac{G}{\rho}$

$$Br = 1.9833$$

Finally, the product of $Re \cdot Pr \cdot Br$ is 7768.06.

From the plot of Gz vs. $Re \cdot Pr \cdot Br$ (Fig. 9.8) [9], which is obtained by measuring the flow length at different values of spiral height, melt temperature, and flow rate, the Graetz number corresponding to the calculated product of $Re \cdot Pr \cdot Br$ is used to find the flow length L .

Symbols and units used in the formulas above:

Br Brinkman number

c_p Specific heat kJ/kg·K

$\dot{\gamma}$ Shear rate s^{-1}

G Mass flow rate kg/h

Gz Graetz number

H Height of the spiral mm

H^* Half-height of the spiral mm

L Length of the spiral mm

n_r Reciprocal of the power law exponent

Pr Prandtl number

\dot{Q}_0 Volume flow rate m^3/s

Re Reynolds number

T_M Melt temperature $^{\circ}C$

T_W Mold temperature $^{\circ}C$

V_e Velocity of the melt front m/s

W Width of the spiral mm

λ Thermal conductivity W/m·K

ρ Melt density g/cm^3

η Melt viscosity Pa·s

In the case of thermosetting resins, the flow can be defined as a measure of melt viscosity, gelation rate, and subsequent polymerization or cure [18].

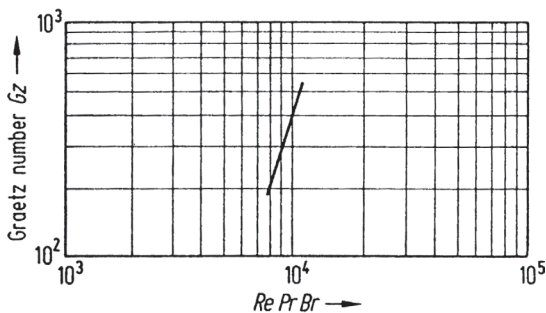


Figure 9.8 Dimensionless groups for determining the flow length L in a spiral test

■ 9.2 Machine-Related Parameters

9.2.1 Injection Unit

The average travel velocities of injection units (Fig. 9.9) [1] are given in Table 9.5 [1]. Table 9.6 [1] shows the common forces with which the nozzle is in contact with the sprue bushing. This contact pressure prevents the melt from leaking into the open at the interface between the nozzle and sprue bushing [1].

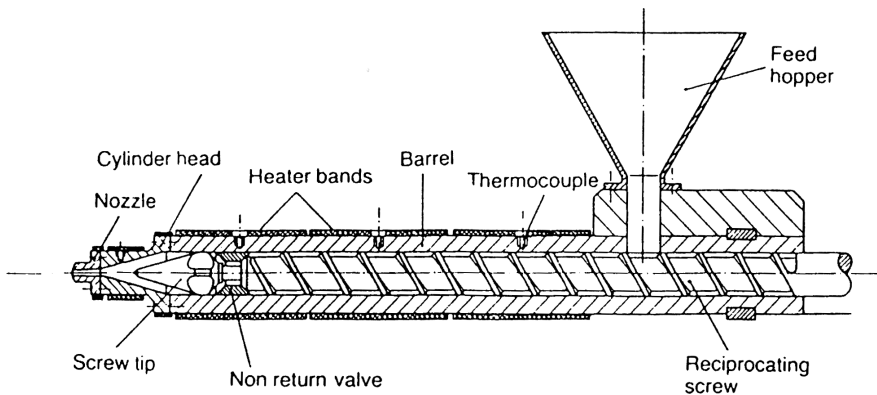


Figure 9.9 Components of a reciprocating screw injection [1]

Table 9.5 Travel Velocity of the Injection Unit [1]

Clamping force kN	Maximum velocity mm/s	Minimum velocity mm/s
< 500	300/400	20/40
501/2000	250/300	30/50
2001/10 000	200/250	40/60
> 10 000	200	50/100

Table 9.6 Contact Force Between Nozzle and Sprue Bushing [1]

Clamping force kN	Contact force kN
500	50/80
1000	60/90
5000	170/220
10 000	220/280
20 000	250/350

9.2.2 Injection Molding Screw

The plastication of solids in the reciprocating screw of an injection molding machine is a batch process consisting of two phases. During the stationary phase of the screw, melting takes place mainly by conduction heating from the barrel. The melting during screw rotation time of the molding cycle is similar to that in an extrusion screw but time-dependent. At long times of screw rotation, it approaches the steady state condition of extrusion melting [6, 7].

Design of injection molding screws can be performed by using the software of Rao [8]. Essential dimensions are the lengths and depths of the feed zone and the metering zone (Fig. 9.10).

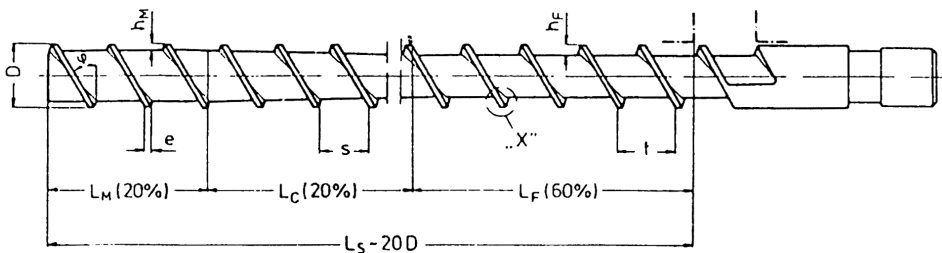


Figure 9.10 Dimensions of an injection molding screw [1]

Table 9.7 shows these data for several screw diameters [1].

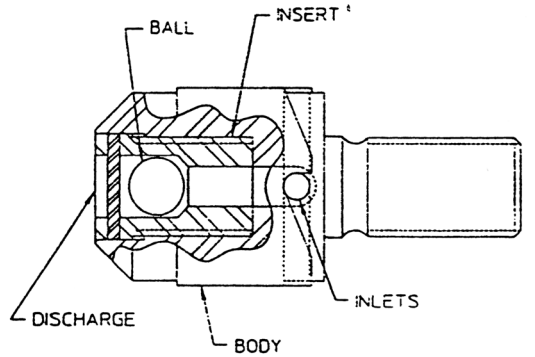
Table 9.7 Significant Screw Dimensions for Processing Thermoplastics [1]

Diameter	Flight depth (feed) h_F mm	Flight depth (metering) h_M mm	Flight depth ratio	Radial flight clearance mm
30	4.3	2.1	2:1	0.15
40	5.4	2.6	2.1:1	0.15
60	7.5	3.4	2.2:1	0.15
80	9.1	3.8	2.4:1	0.20
100	10.7	4.3	2.5:1	0.20
120	12	4.8	2.5:1	0.25
> 120	max 14	max 5.6	max 3:1	0.25

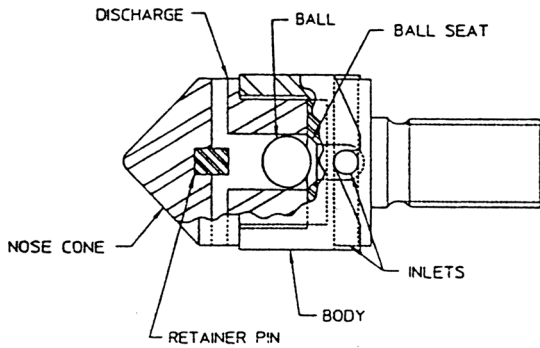
Screw geometries for other polymers are given by Johannaber [1].

9.2.2.1 Nonreturn Valves

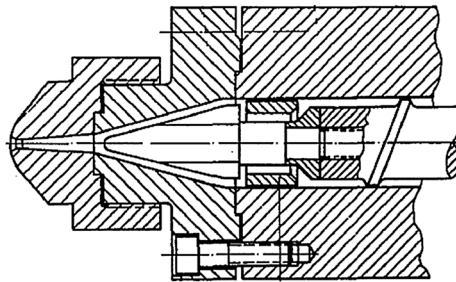
A nonreturn valve is a component at the tip of the screw that prevents back flow of the plasticated material during the injection and holding pressure stages. A comparison between the main categories of nonreturn valves (Fig. 9.11) is given in Table 9.8 [3].



Front Discharge Ball Check



Side Discharge Ball Check



Sliding-Ring Type Nonreturn Valve

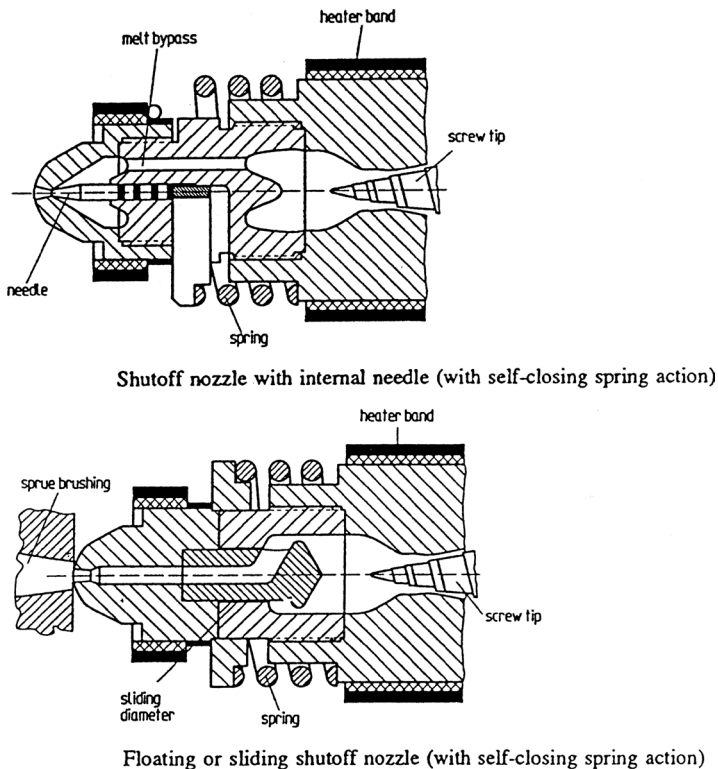
Figure 9.11 Nonreturn valves [1, 3]

Table 9.8 Comparison between Sliding Ring Valves and Ball Check Valves [21]

Sliding ring valve – Advantages	Ball check valve – Advantages
1. Greater streamlining for lower material degradation, 2. suitable for heat sensitive materials, 3. less barrel wear, 4. less pressure drop across valve, 5. well suited for vented operation, and 6. easy to clean.	1. More positive shut off and 2. better shot control.
Disadvantages	Disadvantages
1. Lower positive shut-off in large machines and 2. lower shot control.	1. Less streamlined, hence more degradation of materials, 2. more barrel wear and galling, 3. greater pressure drop, hence more heat, 4. poor for vented operation, and 5. harder to clean.

9.2.2.1.1 Nozzle

The plasticating barrel ends at the mold in a nozzle, which is forced against the sprue bushing of the mold prior to injection and produces a force locking connection there [1]. Examples of commonly used types of nozzles are given in Fig. 9.12 [1].

**Figure 9.12** Examples of nozzles [1]

9.2.3 Injection Mold

The quantitative description of the important mold filling stage has been made possible by the well-known computer programs like MOLDFLOW [11], CADMOULD [12], C-MOLD [10], and others.

The purpose of this section is to touch upon the basic principles of designing injection molding dies using rheological and thermal properties of polymers.

9.2.3.1 Runner Systems

The pressure drop along the gate or runner of an injection mold can be calculated from the same relationships used for dimensioning extrusion dies.

Example:

A part is to be made from polycarbonate using a runner of length 100 mm and diameter 3 mm and with the melt at a temperature 300 °C. The volume flow rate of the plastic melt through the runner is 2.65 cm³/s. The pressure drop in the runner is to be calculated.

Solution:

$$\text{shear rate } \dot{\gamma} = \frac{4\dot{Q}}{\pi R^3} = \frac{4 \cdot 2.65 \cdot 10^3}{\pi \cdot 1.5^3} = 1000 \text{ s}^{-1}$$

At 300 °C, a shear rate of 1000 s⁻¹ corresponds to a viscosity $\eta = 420 \text{ Pa} \cdot \text{s}$, according to the resin manufacturer's data.

The shear stress

$$\tau = \eta \cdot \dot{\gamma} = 420 \cdot 1000 = 0.42 \text{ MPa}$$

The pressure drop across the runner can be calculated by using

$$\Delta p = \frac{2 \cdot \tau \cdot L}{R} = \frac{2 \cdot 0.42 \cdot 100}{1.5} = 56 \text{ MPa}$$

It is accepted practice that the pressure drop across the runner should be less than 70 MPa [17]. Otherwise the size of the runner should be increased. The pressure drop in runners of noncircular cross sections can be calculated as just shown.

Different cross sections for runners, their advantages, disadvantages, and practical design relationships are summarized in Fig. 9.13 [17].

Empirical guidelines for dimensioning cross sections of runners are presented in Fig. 9.14 [17].

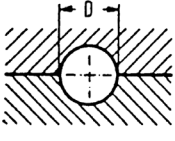
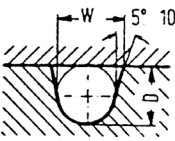
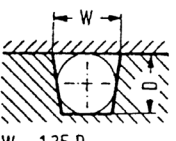
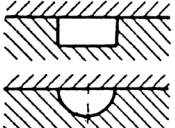
Circular cross-section	Cross sections for runners
 <p data-bbox="161 354 308 382">$D = s_{\max} + 1,5 \text{ mm}$</p>	<p data-bbox="400 214 1052 318">Advantages: smallest surface relative to cross-section, slowest cooling rate, low heat and frictional losses, center of channel freezes last therefore effective holding pressure</p> <p data-bbox="400 327 1008 382">Disadvantages: Machining into both mold halves is difficult and expensive</p>
<p data-bbox="161 445 365 473">Parabolic cross-section</p>  <p data-bbox="161 627 252 655">$W = 1,25 \cdot D$</p> <p data-bbox="161 664 308 691">$D = s_{\max} + 1,5 \text{ mm}$</p>	<p data-bbox="400 445 1052 527">Advantages: best approximation of circular cross section, simpler machining in one mold half only (usually movable side for reasons of ejection)</p> <p data-bbox="400 536 1026 591">Disadvantages: more heat losses and scrap compared with circular cross section</p>
<p data-bbox="144 713 371 740">Trapezoidal cross-section</p>  <p data-bbox="144 882 233 910">$W = 1,25 \cdot D$</p>	<p data-bbox="400 713 749 740">Alternative to parabolic cross section</p> <p data-bbox="400 749 1001 804">Disadvantages: more heat losses and scrap than parabolic cross section</p>
	<p data-bbox="400 919 837 946">Unfavorable cross sections have to be avoided</p>

Figure 9.13 Advantages and disadvantages of some runner cross sections [17]

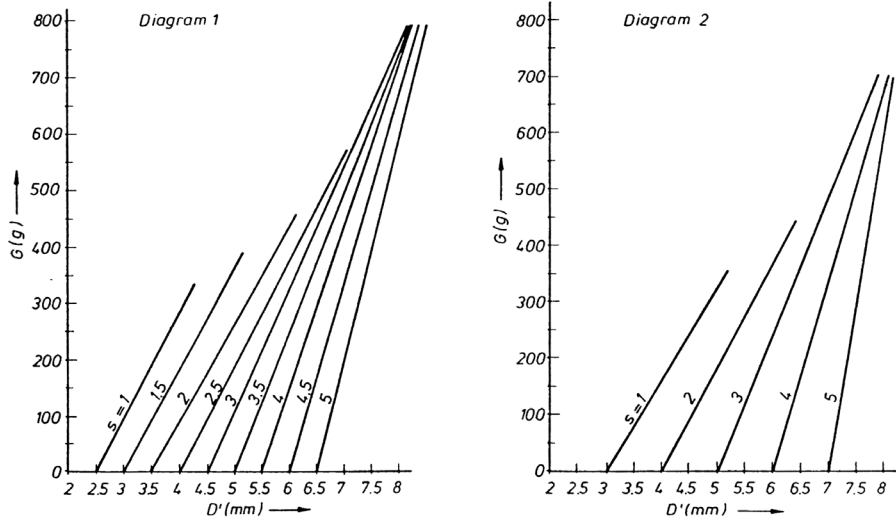
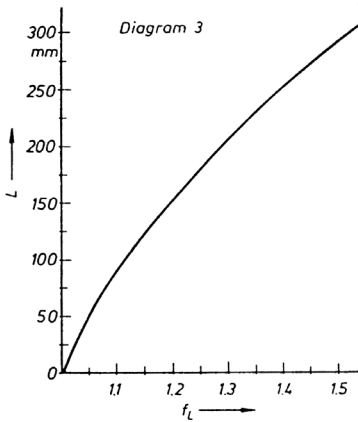


Diagram 1
applicable for PS, ABS, SAN, CAB

Diagram 2
applicable for PE, PP, PA, PC, POM



Symbols

- s: wall thickness of part (mm)
- D': diameter of runner (mm)
- G: weight of part (g)
- L: length of runner to one cavity (mm)
- f_L: correction factor

Procedure (Diagram 3)

1. determine G and s
2. take D' from diagram for material considered
3. determine L
4. take f_L from diagram 3
5. correct diameter of runner: $D = D' \cdot f_L$

Figure 9.14 Nomogram for dimensioning runner cross sections [17]

9.2.3.2 Design of Gates

Suggested dimensions of some commonly used gates are shown in Fig. 9.15 [20], and those of sprues in Fig. 9.16 [17].

By means of the software mentioned at the of this chapter, the entire melt entry system of the mold as well as the mold can be designed with success.

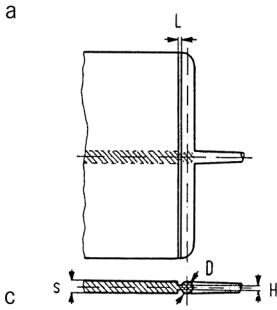
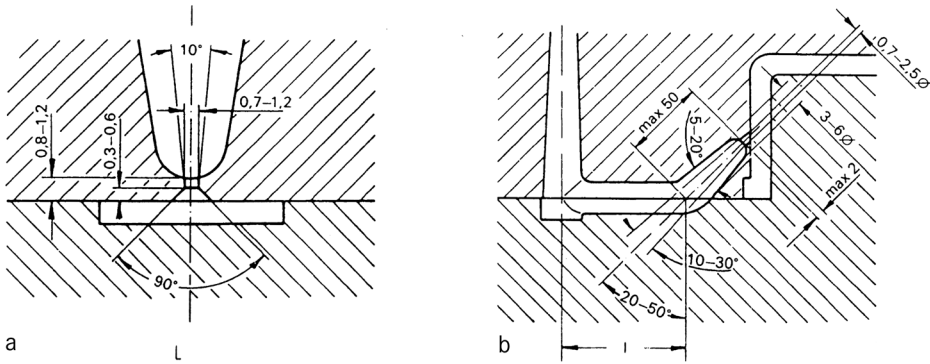


Fig. 175 Edge gate with circular distributor channel [1, 5]

$D = s$ to $\frac{4}{3}s + k$
 $k = 2$ mm for short flow lengths and thick sections
 $k = 4$ for long flow lengths and thin sections
 $L = (0.5 \text{ to } 2.0)$ mm
 $H = (0.2 \text{ to } 0.7)s$

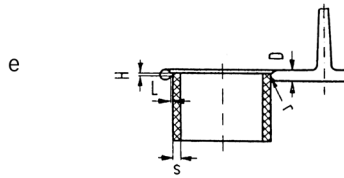
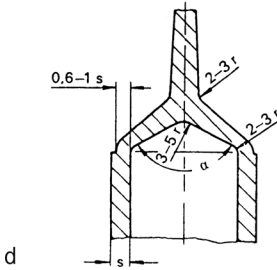
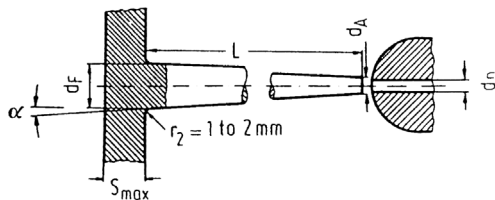


Fig. 185 Ring gate with circular cross section [5, 6]

$D = s + 1.5$ mm to $\frac{4}{3}s + k$
 $L = 0.5$ to 1.5 mm
 $H = \frac{2}{3}s$ to 1 to 2 mm
 $r = 0.2s$
 $k = 2$ for short flow lengths and thick sections
 $k = 4$ for long flow lengths and thin sections

Figure 9.15 Guidelines for dimensioning gates [17];

a: pinpoint, b: tunnel, c: edge gate with circular distributor channel, d: disk gate, and e: ring gate with circular cross section



$$d_F \cong S_{max} + 1.5 \text{ mm}$$

$$d_A \cong d_D + 1 \text{ mm}$$

$$\alpha \cong 1^\circ \dots 2^\circ$$

$$\text{tg } \alpha \cong \frac{d_F - d_A}{2L}$$

Figure 9.16 Guidelines for dimensioning a sprue [17]

9.2.3.3 Injection Pressure and Clamp Force

To determine the size of an injection molding machine suited to produce a given part, knowledge of the clamp force required by the mold is important in order to prevent the mold from flashing.

As already mentioned, the mold filling process was treated extensively in the programs [10] and [12], and later on by Bangert [13]. Analytical expressions for the injection pressure and clamp force have been given by Stevenson [14] on the basis of a model for mold filling. The main parameters characterizing this model are fill time τ and Brinkman number Br , which can be used as machine related parameters for describing injection molding in general. According to the solution procedure of Stevenson [14], injection pressure and clamp force are calculated assuming isothermal flow of melt in the cavity, and then modified to obtain actual values. The empirical relationships used for this modification are functions of fill time and Brinkman number.

The following example shows the calculation of fill time and Brinkman number for a disc-shaped cavity [14]:

The material is ABS with $n_R = 0.2655$, which is the reciprocal of the power law exponent n . Calculate fill time and Brinkman number.

The viscosity constant [8] is	$k_r = 3.05 \cdot 10^4$
Constant injection rate	$\dot{Q} = 160 \text{ cm}^3/\text{s}$
Part volume	$V = 160 \text{ cm}^3$
Half-thickness of the disc	$b = 1.05 \text{ mm}$
Radius of the disc	$r_2 = 120 \text{ mm}$
Number of gates	$N = 1$
Inlet melt temperature	$T_m = 245 \text{ }^\circ\text{C}$
Mold temperature	$T_w = 50 \text{ }^\circ\text{C}$
Thermal conductivity of the melt	$\lambda = 0.174 \text{ W}/(\text{m} \cdot \text{K})$
Thermal diffusivity of the polymer	$a = 7.72 \cdot 10^{-4} \text{ cm}^2/\text{s}$
Melt flow angle [14]	$\Theta = 360^\circ$

Solution:

The dimensionless fill time τ which characterizes the cooling of the flowing melt in the cavity is defined as [14]

$$\tau = \frac{V \cdot a}{\dot{Q} \cdot b^2} \quad (9.7)$$

Inserting the numerical values, we have

$$\tau = \frac{160 \cdot 7.72 \cdot 10^{-4}}{160 \cdot (0.105)^2} = 0.07$$

The Brinkman number, which characterizes viscous heating is given by

$$\text{Br} = \frac{b^2 \cdot kr}{10^4 \cdot \lambda \cdot (T_M - T_W)} \cdot \left[\frac{\dot{Q} \cdot 360}{N \cdot Q \cdot 2\pi \cdot b^2 \cdot r_2} \right]^{(1+n_r)} \quad (9.8)$$

Introducing the given values, we get

$$\text{Br} = \frac{0.105^2 \cdot 3.05 \cdot 10^4}{10^4 \cdot 0.174 \cdot 195} \left(\frac{160 \cdot 360}{1 \cdot 360 \cdot 2\pi \cdot (0.105)^2 \cdot 12} \right)^{1.2655} = 0.771$$

Table 9.9 shows the results of simulating the mold filling of a large rectangular open container (Fig. 9.17) [17] according to the model of Stevenson [14].

Table 9.9 Simulations of Injection Pressure and Clamp Force at Different Processing Conditions [14]

Resin	N	T_1 K	T_w K	Br	Δp MPa	F kN
A	1	501	301	1.381	302	191000
A	1	520	301	0.962	273	175000
A	1	500	321	1.536	290	181000
B	1	500	301	0.849	229	147000
A	4	500	301	0.625	192	67800
B	4	500	301	0.299	113	40400

Symbols in Table 9.9:

T_1 : inlet melt temperature

T_w : mold wall temperature

Δp : injection pressure drop

F : clamp force

N : Number of gates

Operating Conditions:

injection rate = 2000 cm³/s

fill time = 3.81 s

half-thickness of the part = 0.127 cm

dimensionless fill time τ = 0.1824

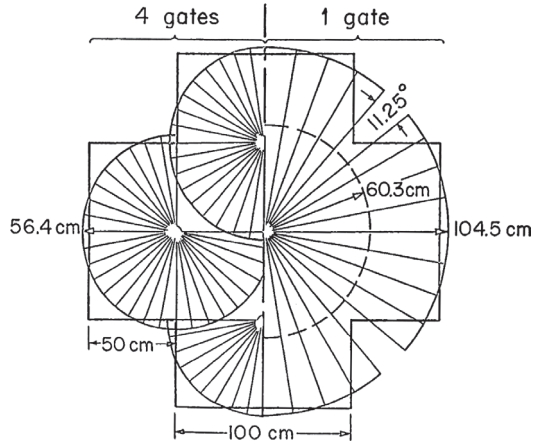


Figure 9.17 Mold filling of rectangular open container according to the model of Stevenson [14]

Relative to the standard conditions, the results in Table 9.9 show that Δp is decreased by 10% when T_1 is increased 20 °C, by 4% when T_w is increased 20 °C, by 24% when the material is changed, by 37% when the number of gates is increased to four, and by 63% when all of the above changes are made. The optimal conditions that correspond to the lowest Δp and F occur when these changes are combined with the change of the resin.

A rough estimate of the clamp force can be made as follows:

The pressure drop in a plate mold Δp_{IN} for the melt flow of an isothermal, Newtonian fluid can be calculated from

$$\Delta p_{IN} = \frac{12 \cdot \dot{Q} \cdot \eta \cdot L}{W \cdot H^3} \tag{9.9}$$

Substituting the injection rate for the volume flow rate \dot{Q} we get

$$\dot{Q} = \frac{v}{t} \tag{9.10}$$

where $v = W \cdot H \cdot L$
 and $t = \text{injection time} = L/u$
 with $u = \text{injection velocity}$

Introducing the equations above into Eq. 9.9 we obtain

$$\Delta p_{IN} = \frac{12 \cdot L}{H} \cdot \frac{1}{H} \cdot u \cdot \eta \tag{9.11}$$

Example: (with symbols and units in Eq. 9.11)

part thickness	$H = 1 \text{ mm}$
flow length	$L = 100 \text{ mm}$
injection velocity	$u = 100 \text{ mm/s}$
melt viscosity	$\eta = 250 \text{ Pa} \cdot \text{s}$

Solution:

$$\Delta p_{\text{IN}} = 12 \cdot \frac{100}{1} \cdot \frac{1}{1} \cdot \frac{100 \cdot 250}{10^5} = 300 \text{ bar}$$

In Fig. 9.18, Δp_{IN} is plotted over the part thickness H for different ratios of flow length L to part thickness [25]. The injection velocity is assumed to be 10 cm/s and the melt viscosity 250 Pa · s.

The pressure Δp_{IN} is then corrected by the following correction factors [26]:

Correction Factor CF_{shape}

Depending on the complicity of the part geometry the factor CF_{shape} can have values between 1.1 to 1.3.

Correction Factor CF_{resin}

The correction factors for the flow behavior of the resin CF_{resin} are given in Table 9.10 for some resins.

Table 9.10 Correction Factor CF_{resin} [16]

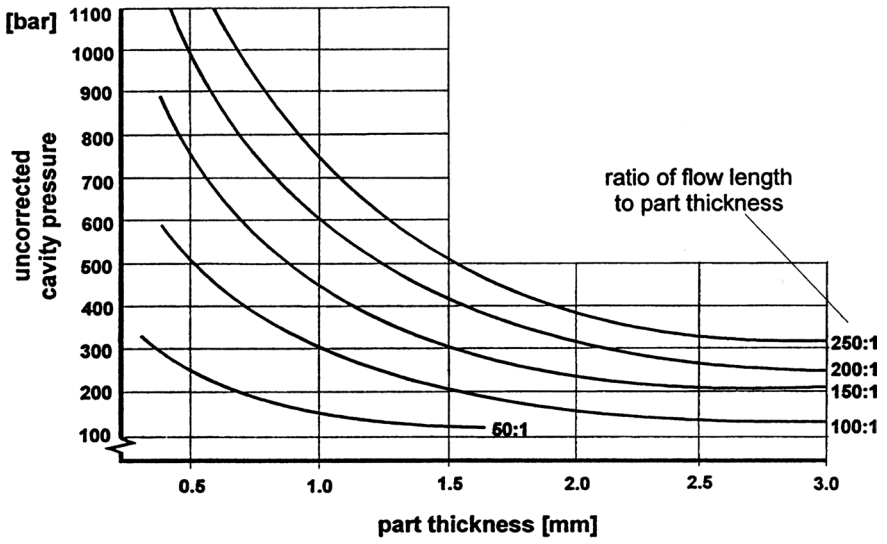
Resin	CF_{resin}
PE, PP, PS	1.0
PMMA, PPO	1.5
PA, SB	1.2
PC, PVC	1.7
ABS, SAN, CA	1.3

Finally, the actual cavity pressure Δp

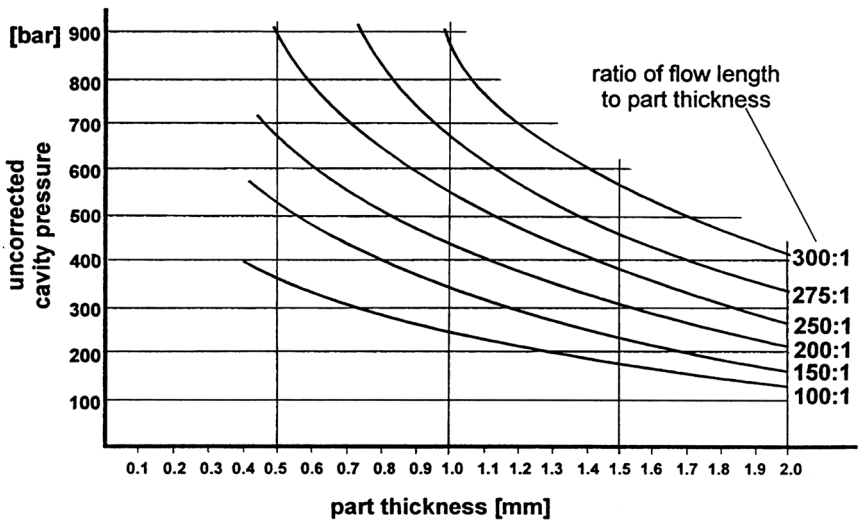
$$\Delta p = \Delta p_{\text{IN}} \cdot CF_{\text{shape}} \cdot CF_{\text{resin}}$$

and the clamp force F [kN]

$$F = \frac{\Delta p(\text{bar}) \cdot \text{projected area of the part (cm}^2\text{)}}{100}$$



(a)



(b)

Figure 9.18 Cavity pressure as a function of part thickness and ratio of flow length to part thickness [16]

Example:

Disk-shaped mold (see Fig. 9.17)

Thickness	H	= 1 mm
Radius	R	= 100 mm
Correction factor	CF_{shape}	= 1.2
Resin: ABS		
CF_{resin} from Table 9.10	CF_{resin}	= 1.3

Solution:

Ratio of flow length to part thickness L/H

$$L/H = 100$$

Δp_{IN} from Fig. 9.18 for $L/H = 100$ and $H = 1$

$$\Delta p_{\text{IN}} = 300 \text{ bar}$$

Actual cavity pressure Δp

$$\Delta p = 300 \cdot 1.2 \cdot 1.3 = 468 \text{ bar}$$

Clamp force F (kN)

$$F = \frac{468 \cdot 314}{100} \approx 1470 \text{ kN}$$

Two-dimensional and three-dimensional diagrams are helpful in the practice for finding out the useful working range of an injection molding machine [18].

Cooling of Melt in Mold

The analytical solution for the transient one-dimensional heat conduction for a plate can be written as [13]

$$t_K = \frac{S^2}{\pi^2 \cdot a} \cdot \ln \left[\frac{4}{\pi} \left(\frac{T_w - T_a}{T_w - T_b} \right) \right] \quad (9.12)$$

Although this equation is valid only for amorphous polymers, it has given good results in the practice for semicrystalline and crystalline polymers as well, so that its general use for all thermoplastic materials is justified.

Example:

Cooling of a part in an injection mold for the following conditions [8]:

resin: PE-LD

thickness of the plate $s = 12.7 \text{ mm}$

temperature of the melt $T_a = 243.3 \text{ }^\circ\text{C}$

mold temperature $T_w = 21.1 \text{ }^\circ\text{C}$

demolding temperature $T_b = 76.7 \text{ }^\circ\text{C}$

thermal diffusivity of the melt $a = 1.29 \cdot 10^{-3} \text{ cm}^2/\text{s}$

The temperature T_b in Eq. 9.12 refers to the centerline temperature of the part.

Solution:

The temperature ratio θ_{T_b} :

$$\theta_{T_b} = \frac{T_b - T_w}{T_a - T_w} = \frac{76.7 - 21.1}{243.3 - 21.1} = 0.25$$

cooling time t_k according to Eq. 9.12

$$t_k = \frac{1.27^2}{\pi^2 \cdot 1.29 \cdot 10^{-3}} \cdot \ln\left(\frac{4}{\pi} \cdot \frac{1}{0.25}\right) = 206.5 \text{ s}$$

The cooling time t_k can also be found from Fig. 9.19 in which the ratio θ_{T_b} is plotted over the Fourier number for bodies of different geometry [23].

Fourier number F_0 from Fig. 9.19 at $\theta_{T_b} = 0.25$

$$F_0 = 0.66$$

Cooling time t_k :

$$x = \frac{s}{2} = \frac{12.7}{2} = 6.35 \text{ mm}$$

$$F_0 = \frac{a \cdot t_k}{x^2} = \frac{1.29 \cdot 10^{-3} \cdot t_k}{(0.635)^2} = 0.66$$

$$t_k \approx 206 \text{ s}$$

The cooling time as a function of wall thickness of the molding is shown in Fig. 9.20.

Calculations of cooling time based on the average demolding temperature are given in the book by Rao [8].

Convective heat transfer is to be taken into account if the mold is cooled by a coolant such as circulating water by calculating the Biot number.

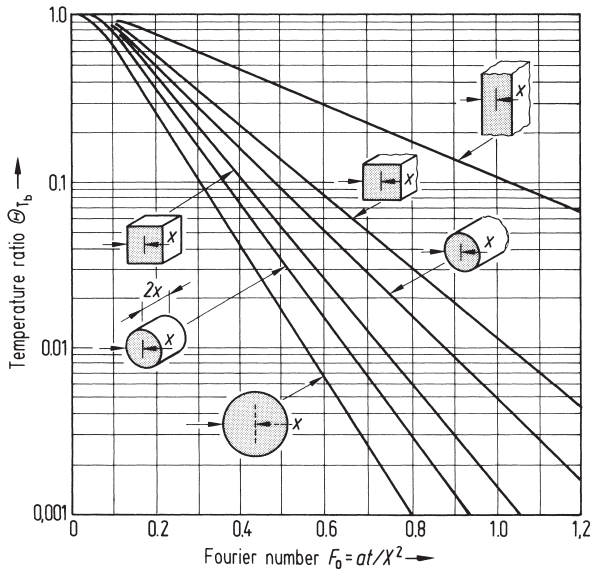


Figure 9.19 Axis temperature for multidimensional bodies [23]

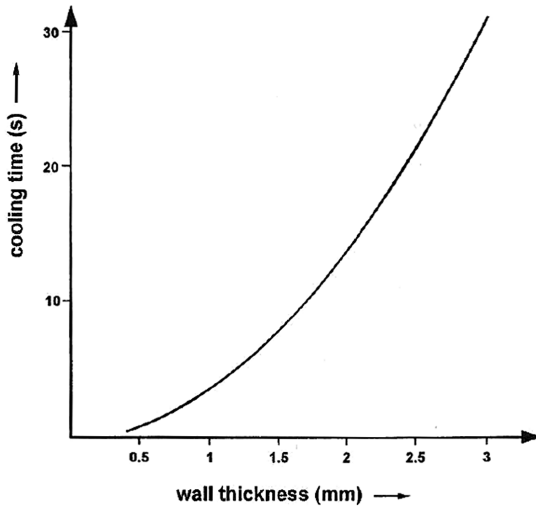


Figure 9.20 Cooling time vs. wall thickness

In practice the temperature of the mold wall is not constant, as it is influenced by the heat transfer between the melt and the cooling water. Therefore, the geometry of the cooling channel lay-out, thermal conductivity of the material, and velocity of cooling water affect the cooling time significantly (Fig. 9.21).

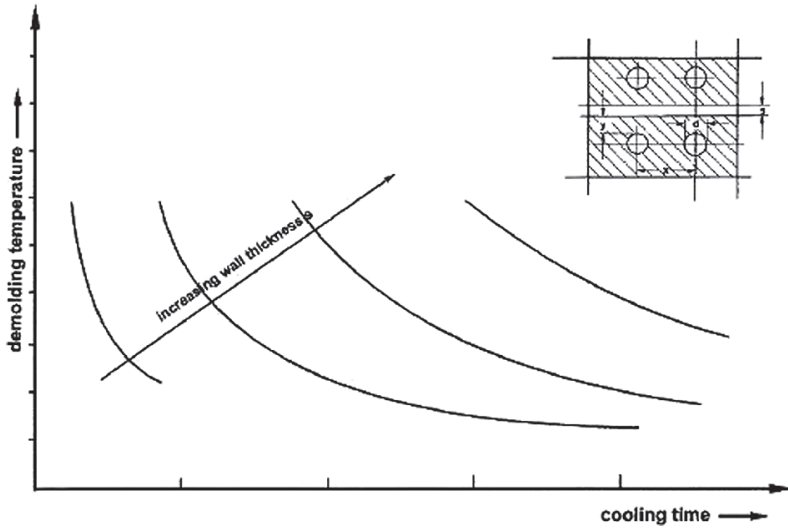


Figure 9.21 Cooling time as a function of demolding temperature and wall thickness

9.2.4 Mechanical Design of Mold

The cooling channels should be as close to the surface of the mold as possible so that heat can flow out of the melt in the shortest time possible. However, the strength of the mold material sets a limit to the distance between the cooling channel and the mold surface. The allowable distance z (Fig. 9.22) taking the strength of the mold material into account was calculated by Lindner [24] according to the following equations:

$$\sigma_b = \frac{0.5 \cdot p \cdot d^2}{z^2} \quad (9.13)$$

$$\tau = \frac{0.75 \cdot p \cdot d}{z} \quad (9.14)$$

$$f = \frac{1000 \cdot p \cdot d^2}{z} \left(\frac{d^2}{32 \cdot E \cdot z^2} + \frac{0.15}{G} \right) \quad (9.15)$$

- where p = melt pressure N/mm²
 d, z = distances mm, see Fig. 9.22
 E = tensile modulus N/mm²
 G = shear modulus N/mm²
 σ_b = tensile stress N/mm²
 τ = shear stress N/mm²
 f = deflection of the mold material above the cooling channel μm

The minimization of the distance z such that the conditions

$$f \leq f_{\max}$$

$$\sigma_b \leq \sigma_{b\max}$$

$$\tau \leq \tau_{\max}$$

(f_{\max} : maximum deflection; $\sigma_{b\max}$: allowable tensile stress; τ_{\max} : allowable shear stress) are satisfied can be accomplished by a computer program [18]. The results of a sample calculation are shown in Table 9.11.

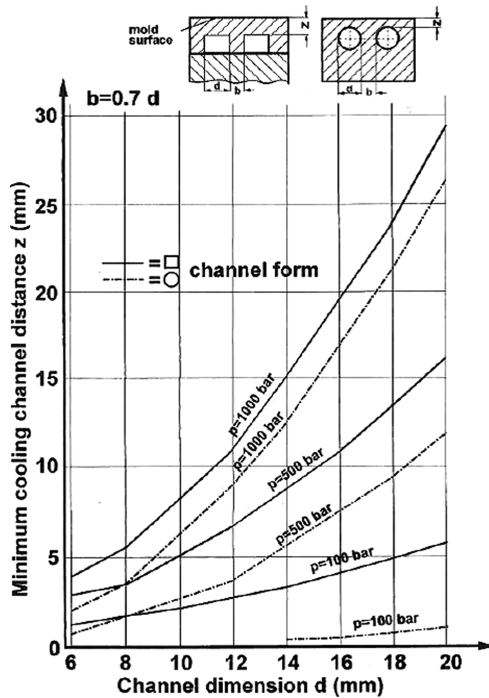


Figure 9.22 Cooling channel distance z for different cavity pressures and channel dimensions with steel as mold material

Table 9.11 Results of Optimization of Cooling Channel Distance

Input	Output
melt pressure $p = 4.9 \text{ N/mm}^2$	channel distance $z = 2.492 \text{ mm}$
maximum deflection $f_{\max} = 2.5 \mu\text{m}$	deflection $f = 2.487 \mu\text{m}$
modulus of elasticity $E = 70588 \text{ N/mm}^2$	tensile stress $\sigma = 39.44 \text{ N/mm}^2$
modulus of shear $G = 27147 \text{ N/mm}^2$	shear stress $\tau = 14.75 \text{ N/mm}^2$
allowable tensile stress $\sigma_{b\max} = 421.56 \text{ N/mm}^2$	
allowable shear stress $\tau_{\max} = 294.1 \text{ N/mm}^2$	
channel dimension $d = 10 \text{ mm}$	

The equations given above are approximately valid for circular channels as well. The distance from wall to wall of the channel in this case should be roughly around channel length l or channel diameter depending on the strength of mold material. Figure 9.22 shows for steel as mold material the minimum cooling channel distance z for different cavity pressures.

■ 9.3 Melting in Injection Molding Screws

In general, problems occurring during injection molding have their origin in mold design. However, with the widespread use of the reciprocating screw for conveying and plasticating, problems concerning the quality of the melt are being increasingly encountered. As in the case of plasticating extrusion, in order to achieve high part quality, the screw must be able to produce a fully plasticated homogeneous melt. Thus, the part quality is intimately connected to the plastication in the screw. This section shows how the melting performance of the reciprocating screw can be predicted through an extension of the model of Donovan [6] to include a simplified melting model [7–9]. The resulting equations allow facile solutions to be found even with a handheld calculator.

9.3.1 Model

During the stationary or nonrotating phase of the screw, melting of the resin takes place mainly by conduction heating from the barrel (Fig. 9.23) [3].

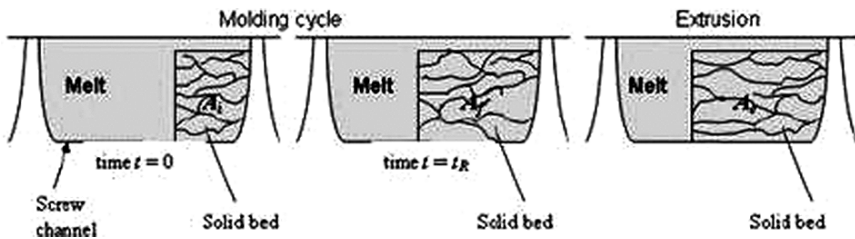


Figure 9.23 Change of solid bed during screw rotation in comparison to steady-state extrusion: A_s : solid bed area at the start of screw rotation; A_s' : solid bed area at the end of screw rotation $t = t_R$; A_s' : solid bed area for the steady-state extrusion; A_s' : cross-sectional area of solid bed at any position; A_T : cross-sectional area for screw channel; $A^* = A_s'/A_T$

The parameter K characterizing the conduction melting is given by [6]

$$\frac{(T_m - T_b) \cdot \lambda_m \cdot \exp(-K^2 / 4\alpha_m)}{\sqrt{\pi \cdot \alpha_m} \cdot \operatorname{erf}(K / 2\sqrt{\alpha_m})} - \frac{(T_r - T_m) \cdot \lambda_s \cdot \exp(-K^2 / \alpha_s)}{\sqrt{\pi \cdot \alpha_s} \cdot \operatorname{erfc}(K / 2\sqrt{\alpha_s})} = \frac{-10^6 \cdot i_m \cdot \rho_m \cdot K}{2} \quad (9.16)$$

with

$$\alpha_m = 10^{-6} \lambda_m / (\rho_m \cdot c_{p_m}) \quad (9.17)$$

and

$$\alpha_s = 10^{-6} \lambda_s / (\rho_s \cdot c_{p_s}) \quad (9.18)$$

By using the equations above, the parameter K can be obtained easily by a simple iteration. The following sample calculation for LDPE illustrates the application of Eq. 9.16.

Sample calculation for K :

Melt thermal conductivity	$\lambda_m = 0.225 \text{ W/(m K)}$
Melt density	$\rho_m = 0.78 \text{ g/cm}^3$
Melt specific heat	$c_{p_m} = 2.4 \text{ kJ/(kg K)}$
Solid thermal conductivity	$\lambda_s = 0.35 \text{ W/(m K)}$
Solid density	$\rho_s = 0.92 \text{ g/cm}^3$
Solid specific heat	$c_{p_s} = 1.9 \text{ kJ/(kg K)}$
Latent heat of fusion	$i_m = 130 \text{ kJ/kg}$
Polymer melting point	$T_m = 110 \text{ }^\circ\text{C}$
Barrel temperature	$T_b = 200 \text{ }^\circ\text{C}$
Solid bed temperature	$T_r = 20 \text{ }^\circ\text{C}$

In this sample calculation, K was found to be $5.457 \cdot 10^{-4} \text{ (m} / \sqrt{\text{s}})$. For given barrel and solid bed temperatures, K is dependent only on the thermal properties of the resin. The value of K is calculated for three resins in Table 9.12.

Table 9.12 Calculated Parameter K for Three Resins

Resin	$K \text{ (m} / \sqrt{\text{s}})$
LDPE	$5.46 \cdot 10^{-4}$
PP	$1.08 \cdot 10^{-3}$
PA6	$8.19 \cdot 10^{-4}$

The change of the solid bed profile is calculated from the equations derived from the model of Donovan [6] and extended to include a simplified melting model for extrusion melting. These are arranged in the following to facilitate easy iteration and calculation.

$$A_f^* - A_i^* = A_f^* \left[K \sqrt{t_T - t_R + (\delta_i / 10^4 K^2)} - (\delta_i / 100) \right] / 10^{-3} H \quad (9.19)$$

$$A_f^* = A_e^* - \left[\frac{A_f^* - A_i^*}{1 - \exp(-\beta \cdot 2\pi N t_R / 60)} \right] \exp(-\beta \cdot 2\pi N t_R / 60) \quad (9.20)$$

$$A_i^* = A_e^* - \left[\frac{A_f^* - A_i^*}{1 - \exp(-\beta \cdot 2\pi N t_R / 60)} \right] \quad (9.21)$$

The melt film thickness δ_i can be approximated by the relationship for a linear temperature profile in the melt film, and is given by [7, 8]

$$\delta_i = \delta_{av} = 0.5 \left\{ \frac{[2\lambda_m(T_b - T_m) + \eta_f v_j^2 \cdot 10^{-4}] W}{10^3 v_{bx} \rho_m [c p_s (T_m - T_s) + i_m]} \right\}^{0.5} \quad (9.22)$$

The average temperature in the melt film is obtained from [7]

$$\bar{T}_f = 0.5 \cdot (T_b - T_m) + 10^{-4} \eta_f v_j^2 / 12\lambda_m \quad (9.23)$$

9.3.2 Calculation Procedure

Step 1: Calculate K using Eq. 9.16.

Step 2: Calculate δ_{av} with Eqs. 9.22 and 9.23. Substitute δ_i with δ_{av} .

Step 3: Calculate the solid bed ratio A_e^* for steady-state extrusion with the simplified model for a linear temperature profile [7].

Step 4: Find the solid bed ratio A_f^* at the end of the screw rotation using the Eq. 9.20.

Step 5: Calculate A_i^* , the solid bed ratio at the start of screw rotation from Eq. 9.21.

The following sample calculation shows the symbols and units of the variables occurring in the previous equations.

9.3.3 Sample Calculation

The thermal properties for LDPE and the barrel temperature are as given in the previous calculation for the parameter K . Furthermore,

$$\text{Total cycle time} \quad t_T = 45 \text{ s}$$

$$\text{Screw rotation time} \quad t_R = 22 \text{ s}$$

Empirical parameter for all polymers: β	= 0.005
Screw speed	$N = 56$ rpm
Channel depth	$H = 9.8$ mm
Channel width	$W = 52.61$ mm
Cross-channel velocity of the melt	$v_{bx} = 5.65$ cm/s
Relative velocity of the melt	$v_j = 15.37$ cm/s
Solids temperature	$T_s = 20$ °C

By inserting these values into Eqs. 9.19 through 9.23 and by iteration, the following target values are obtained:

Melt viscosity in the film $\eta_f = 211$ Pa·s

Average temperature of the melt in the film $\bar{T}_f = 172.8$ °C.

Average thickness of the melt film $\delta_{av} = 7.678 \cdot 10^{-3}$ cm.

Using $K = 5.6 \cdot 10^{-4}$, the solid bed ratios are found to be:

The solid bed ratio at the end of screw rotation $A_f^* = 0.583$;

The solid bed ratio at the start of screw rotation, $A_i^* = 0.429$.

The solid bed ratio for steady-state extrusion, A_e^* , is calculated from the simplified melting model for extrusion [8]. Its numerical value for the conditions above is $A_e^* = 0.75$.

9.3.4 Results of Simulation

In all following figures, the steady-state extrusion profile begins at the position of the stroke. The temperature of the melt refers to the temperature at the end of the screw for the case of steady-state extrusion. The solid bed ratio A^* is the ratio between the cross-sectional area of the solid bed A_s and the total cross-sectional area of the channel A_T . In Fig. 9.24, the effect of the resin type on the solid bed profiles is presented. It appears that the conductivity parameter K and the melt viscosity affect these profiles significantly, even if screw rotation and cycle times remain the same. It can be seen from Fig. 9.25 that the barrel temperature has little effect on the plastication process in the screw.

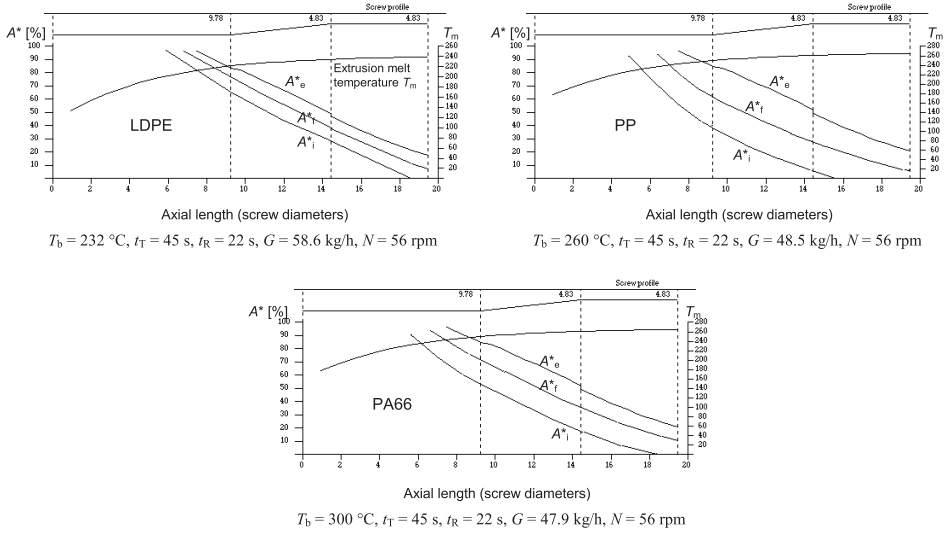


Figure 9.24 Effect of polymer on the melting profiles

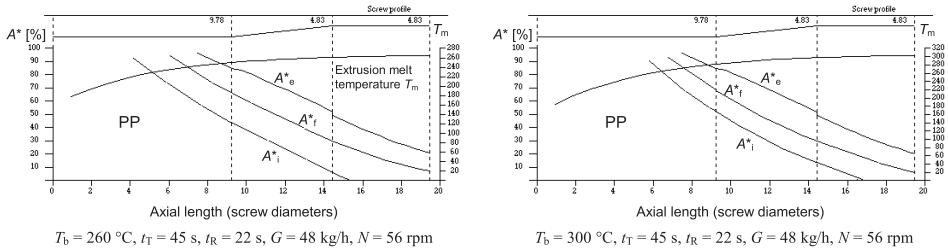


Figure 9.25 Effect of barrel temperature on the melting profiles for PP

As Fig. 9.26 depicts, slow screw speed and a high percentage of screw rotation time compared to the total cycle time strongly favor melting, which has also been found by Donovan [6]. The marked influence of screw geometry on melting becomes clear from and Fig. 9.27.

As can be expected, melting is much faster in the case of the shallower channel.

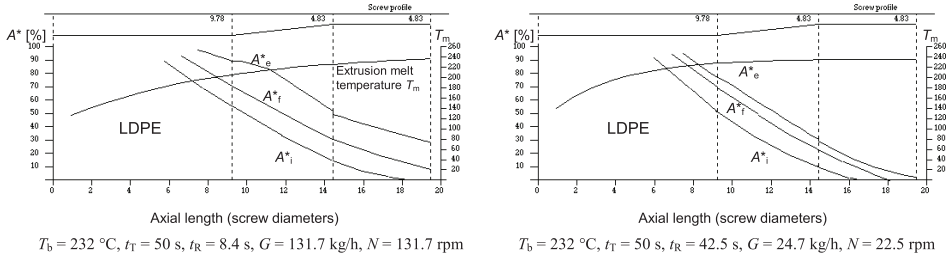


Figure 9.26 Effect of screw rotation time and screw speed on melting of LDPE

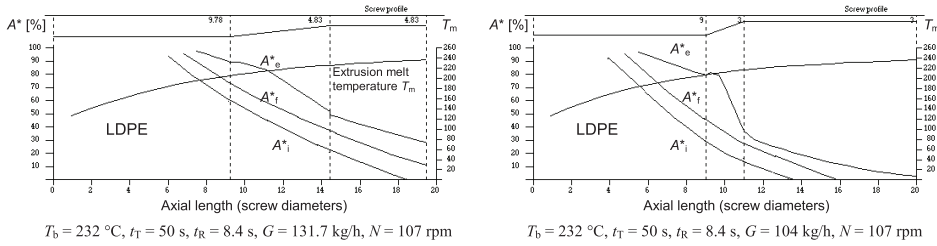


Figure 9.27 Effect of screw geometry on the melting for LDPE

9.3.5 Screw Dimensions

Essential dimensions of injection molding screws for processing thermoplastics are given in Table 9.13 for several screw diameters [1] and depicted in Fig. 9.28.

Table 9.13 Significant Screw Dimensions for Processing Thermoplastics

Diameter (mm)	Flight depth (feed) h_F (mm)	Flight depth (metering) h_M (mm)	Flight depth ratio	Radial flight clearance (mm)
30	4.3	2.1	2 : 1	0.15
40	5.4	2.6	2.1 : 1	0.15
60	7.5	3.4	2.2 : 1	0.15
80	9.1	3.8	2.4 : 1	0.20
100	10.7	4.3	2.5 : 1	0.20
120	12	4.8	2.5 : 1	0.25
> 120	max 14	max 5.6	max 3 : 1	0.25

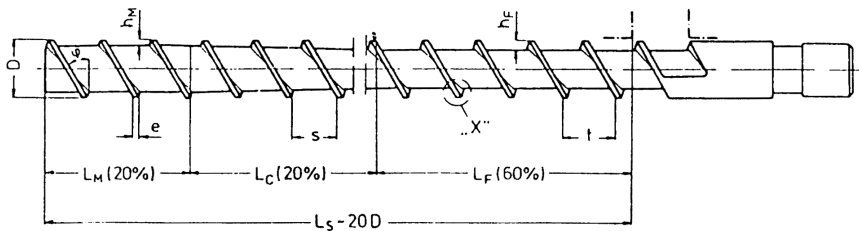


Figure 9.28 Dimensions of an injection molding screw [1]

■ 9.4 Injection Mold

The problems encountered in injection molding are often related to mold design.

The quantitative description of the important mold filling stage has been made possible by the well-known software MOLDFLOW [11]. The purpose of this section is to present practical calculation procedures that can be handled even by hand-held calculators.

9.4.1 Runner Systems

The pressure drop along the gate or runner of an injection mold [15] can be calculated as follows:

9.4.2 Calculated Example

For the following conditions, the isothermal pressure drop Δp_0 and the adiabatic pressure drop Δp are to be determined:

For polystyrene with the following viscosity constants according to [29]

A_0	=	4.4475
A_1	=	-0.4983
A_2	=	-0.1743
A_3	=	0.03594
A_4	=	-0.002196
c_1	=	4.285
c_2	=	133.2
T_0	=	190 °C
flow rate	\dot{m} =	330.4 kg/h
melt density	ρ_m =	1.12 g/cm ³
specific heat	c_{p_m} =	1.6 kJ/(kg · K)
melt temperature	T =	230 °C
length of the runner	L =	101.6 mm
radius of the runner	R =	5.08 mm

Solution**a) Isothermal flow** $\dot{\gamma}_a$ from

$$\dot{\gamma}_a = \frac{4 \dot{Q}}{\pi R^3} = \frac{4 \cdot 330.4}{3.6 \cdot \pi \cdot 1.12 \cdot 0.508^3} = 795.8 \text{ s}^{-1}$$

 $(\dot{Q} = \text{volume flow rate cm}^3/\text{s})$ a_T from

$$a_T = 10^{\frac{-c_1(T-T_0)}{c_2+(T-T_0)}} = 10^{\frac{-4.285(230-190)}{133.2+(230-190)}} = 10^{-0.9896} = 0.102$$

Power law exponent [29]

$$n = 5.956$$

 η_a viscosity [29]

$$\eta_a = 132 \text{ Pa} \cdot \text{s}$$

 τ shear stress

$$\tau = 105013.6 \text{ Pa}$$

 K :

$$K = 9.911 \cdot 10^{-28}$$

Die constant G_{circle}

$$G_{\text{circle}} = \left(\frac{\pi}{4} \right)^{\frac{1}{5.956}} \cdot \frac{(5.08 \cdot 10^{-3})^{\frac{1}{5.956}+1}}{2 \cdot 0.1016} = 1.678 \cdot 10^{-3}$$

 Δp_0 with $\dot{Q} = 8.194 \cdot 10^{-5} \text{ m}^3/\text{s}$:

$$\Delta p_0 = \frac{10^{-5} \cdot (8.194 \cdot 10^{-5})^{\frac{1}{5.956}}}{(9.911 \cdot 10^{-28})^{\frac{1}{5.956}} \cdot 1.678 \cdot 10^{-3}} = 42 \text{ bar}$$

b) Adiabatic flowThe relationship for the ratio $\frac{\Delta p}{\Delta p_0}$ is [8]

$$\frac{\Delta p}{\Delta p_0} = \frac{\ln \chi_L}{\chi_L - 1}$$

where

$$\chi_L = 1 + \frac{\beta \cdot \Delta p_0}{\rho_m \cdot c_{pm}}$$

Temperature rise:

$$\Delta T = \frac{\Delta p}{10 \cdot \rho_m \cdot c_{pm}} = \frac{42}{10 \cdot 1.12 \cdot 1.6} = 2.34 \text{ K}$$

For polystyrene

$$\beta = 0.026 \text{ K}^{-1}$$

$$\chi_L = 2.34 \cdot 0.026 = 1.061$$

Finally, Δp

$$\Delta p = \Delta p_0 \frac{\ln \chi_L}{\chi_L - 1} = \frac{42 \cdot \ln 1.061}{0.061} = 40.77 \text{ bar}$$

In the adiabatic case, the pressure drop is smaller because the dissipated heat is retained in the melt.

9.4.3 Mold Filling

As already mentioned, the mold filling process is treated extensively in commercial simulation programs and by Bangert [13]. In the following sections the more transparent method of Stevenson is given with an example.

To determine the size of an injection molding machine in order to produce a given part, knowledge of the clamping force exerted by the mold is important, as this force should not exceed the clamping force of the machine.

9.4.4 Injection Pressure

The isothermal pressure drop for a disc-shaped cavity is given as [14]

$$\Delta p_1 = \frac{K_r}{10^5 (1 - n_R)} \left[\frac{360 \cdot \dot{Q} \cdot (1 + 2 \cdot n_R)}{N \cdot \Theta \cdot 4\pi \cdot n_R \cdot r_2 \cdot b^2} \right]^{n_R} \cdot \left(\frac{r_2}{b} \right) \quad (9.24)$$

The fill time τ is defined as [14]

$$\tau = \frac{V \cdot a}{\dot{Q} \cdot b^2} \quad (9.25)$$

The Brinkman number is given by [14]

$$\text{Br} = \frac{b^2 \cdot K_r}{10^4 \cdot \lambda \cdot (T_M - T_W)} \cdot \left[\frac{\dot{Q} \cdot 360}{N \cdot \Theta \cdot 2\pi \cdot b^2 \cdot r_2} \right]^{(1+n_R)} \quad (9.26)$$

9.4.5 Calculated Example with Symbols and Units

Given data:

The part has the shape of a round disc.

The material is ABS with $n_R = 0.2565$, which is the reciprocal of the power law exponent n . The constant K_r , which corresponds to the viscosity η_p , is $K_r = 3.05 \cdot 10^4$.

Constant injection rate	$\dot{Q} = 160 \text{ cm}^3/\text{s}$
Part volume	$V = 160 \text{ cm}^3$
Half thickness of the disc	$b = 2.1 \text{ mm}$
Radius of the disc	$r_2 = 120 \text{ mm}$
Number of gates	$N = 1$
Inlet melt temperature	$T_M = 518 \text{ K}$
Mold temperature	$T_W = 323 \text{ K}$
Thermal conductivity of the melt	$\lambda = 0.174 \text{ W}/(\text{m}\cdot\text{K})$
Thermal diffusivity of the polymer	$a = 7.72 \cdot 10^{-4} \text{ cm}^2/\text{s}$
Melt flow angle [14]	$\Theta = 360^\circ$

The isothermal pressure drop in the mold Δp_1 will now be determined.

Solution:

Applying Eq. 9.24 for Δp_1

$$\begin{aligned} \Delta p_1 &= \frac{3.05 \cdot 10^4}{10^5 (1 - 0.2565)} \left[\frac{360 \cdot 160 \cdot (1 + 2 \cdot 0.2565)}{1 \cdot 360 \cdot 4\pi \cdot 12 \cdot 0.105^2} \right]^{0.2565} \cdot \left(\frac{12}{0.105} \right) \\ &= 254 \text{ bar} \end{aligned}$$

Dimensionless fill time τ from Eq. 9.25:

$$\tau = \frac{160 \cdot 7.72 \cdot 10^{-4}}{160 \cdot 0.105^2} = 0.07$$

Brinkman number from Eq. 9.26:

$$\begin{aligned} \text{Br} &= \frac{0.105^2 \cdot 3.05 \cdot 10^4}{10^4 \cdot 0.174 \cdot 195} \cdot \left[\frac{160 \cdot 360}{1 \cdot 360 \cdot 2\pi \cdot 0.105^2 \cdot 12} \right]^{1.2655} \\ &= 0.771 \end{aligned}$$

From the experimental results of Stevenson [14] the following empirical relation was developed to calculate the actual pressure drop in the mold:

$$\ln \left(\frac{\Delta p}{\Delta p_1} \right) = 0.337 + 4.7 \tau - 0.093 \text{Br} - 2.6 \tau \cdot \text{Br} \quad (9.27)$$

The actual pressure drop Δp is therefore from Eq. 9.27

$$\Delta p = 1.574 \cdot \Delta p_1 = 1.574 \cdot 254 = 400 \text{ bar}$$

Clamping Force

The calculation of clamping force is similar to that of the injection pressure. First, the isothermal clamping force is determined from [14]

$$\ln(F/F_1) = 0.372 + 7.6 \tau - 0.084 \text{Br} - 3.538 \tau \cdot \text{Br} \quad (9.28)$$

where $F_1(r_2)$ = isothermal clamping force N.

$F_1(r_2)$ for the example above

$$\begin{aligned} F_1(r_2) &= 10 \cdot \pi \cdot 12^2 \left(\frac{1 - 0.2655}{3 - 0.2655} \right) \cdot 254 \\ &= 308.64 \text{ kN} \end{aligned}$$

The actual clamping force can be obtained from the following empirical relationship, which was developed from the results published in [14].

$$\ln(F/F_1) = 0.372 + 7.6 \tau - 0.084 \text{Br} - 3.538 \tau \cdot \text{Br} \quad (9.29)$$

Hence the actual clamping force F

$$F = 1.91 \cdot 308.64 = 589.5 \text{ kN}$$

The above relationships are valid for a disc-shaped cavity. Other geometries of the mold cavity can be taken into account on this basis in the manner described by Stevenson [14].

■ 9.5 Flow Characteristics of Injection Molding Resins

One of the criteria for resin selection to make a given part is whether the melt is an easy flowing type or whether it exhibits significantly viscous behavior. To determine the flowability of the polymer melt, the spiral test, which consists of injecting the melt into a spiral shaped mold shown in Fig 9.29, is used. The length of the spiral serves as a measure of the ease of flow of the melt in the mold, and enables mold and part design suited to material flow.

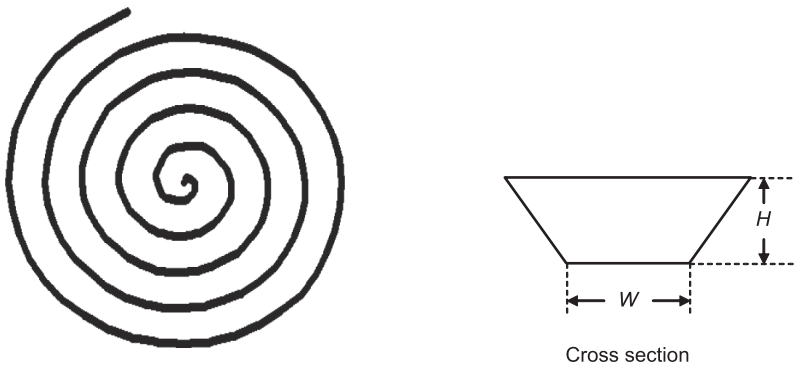


Figure 9.29 Schematic representation of spiral form

The parameters involved in the flow process are resin viscosity, melt temperature, mold wall temperature, axial screw speed, injection pressure, and geometry of the mold. To minimize the number of experiments required to determine the flow length, a semi-empirical model based on dimensional analysis is given in this section. The modified dimensionless numbers used in this model taking non-Newtonian melt flow into account are the Graetz number, Reynolds number, Prandtl number, Brinkman number, and Euler number. Comparison between experimental data obtained with different thermoplastic resins and the model predictions showed good agreement, confirming the applicability of the approach to any injection molding resin [28].

The experimental flow curves obtained at constant injection pressure under given melt temperature, mold temperature, and axial screw speed are given schematically in Fig. 9.30 for a resin type at various spiral depths with melt flow rate of the polymer brand as a parameter. By comparing the flow lengths with one another at any spiral depth also called wall thickness, the flowability of the resin brand in question with reference to another brand can be inferred [8, 18].

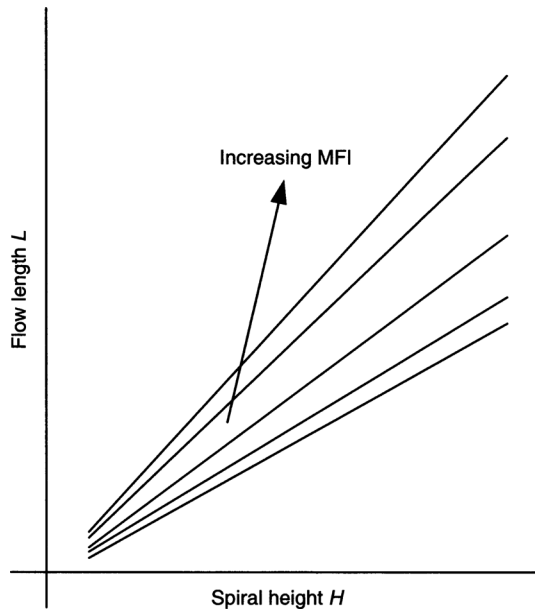


Figure 9.30 Schematic flow curves

9.5.1 Model

The transient heat transfer and flow processes accompanying melt flow in an injection mold can be analyzed by state-of-the-art commercial software packages. However, for simple mold geometries, such as the one used in the spiral test, it is possible to predict the melt flow behavior on the basis of dimensionless numbers and obtain formulae useful in practice. These relationships can be easily calculated with a handheld calculator offering quick estimates of the target values. Due to the nature of non-Newtonian flow, the dimensionless numbers used to describe flow and heat transfer processes of Newtonian fluids have to be modified for polymer melts. According to the authors [19–21], the movement of a melt front in a rectangular cavity can be correlated by the Graetz number, Reynolds number, Prandtl number, and Brinkman number. As the flow length in a spiral test depends significantly on the injection pressure (Fig. 9.31) the Euler number [21] is included in the present work in order to take the effect of injection pressure on the flow length.

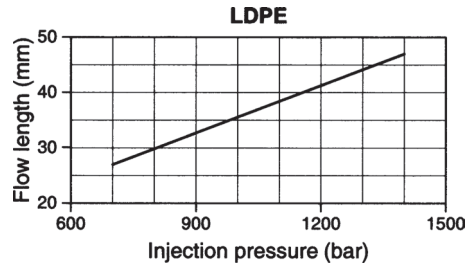


Figure 9.31 Effect of injection pressure on flow length

The Graetz number Gz based on the flow length is given by

$$Gz = \frac{G \cdot c_p}{\lambda \cdot L} \quad (9.30)$$

with G melt throughput, c_p specific heat, λ thermal conductivity of the melt, and L spiral length in the spiral test.

The mean velocity of the melt front V_e in the cavity is defined by

$$V_e = \frac{Q}{A} \quad \text{with} \quad Q = \frac{G}{\rho} \quad (9.31)$$

where Q is the volume throughput, A , the area of the spiral cross section Fig. 9.29, and ρ the density of the melt. The area A follows from

$$A = W \cdot H + H^2 \cdot \tan \alpha \quad (9.32)$$

with W the base width of the spiral and H spiral height or wall thickness, as shown in Fig. 9.29.

9.5.2 Melt Viscosity and Power Law Exponent

Melt viscosity and power law exponent can be calculated by means of the rheological models according to Carreau, Münstedt, Klein and Ostwald, and de Waele, as shown by Rao [8].

The shear rate $\dot{\gamma}$ is obtained from

$$\dot{\gamma} = \frac{6 \cdot Q}{W_{\text{mean}} \cdot H^2} \quad \text{where} \quad W_{\text{mean}} = W + H \cdot \tan \alpha \quad (9.33)$$

The following dimensionless numbers are obtained from [19-21]:

$$\text{Reynolds number } \text{Re} = \frac{V_e^{(2-n_r)} \cdot \rho \cdot H^{*n_r}}{k^*} \quad (9.34)$$

with $H^* = 0.5 \cdot H$ and $k^* = \eta_a \cdot \dot{\gamma}^{(1-n_r)}$

$$\text{Prandtl number } \text{Pr} = \frac{k^* \cdot c_p \cdot H^{*(1-n_r)}}{\lambda \cdot V_e^{(1-n_r)}} \quad (9.35)$$

$$\text{Brinkman number } \text{Br} = \frac{k^* \cdot V_e^{(1+n_r)} \cdot H^{*(1-n_r)}}{\lambda \cdot (T_M - T_W)} \quad (9.36)$$

$$\text{Euler Number } \text{Eu} = \frac{100 \cdot p_I}{\rho \cdot V_e^2} \quad (9.37)$$

where p_I is the injection pressure.

9.5.3 Experimental Results and Discussion

The experimental flow curves for four different resins measured at constant injection pressure under different processing conditions and spiral wall thicknesses are given in Fig. 9.32. The flow length as a function of injection pressure is shown in Fig. 9.31 for LDPE, as an example. The Graetz numbers calculated from the experimentally determined spiral lengths at different operating conditions and resins are plotted as function of the product $\text{Re} \cdot \text{Pr} \cdot \text{Br} \cdot \text{Eu}$, as shown in Fig. 9.33. As can be seen here, the correlation of the Graetz number with this product is good and thus, for any particular material the spiral length can be predicted from this relationship.

$$\text{Gz} = f(\text{Re} \cdot \text{Pr} \cdot \text{Br} \cdot \text{Eu}) \quad (9.38)$$

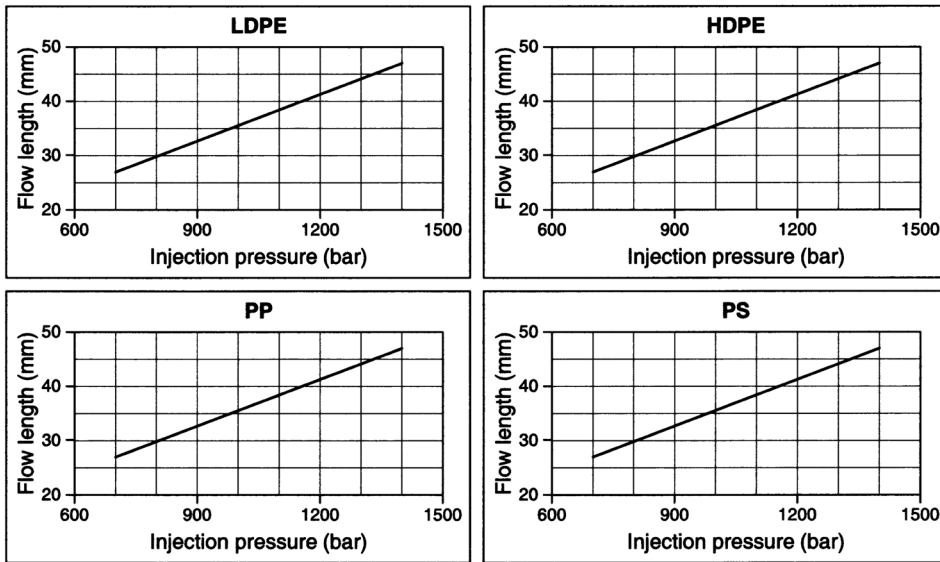


Figure 9.32 Experimental flow curves for LDPE, HDPE, PP, and PS

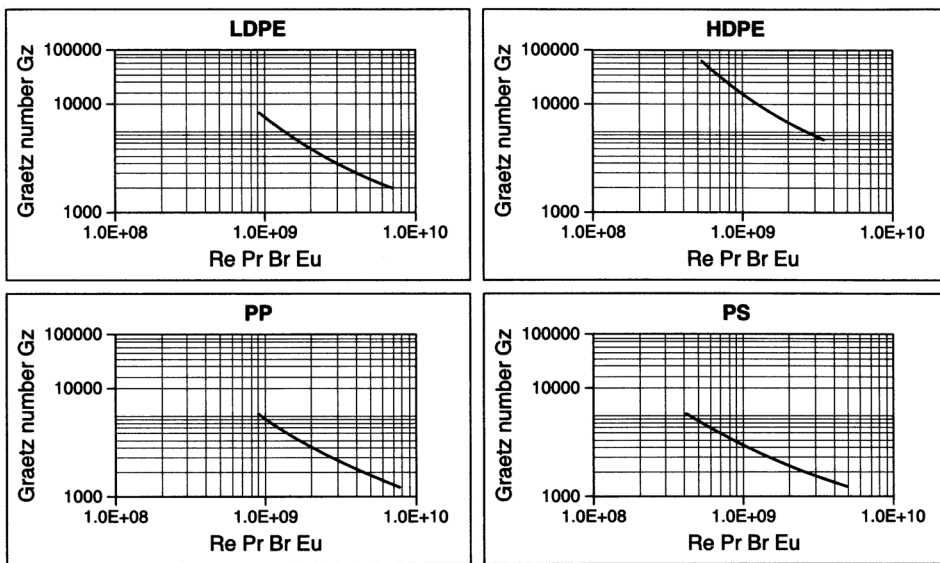


Figure 9.33 Graetz number as a function of the product of Re, Pr, Br, and Eu

Figure 9.34 shows the good agreement between measured and calculated spiral lengths for the experimentally investigated resins.

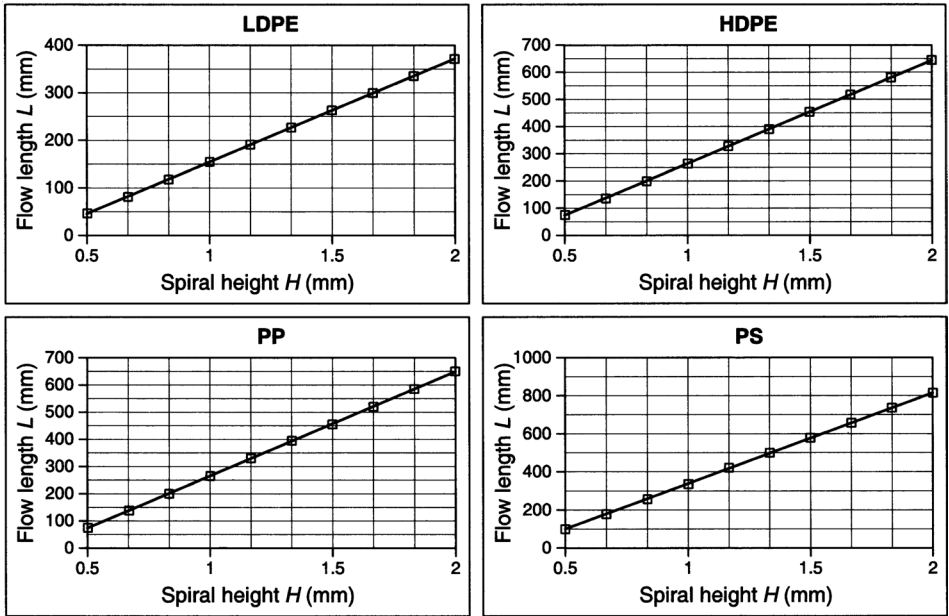


Figure 9.34 Comparison between measured and calculated flow length

9.5.4 Sample Calculation

The example given here shows how the flow length of a given resin can be calculated from Eq. 9.38). For the following input values:

$$W = 10 \text{ mm}$$

$$H = 2 \text{ mm}$$

$$\rho = 1.06 \text{ g/cm}^3$$

$$c_p = 2 \text{ kJ/kg}\cdot\text{K}$$

$$\lambda = 1.5 \text{ W/K}\cdot\text{m}$$

$$T_M = 270 \text{ }^\circ\text{C}$$

$$T_W = 70 \text{ }^\circ\text{C, and}$$

$$G = 211.5 \text{ kg/h, as well as}$$

$$A_0 = 4.7649$$

$$A_1 = -0.4743$$

$$A_2 = -0.2338$$

$$A_3 = 0.081$$

$$A_4 = -0.01063$$

$$c_1 = 4.45$$

$$c_2 = 146.3, \text{ and}$$

$$T_0 = 190 \text{ }^\circ\text{C},$$

The following output is obtained:

$$\text{Re} = 0.05964,$$

$$\text{Pr} = 76625.34,$$

$$\text{Br} = 1.7419, \text{ and}$$

$$\text{Eu} = 10825.84.$$

The Graetz number Gz for the product $\text{Re}\cdot\text{Pr}\cdot\text{Br}\cdot\text{Eu}$ follows from Fig. 9.33.

$$Gz = 217.63.$$

$$\text{Hence } L = 420 \text{ mm.}$$

■ 9.6 Cooling of Melt in the Mold

In order to manufacture articles of high quality, mold design must take thermal, mechanical, and rheological design criteria into account. As mentioned earlier, commercial software systems [10–12] available today are of great value in accomplishing optimal mold design. But in daily practice, where quick estimates of the parameters involved are needed, the application of sophisticated software can be time consuming and costly.

This section deals with an easily applicable method of optimizing the mold design from thermal, mechanical, and rheological considerations [18]. The equations involved can be solved even by handheld calculators.

The numerical solution of the Fourier equation is first presented here for crystalline and amorphous polymers [8].

9.6.1 Crystalline Polymers

The enthalpy temperature diagram of a crystalline polymer shows that there is a sharp enthalpy rise in the temperature region where the polymer begins to melt. This is caused by the latent heat of fusion absorbed by the polymer when it is heated and has to be taken into account when calculating cooling curves of crystalline polymers. By defining an equivalent temperature for the latent heat (Fig. 9.35), Gloor [22] calculated the temperature of a slab using the Fourier equation for the non-steady-state heat conduction.

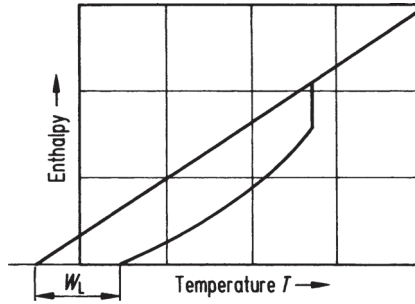


Figure 9.35 Representation of temperature correction for latent heat [22]

The numerical solution using the correction introduced by Gloor [22] was given in [8] on the basis of the method of differences after Schmidt [27]. The time interval used in this method is

$$\Delta t = \frac{c_p \cdot \rho \cdot \Delta x^2}{\lambda \cdot M} \tag{9.39}$$

- Where Δt = time interval
- Δx = thickness of a layer
- M = number of layers, into which the slab is divided, beginning from the midplane of the slab (Fig. 9.36)

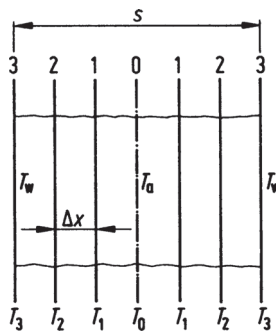


Figure 9.36 Nomenclature for numerical solution of non-steady state conduction in a slab [27]

The mold temperature and the thermodynamic properties of the polymer are assumed to be constant during the cooling process. The temperature at which the latent heat is evolved and the temperature correction W_L (Fig. 9.35) are obtained from the enthalpy diagram as suggested by Gloor [22]. An arbitrary difference of about 6°C is assigned between the temperature of latent heat release at the mid-plane and the temperature at the outer surface of the slab.

Figure 9.37 shows a sample plot of temperature as a function of time for a crystalline polymer.

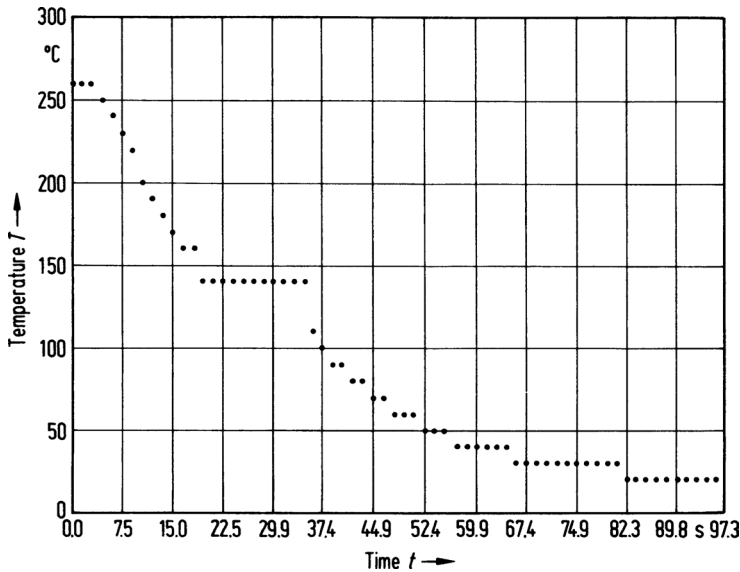


Figure 9.37 Plot of midplane temperature vs. time for a crystalline polymer [8]

9.6.2 Amorphous Polymers

Amorphous polymers do not exhibit the sharp enthalpy change as do crystalline plastics when passing from liquid to solid. Consequently, when applying the numerical method of Schmidt [27], the correction for the latent heat can be left out in the calculation. A sample plot calculated with the computer program [18] is shown in Fig. 9.38 for amorphous polymers. It should be mentioned here that the analytical solutions for non-steady heat conduction given serve as good approximations for crystalline as well as for amorphous polymers.

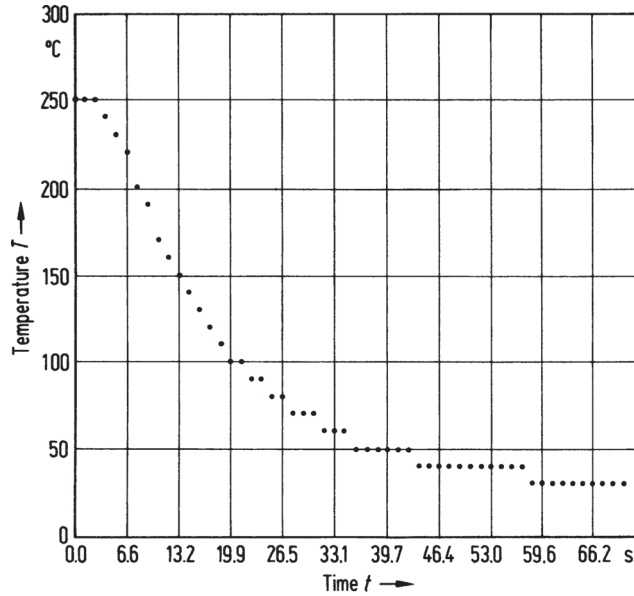


Figure 9.38 Plot of midplane temperature vs. time for an amorphous polymer [8]

9.6.3 Calculations with Varying Mold Wall Temperature

In practice, the mold wall temperature T_w (Fig. 9.36) during part cooling is not constant because it is influenced by the heat transfer between the melt and the cooling water. Therefore, the effect of the geometry of the cooling channel layout, the thermal conductivity of the mold material, and the velocity of the cooling water on the cooling time have to be taken into account.

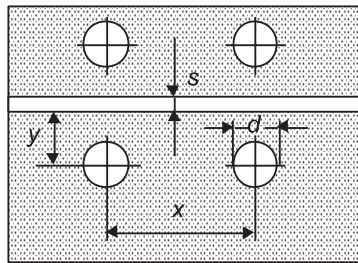


Figure 9.39 Schematic geometry of cooling channels

The heat transferred from the melt to the cooling media can be expressed as [23]

$$\dot{Q}_{AB} = 10^{-3} [(T_M - T_E)c_{p_m} + i_m] \rho_m \frac{s}{2} x \quad [\text{kJ}/\text{m}] \tag{9.40}$$

The heat received by the cooling agent (water) in the time t_k amounts to

$$\dot{Q}_W = 10^{-3} t_k \left(\frac{1}{\lambda_{ST} S_e} + \frac{1}{\alpha 10^{-3} 2\pi R} \right)^{-1} \times (T_W - T_{\text{water}}) \quad [\text{kJ/m}] \quad (9.41)$$

The cooling time t_k can be determined from

$$t_k = \frac{s^2}{\pi^2 a} \cdot \ln \left[\frac{4 \left(\frac{T_M - T_W}{T_E - T_W} \right)}{\pi} \right] \quad (9.42)$$

with the thermal diffusivity

$$a = \lambda_m / \rho_m c_{p_m} \quad (9.43)$$

The influence of the cooling channel layout on heat conduction can be taken into account by the shape factor S_e according to [19, 23]

$$S_e = \frac{2\pi}{\ln \left[\frac{2x \sinh(2\pi y / x)}{\pi d} \right]} \quad (9.44)$$

Using the values for the properties of water, the heat transfer coefficient α follows from [8]

$$\alpha = \frac{0.031395}{d} \cdot \text{Re}^{0.8} \quad (9.45)$$

With Re = Reynolds number.

The mold temperature T_W can now be calculated iteratively from the heat balance $\dot{Q}_{AB} = \dot{Q}_W$.

9.6.3.1 Sample Calculation with Symbols and Units

Part thickness	s	= 2 mm
Distance x	x	= 30 mm
Distance y	y	= 10 mm
Diameter of cooling channel	d	= 10 mm
Mold temperature	T_M	= 250 °C
Demolding temperature	T_E	= 90 °C
Latent heat of fusion of polymer	i_m	= 130 kJ/kg
Specific heat of the melt	c_{p_m}	= 2.5 kJ/(kg K)
Melt density	ρ_m	= 0.79 g/cm ³
Thermal conductivity of the melt	λ_m	= 0.16 W/(m K)

Kinematic viscosity of cooling water $\nu = 1.2 \cdot 10^{-6} \text{ m}^2/\text{s}$

Velocity of cooling water $u = 1 \text{ m/s}$

Temperature of cooling water $T_{\text{water}} = 15 \text{ }^\circ\text{C}$

Thermal conductivity of mold steel $\lambda_{ST} = 45 \text{ W/(m K)}$

With the data above, the heat received from the melt is $\dot{Q}_{AB} = 12.56 \text{ kJ/m}$, $S_e = 3.091$, $\text{Re} = 8333$, and $\alpha = 4300 \text{ W/(m}^2 \text{ K)}$. From the heat balance $\dot{Q}_{AB} = \dot{Q}_W = 12.56$ we obtain by iteration $T_W = 37.83 \text{ }^\circ\text{C}$ and, finally the cooling time t_k from Eq. 9.42 to be $t_k = 8.03 \text{ s}$.

9.6.3.2 Iteration Procedure

The iterative calculation used to obtain the mold wall temperature T_W is performed according to the termination criteria

$$(\dot{Q}_{AB} - \dot{Q}_W) / \dot{Q}_{AB} < \varepsilon$$

where ε is a given error bound as a tolerance. The iteration may be performed by adding a certain minimal value to the assumed mold wall temperature T_W until the termination condition is satisfied.

9.6.3.3 Results of Calculations with the Model

Figure 9.40 shows the effect of the distance y on the cooling time at two different water temperatures. It can be seen that the same cooling time can be obtained as with a lower water temperature when the cooling channels are placed closer to the mold wall, as shown in Fig. 9.41. As Fig. 9.42 depicts, the heat transfer from the melt to the coolant increases insignificantly beyond a certain coolant velocity.

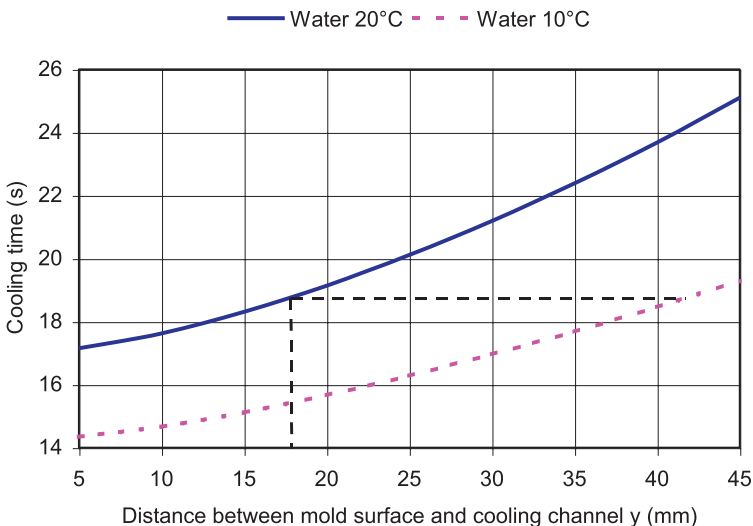


Figure 9.40 Effect of cooling channel distance y on cooling time

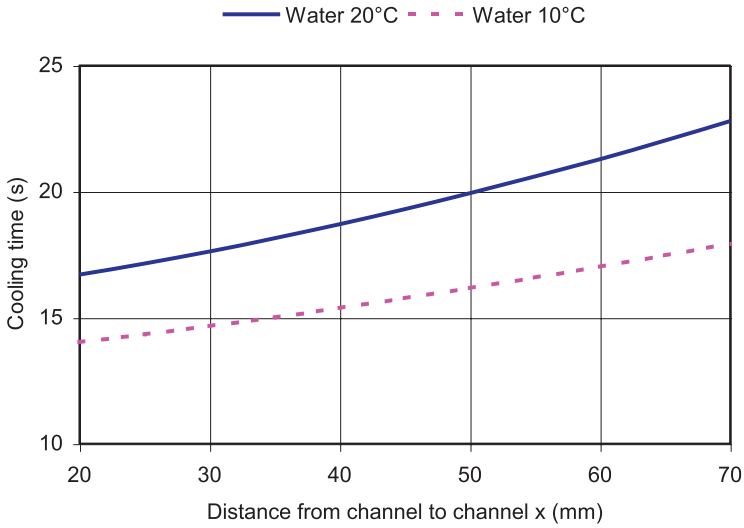


Figure 9.41 Effect of cooling channel distance x on cooling time

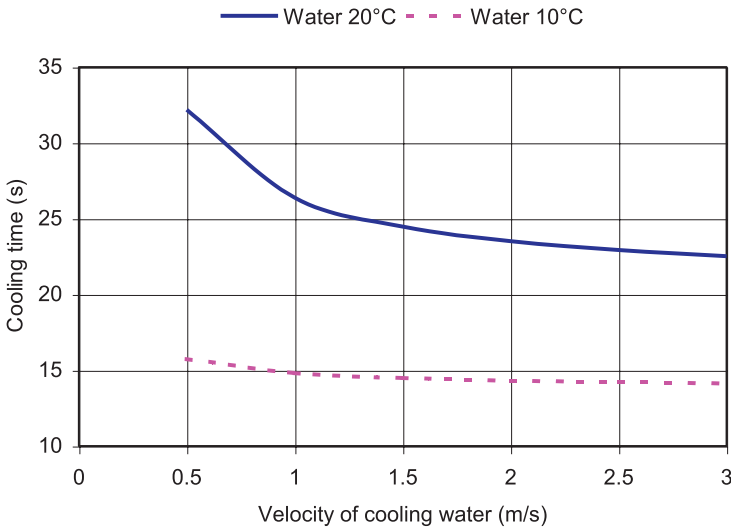


Figure 9.42 Influence of the velocity of cooling water on cooling time

Using the model and the polymers PS, LDPE, and PA as examples, cooling times were calculated and presented in Figs. 9.43 to 9.45 as functions of demolding temperatures.

In these calculations, the distances x and y were kept constant at 30 mm and 12 mm, respectively. Other quantities used were $u = 1$ m/s, $T_{\text{water}} = 20$ °C, and $\lambda_{ST} = 45$ W/(m·K). The resin-dependent properties were used according to the resin in question. The model also allows the simulation of the effect of thermal conductivity

of the mold material as given in Eq. 9.41 (see Figure 9.46). The effect of the temperature of cooling water on cooling time is shown in Figure 9.47.

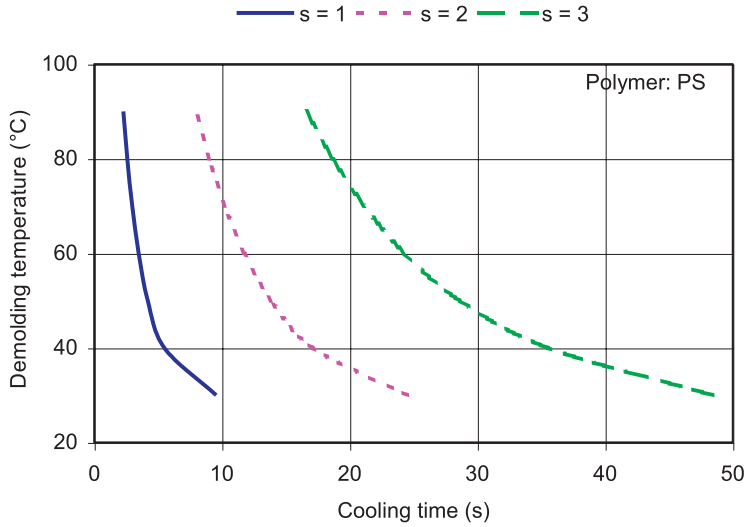


Figure 9.43 Relationship between demolding temperature and cooling time for PS

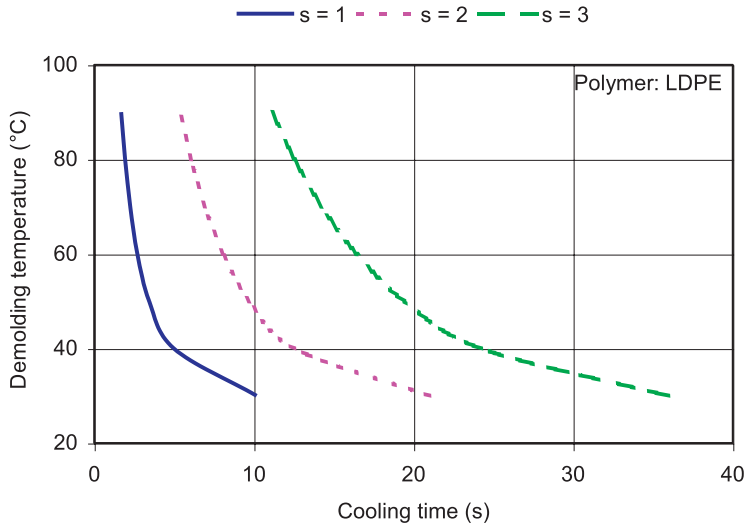


Figure 9.44 Relationship between demolding temperature and cooling time for LDPE

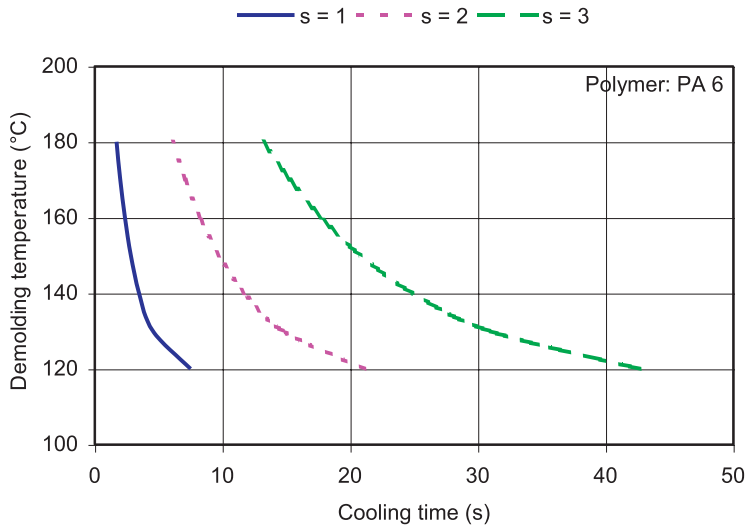


Figure 9.45 Relationship between demolding temperature and cooling time for PA 6

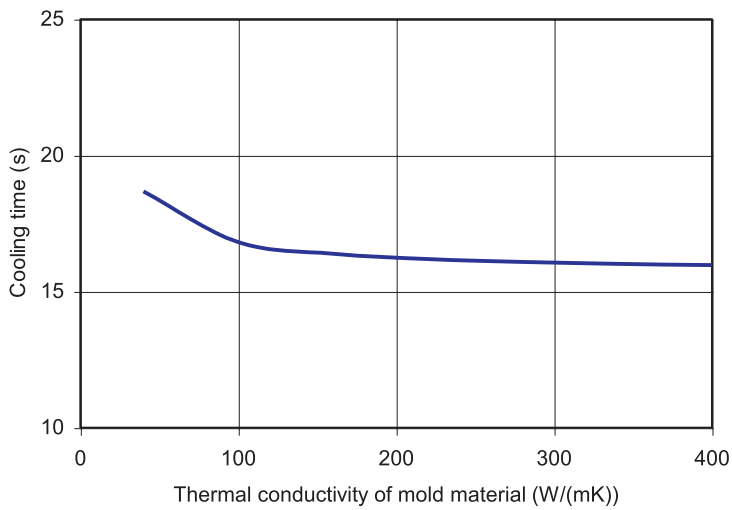


Figure 9.46 Effect of thermal conductivity of mold material on cooling time

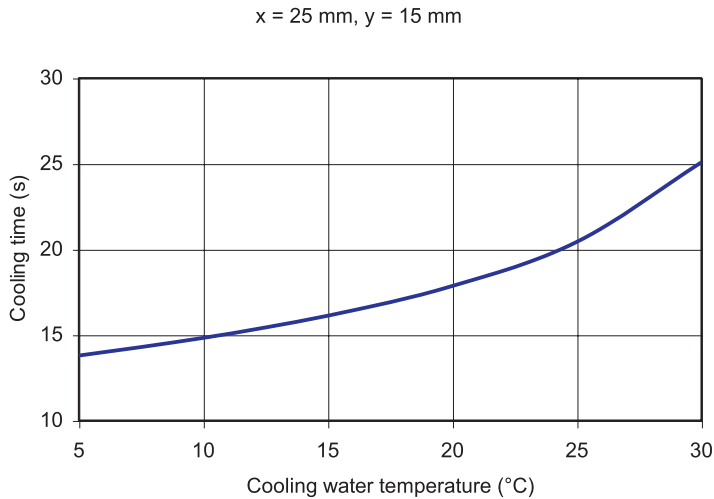


Figure 9.47 Influence of the temperature of cooling water on cooling time

■ 9.7 Rheological Design of the Mold

The distribution of the melt in the runner systems of multicavity molds [15] plays a key role in determining the quality of the part. In order to achieve this aim at low pressures, it is important to be able to predict the pressure drop of the melt flow in the relevant channels accurately. Starting with the resin rheology, the design procedure given next deals with easily applicable practical relationships [8] for calculating the pressure drop in flow channels of different geometries, which are commonly encountered in injection molds.

The power law exponent n can be calculated from Klein's equation, where a_1 , a_{11} , and a_{12} are the viscosity coefficients in the Klein viscosity model, and T is the melt temperature in °F [25].

The shear rates and geometry constants for the channel shapes commonly encountered in injection molds are given in [8].

9.7.1 Sample Calculation

Calculate the pressure drop of a LDPE melt flowing at 200 °C through a round channel with a length of 100 mm and a diameter of 25 mm at a mass flow rate $\dot{m} = 36 \text{ kg/h}$ with a melt density $\rho_m = 0.7 \text{ g/cm}^3$.

Solution:

Volume flow rate:

$$\dot{Q} = \dot{m} / \rho_m = 36 / (3.6 \cdot 0.7) = 1.429 \cdot 10^{-5} \text{ m}^3/\text{s}$$

Shear rate:

$$\dot{\gamma} = 4\dot{Q} / (\pi R^3) = 4 \cdot 1.429 \cdot 10^{-5} / (\pi \cdot 0.0125^3) = 9.316 \text{ s}^{-1}$$

With the viscosity coefficients in the Klein polynomial [25]

$$\ln \eta = a_0 + a_1 \ln \dot{\gamma} + a_{11} \ln \dot{\gamma}^2 + a_2 T + a_{22} T^2 + a_{12} T \ln \dot{\gamma}$$

$$a_0 = 3.3388, a_1 = -0.635, a_{11} = -0.01815, a_2 = -0.005975, a_{22} = -0.0000025, \\ a_{12} = 0.0005187, \text{ and } T = 1.8 \cdot 200 + 32 = 392 \text{ }^\circ\text{F};$$

$$\eta \text{ at } \dot{\gamma} = 9.316 \text{ s}^{-1} \text{ gives } \eta = 4624.5 \text{ Pa} \cdot \text{s}.$$

The power law exponent n is calculated to be $n = 2.052$.

$$\text{Wall shear stress } \tau = \eta \cdot \dot{\gamma} = 43077 \text{ N/m}^2.$$

$$\text{Factor of proportionality, } K = 2.8665 \cdot 10^{-9}.$$

Geometry constant G_{circle}

$$G_{\text{circle}} = (\pi / 4)^{1/2.052} \cdot \frac{0.0125^{3/2.052+1}}{2 \cdot 0.1} = 9.18 \cdot 10^{-5}$$

Finally, $\Delta p = (1.429 \cdot 10^{-5})^{1/2.052} / (2.8665 \cdot 10^{-9})^{1/2.052} \cdot 9.18 \cdot 10^{-5} = 689371 \text{ N/m}^2 =$
 or $\Delta p = 689371 \text{ Pa} = 6.89371 \text{ bar}.$

Figure 9.48 shows the calculated pressure drop Δp as function of the mass flow rate \dot{m} of the melt at 200 °C for a viscous LDPE flowing through a round channel with the tube radius as a parameter. The appropriate runner diameter can be easily found from similar diagrams for any resin by applying the previous equations.

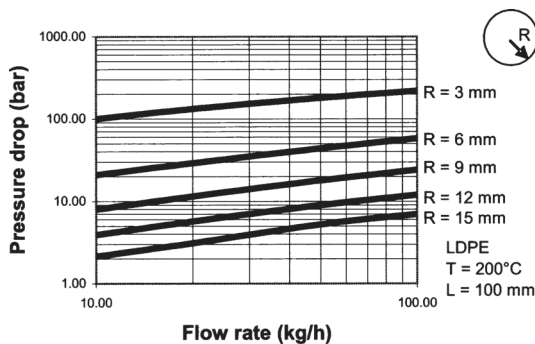


Figure 9.48 Pressure drop vs. flow rate for a circular cross section for LDPE

The effect of melt viscosity on the pressure drop is given in Fig. 9.49. As can be expected, the pressure drop for the easy flowing PET is much lower than that of LDPE.

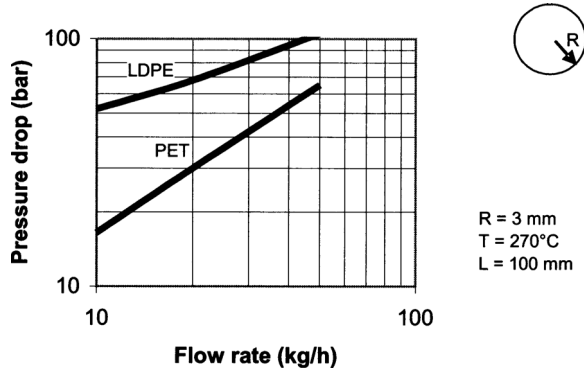


Figure 9.49 Effect of melt viscosity on pressure drop

The calculation procedure allows a quick and easy prediction of the influence of the melt temperature, as depicted in Fig. 9.50.

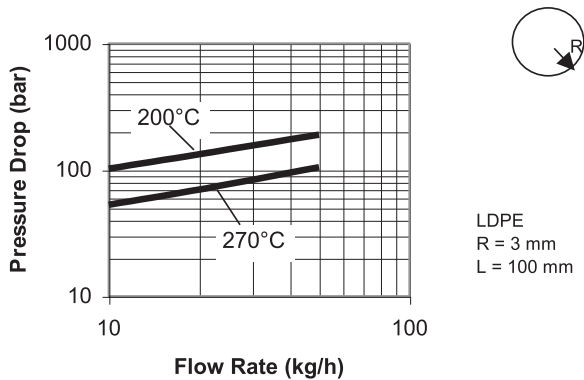


Figure 9.50 Effect of melt temperature on pressure drop

In addition, the effect of the geometry of the runner cross section can also be easily simulated by means of the relationships given in [8] and Fig. 9.51, for a square cross-sectional area compared to a circle for the same cross-sectional area under otherwise equal conditions.

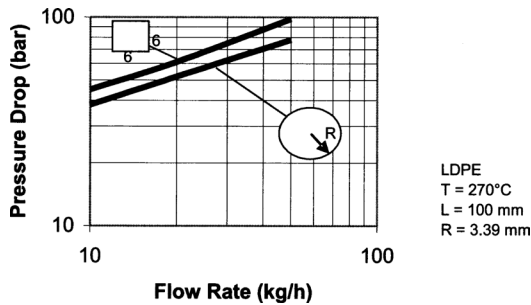


Figure 9.51 Effect of channel shape on pressure drop

9.7.2 General Channel Shape

For channel shapes other than a circle, the equation of Schenkel [26] can be used with close accuracy. A circle with $n = 1$ leads correctly to R_{rh} , the radius of the circle. Using this equation, the pressure drop is calculated for the shape shown in Fig. 9.52 and plotted over the flow rate. In this case, the substitute radius is obtained, and then the same calculation procedure as for the round channel is applied.

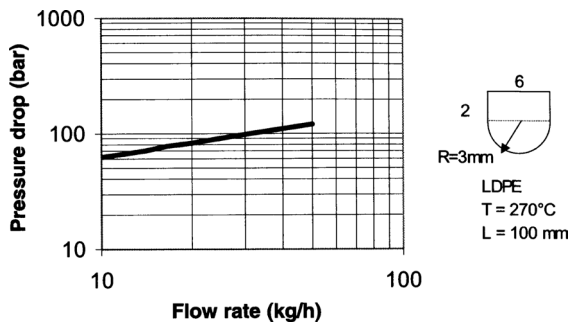


Figure 9.52 Pressure drop for a noncircular channel with $R_{rh} = 2.77$ mm and $n = 2.052$

■ 9.8 References

- [1] *Johannaber, F.*: Injection Molding Machines, 4th ed., Hanser, Munich, 2007
- [2] *Mckelvey, J.M.*: Polymer Processing, John Wiley, New York, 1962
- [3] *Poetsch, G., Michaeli, W.*: Injection Molding – An Introduction, Hanser, Munich, 2007
- [4] *Zoellner, O., Sagenschneider, U.*: Kunstst. 84, 1994, 8, p 1022
- [5] *Hensen, F.* (Ed.): Plastics Extrusion Technology, Hanser, Munich, 1988

- [6] *Donovan, R. C.*: Polym. Eng. Sci. 11, 1971, pp 353, 361
- [7] *Tadmor, Z., Klein, I.*: Engineering Principles of Plasticating Extrusion, Van Nostrand Reinhold, New York, 1970
- [8] *Rao, N. S.*: Design Formulas for Plastics Engineers, Hanser, Munich, 1991
- [9] *Rao, N. S. et al.*: Proceedings of SPE ANTEC, 2001
- [10] C-Mold: Advanced CAE Technology Inc., USA
- [11] *Austin, C.*: CAE for Injection Molding, Hanser, Munich, 1983
- [12] CADMOULD: IKV Aachen, Germany
- [13] *Bangert, H.*: Doctoral Thesis, RWTH, Aachen, 1981
- [14] *Stevenson, J. F.*: Polym. Eng. Sci. 18, 1978, p 573
- [15] *Paulson, D. C.*: Pressure Losses in the Injection Mold, Modern Plastics, 1967, p 119
- [16] Brochure: Mannesman-Demag, 1992
- [17] *Rao, N. S., O'Brien, K.*: Design Data for Plastics Engineers, Hanser, Munich, 1998
- [18] *Rao, N. S. et al.*: Proceedings of SPE ANTEC, 2003
- [19] *Throne, J. F.*: Plastics Process Engineering, Marcel Dekker Inc., New York, 1979
- [20] *Kamal, M. R., Kenig, S.*: Polym. Eng. Sci. 12, 1972
- [21] *Perry, R. H., Green, D.*: Perry's Chemical Engineering Handbook, 1984
- [22] *Gloor, W. E.*: Heat Transfer Calculations, Technical Papers Volume IX-C
- [23] VDI-Wärmeatlas, VDI-Verlag, Düsseldorf, 1984
- [24] *Lindner, E.*: Designing Injection Molds (German), VDI-Verlag, Duesseldorf, 1974, p 109
- [25] *Klein I., Marschall, D. I., Friehe, C. A.*: SPE J. 21, 1965, p 1299
- [26] *Schenkel, G.*: Private Communication
- [27] *Schmidt, E.*: Einführung in die Technische Thermodynamik, Springer, Berlin, 1962
- [28] *Rao, N.*: Kunstst. 73, 1983, p 696
- [29] *Münstedt, H.*: Kunstst. 68, 1978, p 92

■ 9.9 Appendix

Below is a list of programs with brief descriptions.

VISRHEO: This program calculates the viscosity coefficients occurring in four different viscosities models commonly used; namely, Carreau, Münstedt, Klein, and the Power law, on the basis of measured flow curves, and stores these coefficients automatically in a resin data bank.

TEMPMELT: This program calculates the solids melting profile of a multizone screw taking non-Newtonian melt flow into account. A resin data bank containing thermal and rheological properties of different viscosity models is part of the program.

VISSCALE: This program is used to scale up multizone single screws. The resin data bank is included.

VIOUTPUT: This program determines the output of a single screw extruder for a given screw speed or screw speed for a given output. The resin data bank is part of the program.

VISPIDER: This program is for designing spider dies; includes resin data bank.

VISPGAP: This program is for designing spiral mandrel dies; includes resin data bank.

VISCOAT: This program is for designing coat-hanger type dies; includes resin data bank.

All the programs can be obtained from *raonatti@t-online.de*

Index

A

absorption 100

B

barrel screw 118
Barr screw 112
Biot number 174
blown film 155
Brinkman number, Br 174, 204
bulk modulus K 11

C

chemical resistance 101
color 95
comparative tracking index (CTI)
90
composites 103
compounding 167
contact temperature 35
cooling of channels 231
cooling of melt 231
– crystalline polymers 231
cooling time 234
creep modulus 12
creep rupture 14

D

Deborah number 174
design of mold 212
dielectric strength 88

die swell 67
diffusion coefficient 100
dimensionless number 173
drying temperatures 191

E

elastomers 106
enthalpy h 32
extruder output 118
extrusion cooling 170
extrusion dies 145
extrusion screws 112

F

fatigue 15
flammability 38
fluid, non-Newtonian 45

G

gates 202
gloss 155

H

heat deflection temperature (HDT)
36

I

- impact strength 19
- injection molding 185
 - clamp force 204
 - mold 185
 - pressure 188
 - processing temperature 189
 - resin 191
 - runner system 220
 - screw 197

L

- liquid-crystal polymers 104
- loss tangent 89

M

- melt flow index (MFI) 63
- mold shrinkage 188

N

- normal stress coefficient 65

P

- permeability 99
- pipe extrusion 147

R

- reinforced plastics 103
- relaxation modulus 14
- rheological models 51

S

- shear compliance, J_e 66
- sheet extrusion 161
- specific volume v 26
- spider die 147
- surface resistivity 87

T

- thermal conductivity 32
- thermoforming 163
- twin screws 114

V

- velocity 44
- volume resistivity 87

W

- weathering resistance 100

Natti S. Rao

Basic Polymer Engineering Data

Whether working on a machine component's layout, product design, or process optimization, the plastics engineer needs to apply a multitude of polymer property values. Although there are comprehensive overviews of property data for polymers available, books offering both resin and machine design data are very rare.

This book not only provides a quick reference on basic design data for resins, machines, parts, and processes, it also shows how to apply these data to solve practical problems. Numerous examples are given to illustrate the appropriate application of the data presented. The user can even carry out most of the calculations involved with a handheld calculator.

The approach is unassuming and very practical to enable engineers, scientists, and students dealing with polymers to apply the concepts described in this book in their daily work.

Contents:

- Mechanical Properties of Solid Polymers
- Thermal Properties of Solid and Molten Polymers
- Transport Properties of Molten Polymers
- Electrical Properties
- Optical Properties of Solid Polymers
- External Influences
- Extrusion
- Blow Molding
- Injection Molding

HANSER

www.hanserpublications.com

Hanser Publications

ISBN 978-1-56990-649-1



9 781569 906491